Advances in Clinical and Experimental Medicine

MONTHLY ISSN 1899-5276 (PRINT) ISSN 2451-2680 (ONLINE) www.advances.umw.edu.pl

2021, Vol. 30, No. 11 (November)

Impact Factor (IF) – 1.727
Ministry of Science and Higher Education – 40 pts
Index Copernicus (ICV) – 166.39 pts

Wroclaw Medical University

Advances
in Clinical and Experimental
Medicine

Advances
in Clinical and Experimental Medicine

ISSN 1899-5276 (PRINT) ISSN 2451-2680 (ONLINE) www.advances.umw.edu.pl

MONTHLY 2021
Vol. 30, No. 11
(November)

Advances in Clinical and Experimental Medicine (*Adv Clin Exp Med*) publishes high quality original articles, research-in-progress, research letters and systematic reviews and meta-analyses of recognized scientists that deal with all clinical and experimental medicine.

Editorial Office
ul. Marcinkowskiego 2–6
50-368 Wrocław, Poland
Tel.: +48 71 784 11 36
E-mail: redakcja@umw.edu.pl

Publisher
Wroclaw Medical University
Wybrzeże L. Pasteura 1
50-367 Wrocław, Poland

Online edition is the original version of the journal

Editorial Policy

Advances in Clinical and Experimental Medicine (Adv Clin Exp Med) is an independent multidisciplinary forum for exchange of scientific and clinical information, publishing original research and news encompassing all aspects of medicine, including molecular biology, biochemistry, genetics, biotechnology and other areas. During the review process, the Editorial Board conforms to the "Uniform Requirements for Manuscripts Submitted to Biomedical Journals: Writing and Editing for Biomedical Publication" approved by the International Committee of Medical Journal Editors (www.ICMJE.org/). The journal publishes (in English only) original papers and reviews. Short works considered original, novel and significant are given priority. Experimental studies must include a statement that the experimental protocol and informed consent procedure were in compliance with the Helsinki Convention and were approved by an ethics committee.

For all subscription-related queries please contact our Editorial Office:
redakcja@umw.edu.pl

For more information visit the journal's website:
www.advances.umw.edu.pl

Pursuant to the ordinance No. 134/XV R/2017 of the Rector of Wroclaw Medical University (as of December 28, 2017) from January 1, 2018 authors are required to pay a fee amounting to 700 euros for each manuscript accepted for publication in the journal Advances in Clinical and Experimental Medicine.

Indexed in: MEDLINE, Science Citation Index Expanded, Journal Citation Reports/Science Edition, Scopus, EMBASE/Excerpta Medica, Ulrich's™ International Periodicals Directory, Index Copernicus

Typographic design: Piotr Gil, Monika Kolęda
DTP: Wydawnictwo UMW
Cover: Monika Kolęda
Printing and binding: Soft Vision Mariusz Rajski

Advances
in Clinical and Experimental Medicine

MONTHLY 2021, Vol. 30, No. 11 (November)

ISSN 1899-5276 (PRINT)
ISSN 2451-2680 (ONLINE)
www.advances.umw.edu.pl

Contents

Editorials

Original papers

Impacts of COVID-19 lockdowns on frailty and wellbeing in older people and those living with long-term conditions

Carol Holland[1,A–F], Ian Garner[1,B,C,E,F], Jane Simpson[1,A–C,E,F], Fiona Eccles[1,A–C,E,F], Esperanza Navarro Pardo[2,A,B,C,E,F], Calum Marr[1,A,B,C,E,F], Sandra Varey[1,A,B,E,F]

[1] Centre for Ageing Research, Lancaster University, UK
[2] School of Psychology, University of Valencia, Spain

A – research concept and design; B – collection and/or assembly of data; C – data analysis and interpretation; D – writing the article; E – critical revision of the article; F – final approval of the article

Advances in Clinical and Experimental Medicine, ISSN 1899–5276 (print), ISSN 2451–2680 (online) *Adv Clin Exp Med*. 2021;30(11):1111–1114

Address for correspondence
Carol Holland
E-mail: c.a.holland@lancaster.ac.uk

Funding sources
None declared

Conflict of interest
None declared

Received on November 9, 2021
Accepted on November 22, 2021

Published online on November 25, 2021

Abstract

Lockdowns and social distancing have been important and successful strategies to limit the spread of the coronavirus disease 2019 (COVID-19) virus. However, excess deaths related to non-COVID-19 causes have been reported, suggesting issues around availability and use of health services, particularly for people with conditions needing ongoing medical support. In addition, evidence indicates that a range of age-related diseases and frailty are impacted by physical activity and social engagement, both limited in lockdown situations. It is therefore important to learn from the effects of lockdowns in order to limit any impacts, while still protecting people from the infection. This editorial summarizes two research themes at the Centre for Ageing Research at Lancaster University in the UK, one assessing impacts of lockdown for people living with a long-term neurodegenerative condition, Parkinson's disease, and one assessing longitudinal impacts on frailty and wellbeing, with older adults aged over 70, including those living with at least one long-term condition. Uncertainty related to Parkinson's disease and to COVID-19 amplified each other, and cancelled clinical appointments and limitations on physical activity had very significant impacts on wellbeing for this group. In the longitudinal study, frailty was more severe during lockdown periods. While lockdowns reduce spread of the virus, becoming frailer could make older adults more vulnerable to the effects of the virus during these periods. Regular exercise during lockdown had beneficial effects aiding recovery once restrictions relaxed. These studies suggest factors that could lessen negative impacts of future lockdowns. Maintaining physical activity and providing access to health services during periods of lockdown are suggested as priorities.

Key words: COVID-19, physical distancing, Parkinson's disease, frailty, aged

Cite as
Holland C, Garner I, Simpson J, et al. Impacts of COVID-19 lockdowns on frailty and wellbeing in older people and those living with long-term conditions. *Adv Clin Exp Med*. 2021;30(11):1111–1114. doi: 10.17219/acem/144135

DOI
10.17219/acem/144135

More than 5 million people worldwide have now died of the coronavirus disease 2019 (COVID-19) virus, with many countries also beginning to report excess deaths (deaths in excess of what would be expected for the time of year based on pre-pandemic years) from other causes, related to stretched medical resources or fear of attending hospitals. The World Health Organization (WHO) survey,[1] using data from 105 countries, found that the treatment of noncommunicable conditions had been disrupted by the pandemic, particularly the treatment of hypertension, diabetes, cancer, and cardiovascular emergencies. Non-COVID-19 mortality represents between one and two thirds of the excess mortality in different countries,[2–4] and its causes include heart disease, diabetes, dementia and other causes. This has been attributed to a significant drop in use of healthcare; for example, in Greece, primary care visits dropped by 24.8% and hospital surgical procedures by 23.1%, suggesting that the success of lockdowns in reducing infections and deaths from COVID-19 had come at the expense of non-COVID-19 patients, leaving a significant amount of unmet need in the population.[4]

Work to examine impacts of lockdowns on populations is crucial if we are to learn what works compared to what increases risks and healthcare burdens in the longer term. This is specifically the case for older age groups, given age-related increase in frequency of long-term conditions that need regular and ongoing healthcare support.[5] The greater impact of COVID-19 infection on older adults, particularly those with existing long-term conditions is clear[6] with respiratory issues, morbid obesity, dementia, diabetes, atrial fibrillation, and hypertension, all being risk factors for COVID-19-related hospitalizations.[7,8] Frailty also increases with age, which can be associated with multiple chronic diseases but can also occur in the absence of specific diseases. Frailty is defined as a state of increased vulnerability to negative outcomes[9] and in line with this definition, the outcomes of COVID-19 infection are more severe for frail older adults.[10,11] Therefore, lockdown and social distancing strategies are vital to protect older adults. Moreover, we need to determine what impacts such strategies may have.

It is thus important to understand how lockdown restrictions may have affected older people living with, and without, long-term conditions, but also how they may have influenced frailty levels, and so vulnerability to infection, over the course of the pandemic to date. Physical and social inactivity caused by lockdown may be expected to have both an immediate and lasting effect on older adults' health, given that low exercise and social engagement have been associated with an increased risk of frailty, cognitive decline and dementia.[12–14] Many older adults reported a significant reduction in normal activities they do to promote healthy ageing during lockdown – e.g., in a Spanish study, 65.7% reported doing less physical activity.[15] Therefore, it is important to consider what factors may mitigate adverse effects of lockdown on older adults and those living with long-term conditions, with coping resources, and health behaviors such as physical and social engagement identified as candidate protective factors. Our own work has begun to examine some of these issues, first in a group of people living with a long-term neurodegenerative condition, Parkinson's disease, and second in groups of people aged over 70, half of whom living with multiple long-term conditions.

Our qualitative work with people living with Parkinson's[16] focused on the uncertainty related to living with the illness in a time of pandemic and lockdowns. Four specific themes were extracted from the interview data: (1) COVID-19 is amplifying existing fears and difficulties around the uncertainty of Parkinson's, including those relating to hospitalization, loss of function and independence, accessibility of medication, and worries about treatment if they did get a COVID-19 infection. Many participants also realized that the two sources of uncertainty (their chronic, neurodegenerative illness and COVID-19) amplified each other; (2) Practical and psychological efforts to manage uncertainty. Participants attempted to gain control of the uncertainty of the situation. Their approach to the additional uncertainty created by social restrictions was pragmatic and focused on acceptance. The psychological toll of dealing with COVID-19 against a backdrop of also managing a serious health condition was acknowledged by the participants; (3) Benefit-finding as a way of acknowledging the positive aspects of lockdown: Despite multiple challenges, participants' ability to see the positives was important in balancing the potential psychological distress from having to manage an additional set of stressors, by reassessing priorities and feeling an increase in personal resilience; (4) Risk and future management in the context of uncertainty: While some of the participants' fears related to contracting COVID-19, similar levels of anxiety were also expressed about lockdown causing permanent effects on their health and wellbeing, e.g., due to cancelled health appointments or lack of availability of physical and social activity.

A key learning point was that the clinical appointments being cancelled during the pandemic was particularly worrying, given evidence on the role of healthcare communication and support in reducing illness uncertainty and communicating hope, especially during healthcare crises.[17] Supporting this, Parkinson's UK report, based on a large quantitative survey, also found loss of physical exercise was a problem, due to its impact on both physical and mental wellbeing and significant problems with loss of medical appointments.[18]

In our second study (unpublished data), potential changes in physical and mental wellbeing in older adults were assessed across a 12-month period through lockdown variations to determine how frailty may change in relation to restrictions, focusing on a multidimensional approach to frailty and its measurement.[19] We also aimed to consider if coping resources mitigate any deterioration in health and

wellbeing associated with lockdown, and how frequency of physical activity and experienced social isolation may influence change in frailty, loneliness, quality of life, and perceptions of environmental age-friendliness (physical and social accessibility, community support and outreach).

Seventy participants were recruited in England and Spain, time periods illustrated in Fig. 1. While lockdowns were similar between the countries, the first lockdown, during which we conducted our first assessment (our Time 1), was stricter in Spain with people not being allowed out just for a walk, while in the UK residents were encouraged to take daily exercise. Also, at the time of our fourth assessment (Time 4), restrictions were increasing again in the regions of England where our participants were located. The last assessment was in June 2021 by which time all participants had been vaccinated.

Volunteers, all living independently, were aged over 70, with 50 participants in England and 20 in Spain. Overall, 24 participants were considered 'high risk' as determined using the UK National Health Service (NHS) lists of high-risk conditions,[20] meaning they had at least one long-term health condition that made them more vulnerable to severe effects of COVID-19.

Assessments included measures of: multidimensional frailty; quality of life; loneliness; age-friendliness of their environment; physical activity (days a week they engaged in at least 30 min of exercise); social contact; coping resources (what things were helping them cope during the pandemic, e.g., family support, community groups or watching TV).

Results showed that the average frailty was highest at the time of the first assessment when restrictions were at their most stringent (it was higher in Spain), then decreased in severity in both countries to the third assessment, representing a time period with lower restrictions. Among the Spanish group, frailty continued to decrease but in the English group, frailty rose again at the fourth assessment, corresponding to a period in which our participants were subject to the stricter of the UK "tiered" lockdowns and to the beginning of the darker evenings and harsher winter than expected in Spain. At our final assessment, one year after the first, all participants had received two doses of a COVID-19 vaccine and social distancing had largely eased. At this point, frailty was significantly lower than in the strict first lockdown.

We also found changes in how participants viewed their environment. Across both countries, participants seemed to view their environment as more age-friendly, more able to meet their needs, e.g., for access to general practitioner (GP) surgeries or social engagement, when fewer lockdown restrictions were in place.

A year after the first lockdown, participants viewed their environment as significantly more age-friendly than at the beginning. We did not find any evidence to suggest that quality of life or loneliness showed significant changes over time, but we did find an impact of level of physical exercise on changes in frailty. Participants who engaged in exercise more frequently during lockdown showed a greater decrease in frailty severity as restrictions were eased. Having more or fewer coping resources did not seem to affect changes in frailty in this study.

The key learning points are:

(i) Frailty in older adults, including those with underlying health conditions that put them at higher risk

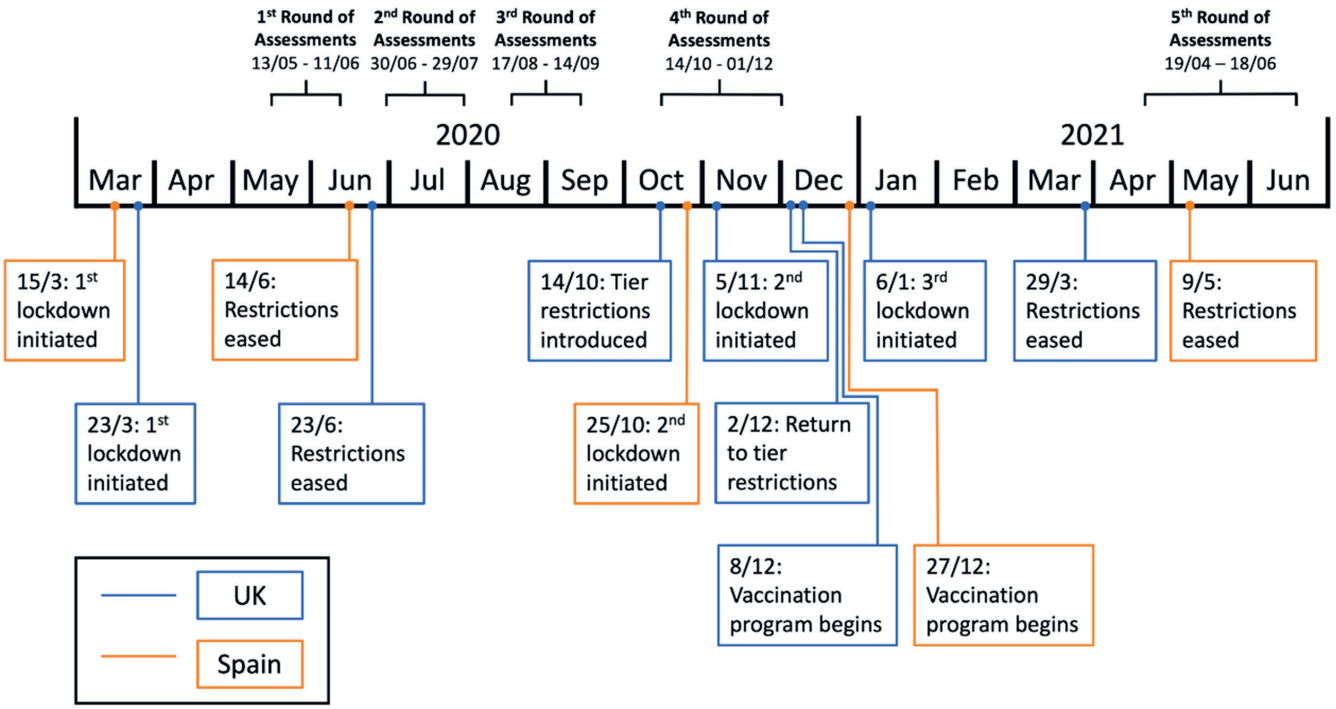

Fig. 1. Study timeline

of COVID-19 infection, was more severe during periods of lockdown compared to when restrictions were eased. While periods of lockdown and strict social distancing clearly reduce the spread of the virus, becoming frailer because of lockdown may mean that older adults could be more vulnerable to serious effects of the virus during these periods. There is an important need for strategies to help in reducing frailty in older adults while such restrictions are in place;

(ii) Regular exercise during lockdown can have beneficial long-term effects aiding recovery once restrictions relax. Helping older adults, especially those living with frailty, to remain physically active during periods of high restrictions should be an important consideration going forward.

In conclusion, lockdowns, social distancing restrictions and pauses in healthcare accessibility could have specific negative consequences for older people, particularly those living with long-term conditions that need ongoing treatment and support. While lockdowns protect the most vulnerable, these studies suggest factors that could lessen negative impacts of future lockdowns. Maintaining physical activity, supporting a sense of control and a supportive environment, as well as providing access to services such as GP or outpatient appointments during periods of lockdown are shown to be key priorities.

ORCID iDs

Carol Holland https://orcid.org/0000-0001-7109-6554
Ian Garner https://orcid.org/0000-0002-9349-5377
Jane Simpson https://orcid.org/0000-0001-5071-4077
Fiona Eccles https://orcid.org/0000-0003-1484-2703
Esperanza Navarro Pardo https://orcid.org/0000-0002-9355-2909
Calum Marr https://orcid.org/0000-0003-3878-9505
Sandra Varey https://orcid.org/0000-0002-6148-6425

References

1. World Health Organization. Pulse survey on continuity of essential health services during the COVID-19 pandemic: Interim report, 27 August 2020. https://www.who.int/publications/i/item/WHO-2019-nCoV-EHS_continuity-survey-2020.1. Accessed November 6, 2021.
2. Woolf SH, Chapman DA, Sabo RT, Weinberger DM, Hill L. Excess deaths from COVID-19 and other causes, March-April 2020. *JAMA*. 2020;324(5):510–513. doi:10.1001/jama.2020.11787
3. Kontopantelis E, Mamas MA, Deanfield J, Asaria M, Doran T. Excess mortality in England and Wales during the first wave of the COVID-19 pandemic. *J Epidemiol Community Health*. 2021;75(3):213–223. doi:10.1136/jech-2020-214764
4. Kondilis E, Tarantilis F, Benos A. Essential public healthcare services utilization and excess non-COVID-19 mortality in Greece. *Public Health*. 2021;198:85–88. doi:10.1016/j.puhe.2021.06.025
5. Department of Health. Long Term Conditions Compendium of Information, Third Edition. https://assets.publishing.service.gov.uk/government/uploads/system/uploads/attachment_data/file/216528/dh_134486.pdf. Accessed November 6, 2021.
6. Levin AT, Hanage WP, Owusu-Boaitey N, Cochran KB, Walsh SP, Meyerowitz-Katz G. Assessing the age specificity of infection fatality rates for COVID-19: Systematic review, meta-analysis, and public policy implications. *Eur J Epidemiol*. 2020;35(12):1123–1138. doi:10.1007/s10654-020-00698-1
7. Atkins JL, Masoli JAH, Delgado J, et al. Preexisting comorbidities predicting COVID-19 and mortality in the UK biobank community cohort. *J Gerontol A Biol Sci Med Sci*. 2020;75(11):2224–2230. doi:10.1093/gerona/glaa183
8. Onder G, Rezza G, Brusaferro S. Case–fatality rate and characteristics of patients dying in relation to COVID-19 in Italy. *JAMA*. 2020;323(18):1775–1776. doi:10.1001/jama.2020.4683
9. Clegg A, Young J, Iliffe S, Rikkert MO, Rockwood K. Frailty in elderly people. *Lancet*. 2013;381(9868):752–762. doi:10.1016/S0140-6736(12)62167-9
10. Hewitt J, Carter B, Vilches-Moraga A, et al. The effect of frailty on survival in patients with COVID-19 (COPE): A multicentre, European, observational cohort study. *Lancet Public Health*. 2020;5(8):e444–e451. doi:10.1016/S2468-2667(20)30146-8
11. Petermann-Rocha F, Hanlon P, Gray SR, et al. Comparison of two different frailty measurements and risk of hospitalisation or death from COVID-19: Findings from UK Biobank. *BMC Med*. 2020;18(1):355. doi:10.1186/s12916-020-01822-4
12. Apóstolo, J, Cooke R, Bobrowicz-Campos E, et al. Effectiveness of interventions to prevent pre-frailty and frailty progression in older adults: A systematic review. *JBI Database System Rev Implement Rep*. 2018;16(1):140–232. doi:10.11124/JBISRIR-2017-003382
13. Gale CR, Westbury L, Cooper C. Social isolation and loneliness as risk factors for the progression of frailty: The English Longitudinal Study of Ageing. *Age Ageing*. 2018;47(3):392–397. doi:10.1093/ageing/afx188
14. Oliveira JS, Pinheiro MB, Fairhall N, et al. Evidence on physical activity and the prevention of frailty and sarcopenia among older people: A systematic review to inform the World Health Organization physical activity guidelines. *J Phys Act Health*. 2020;17(12):1247–1258. doi:10.1123/jpah.2020-0323
15. Rodríguez-Gonzalez R, Facal D, Martinez-Santos AE, Gandoy-Crego M. Psychological, social and health-related challenges in Spanish older adults during the lockdown of the COVID-19 first wave. *Front Psychiatry*. 2020;11:588949. doi:10.3389/fpsyt.2020.588949
16. Simpson J, Zarotti N, Varey S, et al. 'It's a double whammy': A qualitative study of illness uncertainty in individuals with Parkinson's disease in the context of COVID-19. *Chronic Illn*. 2021;17423953211043101. doi:10.1177/17423953211043101
17. Hansen BS, Rørtveit K, Leiknes I, et al. Patient experiences of uncertainty: A synthesis to guide nursing practice and research. *J Nurs Manag*. 2012;20(2):266–277. doi:10.1111/j.1365-2834.2011.01369.x
18. Simpson J, Eccles FJR, Doyle C. The impact of coronavirus restrictions on people affected by Parkinson's: The findings from a survey by Parkinson's UK. Lancaster, UK: Lancaster University; 2020. https://www.parkinsons.org.uk/news/how-have-coronavirus-covid-19-restrictions-impacted-people-affected-parkinsons. Accessed November 6, 2021.
19. Garner IW, Burgess AP, Holland CA. Developing and validating the Community-Oriented Frailty Index (COM-FI). *Arch Gerontol Geriatr*. 2020;91:104232. doi:10.1016/j.archger.2020.104232
20. National Health Service. Who is at high risk from coronavirus (clinically extremely vulnerable). https://www.nhs.uk/conditions/coronavirus-covid-19/people-at-higher-risk/who-is-at-high-risk-from-coronavirus-clinically-extremely-vulnerable. Accessed November 6, 2021.

Out-of-hospital sepsis recognition by paramedics improves the course of disease and mortality: A single center retrospective study

Martin Floer[1,A–F], Mario Ziegler[2,3,A–F], Bodo Lenkewitz[3,A–F], Agneta Auer[1,A–F], Tobias Meister[1,A–F]

[1] The First Department of Medicine, Klinikum Ibbenbüren, Germany
[2] Helios Albert-Schweitzer-Hospital, Northeim, Germany
[3] Emergency Medical Service, Northeim, Germany

A – research concept and design; B – collection and/or assembly of data; C – data analysis and interpretation;
D – writing the article; E – critical revision of the article; F – final approval of the article

Advances in Clinical and Experimental Medicine, ISSN 1899–5276 (print), ISSN 2451–2680 (online) *Adv Clin Exp Med*. 2021;30(11):1115–1125

Address for correspondence
Martin Floer
E-mail: martinfloer@web.de

Funding sources
None declared

Conflict of interest
None declared

Acknowledgements
We would like to thank the Helios Albert-Schweitzer-Hospital in Northeim, especially medical controller Michael Mehrmann, for supporting this work by granting access to the clinical information system. We would like to thank Karly Conrads (MSc) for her correction of this paper as a native speaker.

Received on March 26, 2021
Reviewed on May 11, 2021
Accepted on July 20, 2021

Published online on August 20, 2021

Abstract

Background. Early recognition of sepsis and a prompt initiation of goal-directed therapy is important for sepsis survival. Little is known about the impact of early recognition of sepsis in the out-of-hospital setting when paramedics are the 1st medical professionals arriving on the scene.

Objectives. To characterize the impact of sepsis recognition by paramedics in the 1st out-of-hospital contact and to establish a predictive model by combining preclinical patient characteristics.

Materials and methods. In this retrospective single-center cohort study, we included a total of 263 patients diagnosed with sepsis after admission to the emergency department and correlated them to the emergency medical protocols of the paramedics who have seen the patient out-of-hospital.

Results. Only 25 patients were correctly diagnosed by paramedics out-of-hospital. If sepsis was diagnosed, the median time to antibiotic administration was significantly lower (136.50 min compared to 206.98 min, $p = 0.0069$) and mortality was reduced from 22.8% to 8% ($p = 0.0292$). We have identified predictors for prognosis and calculated a predictive model with a modified quick Sepsis-related Organ Failure Assessment (qSOFA) score, which fits the needs for out-of-hospital usage and results in a better discrimination of vitally threatened patients (receiver operating characteristic (ROC) area under curve (AUC) of 0.641 compared to 0.719), as compared to the standard qSOFA.

Conclusions. Sepsis recognition by paramedics at the 1st out-of-hospital contact significantly reduces sepsis mortality. The qSOFA and modified qSOFA are suitable tools for sepsis recognition, and have an impact on mortality and disease management when used.

Key words: paramedic, emergency medicine, qSOFA, sepsis, out-of-hospital

Cite as
Floer M, Ziegler M, Lenkewitz B, Auer A, Meister T. Out-of-hospital sepsis recognition by paramedics improves the course of disease and mortality: A single center retrospective study. *Adv Clin Exp Med*. 2021;30(11):1115–1125. doi:10.17219/acem/140357

DOI
10.17219/acem/140357

Background

Sepsis is a severe disease associated with high rates of mortality and morbidity.[1] The treatment of septic patients is often expensive.[2] Moreover, despite advances in intensive care, the diagnosis of sepsis and its underlying disease remains challenging and time-consuming.[3] The availability of an early predictive model of sepsis for the initiation of goal-directed therapy is necessary. Guidelines from the Surviving Sepsis Campaign have helped to establish structures for the successful treatment of sepsis, especially in hospitalized patients.[4] However, only limited capabilities exist in preclinical emergency services for diagnostic procedures.[5]

In some projects, so-called sepsis kits have been established to improve sepsis survival in a preclinical setting. However, randomized controlled trials evaluating these kits are not sufficiently available and have been difficult to establish.[6] The quick Sepsis-related Organ Failure Assessment (qSOFA) score has been developed recently using guidelines for the rapid assessment of septic conditions. This scoring system uses respiratory rate, disturbance of consciousness, and systolic blood pressure (SBP) as parameters. They can be easily assessed during preclinical emergency service.[7] There is an ongoing scientific debate on the performance of this score as a predictor of outcome.[8] Other scoring systems like the Mortality in Emergency Department Sepsis (MEDS) score and the Modified Early Warning Score (MEWS) may perform better, but are more difficult to establish under preclinical conditions.[9,10] The qSOFA criteria might be also useful in some differential diagnostic aspects that are important for preclinical medicine.

The treatment outcome parameters for sepsis patients are established and described. Among these, the time to antibiotic treatment, lactic acid levels and hemodynamic parameters are the most important.[11] Research in the field of sepsis at this interface is nearly non-existent for out-of-hospital emergency service systems, thus further research is needed in this area.[12] The development of a risk assessment tool for death in patients with preclinical sepsis may be helpful in identifying sepsis patients at the earliest possible time point, and aid in providing adequate and rapid diagnostics work-up and surveillance.

Objectives

It was hypothesized that early sepsis recognition by paramedics at 1st out-of-hospital contact would have an impact on the mortality and morbidity of sepsis. We have also searched for predictive parameters that can be assessed by paramedics, and aimed to establish a predictive model for sepsis prognosis by combining out-of-hospital patient characteristics.

Materials and methods

Study design

This study is a retrospective single-center study. Sepsis survivors and non-survivors who were rushed to the hospital by ambulance were identified and used as the 2 cohorts for this study.

Setting

Sepsis patients interacting with emergency medical services (EMS) in the county of Northeim, Germany and the Helios Albert-Schweitzer-Hospital, Northeim, Germany, were considered for inclusion in the study.

Participants

The patient group was identified by hospital release documentation ICD-10 code A41 (sepsis) and R65 (systemic inflammatory response syndrome – SIRS) after final release or death in hospital. Data were collected from the clinic information system (CIS) of the hospital and the records of the EMS. A total of 263 patients were identified. Data were obtained from the period of January 1, 2012 to December 31, 2018. The exclusion criteria were age under 18 years and missing documentation in the CIS system. All parameters were obtained according to the Declaration of Helsinki and to the rules of the European Union. The study was approved by the ethics committee at the University of Göttingen (approval No. 4/8/17). Data were collected in a Microsoft Excel 2013 (Microsoft Corp., Redmond, USA) table and pseudonymized.

Variables

The primary outcome parameters for mortality rate were death in hospital and length of hospital stay for morbidity rate. The secondary parameters were as follows: age, sex, coronary heart disease, diabetes, residential care, hypertension, chronic kidney disease, liver cirrhosis, malignancy, immunodeficiency, septic urinary tract infection, septic pneumonia, other foci, Allgower's index, preclinical respiratory rate >22/min, preclinical heart rate, preclinical Glasgow Coma Scale (GCS) <14, preclinical lowest SBP, preclinical qSOFA, preclinical O_2 saturation, preclinical temperature >38.5°C, preclinical diagnosis of sepsis (yes or no), hospital respiratory rate >22/min, hospital heart rate, hospital O_2 saturation, hospital GCS <14, preclinical lowest SBP, hospital qSOFA, length of intensive care stay, length of hospital stay, death in hospital, denial of resuscitation order, preclinical antibiotics, hospital antibiotics, time of antibiotics administration, MEWS, Manchester triage category, laboratory tests like thrombocyte count, bilirubin, creatinine, lactic acid level, high sensitive troponin,

leucocyte count, procalcitonin and blood culture results, need for dialysis, and type of antibiotic treatment.

Sample size

The required sample size was not calculated since this was a retrospective proof of concept study.

Statistical analyses

Descriptive statistics were calculated using IBM SPSS v. 27 (SPSS Statistics for Windows; IBM Corp., Armonk, USA). Values are presented as number (n) and percentage, means ± standard deviation (SD), or median ± interquartile range (IQR). Detailed explanations are included in the figure captions.

For tests of statistical significance, t-tests were performed, with a $p < 0.05$ considered significant. For comparisons of n in contingency tables, χ^2 tests were performed where applicable, with a $p < 0.05$ considered significant. We used Q–Q plots to determine a normal distribution for the following variables: age, preclinical SBP, emergency department SBP, preclinical temperature, and emergency department temperature. Non-normality was seen for lactate. After Box–Cox transformation with lambda = 0.1, a normal distribution was achieved and a two-tailed unpaired t-test was performed. For emergency department vigilance, a non-normal distribution was seen. After Box–Cox transformation with lambda = 6.7934, a normal distribution was approximated, but it still did not satisfy the Shapiro–Wilk test. Therefore, a Mann–Whitney U test was used to test for significance in this case.[13]

A receiver operator characteristic (ROC) curve analysis was performed to calculate the correlations of qSOFA and our modified qSOFA with death due to sepsis. Points on the ROC curve nearest the upper left corner were chosen for cut-off values as this resulted in optimal sensitivity and specificity. The predictive model $P_{sepsisdeath}$, indicating the probability for sepsis death by means of multivariate logistic regression, was calculated separately.[13] The $P_{sepsisdeath}$ was calculated by using variables in our modified qSOFA with the following parameters: age, preclinical GCS, and preclinical SBP. For immunodeficiency, 1 indicated immunodeficiency and 0 indicated no immunodeficiency. The predictive factor X was generated as the weighted sums of the predictive factor values, weighed with their regression coefficients from the final binary logistic regression analysis[13] (algorithm: X = 0.024 * [age] – 0.088 * [out of hospital GCS] – 0.021 * [out of hospital SBP] – 0.558 * [1 if immunodeficiency is positive, otherwise 0] + 0.430). The probability of sepsis death ($P_{sepsisdeath}$) was calculated as follows (Eq. 1):

$$p = \frac{1}{1 + e^x}$$

For boxplots of predicted vs real mortality, we grouped patients into quartiles based on their individual mortality likeliness.

Results

We identified 263 sepsis patients who were seen between 2012 and 2018 by the EMS and brought to the emergency department. Sixty-one of them died of sepsis and 202 survived. Between these 2 groups, no differences were found for sex distribution, coronary heart disease, diabetes, dementia, residential care, hypertension, chronic kidney disease, dialysis, liver cirrhosis, or cancer history. Sepsis death was associated with age (83.10 compared to 79.51 years, $p = 0.0385$; Table 1) and the presentation of acute kidney injury (77.7% compared to 61.98%, $p = 0.0346$). For immunodeficiency status, a strong positive tendency was found, but it did not reach significance (11.5% compared to 21.8%, $p = 0.0743$; Table 1). The mean out-of-hospital qSOFA was 1.49 in the non-survivor group and 0.9 in the survivor

Table 1. Significant demographic data, laboratory results and scores

Parameter	Died (n = 61)	Survived (n = 202)	p-value	df#
Age [years]	83.10 ±11.158	79.51 ±12.003	0.0385 (t-test)	261
Acute kidney injury, (n, %)	46, 77.7%	125, 61.9%	0.0346 (χ^2 test)	1
Immunodeficiency*, (n, %)	7, 11.5%	44, 21.8 %	0.0743 (χ^2 test)	1
Lactate [mmol/L]	3.88 ±3.84	2.02 ±2.53	0.0008 (t-test)	108
Preclinical SBP [mm Hg]	107.61 ±33.82	124.37 ±31.39	<0.0001 (t-test)	255
Emergency department SBP [mm Hg]	109.98 ±34.45	129.40 ±33.46	<0.0001 (t-test)	93
Preclinical temperature [°C]	36.53 ±1.21	37.57 ±1.53	<0.0001 (t-test)	119
Emergency department temperature [°C]	36.39 ±1.10	37.46 ±1.44	<0.0001 (t-test)	251
Emergency department qSOFA score	1.49 ±0.95	0.90 ±0.81	<0.0001 (t-test)	255
Emergency department vigilance GCS score ≥15 (n, %)	12.80 ±2.41	13.68 ±1.92	0.0045 (U test)	249

* all patients with ongoing chemotherapy, immunosuppression or hereditary or acquired immunodeficiency; n – number; #df – degrees of freedom; SBP – systolic blood pressure; GCS – Glasgow Coma Scale; qSOFA – quick Sepsis-related Organ Failure Assessment.

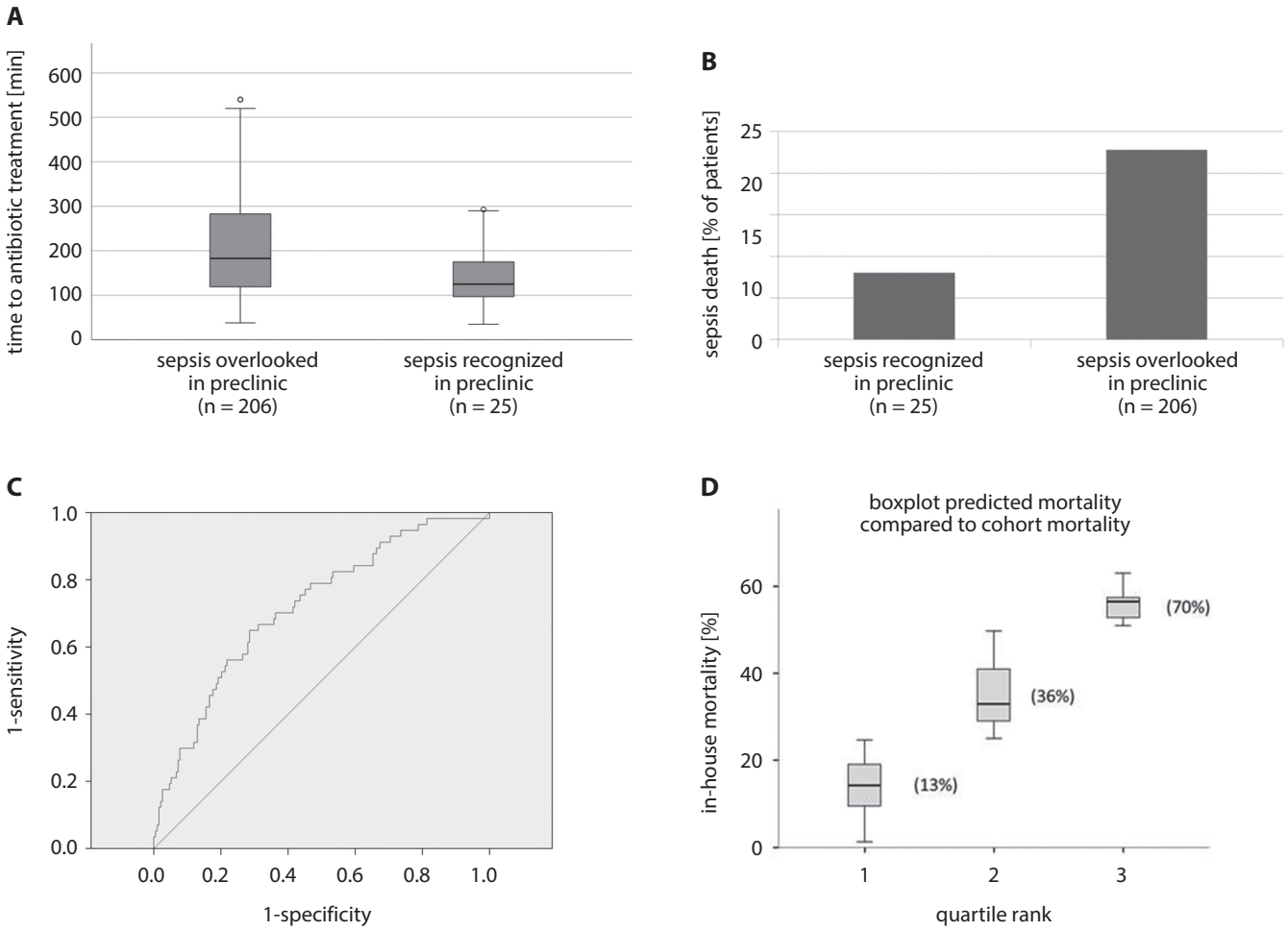

Fig. 1. Boxplot Fig. 1A and 1D include the median as center while the boxes represent the 1st and 3rd quartiles, and therefore, enclose the interquartile range. The whiskers show the minimum and maximum values, and the little circles represent statistical outliers

A. Time to antibiotic treatment as compared to sepsis recognition by paramedics, p = 0.0069; B. Death toll in both groups (%), p = 0.0292; C. ROC analysis of our modified sepsis score, AUC = 0.719 (95% CI = 0.644–0.794); D. Prediction of sepsis death based only on the knowledge of our modified out-of-hospital sepsis score parameters (containing age, out-of-hospital GCS, out-of-hospital SBP, and immunodeficiency). Results are displayed as boxplots with confidence interval; 1st quartile – death probability 0–25%; 2nd quartile – death probability 25–50%; 3rd quartile – death probability 50–75%.
The real measured mortality in our cohort is shown in brackets. There is a good correlation of predicted and actual mortality by this modification.

group (p < 0.0001). It was also found that preclinical SBP (107.61 mm Hg compared to 124.37 mm Hg, p < 0.0001) and preclinical body temperature (36.53°C compared to 37.46°C, p < 0.0001; Table 1) were significantly lower in the sepsis death group. No differences were seen in preclinical average blood pressure (BP), heart rate, vigilance, respiration rate, or oxygen saturation. Interestingly, these findings were also true for the vital parameters taken in the emergency department, but a significant signal for vigilance, as measured with the GCS (12.80 compared to 13.68, p = 0.0048; Table 1), was observed between non-survivors and survivors.

Regarding the reason for sepsis (urinary tract sepsis, pneumonia, abdominal infection, other reasons), no significant differences were found between the sepsis death group and the survival group. A total of 114 positive blood cultures and 149 negative blood cultures were found. The main disease-causing agent was *Escherichia coli*, followed by *Staphylococcus aureus* and *Klebsiella* spp.

The laboratory parameters taken in the emergency department revealed a positive association with sepsis death and lactic acid levels (3.88 mmol/L compared to 2.02 mmol/L, p = 0.0008; Fig. 1), whereas no correlation was found with thrombocyte levels, leucocyte levels, bilirubin concentration, creatinine levels, C-reactive protein (CRP) levels, or increased procalcitonin levels.

Sepsis was recognized by paramedics in only 25 patients and 238 did not have a suspected diagnosis of sepsis by EMS paramedics (Table 2). If sepsis was diagnosed by EMS, a noteworthy decrease in time to the first antibiotic administration as compared to a non-diagnosed sepsis was found (136.50 min compared to 206.98 min after the arrival of EMS on the scene, p = 0.0069; Fig. 1). A remarkable increase in mortality was also found if sepsis was not initially diagnosed by EMS personnel (8% compared to 22.8%, p = 0.0292) before hospital admission (Fig. 1).

If sepsis was not suspected, several misleading diagnoses were documented by paramedics upon delivery

Table 2. EMS diagnosis sepsis, outcome

Outcome	Sepsis recognized (n = 25)	Sepsis not recognized (n = 238)	p-value	df
Mean time to antibiotic treatment [min]*	136.50 ±81.08	206.98 ±117.28	0.0069 (t-test)	182
Died, n (%)	2 (8.0)	59 (22.8)	0.0292 (χ^2 test)	1

*time between arrival of the EMS at the scene and antibiotic administration; df – degrees of freedom.

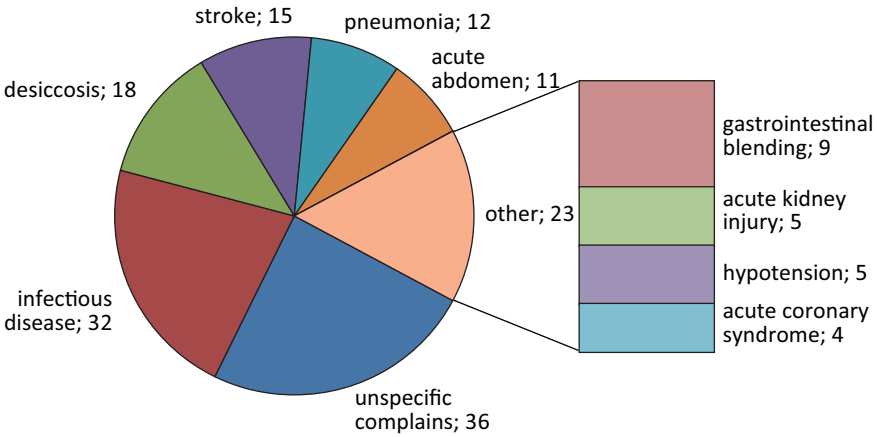

Fig. 2. Top 10 misleading diagnoses by paramedics (n)

Table 3. Top 5 EMS alternative diagnosis instead of sepsis

EMS alternative diagnosis instead of sepsis – top 10	n
Unspecific complaints	36
Infectious disease	32
Desiccosis	18
Stroke	15
Pneumonia	12

EMS – emergency medical services.

to the emergency department (Fig. 2). The most often diagnosis was "unspecific complaints," followed by "unspecific infectious disease" and desiccosis (Table 3).

Interestingly, most patients were transported by a type B ambulance (emergency ambulance) according to Euronorm (EN) 1789 (48%). Only 31% of patients were transported by a type C ambulance (mobile intensive care unit; EN 1789) and 21% had a type C ambulance accompanied by an emergency physician.

The duration of stay in the intensive care unit (ICU) did not differ between non-survivors and survivors, and no significant difference was seen after subdivision of the preclinical qSOFA 1 or 2–3 (3.5 compared to 5 days, p = 0.109). There was only a tendency for longer stays with a higher qSOFA (>1) on admission.

The out-of-hospital qSOFA and in-hospital mortality were correlated using a ROC. In our cohort, qSOFA correlated with an area under curve (AUC) of 0.641 (95% CI = 0.559–0.723) for predicting sepsis death.

If we use a modified sepsis score (with parameters age, out-of-hospital GCS, out-of-hospital SBP, and presence of immunodeficiency – Fig. 2), the AUC was more exact with 0.719 (95% CI = 0.644–0.794), as compared to the original qSOFA. We have chosen to implement the aspect of immunodeficiency since this parameter showed a strong tendency, but lacked significance (p = 0.0743).

Next, we checked the abovementioned modified sepsis score (Fig. 1C) by calculating the individual probability of sepsis death. Three groups were formed according to the mathematical division into quartile ranks (1st quartile – death probability 0–25%, 2nd quartile – death probability 25–50%, 3rd quartile – death probability 50–75%; Fig. 1D). Since the 4th quartile (death probability 75–100%) encompassed no patients, it was excluded. The results of this calculation based on the abovementioned parameters are shown as boxplots representing the mean and IQR (25–75%) of the corresponding box for the specific quartile rank; therefore, representing the probability of death due to sepsis. The actual measured mortality in our cohort is shown in brackets (Fig. 1D). A very good prediction of the real in-hospital mortality was found when the modified version of the out-of-hospital sepsis score was used.

Discussion

Our main finding was that, if sepsis was suspected by EMS, an improved outcome was detected. This finding is consistent with previously published data.[14] On the other hand, there are reports that did not detect an improved outcome even if EMS was involved in sepsis cases.[15] The reasons for these conflicting results remain unclear. One could speculate that situational awareness might play a role. The qSOFA is therefore a useful tool to establish this awareness in the out-of-hospital context. Further

investigation after implementation of the so-called sepsis bundles and routine qSOFA scoring in the preclinical setting might help solve this problem.

In the majority of cases, sepsis was not recognized by EMS personnel. Mainly, unspecific complaints were given as admission diagnoses on arrival at the emergency department. It is well known that especially elderly patients being brought to emergency departments with unspecified complaints in 60% of cases have a serious disease.[16] The most frequent reasons for misdiagnosis in the geriatric setting are concealed or less typical symptoms, multi-morbidity, as well as communication problems.[17] In this context, it is not surprising that most patients were transported with type B EN1789 patient transport ambulances.

The overall sepsis mortality rate in the current cohort between 2012 and 2018 was 23.2%. Stevenson et al.[18] reported a mortality rate of 29% for severe sepsis in the decade 2010–2020. Therefore, it can be concluded that the current cohort was not undertreated; in fact, these patients performed better than average. Looking at the demographics, it was found that age, acute kidney injury and immunosuppression (defined as any state of ongoing antitumor chemotherapy, medical immunosuppression, and hereditary or acquired immunodeficiency) influenced sepsis mortality. These findings are consistent with literature.[19] A positive correlation of out-of-hospital qSOFA and emergency department qSOFA with mortality was found, which is also consistent with literature.[20] A preclinical normal or slightly lowered body temperature (mean 36.4°C) was associated with sepsis death, as compared to a normal or slightly elevated body temperature (mean 37.5°C). While the role of fever in sepsis has been widely discussed and sparked controversy, the impact on mortality is generally low.[21] Kushimoto et al.[22] found that body temperature lower than 36.5°C to be associated with sepsis death, which is in accordance with our data.

Interestingly, a signal for the parameters average BP and GCS in the emergency department was found, which was not detected during patient transport. This time-dependent phenomenon shows the dynamic status of septic shock and is known in literature.[23]

The reasons for sepsis and sepsis death, as well as blood culture results, did not differ between the survivor and non-survivor groups, therefore excluding intensive care treatment bias in our cohort.

Elevated lactic acid levels were associated with death in the current cohort, which has also been described in the literature.[24] The data showed no significant difference in the duration of stay in ICU between the non-survivors and survivors. Patients with a higher qSOFA had only a tendency for longer stays. Not surprisingly, survivors had a longer hospital stay as compared to patients in the non-survivor group. Again, this finding is consistent with previously published data.[25] The ROC analysis revealed a good correlation of qSOFA with sepsis death in the current study. Brink et al.[26] recently published a qSOFA AUC with similar results; therefore, we are confident that our data is reliable.

In the current study, the qSOFA was modified by integrating easy to determine preclinical parameters like age, GCS, SBP, and anamnesis of immunodeficiency. ROC analysis revealed an even better correlation of these preclinical parameters with in-hospital death as compared to the original qSOFA. Therefore, a relatively exact prediction model for the current cohort was established. With this score model, a preclinical tool could be developed that allows for increased awareness of a septic condition and might enable prompt medical treatment, critical for sepsis treatment. We plan to establish a web-based calculator, which might help to further evaluate this score and could be a helpful tool for out-of-hospital sepsis recognition. Further evaluation may have a clinical impact on in-hospital mortality. The EMS in Northeim had already introduced a sepsis bundle in 2018 after obtaining our results. Further scientific evaluation of the future developments may be interesting.

Limitations

Our study is limited by the retrospective single-center design. Therefore, our data are not able to prove that the recognition of sepsis by paramedics will always improve sepsis outcome. Multicenter randomized trials are needed to provide further evidence. We did not calculate the required sample size, since this was a proof of concept study. Thus, the current study may be underpowered.

We identified our cohort retrospectively by selecting cases that were documented with ICD-10 codes A41 and R65 as the main diagnoses. These diagnoses are based on systemic inflammatory response syndrome (SIRS) criteria. One might criticize that this is a selection bias, since qSOFA-positive patients who did not fit SIRS criteria might have escaped our attention. Although we cannot exclude selection bias, recent work[27] showed that SIRS criteria are superior to the qSOFA in their ability to identify sepsis cases.

Conclusions

Preclinical recognition of sepsis by paramedics may result in an improved clinical outcome. Our data may help improve preclinical sepsis recognition by paramedics. Although further investigation is needed, our modified scoring system could be a promising tool.

Supplementary files

We have examined all the metric variables for normal distributions by using Q–Q plots. Normal distributions were seen for age, preclinical SBP, emergency department SBP, preclinical temperature, and emergency department

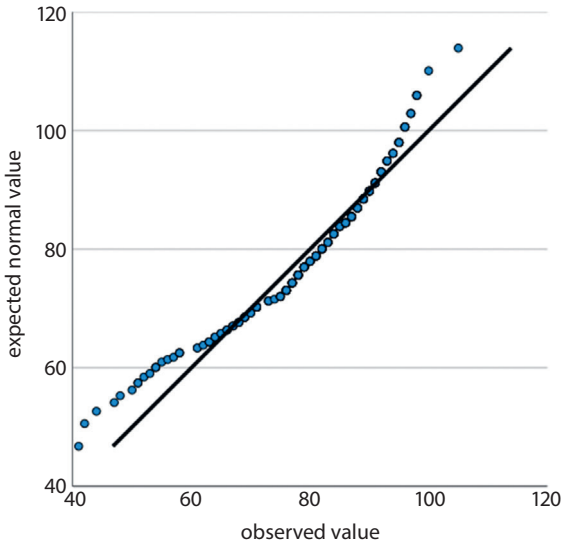

Supplementary Fig. 1. Normal Q-Q plot of age

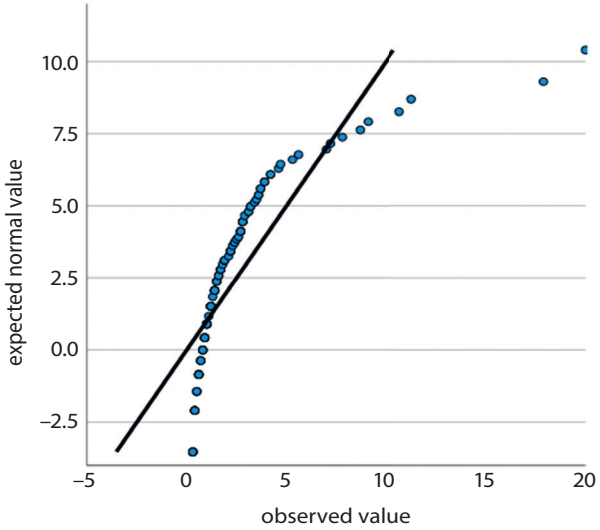

Supplementary Fig. 2. Normal Q-Q plot of 1. lactate [mmol/L]

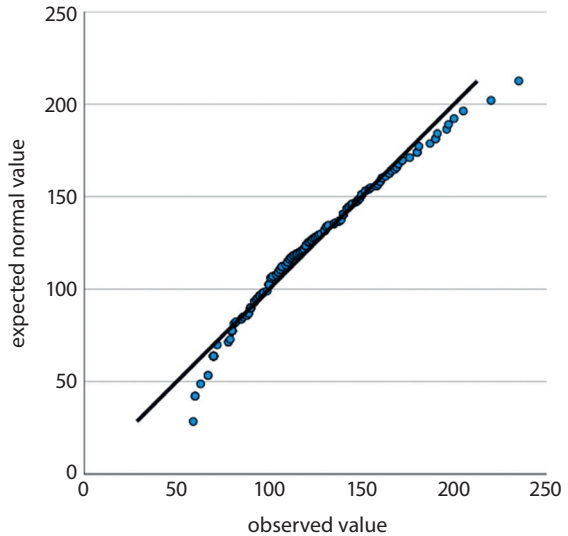

Supplementary Fig. 3. Normal Q-Q plot of preclinical systolic blood pressure (SBP)

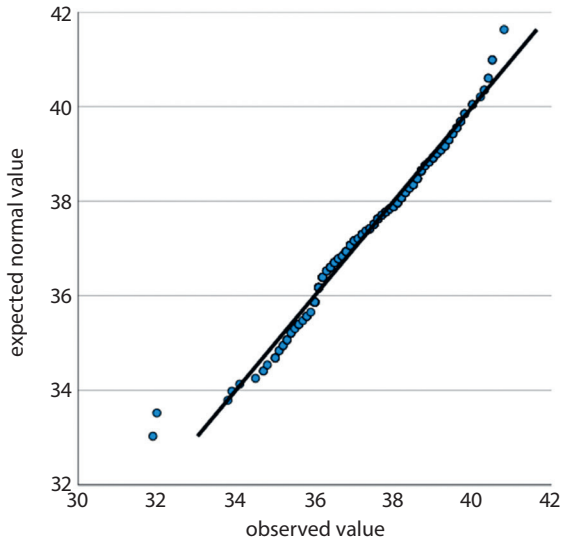

Supplementary Fig. 4. Normal Q-Q plot of preclinical temperature

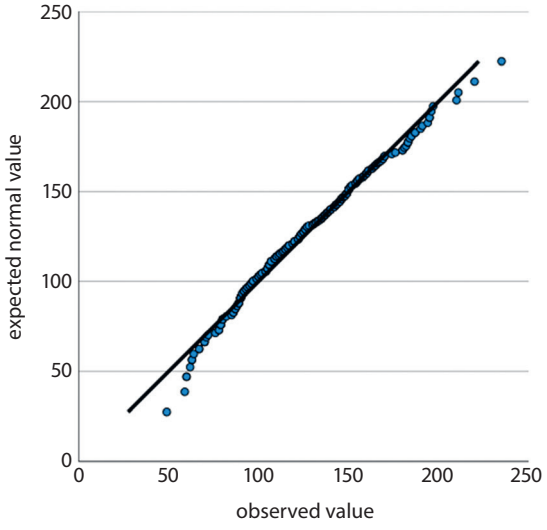

Supplementary Fig. 5. Normal Q-Q plot of systolic blood pressure (SBP) at the emergency department

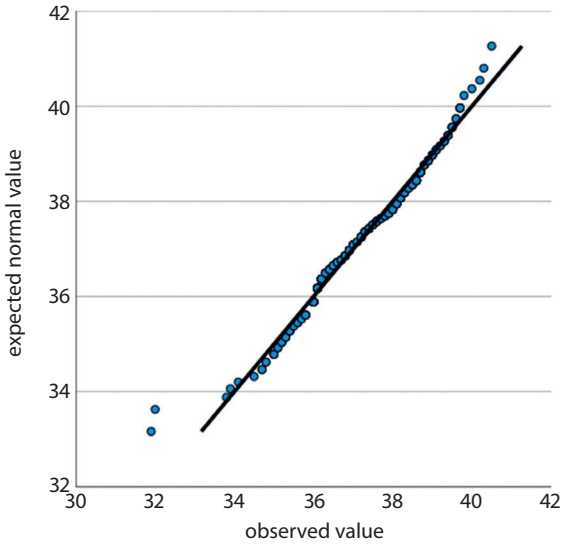

Supplementary Fig. 6. Normal Q-Q plot of temperature at the emergency department

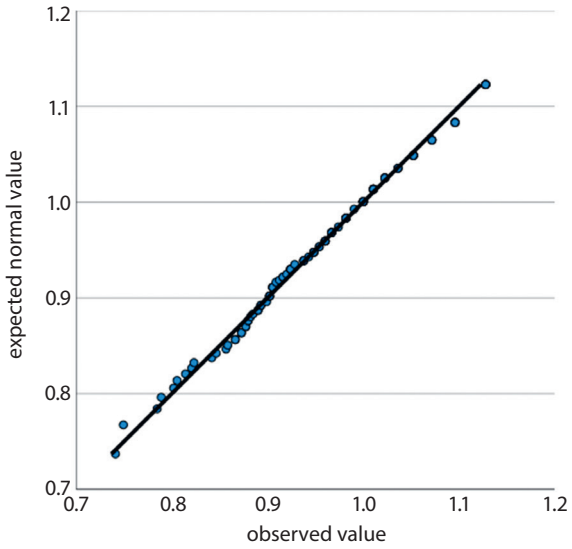

Supplementary Fig. 7. Normal Q-Q plot of 1. Lactate transformed

temperature. Non-normality was seen for lactic acid (lactate). After Box–Cox transformation with lambda = 0.1, normal distribution was achieved and a two-tailed unpaired t-test showed a p = 0.0008. For emergency department vigilance, a non-normal distribution was seen. After Box–Cox transformation with lambda = 6.7934, a normal distribution was approximated but did not satisfy the Shapiro–Wilk test. Therefore a Mann–Whitney U test was used to test for significance. All results from regression analysis and Q–Q plots as well as and transformation results are provided as supplementary file.

ORCID iDs

Martin Floer https://orcid.org/0000-0002-8572-9372
Mario Ziegler https://orcid.org/0000-0002-6878-7079
Bodo Lenkewitz https://orcid.org/0000-0003-4487-2022
Agneta Auer https://orcid.org/0000-0002-3672-8437
Tobias Meister https://orcid.org/0000-0002-7664-8108

References

1. Brunkhorst FM. Epidemiologie, Okonomie und Praxis – Ergebnisse der deutschen Prävalenzstudie des Kompetenznetzwerkes Sepsis (SepNet). *Anasthesiol Intensivmed Notfallmed Schmerzther.* 2006;41(1):43–44. doi:10.1055/s-2005-921227
2. Zaccone V, Tosoni A, Passaro G, et al. Sepsis in internal medicine wards: Current knowledge, uncertainties and new approaches for management optimization. *Ann Med*. 2017;49(7):582–592. doi:10.1080/07853890.2017.1332776
3. Singer M, Deutschman CS, Seymour CW, et al. The Third International Consensus Definitions for Sepsis and Septic Shock (Sepsis-3). *JAMA*. 2016;315(8):801–810. doi:10.1001/jama.2016.0287
4. Rhodes A, Evans LE, Alhazzani W, et al. Surviving Sepsis Campaign: International Guidelines for Management of Sepsis and Septic Shock: 2016. *Intensive Care Med*. 2017;43(3):304–377. doi:10.1007/s00134-017-4683-6
5. Christie A, Costa-Scorse B, Nicholls M, Jones P, Howie G. Accuracy of working diagnosis by paramedics for patients presenting with dyspnoea. *Emerg Med Australas*. 2016;28(5):525–530. doi:10.1111/1742-6723.12618
6. Wang HE, Weaver MD, Shapiro NI, Yealy DM. Opportunities for emergency medical services care of sepsis. *Resuscitation*. 2010;81(2):193–197. doi:10.1016/j.resuscitation.2009.11.008
7. Peake SL, Delaney A, Bailey M, Bellomo R; ARISE Investigators. Potential impact of the 2016 Consensus Definitions of Sepsis and Septic Shock on Future Sepsis Research. *Ann Emerg Med*. 2017;70(4):553–561.e1. doi:10.1016/j.annemergmed.2017.04.007
8. Askim Å, Moser F, Gustad LT, et al. Poor performance of quick-SOFA (qSOFA) score in predicting severe sepsis and mortality: A prospective study of patients admitted with infection to the emergency department. *Scand J Trauma Resusc Emerg Med*. 2017;25(1):56. doi:10.1186/s13049-017-0399-4
9. Cochon L, Ovalle A, Nicolás JM, Baez AA. Acute Care Diagnostic Collaboration: Bayesian modeling comparative diagnostic assessment of lactate, procalcitonin and CRP in risk stratified population by Mortality in ED (MEDS) score. *Am J Emerg Med*. 2017;35(4):564–568. doi:10.1016/j.ajem.2016.12.012
10. Shapiro NI, Wolfe RE, Moore RB, Smith E, Burdick E, Bates DW. Mortality in Emergency Department Sepsis (MEDS) score: A prospectively derived and validated clinical prediction rule. *Crit Care Med*. 2003;31(3):670–675. doi:10.1097/01.CCM.0000054867.01688.D1
11. Innocenti F, Tozzi C, Donnini C, et al. SOFA score in septic patients: Incremental prognostic value over age, comorbidities, and parameters of sepsis severity. *Intern Emerg Med*. 2018;13(3):405–412. doi:10.1007/s11739-017-1629-5
12. Fischer M, Kehrberger E, Marung H, et al. Eckpunktepapier 2016 zur notfallmedizinischen Versorgung der Bevölkerung in der Prähospitalphase und in der Klinik. *Notfall Rettungsmed.* 2016;19:387–395. https://doi.org/10.1007/s10049-016-0187-0
13. Meister T, Uphoff MA, Heinecke A, et al. Novel score for prediction of malignant bile duct obstruction based on biochemical and clinical markers. *Aliment Pharmacol Ther*. 2015;41(9):877–887. doi:10.1111/apt.13152
14. Barbara P, Graziano C, Caputo W, Litvak I, Battinelli D, Hahn B. The quick sequential organ failure assessment (qSOFA) identifies septic patients in the out-of-hospital setting. *Am J Emerg Med*. 2018;36(6):1022–1026. doi:10.1016/j.ajem.2018.01.073
15. Band RA, Gaieski DF, Hylton JH, Shofer FS, Goyal M, Meisel ZF. Arriving by emergency medical services improves time to treatment endpoints for patients with severe sepsis or septic shock. *Acad Emerg Med*. 2011;18(9):934–940. doi:10.1111/j.1553-2712.2011.01145.x
16. Nemec M, Koller MT, Nickel CH, et al. Patients presenting to the emergency department with non-specific complaints: The Basel Non-specific Complaints (BANC) study. *Acad Emerg Med*. 2010;17(3):284–292. doi:10.1111/j.1553-2712.2009.00658.x
17. Rutschmann OT, Chevalley T, Zumwald C, Luthy C, Vermeulen B, Sarasin FP. Pitfalls in the emergency department triage of frail elderly patients without specific complaints. *Swiss Med Wkly*. 2005;135(9–10):145–150. PMID:15832233
18. Stevenson EK, Rubenstein AR, Radin GT, Wiener RS, Walkey AJ. Two decades of mortality trends among patients with severe sepsis: A comparative meta-analysis. *Crit Care Med*. 2014;42(3):625–631. doi:10.1097/CCM.0000000000000026
19. Raith EP, Udy AA, Bailey M, et al. Prognostic accuracy of the SOFA Score, SIRS Criteria, and qSOFA score for in-hospital mortality among adults with suspected infection admitted to the intensive care unit. *JAMA*. 2017;317(3):290–300. doi:10.1001/jama.2016.20328
20. Song JU, Sin CK, Park HK, Shim SR, Lee J. Performance of the quick Sequential (sepsis-related) Organ Failure Assessment score as a prognostic tool in infected patients outside the intensive care unit: A systematic review and meta-analysis. *Crit Care*. 2018;22(1):28. doi:10.1186/s13054-018-1952-x
21. Ludwig J, McWhinnie H. Antipyretic drugs in patients with fever and infection: Literature review. *Br J Nurs*. 2019;28(10):610–618. doi:10.12968/bjon.2019.28.10.610
22. Kushimoto S, Gando S, Saitoh D, et al. The impact of body temperature abnormalities on the disease severity and outcome in patients with severe sepsis: An analysis from a multicenter, prospective survey of severe sepsis. *Crit Care*. 2013;17(6):R271. doi:10.1186/cc13106
23. Hwang SY, Jo IJ, Lee SU, et al. Low accuracy of positive qSOFA criteria for predicting 28-day mortality in critically ill septic patients during the early period after emergency department presentation. *Ann Emerg Med*. 2018;71(1):1–9.e2. doi:10.1016/j.annemergmed.2017.05.022

24. Baysan M, Baroni GD, van Boekel AM, Steyerberg EW, Arbous MS, van der Bom JG. The added value of lactate and lactate clearance in prediction of in-hospital mortality in critically ill patients with sepsis. *Crit Care Explor*. 2020;2(3):e0087. doi:10.1097/CCE.0000000000000087
25. Goulden R, Hoyle MC, Monis J, et al. qSOFA, SIRS and NEWS for predicting inhospital mortality and ICU admission in emergency admissions treated as sepsis. *Emerg Med J*. 2018;35(6):345–349. doi:10.1136/emermed-2017-207120
26. Brink A, Alsma J, Verdonschot RJCG, et al. Predicting mortality in patients with suspected sepsis at the emergency department; A retrospective cohort study comparing qSOFA, SIRS and National Early Warning Score. *PLoS One*. 2019;14(1):e0211133. doi:10.1371/journal.pone.0211133
27. Serafim R, Gomes JA, Salluh J, Póvoa P. A comparison of the quick-SOFA and Systemic Inflammatory Response Syndrome Criteria for the diagnosis of sepsis and prediction of mortality: A systematic review and meta-analysis. *Chest*. 2018;153(3):646–655. doi:10.1016/j.chest.2017.12.015

Table S1. Statistical analysis for normal distribution

Table S1A. Model description

Model name		MOD_1
Series or sequence	1	age
	2	lactic acid
	3	preclinical SBP
	4	preclinical temperature
	5	SBP at the emergency department
	6	temperature at the emergency department
	7	lactate-transformed
Transformation		none
Non-seasonal differencing		0
Seasonal differencing		0
Length of seasonal period		no periodicity
Standardization		not applied
Distribution	type	normal
	location	estimated
	scale	estimated
Fractional rank estimation method		Blom's
Rank assigned to ties		mean rank of tied values

Legend:
df – degrees of freedom; Exp(B) – exponent (B); SBP – systolic blood pressure; SE – standard error; Sig. – significance; Wald – Wald test; GCS pre – preclinical Glasgow Coma Scale

Table S1B. Case processing summary (part 1)

Case processing summary (1)		Age	Lactic acid	Preclinical SBP	Preclinical temperature
Series or sequence length		263	263	263	263
Number of missing values in the plot	user-missing	0	0	0	0
	system-missing	0	153	6	9

Table S1C. Case processing summary (part 2)

Case processing summary (2)		SBP at the emergency department	Temperature at the emergency department	Lactate-transformed
Series or sequence length		263	263	263
Number of missing values in the plot	user-missing	0	0	0
	system-missing	8	10	153

Table S1D. Estimated distribution parameters (part 1)

Estimated distribution (1)		Age	Lactic acid	Preclinical SBP	Preclinical temperature
Normal distribution	location	80.342205	2.582727	120.521401	37.329921
	scale	11.8883485	3.0865752	32.6686808	1.5284038

Table S1E. Estimated distribution parameters (part 2)

Estimated distribution (2)		SBP at the emergency department	Temperature at the emergency department	Lactate-transformed
Normal distribution	location	124.909804	37.214625	0.953582
	scale	34.6133267	1.4401222	0.0855219

Table S2. Logistic regression analysis

Table S2A. Case processing summary

Unweighted cases[a]		Number of cases	Percentage
Selected cases	included in analysis	252	95.8
	missing cases	11	4.2
	total	263	100
Unselected cases		0	0
Total		263	100

Legend:
df – degrees of freedom; Exp(B) – exponent (B); SBP – systolic blood pressure; SE – standard error; Sig. – significance; Wald – Wald test; GCS pre – preclinical Glasgow Coma Scale

Table S2B. Classification table

Classification	Observed		Predicted		
			died: yes (1), no (0)		percentage correct
			0	1	
Step 0	died: yes (1), no (0)	0	195	0	100
		1	57	0	0
	overall percentage				77.4

Table S2C. Variables in the equation

Variables included		B	SE	Wald	df	Sig.	Exp(B)
Step 0	constant	–1.230	0.151	66.724	1	0	0.292

Table S2D. Variables excluded from equation

Variables excluded			Score	df	Sig.
Step 0	variables	age	4.510	1	0.034
		immunodeficiency: yes (1), no (0)	2.647	1	0.104
		preclinical SBP	15.542	1	0.000
		GCS pre	5.013	1	0.025
	overall statistics		23.429	4	0.000

Table S2E. Model coefficients test

Model coefficients		χ^2	df	Sig.
Step 1	step	25.104	4	0.000
	block	25.104	4	0.000
	model	25.104	4	0.000

Table S2F. Statistical model summary

Model summary	–2 Log likelihood	Cox & Snell R square	Nagelkerke R square
Step 1	244.351[a]	0.095	0.144

Table S2G. Classification table

Classification	Observed		Predicted		
			died in the hospital: yes (1), no (0)		percentage correct
			0	1	
Step 1	died: yes (1), no (0)	0	192	3	98.5
		1	50	7	12.3
	overall percentage				79.0

Table S2H. Variables in the equation (calculation for significance)

Variables for equation		B	SE	Wald	df	Sig.
Step 1[a]	age	0.024	0.015	2.566	1	0.109
	immunodeficiency: yes (1), no (0)	–0.558	0.465	1.439	1	0.230
	preclinical SBP	–0.021	0.006	12.949	1	0
	GCS pre	–0.088	0.070	1.585	1	0.208
	constant	0.430	1.699	0.064	1	0.800

Table S2I. Exponent (B) summary

Exponent (B) summary		Exp(B)
Step 1[a]	age	1.024
	immunodeficiency: yes (1), no (0)	0.572
	preclinical SBP	0.980
	GCS pre	0.916
	constant	1.538

Effects of position on non-stress test results and maternal satisfaction

Salime Mucuk[A–F], Tülay Bülbül[B,E,F]

Department of Nursing, Division of Obstetrics and Gynecology Nursing, Faculty of Health Sciences, Erciyes University, Kayseri, Turkey

A – research concept and design; B – collection and/or assembly of data; C – data analysis and interpretation;
D – writing the article; E – critical revision of the article; F – final approval of the article

Advances in Clinical and Experimental Medicine, ISSN 1899–5276 (print), ISSN 2451–2680 (online) *Adv Clin Exp Med*. 2021;30(11):1127–1132

Address for correspondence
Salime Mucuk
E-mail: mucukslm@gmail.com

Funding sources
None declared

Conflict of interest
None declared

Received on April 10, 2021
Reviewed on April 26, 2021
Accepted on July 13, 2021

Published online on September 9, 2021

Abstract

Background. The non-stress test (NST) is a simple non-invasive procedure commonly used in obstetrics clinics to assess fetal health. It is important that mothers feel comfortable during the NST and that the test results are obtained quickly.

Objectives. To determine the effects of maternal position on NST results and participants' satisfaction during the procedure.

Materials and methods. This was a randomized controlled experimental study conducted at the Department of Obstetrics and Gynecology Polyclinic of Erciyes University Hospital (Kayseri, Turkey) between October 2017 and March 2018. During the NST, either the supine, semi-Fowler or left lateral position was utilized. Questionnaire forms and NST tracings were collected from 275 participating mothers and analyzed. The χ^2 test was used to determine whether the distribution of categorical variables differed between groups. The Kruskal–Wallis test was used to determine whether median scores differed between groups. A p-value <0.05 was considered statistically significant.

Results. Most participants in the left lateral (78.9%) and semi-Fowler positions (88.4%) reported feeling satisfied compared to only 24.2% of participants in the supine position ($p < 0.001$). Participants also felt more comfortable in the left lateral (92.2%) and semi-Fowler positions (87.2%). In the supine position, most participants (68.7%) reported experiencing back pain ($p < 0.001$). There were no significant differences among groups in terms of basal heart rate ($p = 0.497$), reactivity time ($p = 0.421$) or percentage of reactivity ($p = 0.676$). The number of accelerations was 5.0 in the left lateral position, 4.5 in the semi-Fowler position and 4.0 in the supine position ($p = 0.051$).

Conclusions. Our findings support the use of the semi-Fowler and left lateral positions during the NST. Participants reported high satisfaction in these positions and felt more comfortable, and no procedure-related problems occurred.

Key words: non-stress test, maternal position, maternal satisfaction

Cite as
Mucuk S, Bülbül T. Effects of position on non-stress test results and maternal satisfaction. *Adv Clin Exp Med*. 2021;30(11):1127–1132. doi:10.17219/acem/ 140196

DOI
10.17219/acem/140196

Background

The non-stress test (NST) is used to interpret changes in fetal heart rate (FHR) in relation to fetal body movements during the antenatal period. It is a commonly used method to assess antenatal fetal health, provide a timely diagnosis and prevent complications that may occur due to intrauterine asphyxia.[1–4]

Maternal position during the NST is an important factor for reducing procedure-related problems. At our clinic, nurses typically put mothers in a supine position because it allows for easy administration of the NST. However, in this position, venous return and cardiac output may decrease, particularly due to the pressure caused by the enlarged uterus upon the inferior vena cava, and supine hypotensive syndrome may occur. Furthermore, decreased uteroplacental circulation and fetal oxygenation may negatively affect NST results. Thus, the lateral recumbent, semi-Fowler or sitting positions may be more acceptable positions for the NST to avoid inducing supine hypotension or maternal discomfort, such as a backache.[1,5–13] In addition, it is important that mothers feel comfortable with the position they take during the NST because it lasts on average 20–40 min. During the procedure, most mothers complain of a backache caused by the supine position and boredom from being in the same position. Since the position during the NST should be comfortable and satisfactory for the mothers, identifying the effect of different positions on test results and maternal satisfaction will aid in improving the NST procedure.

Objectives

In the literature, there are limited studies on the effect of maternal position on NST results and mothers' satisfaction. Thus, the current study aimed to address these research gaps.

Materials and methods

Study population

This was a randomized controlled experimental study conducted in the Department of Obstetrics and Gynecology, Polyclinic at Erciyes University Hospital (Kayseri, Turkey) between October 2017 and March 2018. Pregnant women who attended the polyclinic for prenatal exams were included in this study.

The required sample size was calculated using the NCSS-PASS software (NCSS LLC, East Kaysville, USA). Based on the study by Nathan et al., the number of women needed for each group was determined ($\alpha = 0.05$, power = 0.80) to be at least 50.[14] However, 100 participants were assigned to each group due to the possibility that mothers might want to change position during the procedure, withdraw from the study or for some other reason. The study inclusion criteria were as follows: patients at 32 to 42 gestational weeks, who did eat at least 2 h before the test, and did not use alcohol or cigarettes before the test, not taking any barbiturate derivative medicine, able to communicate verbally, and consented to participate in the study. Participants with complications of pregnancy such as hypertension, diabetes, intrauterine growth restriction, or fetal anomalies were excluded. Participants who met the inclusion criteria were assigned to 1 of the 3 maternal positions during the antepartum NST according to a computerized randomization list.

Measurements

Data were collected from questionnaires and NST tracings. The questionnaire included socio-demographic information, obstetric characteristics, vital signs, and satisfaction with the allocated position. The satisfaction questions concerned feeling any discomfort during the NST procedure, satisfaction with the position and position preference. Heart rate, systolic and diastolic blood pressure (SBP and DBP), and respiration rate were recorded as well.

An external electronic fetal monitor (Hewlett Packard Series 50A; Hewlett-Packard GmbH, Böblingen, Germany) was used to measure FHR and uterine activity in each study participant. The bedside monitor unit received information about the FHR and uterine activity from sensors or transducers, processed the information, and provided output in the form of a numeric display and a printed strip.

Procedure

Pregnant women who attended the polyclinic for prenatal exams were included in this study. Participants were informed about the aim of the study and those who met the inclusion criteria were randomly assigned to 1 of the 3 maternal positions (supine, semi-Fowler or left lateral) during the antepartum NST. The NST for each participant took the average of 20 min. All tests were carried out between 9:00 AM and 12.00 PM. The mother's vital signs were measured after resting for 5–10 min. Reactivity time and rate, basal speed, and the number of accelerations and decelerations were recorded from the NST strips after testing concluded.

Statistical analyses

Statistical analyses were performed using IBM SPSS Statistics v. 26 (IBM Corp., Armonk, USA). Descriptive statistics were given as the number (n), percent (%), median (M), 1st quartile (Q1), and 3rd quartile (Q3). The distribution of numerical data was evaluated using the Shapiro–Wilk normality test. Comparisons of numerical variables between groups were performed using the Kruskal–Wallis test. The Fisher's exact test was used to compare categorical variables.[15] If there was a significant difference in the χ^2 test,

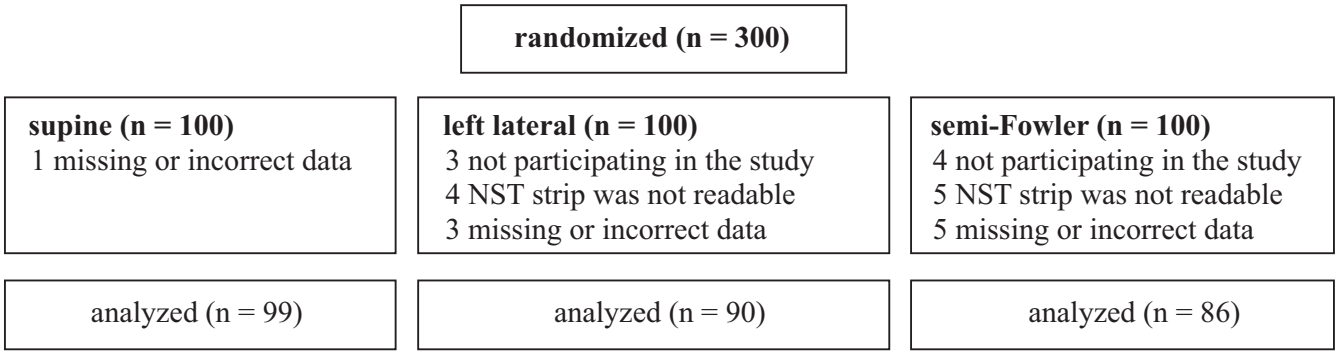

Fig. 1. Study flowchart

the differences between the groups in the categories were determined using the Bonferroni-corrected 2 proportion Z-test. A p-value <0.05 was considered statistically significant.

A complete study flowchart is presented as Fig. 1.

Ethical approval

This study was approved by the Ethics Committee of Erciyes University (approval No. 2013/427). All patients were informed about the purpose of the study and provided written and oral consent. The Declaration of Helsinki was complied with at all stages of the study.

Results

As shown in Table 1, the experimental groups were similar to each other in terms of mean age (p = 0.738), height (p = 0.095), weight (p = 0.425), number of pregnancies (p = 0.767), gestational age (p = 0.844), heart rate (p = 0.127), SBP (p = 0.310), DBP (p = 0.416), respiration rate (p = 0.623), and education level (p = 0.545). There was no statistically significant difference among the groups in terms of basal heart rate (p = 0.497). The number of accelerations was 5.0 in the left lateral position, 4.5 in the semi-Fowler position and 4.0 in the supine position (p = 0.051). No significant differences were found in terms of reactivity time (p = 0.421), reactivity rate (p = 0.676) or percentage of deceleration (p = 0.748) among the 3 groups (Table 2).

Most participants in the left lateral (78.9%) and semi-Fowler positions (88.4%) reported being satisfied. Only 24.2% of participants were satisfied in the supine position and 53.5% reported dissatisfaction with this position (p < 0.001), with 71.7% reporting discomfort. In contrast, discomfort was reported by only 7.8% of participants in the left lateral position and 12.8% in the semi-Fowler position (p < 0.001). In the supine position, most participants (68.7%) reported back pain (p < 0.001). Most participants

Table 1. Comparison of participant characteristics by position

Participant characteristics	Supine n = 99	Left lateral n = 90	Semi-Fowler n = 86	Test statistics	
				H/χ^2	p-value
Continuous variables, M (Q_1–Q_3)					
Age [years]	27.0 (24.0–33.0)	28.5 (24.8–33.0)	28.0 (23.0–33.0)	0.606	0.738
Height [cm]	160.0 (158.0–165.0)	160.0 (156.8–165.0)	162.5 (158.0–167.0)	4.716	0.095
Weight [kg]	78.0 (70.0–87.0)	76.5 (69.8–86.0)	74.0 (68.0–85.0)	1.711	0.425
Pregnancies [number]	3.0 (2.0–4.0)	3.0 (1.0–3.0)	3.0 (2.0–4.0)	0.530	0.767
Gestational age [weeks]	38.0 (37.0–39.0)	38.0 (37.0–39.0)	38.0 (37–39)	0.339	0.844
Heart rate [beats/min]	92.0 (80.0–100.0)	87.0 (80.0–94.5)	88.0 (80.0–96.5)	4.126	0.127
SBP [mm Hg]	120.0 (110.0–120.0)	117.5 (100.0–120.0)	120.0 (110.0–120.0)	2.343	0.310
DBP [mm Hg]	70.0 (70.0–80.0)	70.0 (60.0–80.0)	70.0 (60.0–80.0)	1.754	0.416
Respiration rate [rate/min]	22.0 (20.0–24.0)	22.0 (20.0–24.0)	22.0 (20.0–24.0)	0.948	0.623
Categorical variables, n (%)					
Education					
primary school	39 (39.4)	39 (43.3)	34 (39.5)		
secondary school	27 (27.3)	18 (20.0)	28 (32.6)	6.998	0.545
high school	22 (22.2)	21 (23.3)	15 (17.4)		
university	11 (11.1)	12 (13.3)	9 (10.5)		

n – number of participants; % – column percentages; M – median; Q_1 – 1st quartile; Q_3 – 3rd quartile; SBP – systolic blood pressure; DBP – diastolic blood pressure; H – Kruskal–Wallis test; χ^2 – χ^2 test.

Table 2. Comparison of non-stress test features in each group

Non-stress test features	Supine n = 99	Left lateral n = 90	Semi-Fowler n = 86	Test statistics	
				H/χ^2	p-value
Continuous variables, M (Q_1–Q_3)					
Reactivity time [min]	8.0 (5.0–12.0)	7.0 (5.0–10.0)	7.0 (5.0–10.0)	1.730	0.421
Basal heart rate [beats]	139.0 (130.0–140.0)	135.0 (130.0–140.0)	135.0 (130.0–140.0)	1.398	0.497
Acceleration [number]	4.0 (2.0–6.0)	5.0 (4.0–8.0)	4.5 (3.0–7.0)	5.941	0.051
Categorical variables, n (%)					
Reactivity reactive nonreactive	 85 (85.8) 14 (14.2)	 81 (90.0) 9 (10.0)	 76 (88.4) 10 (11.6)	0.782	0.676
Deceleration none 1 2 3	 92 (92.9) 5 (5.1) 1 (1.0) 1 (1.0)	 84 (93.3) 5 (5.6) 0 (0.0) 1 (1.1)	 84 (97.7) 2 (2.3) 0 (0.0) 0 (0.0)	4.044	0.748

n – number of participants; % – column percentages; M – median; Q_1 – 1st quartile; Q_3 – 3rd quartile; H – Kruskal–Wallis test; χ^2 – χ^2 test.

Table 3. Distribution of satisfaction with position in each group

Characteristics n (%)	Supine n = 99	Left lateral n = 90	Semi-Fowler n = 86	Test statistics		Pairwise comparisons*		
				χ^2	p-value	supine & left lateral	supine & semi-Fowler	left lateral & semi-Fowler
Satisfaction								
satisfied	24 (24.2)^a	71 (78.9)^b	76 (88.4)^b	113.436	<0.001	<0.001	<0.001	0.106
not satisfied	53 (53.5)^a	3 (3.3)^b	5 (5.8)^b			<0.001	<0.001	0.489
partially satisfied	22 (22.2)^a	16 (17.8)^a	5 (5.8)^b			0.473	0.002	0.019
Discomfort during the process								
yes	71 (71.7)^a	7 (7.8)^b	11 (12.8)^b	109.947	<0.001	<0.001	<0.001	0.325
no	28 (28.3)^a	83 (92.2)^b	75 (87.2)^b			<0.001	<0.001	0.325
Disturbance type								
none	28 (28.3)^a	83 (92.2)^b	76 (88.4)^b	112.948	<0.001	<0.001	<0.001	0.450
back pain	68 (68.7)^a	7 (7.8)^b	10 (11.6)^b			<0.001	<0.001	0.450
respiratory distress	3 (3.0)^a	0 (0.0)^a	0 (0.0)^a			0.248	0.250	–
Preferred position								
right lateral recumbent	16 (16.2)^a	5 (5.6)^{ab}	2 (2.3)^b	110.524	<0.001	0.052	0.002	0.444
left lateral recumbent	20 (20.2)^a	33 (36.7)^b	2 (2.3)^c			0.015	<0.001	<0.001
supine	22 (22.2)^a	7 (7.8)^b	6 (7.0)^b			0.008	0.004	0.999
semi-Fowler	16 (16.2)^a	15 (16.7)^a	63 (73.3)^b			0.999	<0.001	<0.001
right/left lateral recumbent	25 (25.2)^{ab}	30 (33.3)^b	13 (15.1)^a			0.263	0.102	0.005

n – number of participants; % – column percentages; χ^2 – χ^2 test; *significance values for 2 proportion Z-test with Bonferroni correction; $^{a, b, c}$ the same superscript letters indicate no statistically significant difference between the position groups in each rows; & – compared to.

in the semi-Fowler position (73.3%) reported that they would prefer to be in the same position for the next NST (Table 3).

Discussion

This study was conducted to determine the effects of maternal position on NST results and mothers' satisfaction with the procedure. There were no statistically significant differences among our groups in terms of basal FHR or maternal heart rate. The reason for the similar results across groups may be that only healthy pregnancies were included to control for risky situations in this study. The number of accelerations was 5.0, 4.5, and 4.0 in the left lateral, semi-Fowler and supine position, respectively. Similar results were obtained by Cito et al., who found that maternal positions (reclining, sitting, walking) did not result in statistically significant differences in baseline FHR or the number of large accelerations.[1] In a study by Ibrahim et al., using the same positions (left lateral, semi-Fowler and supine) as our study, a higher baseline

FHR and increased number of accelerations were found in the left lateral position, followed by the semi-Fowler position, compared to the supine position.[16] The results obtained by Ibrahim et al. are very similar to ours.

Furthermore, there was no statistically significant difference between the groups in terms of reactivity time in our study, which is consistent with other studies in the literature. A study comparing 4 different positions (sitting-up, semi-Fowler, left lateral, and supine) determined that reactivity time was not significantly different among the groups.[7]

The reactivity rate did not differ significantly among the groups in the current study. In the literature, different results have been obtained in studies comparing different positions during the NST. In a study using the same positions as our study, similar results were obtained: the NST reactivity rate did not show statistically significant differences between the left lateral, semi-Fowler and supine positions.[16] A study comparing the sitting-up, semi-Fowler and semi-Fowler left lateral positions also reported no significant differences between groups in terms of reactive NST rate.[17] Similar results were obtained in a study in which the left lateral and sitting positions were examined, and the reactivity rate was not significantly different between the groups.[18] However, Nathan et al.[14] found that the non-reactive NST rate in the supine position was higher than in the sitting position. In a study comparing the effect of 4 different positions (supine, left lateral, semi-Fowler, and sitting-up), the lowest reactive NST rate was noted in the supine position.[7] Another study reported a positive correlation between maternal and fetal parameters in the left lateral position compared to other positions during the NST.[19]

Maternal satisfaction and comfort during different obstetrical procedures is a fundamental issue for perinatal nursing care. Importantly, maternal comfort, satisfaction and collaboration during the NST may affect the NST results. Thus, this study aimed to assess maternal perceptions of comfortable positions during the antenatal NST. Our results indicated that most of the women in the semi-Fowler position and the left lateral position were satisfied with these positions, while the satisfaction rate was significantly lower for women in the supine position. Furthermore, the rate of women who reported discomfort in the supine position was higher than those in other positions. Specifically, women in the supine position complained of backaches. The back pain may be experienced due to the pressure caused by the enlarged uterus over the lumbosacral region when in the supine position. When women were asked which position they would prefer to take during the NST procedure, most preferred the semi-Fowler position. Based on these findings, the semi-Fowler position and the left lateral position may be more suitable for the NST procedure.

The findings of this study are similar to those of other studies in that the majority of antenatal mothers were reportedly comfortable in the left lateral position. Kaur and Saha stated that around 67% of participants reported being comfortable in the left lateral position during the NST, whereas only 25% of participants supported the sitting position.[18] Essa and Hafez reported that the semi-Fowler and left lateral positions were associated with lower levels of discomfort than the supine position.[12] Another study reported that both maternal fatigue and back pain were reduced in the semi-Fowler position compared to the left lateral position.[20] El Sayed and Mohamady also noted that nearly $^{2}/_{3}$ of participants felt uncomfortable in the supine position compared to the semi-Fowler and left lateral positions.[21] A study investigating the comfort of mothers during antenatal NST procedures reported that the comfort level was higher in the semi-Fowler position than in the supine position.[22] Similar results were obtained in other studies.[8,9] The results of the current study and other studies in the literature seem congruent with physiological changes during pregnancy.

Limitations

The most important limitation of this study is the small sample size, as some variables such as the number of accelerations were very close to the statistical significance level, but did not reach the statistical significance.

Conclusions

Our findings support that the semi-Fowler and left lateral positions are more suitable for the NST. The satisfaction and comfort of mothers in these positions were high and no disturbances such as a backache occurred.

ORCID iDs

Salime Mucuk https://orcid.org/0000-0003-4787-7515
Tülay Bülbül https://orcid.org/0000-0001-5166-0074

References

1. Cito G, Luisi S, Mezzesimi A, Cavicchioli C, Calonaci G, Petraglia F. Maternal position during non-stress test and fetal heart rate patterns. *Acta Obstet Gynecol Scand.* 2005;84(4):335–338. doi:10.1111/j.0001-6349.2005.00644.x
2. Alp Dal N, Ertem G. Evaluation of fetal health. In: Sevil Ü, Ertem G, eds. *Perinatology and Care.* Ankara, Turkey: Nobel Medical Bookstores; 2016:383–386.
3. Umana OD, Siccardi MA. Prenatal non-stress test. StatPearls Publishing; 2020. http://www.ncbi.nlm.nih.gov/pubmed/30725808. Updated August 10, 2020. Accessed December 19, 2020.
4. Nazari S, Hatami E, Tabatabayeechehr M, Bagheri M, Ghorbani M. Diagnostic value of non-stress test interpreted by smart interpretive software. *J Midwifery Reprod Health*. 2018;6(3):1384–1389. doi:10.22038/jmrh.2018.21461.1228
5. Humphries A, Mirjalili SA, Tarr GP, Thompson JMD, Stone P. The effect of supine positioning on maternal hemodynamics during late pregnancy. *J Matern Fetal Neonatal Med.* 2019;32(23):3923–3930. doi:10.1080/14767058.2018.1478958
6. POGP. Goog Practice Statement: Supine lying during pregnancy. *J Pelvic Obstet Gynaecol Physiother.* 2018;122:77–83. https://pogp.csp.org.uk/sites/default/files/journal/2018-08/15_14301043.pdf/. Accessed December 20, 2020.

7. Aluş M, Okumuş H, Mete S, Güçlü S. The effects of different maternal positions on non-stress test: An experimental study. *J Clin Nurs*. 2007; 16(3):562–568. doi:10.1111/j.1365-2702.2006.01570.x
8. Abdallah EL Sayed H, Hassan Mohamady S. Effects of different maternal positions during non-stress test on maternofetal physiological parameters. *Tanta Sci Nurs J.* 2016;10(1):116–131. doi:10.21608/tsnj.2016.71197
9. Sekhavat L, Tabatabaei A. The effect of different maternal position on non-stress test (NST). *World Appl Sci J*. 2014;32(5):853–856. doi:10.5829/idosi.wasj.2014.32.05.83246
10. Samuel R, Karkada S, Fernandes S, Bhat P. Materno foetal physiological parameters in sitting and left lateral position during non-stress test (NST monitoring in pregnancy: A cross over study). *Manipal J Nurs Heal Sci*. 2015;1(2):83–86. http://eprints.manipal.edu/id/eprint/146821/. Accessed December 17, 2020.
11. Khatib N, Weiner Z, Beloosesky R, Vitner D, Thaler I. The effect of maternal supine position on umbilical and cerebral blood flow indices. *Eur J Obstet Gynecol Reprod Biol*. 2014;175(1):112–114. doi:10.1016/j.ejogrb.2013.12.043
12. Essa RM, Hafez SK. Effect of different positions of pregnant women on their comfort and fetal cardiotocographic patterns during Non Stress test. *Int J Res Heal Sci Nurs*. 2018;4(2):1–24. https://gnpublication.org/index.php/hsn/article/view/257/. Accessed December 18, 2020.
13. American College of Obstetricians and Gynecologists (ACOG). Practice bulletin No. 145: Antepartum fetal surveillance. *Obstet Gynecol*. 2014;124(1):182–192. doi:10.1097/01.AOG.0000451759.90082.7b
14. Nathan EB, Haberman S, Burgess T, Minkoff H. The relationship of maternal position to the results of brief nonstress tests: A randomized clinical trial. *Am J Obstet Gynecol*. 2000;182(5):1070–1072. doi:10.1067/mob.2000.105443
15. Mehta CR, Patel NR. A hybrid algorithm for Fisher's exact test in unordered rxc contingency tables. *Commun Stat Theory Methods*. 1986;15(2):387–403. doi:10.1080/03610928608829128
16. Ibrahim HA, Elgzar WT, Saied EAR. The effect of different positions during Non-stress test on maternal hemodynamic parameters, satisfaction, and fetal cardiotocographic patterns. *Afr J Reprod Health*. 2021;25(1):81–89. doi:10.29063/ajrh2021/v25i1.10
17. Kıratlı D, Yavan T, Karaşahin KE, Yenen MC. The effect of different maternal positions on reactivity of the nonstress test, maternal blood pressure and heart rate. *Journal of Dr Behcet Uz Childrens Hospital*. 2018;8(2):101–108. doi:10.5222/buchd.2018.101
18. Kaur VS, Saha PK. A comparative study to assess the effect of different maternal position on reactivity and time consumption for nonstress test. *Nurs Midwifery Res J*. 2015;11(4):145–152. doi:10.33698/NRF0193
19. Gorler A, Rani J, Kannan M. Correlation of maternal positions on maternal and fetal parameters during non-stress test among antenatal mothers at svmch& rc, Puducherry. *TNNMC J Obstet Gynaecol Nurs*. 2021;9(1):14–18. https://www.indianjournals.com/ijor.aspx?target=ijor:tnnmcjogn&volume=9&issue=1&article=003/. Accessed January 16, 2021.
20. Lekshmi S, Annie Annal M, Lavanya S. Effects of different maternal positions on maternal parameters and fetal heart rate among antenatal mothers during non-stress test. *Pondicherry J Nurs*. 2017;11(2): 13–16. https://pjn.sbvjournals.com/doi/PJN/pdf/10.5005/pjn-11-2-13. Accessed December 18, 2020.
21. EL Sayed HA, Mohamady SH. Effects of different maternal positions during non-stress test on maternofetal physiological parameters. *Tanta Sci Nurs J*. 2016;10(1):116–131. doi:10.21608/TSNJ.2016.71197
22. Siby R, Vinsi MS. Relation of semi-Fowler's position and supine position on comfort level of antenatal mothers during non-stress test. *Int J Health Sci Res*. 2019;9(7):115–120. https://www.ijhsr.org/IJHSR_Vol.9_Issue.7_July2019/18.pdf. Accessed December 19, 2020.

Effectiveness of TI-RADS and ATA classifications for predicting malignancy of thyroid nodules

Murat Şahin[1,A–F], Ayten Oguz[2,A,C,E,F], Dilek Tuzun[1,A,B,D–F], Gülsüm Akkus[3,A,B,E,F], Gul Inci Törün[4,A,B,E,F], Abdulkadir Yasir Bahar[5,A,C,F], Hatice Şahin[6,A,B,E,F], Kamile Gül[2,A,C,E,F]

[1] Department of Endocrinology and Metabolism, Kahramanmaraş Sütçü İmam University, Turkey
[2] Department of Endocrinology and Metabolism, Gaziantep Liv Hospital, Turkey
[3] Department of Internal Medicine, Etimesgut Şehit Sait Ertürk State Hospital, Ankara, Turkey
[4] Department of Internal Medicine, Afsin State Hospital, Kahramanmaraş, Turkey
[5] Department of Pathology, Faculty of Medicine, Kahramanmaraş Sütçü İmam University, Turkey
[6] Department of Pulmonology, Kahramanmraş Necip Fazıl State Hospital, Turkey

A – research concept and design; B – collection and/or assembly of data; C – data analysis and interpretation; D – writing the article; E – critical revision of the article; F – final approval of the article

Advances in Clinical and Experimental Medicine, ISSN 1899–5276 (print), ISSN 2451–2680 (online) *Adv Clin Exp Med*. 2021;30(11):1133–1139

Address for correspondence
Murat Şahin
E-mail: muratsahin@me.com

Funding sources
None declared

Conflict of interest
None declared

Received on May 4, 2021
Reviewed on June 27, 2021
Accepted on June 29, 2021

Published online on September 9, 2021

Abstract

Background. Thyroid cancer is one of the most common cancers and is especially common in young patients. Therefore, effective recognition and treatment of thyroid cancer are essential for patient survival.

Objectives. To compare the effectiveness of standard guidelines for predicting thyroid malignancy. To do so, thyroid nodules were classified according to the categories of the American Thyroid Association (ATA) and Thyroid Imaging Reporting and Data System (TI-RADS) guidelines, and compared with fine-needle aspiration biopsy (FNAB) results.

Materials and methods. The study included 1741 thyroid nodules with a final diagnosis in 1121 consecutive patients. The FNAB was recommended for all patients according to ATA guidelines and subsequently performed. The nodules were reclassified according to TI-RADS guidelines.

Results. Comparing nodules classified according to ATA and TI-RADS in terms of ultrasonography (US) features with the Bethesda cytological diagnosis classification System for Reporting Thyroid Cytopathology, 37.6% of the nodules classified in the high-risk category according to the ATA classification were found to be malignant cytology, 10.4% suspicious for malignancy, 4% non-diagnostic, 9.6% indeterminant cytology, and 38.4% benign. According to the TI-RADS risk category, 50% of those with high suspicion were malignant, 13.3% suspicious for malignancy cytology and 36.7% were benign. For the TI-RADS guidelines, the best cutoff value for differentiating benign and malignant nodules was found to be 4.5 (area under the curve (AUC) = 0.962, 95% CI = 0.943–0.981, $p < 0.001$). For the ATA guidelines, the best cutoff value for separating benign and malignant nodules was 4.5 (AUC = 0.917, 95% CI = 0.875–0.959, $p < 0.001$). The diagnostic performances of the TI-RADS and ATA score systems were evaluated using highly suspicious nodules. The sensitivity and specificity of highly suspicious nodules, according to both TI-RADS and ATA guidelines, were both high. Sensitivity and specificity of ATA classification were 80% and 96.3%, respectively. Sensitivity and specificity of TI-RADS classification were 76% and 97.5%, respectively, but positive predictive value was low (63.3% compared to 55.5%).

Conclusions. Both, the ATA and TI-RADS classifications can effectively predict malignancy risk of thyroid nodules and may thus decrease unnecessary FNAB.

Key words: thyroid nodule, ultrasonography, risk of malignancy, fine-needle aspiration

Cite as
Şahin M, Oguz A, Tuzun D, et al. Effectiveness of TI-RADS and ATA classifications for predicting malignancy of thyroid nodules. *Adv Clin Exp Med*. 2021;30(11):1133–1139. doi:10.17219/acem/139591

DOI
10.17219/acem/139591

Background

The frequency of thyroid nodules detection has increased in recent years, largely due to the widespread use of ultrasonography (US) in more places. While the prevalence of thyroid nodules is detected at a rate of 4% with palpation, its prevalence varies between 190 and 347 per 1000 cases when thyroid US is used; in autopsy series where nodules are most clearly evaluated, the prevalence is between 82 and 650 in 1000 autopsies.[1] Thyroid nodules warrant medical attention because of the possibility of cancer development. The incidence of thyroid cancer is increasing all over the world.[2] According to 2020 cancer statistics for the USA, thyroid cancer is most commonly reported in people aged 15–39. Among all cancers that develop between the age of 30 and 39, thyroid cancer is the most common type of cancer in men and the 2nd most common in women.[2]

Because thyroid cancer is one of the most common cancers and occurs in young patients, effective recognition and treatment are very important for the survival of patients. Some evidence-based guidelines have been developed for the evaluation of patients presenting with thyroid nodules. The American Thyroid Association (ATA) recommends thyroid US along with cervical lymph node examination in patients with suspected thyroid nodules.[3] Similarly, the National Comprehensive Cancer Network (NCCN) recommends evaluating the lateral neck compartment lymph nodes along with thyroid US in all patients with an incidentally detected neck mass.[4] When performing thyroid US, the clinical aim is to detect nodules with a high-risk of thyroid cancer. The presence of findings such as microcalcifications, irregular margins and marked hypoechogenicity indicates a higher risk of malignancy. Existing guidelines classify thyroid nodules into risk categories according to the abovementioned suspicious features and make recommendations for biopsy. In the ATA guidelines, fine-needle aspiration biopsy (FNAB) is recommended at 1 cm and above for high- or moderate-suspicion nodules, 1.5 cm and above for low-suspicion nodules and 2 cm and above for very-low-suspicion nodules.[3] In the Thyroid Imaging Reporting and Data System (TI-RADS) developed by the American College of Radiology (ACR), FNAB is recommended at 1 cm and above for nodules in the high-suspicion category, 1.5 cm and above in the moderate-suspicion category and 2.5 cm and above in the mild-suspicion category.[5]

Objectives

The efficacy of FNAB recommendations based on the ATA and TI-RADS guidelines in predicting malignancy of thyroid nodules has been reported in previous studies. Both ATA and TI-RADS guidelines classify nodules into risk groups. Although there are some similarities, the classifications also differ in some aspects. Currently, it is not clear whether these differences in the classifications may result in differences in predicting malignancy. In the present study, we aimed to classify biopsied thyroid nodules according to the risk categories of both guidelines and then evaluate whether there is a difference between the guidelines in predicting malignancy.

Materials and methods

The Ethics Committee of Kahramanmaraş Sütçü İmam University (KSU), Kahramanmaraş, Turkey, approved this retrospective, cross-sectional study (approval No. 22, decision date March 6, 2019).

Subjects

This study included a total of 1741 thyroid nodules (this number was determined using power analysis), with final diagnosis in 1121 consecutive patients (age: 51.54 ±13.53 years). Routine US-guided FNAB (USg-FNAB) was performed according to the 2015 ATA guidelines.[3]

US examination and image analysis

Ultrasound machines (General Electric Logic P5; General Electric, Schenectady, USA) equipped with a 12-MHz linear probe were used for analysis. Generally, USg-FNAB is recommended for all patients with hypoechoic solid nodules ≥1 cm in diameter, isoechoic solid nodules ≥1.5 cm, mixed cystic–solid nodules and spongiform nodules ≥2 cm, and high-risk history with nodules ≥5 mm according to the ATA guidelines. Microcalcification, taller-than-wide shape, irregular margins, and pronounced hypoechogenicity are considered suspicious characteristics. Biopsy was not performed because pure cystic nodules are considered benign.

The nodules were then reclassified in accordance with the ACR TI-RADS guidelines and evaluated in terms of echogenic foci, margin irregularity, taller-than-wide shape, and calcification and microcalcification. The risk category of the nodules was scored according to these features. Nodules were classified as benign (TR1, 0 points), very low suspicion (TR2, 2 points), low suspicion (TR3, 3 points), intermediate suspicion (TR4, 4–6 points), and high suspicion (TR5, ≥7 points).[5]

FNAB

The FNAB was performed by endocrinologists under US guidance using 23–27 gauge needles. The FNAB procedure was performed with the patient lying in the supine position, with the neck extended. During the procedure, a sample was taken from all sides of the nodule. Biopsy was taken from solid parts in mixed echogenic nodules.

Cytopathological analysis

Cytopathological interpretation of FNAB samples was performed using the Bethesda System for Reporting Thyroid Cytopathology.[6] Retrospective reclassification of all nodules according to TI-RADS system was blind regarding the FNAB results.[5]

Statistical analyses

Statistical analyses were performed using IBM SPSS v. 22.0 for Windows (IBM Corp., Armonk, USA). Continuous data are presented as mean ± standard deviation (SD). Categorical variables were evaluated using the McNemar's and Pearson's χ^2 test. Nominal data are given as number of cases and percentage. The independent two-sample t-test was used to compare 2 groups in terms of age and thyroid stimulating hormone (TSH) level. We measured the specificity, sensitivity, negative/positive predictive value (PPV), and accuracy of both guidelines in terms of the diagnosis of malignant thyroid nodules. The malignancy risk of the TI-RADS scores and groups and the ATA risk stratification grades were measured on the basis of the cytopathological findings. The diagnostic performance of the TI-RADS and ATA score systems were evaluated using receiver operating curve (ROC) analysis based on high-suspicion nodules. Differences were considered to be statistically significant when $p < 0.05$.

Results

Demographic and laboratory findings

The malignancy rate was 5.0% (n = 36) in women and 4.9% (n = 8) in men, and the difference was not statistically significant (p = 0.512). The mean age of patients with benign cytology results was 51.68 ±13.39 years and for malignant cases mean age was 50.84 ±16.15 years; the difference was not statistically significant (p = 0.517). Additionally, when patients with malignant and benign cytology results were compared in terms of TSH levels (1.88 ±0.44 compared to 65 ±0.52 mIU/L, respectively), no significant difference was found (p = 0.526).

Thyroid US and USg-FNAB cytological findings

The US findings for the thyroid nodules are shown in Table 1. Ultrasonography-guided FNAB and cytological

Table 1. Ultrasonography findings and cytologic results of thyroid nodules for which fine-needle aspiration biopsy (FNAB) was performed

Ultrasonography findings	Total n (%)	Cytological diagnosis		Cytological diagnosis			p-value
		non-diagnostic	benign	indeterminate	suspicious	malignant	
Total (nodule)	1741	148 (8.5)	1327 (76.2)	191 (11.0)	23 (1.3)	52 (3.0)	–
Total (patient)	1121	84 (7.5)	842 (75.2)	153 (13.6)	16 (1.4)	26 (2.3)	–
Sex							
female	913 (81.4)	63 (6.9)	689 (75.5)	113 (12.4)	12 (1.3)	36 (3.9)	0.006
male	208 (18.6)	20 (9.6)	154 (74.0)	23 (11.1)	3 (1.4)	8 (3.8)	
Size							
subcentimeter	69 (4.0)	7 (10.1)	38 (55.1)	13 (18.8)	3 (4.3)	8 (11.6)	0.000
supracentimeter	1672 (96.0)	141 (8.4)	1289 (77.1)	178 (10.6)	20 (1.2)	44 (2.6)	
Echogenicity							
anechoic	6 (0.4)	3 (50.0)	1 (16.7)	2 (33.3)	0 (0.0)	0 (0.0)	0.000
isoechoic/hyperechoic	1289 (74.0)	99 (7.7)	1027 (79.7)	125 (9.7)	11 (0.9)	27 (2.1)	
hypoechoic	444 (25.5)	46 (10.4)	299 (67.3)	64 (14.4)	12 (2.7)	23 (5.2)	
marked hypoechoic	2 (0.1)	0 (0.0)	0 (0.0)	0 (0.0)	0 (0.0)	2 (100.0)	
Calcification							
absent	1428 (82.1)	119 (8.3)	1107 (77.5)	155 (10.9)	16 (1.1)	31 (2.2)	0.000
macrocalcification	293 (16.8)	29 (9.9)	217 (74.1)	35 (11.9)	4 (1.4)	8 (2.7)	
peripheral calcification	4 (0.2)	0 (0.0)	3 (75.0)	0 (0.0)	0 (0.0)	1 (25.0)	
microcalcification	16 (0.9)	0 (0.0)	0 (0.0)	1 (6.3)	3 (18.8)	12 (75)	
Margins							
regular	1612 (92.6)	133 (8.3)	1297 (80.5)	156 (9.7)	8 (0.5)	18 (1.1)	0.000
irregular	129 (7.4)	15 (11.6)	30 (23.3)	35 (27.1)	15 (11.6)	34 (26.4)	
Composition							
spongiform	9 (0.5)	3 (33.3)	6 (66.7)	0 (0.0)	0 (0.0)	0 (0.0)	0.000
mixed	977 (56.1)	80 (8.2)	788 (80.7)	85 (8.7)	9 (0.9)	15 (1.5)	
solid	755 (43.4)	65 (8.6)	533 (70.6)	106 (14.0)	14 (1.9)	37 (4.9)	
Shape							
ovoid	1694 (97.3)	148 (8.7)	1320 (77.9)	174 (10.3)	17 (1.0)	35 (2.1)	0.000
spheric	47 (2.7)	0 (0)	7 (14.9)	17 (36.2)	6 (12.8)	17 (36.2)	

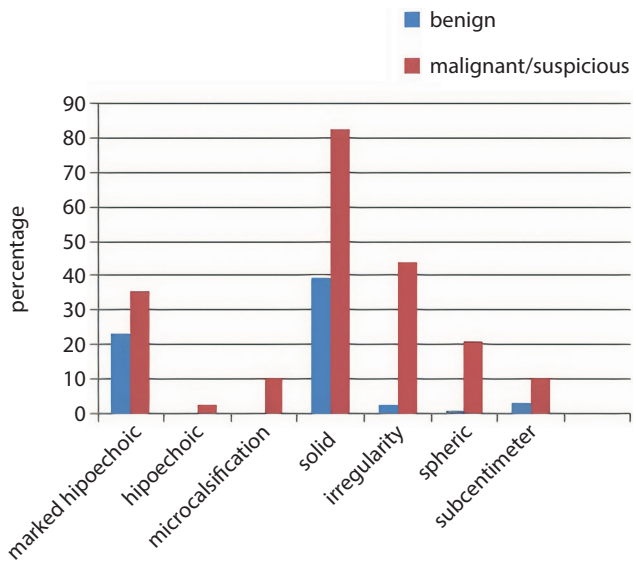

Fig. 1. Percentage distribution of ultrasonography features of nodules with malignant/suspicious or benign cytology

analysis were performed on 1741 nodules of 1121 cases. When non-diagnostic cytology findings were detected after the first USg-FNAB, repeat FNAB was performed. Accordingly, we determined that 1327 out of 1741 nodules were benign (76.2%), 148 were non-diagnostic (8.5%), 191 were indeterminate (in Bethesda classification, indeterminate cytology includes FLUS (follicular lesion of undetermined significance) and AUS (atypia of undetermined significance)) and/or follicular/Hurthle cell neoplasm (11.0%), 23 were suspicious (1.3%), and 52 (3.0%) were malignant cytological findings.

Figure 1 shows the percentage distribution of US features of nodules with malignant/suspicious and benign cytology findings. When malignant/suspicious and benign nodules were compared, hypoechogenicity (36% compared to 23.2%), marked hypoechogenicity (2.7% compared to 0.0%), microcalcification (10.7% compared to 0.0%), solid composition (82.7% compared to 39.8%), taller-than-wide shape (21.3% compared to 1.1%), and margin irregularity (44.0% compared to 3.0%) were significantly more common in malignant/suspicious nodules ($p < 0.001$). Separate tests were performed for each feature and all values were <0.0001. The p-values of each test were shown in Table 1.

Diagnostic performance of ATA and TI-RADS

When we compared the nodules classified according to ATA and TI-RADS in terms of ultrasonography (US) features with the Bethesda cytological diagnosis classification System for Reporting Thyroid Cytopathology, 37.6% of the nodules classified in the high-risk category according to the ATA classification were found to be malignant cytology, 10.4% suspicious for malignancy, 4% non-diagnostic, 9.6% indeterminant cytology, and 38.4% benign. According to the TI-RADS risk category, 50% of those with high suspicion were malignant, 13.3% were suspicious for malignancy cytology and 36.7% were benign. Of note, 12.9% and 0.5% (226 of 1741 and 10 of 1741) of the nodules did not fit any category in the ATA and TI-RADS guidelines, respectively. There was no malignancy in any of these nodules (Table 2).

As suggested by the ROC curve analysis (Fig. 2), for the TI-RADS classification, the best cutoff value in differentiating benign and malignant nodules was found to be 4.5. Accordingly, a nodule with TR5 is likely malignant, and a nodule with TR4 or below is likely benign. The most reliable diagnosis based on TI-RADS was obtained using

Table 2. Cytological diagnosis rate according to the American Thyroid Association (ATA) and Thyroid Imaging Reporting and Data System (TI-RADS) risk categories

Ultrasonography findings	Total n	Cytological diagnosis				
		non-diagnostic n (%)	benign n (%)	indeterminate n (%)	suspicious n (%)	malignant n (%)
ATA risk category						
Out of category	226	35 (15.4)	168 (74.3)	23 (10.2)	0 (0)	0 (0)
Benign	9	0 (0)	9 (90.0)	0 (0)	0 (0)	0 (0)
Very low suspicion	83	3 (3.6)	80 (96.4)	0 (0)	0 (0)	0 (0)
Low suspicion	1269	106 (8.4)	1001 (78.9)	153 (12.1)	9 (0.7)	0 (0)
Intermediate suspicion	29	0 (0.0)	21 (72.4)	3 (10.3)	0 (0)	5 (17.2)
High suspicion	125	5 (4.0)	48 (38.4)	12 (9.6)	13 (10.4)	47 (37.6)
TI-RADS category						
Out of category	10	4 (40.0)	5 (50.0)	1 (10.0)	0 (0)	0 (0)
Benign	216	49 (22.7)	167 (77.3)	0 (0)	0 (0)	0 (0)
Not suspicious	668	41 (6.1)	531 (79.5)	96 (14.4)	0 (0.0)	0 (0)
Slightly suspicious	672	54 (8.0)	520 (77.4)	91 (13.5)	5 (0.7)	2 (0.3)
Intermediately suspicious	85	0 (0)	71 (83.5)	3 (3.5)	6 (7.1)	5 (5.9)
Highly suspicious	90	0 (0)	33 (36.7)	0 (0)	12 (13.3)	45 (50.0)

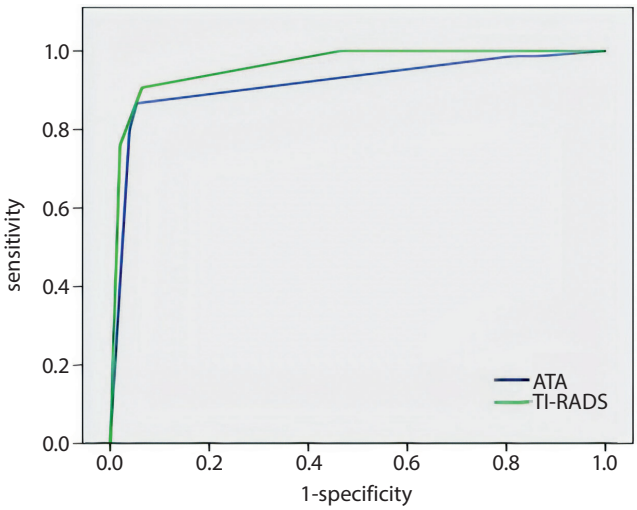

Fig. 2. The receiver operating curve (ROC) of the American College of Radiology (ACR) and American Thyroid Association (ATA) guidelines (TI-RADS – Thyroid Imaging Reporting and Data System)

Table 3. Diagnostic value of the ATA and TI-RADS risk classifications for the detection of malignant/suspicious thyroid nodules

Parameter	ATA-high suspicion	TI-RADS-high suspicion
Sensitivity	60/75 (80.0%)	57/75 (76.0%)
Specificity	1279/1327 (96.3%)	1294/1327 (97.5%)
PPV	60/108 (55.5%)	57/90 (63.3%)
NPV	1279/1294 (98.8%)	1294/1312 (98.6%)
Accuracy	1339/1402 (95.5%)	1351/1402 (96.3%)

Sensitivity – number of true positives divided by the number of true positives plus the number of false negatives; specificity – number of true negatives divided by the number of true negatives plus the number of false positives; positive predictive value (PPV) – number of true positives divided by the number of true positives plus the number of false positives; negative predictive value (NPV) – number of true negatives divided by the number of true negatives plus the number of false negatives; accuracy – number of true positives plus the number of true negatives divided by the number of true positives plus the number of true negatives plus the number of false positives plus the number of false negatives; ATA – American Thyroid Association; TI-RADS – Thyroid Imaging Reporting and Data System.

this cutoff value (area under the curve (AUC) = 0.962, 95% confidence interval (95% CI) = 0.943–0.981, $p < 0.001$). Using the ATA guidelines, the best cutoff value for differentiating benign and malignant nodules was 4.5. This means that if a nodule is in the high-suspicion category, it is likely malignant; if it is in the intermediate or lower-suspicion category, it is likely benign. The most reliable diagnosis based on the ATA guidelines was obtained using this cutoff value (AUC = 0.917, 95% CI = 0.875–0.959, $p < 0.001$).

The diagnostic performances of the TI-RADS and ATA score systems were evaluated based on high-suspicion nodules. The sensitivity and specificity of high-suspicion nodules according to both TI-RADS and ATA were both high (76% compared to 80% and 97.5% compared to 96.3%, respectively), but PPV was low (63.3% compared to 55.5%; Table 3).

Discussion

Thyroid cancers are observed more frequently in women. In a large-scale study, approx. 75% of thyroid cancer cases were reported to be women.[7] In our study, when the sexes were evaluated separately, the rate of cases with malignancy confirmed using FNAB was found to be similar (4.9% in men, 5% in women). However, when all patients who underwent FNAB were evaluated, the majority of patients with malignancy were women. Thus, this finding is consistent with previous findings stating that the incidence of thyroid cancer is higher in women.

In this study, the Bethesda classification was used for pathological evaluation of FNAB performed on the thyroid nodules. The malignancy risk of each category in the Bethesda system has been demonstrated in prior studies: while the risk of malignancy in the benign category is approx. 0–3%, it is 97–99% in the malignant category, which means that the Bethesda system can accurately estimate the risk of malignancy.[6] In the Bethesda system, the non-diagnostic category is applied when the sample is not large enough to reach a conclusion. In a previous study, this category was applied to 16% of first biopsies; when a second biopsy was performed in patients with non-diagnostic results, sufficient samples were taken from most of these patients.[8] In our study, the rate of the non-diagnostic category was 8.5%. It has been suggested that the category of atypia of undetermined significance (AUS)/follicular lesion of undetermined significance (FLUS) in the Bethesda system should be below 7%, if possible, in all thyroid FNAB results, although a value of 10% is more reasonable.[6] In our study, the AUS/FLUS category was 11% of all FNAB results.

The ATA classifies nodules into risk categories and makes FNAB recommendations accordingly. The ATA high-risk category is reported to have an approx. 70–90% malignancy risk. In a study evaluating the malignancy risk of nodules according to the ATA classification, malignancy was detected in approx. 67.5% of the nodules considered high-risk ones.[9] Another study reported a malignancy risk of approx. 83% for high-risk nodules classified using ATA guidelines.[10] In our study, 48% of the nodules classified as high-risk according to the ATA risk category were found to have malignant/suspicious cytology results.

In the TI-RADS classification, points are given according to the characteristics of the nodules and the risk classification of the nodules is made considering the total score. In a study investigating the malignancy risk of the TI-RADS classification, the frequency of malignancy was approx. 20.6% for nodules in the high-suspicion category, from 5.9% to 12.8% for nodules in the moderate-suspicion category, and 4.8% in the mild-suspicion category.[11] In another study comparing the FNAB results of nodules classified according to the TI-RADS classification, the frequency of malignancy/suspected malignancy in TR5 nodules was observed at a rate of 60%. When the benign FNAB results

were examined, it was determined as 100% in the TR2 category, 66% in the TR3 category, 33% in the TR4 category, and 40% in the TR5 category.[12] In another study, malignancy was detected histopathologically in 97.1% of nodules in the TR5 category and 33.3% of nodules in the TR3 category.[13] In our study, similar to the literature, 63.3% of nodules in the TI-RADS TR5 category were found to be histopathologically malignant/suspected for malignancy.

Malignancy risk is significantly higher in high-suspicion nodules compared with other nodules in both the ATA and TI-RADS classifications. Gao et al. reported a malignancy rate of 88% in the TI-RADS TR5 category and the best cutoff value in predicting malignancy according to the ROC curve was TR5. For the ATA risk classification, the risk of malignancy in highly suspicious nodules was found to be 87.3% and the best cutoff value in predicting malignancy according to the ROC curve was the category of highly suspicious nodules.[14] In another study comparing the ATA and TI-RADS risk classifications, the rate of malignancy was found to be 65% in nodules in the ATA high-risk group and 73.6% in nodules in the TI-RADS TR5 category. The authors also found that TI-RADS TR5 and the ATA high-suspicion nodule category were best at distinguishing between benign and malignant nodules. When the sensitivity and specificity of both diagnostic classifications were evaluated, it was observed that the ATA classification was more sensitive and the TI-RADS classification was more specific.[15] In a study conducted by Koc et al., 45 nodules were observed as malignant, 34 of which had FNAB indication for TI-RADS, while 38 nodules had FNAB indication according to the ATA classification. In the same study, the sensitivity of TI-RADS was found to be 48.8% and the specificity was 59.9%, while the sensitivity of the ATA classification was 82.2% and the specificity was 53.47%.[16] A study evaluating the TI-RADS classification found 81.4% malignancy in the TR5 category, 40.1% in the TR4 category, 7.5% in the TR3 category, 2.3% in the TR2 category, and no malignant cytology in the TR1 category. In addition, the study found that the sensitivity of TI-RADS was 96.6%, the specificity was 52.9% and the cutoff category for predicting malignancy was TR4.[17] In a study by Huang et al., when the ATA and TI-RADS classifications were compared, the sensitivity of the ATA classification was 92% and the specificity was 10%, while the sensitivity of the TI-RADS classification was 74% and the specificity was 47%. As a result, the ATA classification was found to be more sensitive, while the TI-RADS classification was more specific.[18] In the present study, when we evaluated the power of both classifications to recognize malignancy, we found that the sensitivity of the ATA risk classification was 80% and the specificity was 96.3%, while the sensitivity of the TI-RADS classification was 76% and the specificity was 97.5%. According to these results, ATA and TI-RADS have high specificity and sensitivity. We also found that the best category for distinguishing malignant and benign nodules was TR5 for TI-RADS and the high-suspicion category for ATA.

While almost all nodules are included in a given category in the ATA and TI-RADS classifications, some nodules are outside of a category. In the ACR-TI-RADS classification, the TR1 category includes nodules scoring 0 and the TR2 category includes nodules scoring 2 points; thus, nodules scoring 1 point do not fall into any category. Similarly, in the ATA classification, some nodules are outside of a category. According to the ATA classification, the high-risk nodule category includes hypoechoic nodules with suspicious features, the moderate-risk category includes hypoechoic nodules without suspicious features, and the low-risk category includes isoechoic nodules without suspicious features. Therefore, isoechoic nodules with suspicious features fall outside of a category. In a prior study, the frequency of nodules that could not be classified according to ATA category was 3.4% and the frequency of malignancy in these nodules was 18.2%.[19] In a study by Lauria Pantano et al., 54 of 1077 nodules included in the study did not fit any category in the ATA classification, and 9 of them were cytologically high-risk ones.[20] In our study, when evaluated according to the ATA category, 12% of the nodules were found to be outside of a category, and 0.5% of these nodules were classified as non-categorized according to the TI-RADS classification. However, no malignancy or suspected malignancy cytology result was observed in any of the nodules that were outside of a category in both classifications.

Limitations

While we compared the risk categories using both guidelines with the FNAB results, we did not compare risk categories with final pathological results after thyroidectomy because we were not able to follow up with sufficient patients.

Conclusions

Our findings support that both the ATA and TI-RADS classifications can effectively predict malignancy risk in thyroid nodules. Both methods are effective at detecting malignancy in patients and preventing unnecessary FNAB.

ORCID iDs

Murat Şahin https://orcid.org/0000-0001-7969-9157
Ayten Oguz https://orcid.org/0000-0002-9518-8610
Dilek Tuzun https://orcid.org/0000-0002-6693-4928
Gülsüm Akkus https://orcid.org/0000-0002-3819-8169
Gul Inci Törün https://orcid.org/0000-0002-6106-4935
Abdulkadir Yasir Bahar https://orcid.org/0000-0002-6963-3389
Hatice Şahin https://orcid.org/0000-0002-3317-3640
Kamile Gül https://orcid.org/0000-0002-2145-770X

References

1. Dean DS, Gharib H. Epidemiology of thyroid nodules. *Best Pract Res Clin Endocrinol Metab*. 2008;22(6):901–911. doi:10.1016/j.beem.2008.09.019

2. American Cancer Society. Cancer Facts & Figures 2020. Atlanta, USA: American Cancer Society; 2020. https://www.cancer.org/content/dam/cancer-org/research/cancer-facts-and-statistics/annual-cancer-facts-and-figures/2020/special-section-cancer-in-adolescents-and-young-adults-2020.pdf.
3. Haugen BR, Alexander EK, Bible KC, et al. 2015 American Thyroid Association Management Guidelines for Adult Patients with Thyroid Nodules and Differentiated Thyroid Cancer: The American Thyroid Association Guidelines Task Force on Thyroid Nodules and Differentiated Thyroid Cancer. *Thyroid*. 2016;26(1):1–133. doi:10.1089/thy.2015.0020
4. National Comprehensive Cancer Network. Thyroid cancer (Version 2.2020). https://www.nccn.org/patients/guidelines/content/PDF/thyroid-patient.pdf. Plymouth Meeting, USA; 2020.
5. Tessler FN, Middleton WD, Grant EG, et al. ACR Thyroid Imaging, Reporting and Data System (TI-RADS): White Paper of the ACR TI-RADS Committee. *J Am Coll Radiol*. 2017;14(5):587–595. doi:10.1016/j.jacr.2017.01.046
6. Cibas ES, Ali SZ. The 2017 Bethesda System for Reporting Thyroid Cytopathology. *Thyroid*. 2017;27(11):1341–1346. doi:10.1089/thy.2017.0500
7. Lim H, Devesa SS, Sosa JA, Check D, Kitahara CM. Trends in thyroid cancer incidence and mortality in the United States, 1974–2013. *JAMA*. 2017;317(13):1338–1348. doi:10.1001/jama.2017.2719
8. Jack GA, Sternberg SB, Aronson MD, Mukamal KJ, Oshin A, Hennessey JV. Nondiagnostic fine-needle aspiration biopsy of thyroid nodules: Outcomes and determinants. *Thyroid*. 2020;30(7):992–998. doi:10.1089/thy.2019.0140
9. Chng CL, Tan HC, Too CW, et al. Diagnostic performance of ata, bta and tirads sonographic patterns in the prediction of malignancy in histologically proven thyroid nodules. *Singapore Med J*. 2018;59(11):578–583. doi:10.11622/smedj.2018062
10. de Macedo BM, Izquierdo RF, Golbert L, Meyer ELS. Reliability of thyroid imaging reporting and data system (TI-RADS), and ultrasonographic classification of the American Thyroid Association (ATA) in differentiating benign from malignant thyroid nodules. *Arch Endocrinol Metab*. 2018;62(2):131–138. doi:10.20945/2359-3997000000018
11. Middleton WD, Teefey SA, Reading CC, et al. Multiinstitutional analysis of thyroid nodule risk stratification using the American College of Radiology thyroid imaging reporting and data system. *Am J Roentgenol*. 2017;208(6):1331–1341. doi:10.2214/AJR.16.17613
12. Singaporewalla RM, Hwee J, Lang TU, Desai V. Clinico-pathological correlation of thyroid nodule ultrasound and cytology using the TIRADS and Bethesda classifications. *World J Surg*. 2017;41(7):1807–1811. doi:10.1007/s00268-017-3919-5
13. George NA, Suresh S, Jiji V, et al. Correlation of TIRADS and Bethesda scoring systems with final histopathology of thyroid nodules: An institutional experience. *Indian J Otolaryngol Head Neck Surg*. 2021;2021:1–6. doi:10.1007/s12070-021-02380-8
14. Gao L, Xi X, Jiang Y, et al. Comparison among TIRADS (ACR TI-RADS and KWAK- TI-RADS) and 2015 ATA Guidelines in the diagnostic efficiency of thyroid nodules. *Endocrine*. 2019;64(1):90–96. doi:10.1007/s12020-019-01843-x
15. Wu XL, Du JR, Wang H, et al. Comparison and preliminary discussion of the reasons for the differences in diagnostic performance and unnecessary FNA biopsies between the ACR TIRADS and 2015 ATA guidelines. *Endocrine*. 2019;65(1):121–131. doi:10.1007/s12020-019-01886-0
16. Koc AM, Adıbelli ZH, Erkul Z, Sahin Y, Dilek I. Comparison of diagnostic accuracy of ACR-TIRADS, American Thyroid Association (ATA), and EU-TIRADS guidelines in detecting thyroid malignancy. *Eur J Radiol*. 2020;2020:109390. doi:10.1016/j.ejrad.2020.109390
17. Xu T, Wu Y, Wu RX, et al. Validation and comparison of three newly-released thyroid imaging reporting and data systems for cancer risk determination. *Endocrine*. 2019;64(2):299–307. doi:10.1007/s12020-018-1817-8
18. Huang BL, Ebner SA, Makkar JS, et al. A multidisciplinary head-to-head comparison of American College of Radiology Thyroid Imaging and Reporting Data System and American Thyroid Association Ultrasound Risk Stratification Systems. *Oncologist*. 2020;25(5):398–403. doi:10.1634/theoncologist.2019-0362
19. Malhi H, Grant E. Both TIRADS and the ATA guidelines provide effective malignancy risk stratification for thyroid nodules. *Clin Thyroidol*. 2016;28(8):238–240. doi:10.1089/ct.2016;28.238-240
20. Lauria Pantano A, Maddaloni E, Briganti SI, et al. Differences between ATA, AACE/ACE/AME and ACR TI-RADS ultrasound classifications performance in identifying cytological high-risk thyroid nodules. *Eur J Endocrinol*. 2018;178(6):595–603. doi:10.1530/EJE-18-0083

Differences in clinical phenotypes of primary Sjögren's syndrome depending on early or late onset

Agata Sebastian[1,A–F], Marta Madej[1,A–F], Maciej Sebastian[2,A–F], Ewa Morgiel[1,B–F], Piotr Wawryka[2,C,E,F], Piotr Wiland[1,A,C,E,F]

[1] Department of Rheumatology and Internal Medicine, Wroclaw University Clinical Hospital, Poland
[2] Department of General, Minimally Invasive and Endocrine Surgery, Wroclaw Medical University, Poland

A – research concept and design; B – collection and/or assembly of data; C – data analysis and interpretation; D – writing the article; E – critical revision of the article; F – final approval of the article

Advances in Clinical and Experimental Medicine, ISSN 1899–5276 (print), ISSN 2451–2680 (online) *Adv Clin Exp Med*. 2021;30(11):1141–1146

Address for correspondence
Marta Madej
E-mail: marta.madej@poczta.fm

Funding sources
None declared

Conflict of interest
None declared

Received on February 6, 2021
Reviewed on May 9, 2021
Accepted on July 12, 2021

Published online on September 22, 2021

Abstract

Background. Previous research suggests that systemic involvement in primary Sjögren's syndrome (pSS) is a marker of disease prognosis.

Objectives. To evaluate pSS disease activity and the clinical phenotype of pSS patients depending on the age at diagnosis with long-term follow-up.

Materials and methods. The study group consisted of patients diagnosed with pSS based on the 2016 pSS classification criteria.

Results. The study group consisted of 46 patients with early-onset pSS (≤35 years of age) and 32 patients with late-onset pSS (≥65 years of age). The study group was identified from a total of 228 patients diagnosed with pSS. There were no differences regarding the frequency of eye and mouth dryness, focus score (FS) ≥1 or anti-SSA/SSB antibodies depending on age. Rheumatoid factor (RF) was more common among older patients ($p > 0.05$). In the overall assessment of disease activity using European League Against Rheumatism (EULAR) Sjögren Syndrome Disease Activity Index (ESSDAI), no differences related to age were observed on the first and last visit (after 36 months on average). Lymphadenopathy and changes in the hematology domain ($p < 0.05$) were more common in patients with the early-onset phenotype. Changes in the lungs and musculoskeletal system occurred regardless of age.

Conclusions. Patients with early-onset pSS differ from those with late-onset pSS in terms of higher incidence of peripheral lymphadenopathy and cytopenia. The involvement of lung tissue and joints as well as dryness symptoms are common in pSS regardless of age. The RF plays a role in the pathomechanism of pSS development.

Key words: disease activity, age, Sjögren's syndrome, antinuclear antibodies

Cite as
Sebastian A, Madej M, Sebastian M, Morgiel E, Wawryka P, Wiland P. Differences in clinical phenotypes of primary Sjögren's syndrome depending on early or late onset. *Adv Clin Exp Med*. 2021;30(11):1141–1146. doi:10.17219/acem/140178

DOI
10.17219/acem/140178

Background

Primary Sjögren's syndrome (pSS) is a systemic autoimmune disease characterized by inflammation of the salivary and lacrimal glands, causing a reduction in exocrine secretion that ultimately leads to clinical presentation of sicca symptoms.[1] Aside from sicca syndrome, a typical symptom is chronic fatigue. The pSS is a heterogeneous disease that, in addition to dryness, presents with involvement of multiple organs and systems (extraglandular manifestations).

Systemic involvement corresponds to disease prognosis.[2] The incidence of pSS is estimated at 61 per 100,000 people in the general population, with the highest prevalence encountered in Europe.[3] Differences regarding the prevalence and incidence of pSS are thought to be due to variation in study design and classification criteria.[3] The disease overwhelmingly affects middle-aged women. The mean age at the time of pSS diagnosis is 56 years, with another peak occurring between 20 and 40 years.[4] Several factors, including age, appear to determine the various clinical phenotypes of pSS.[5] To date, little data have been published regarding the relationship between age and clinical signs of pSS. As a result, the current research findings are divergent and inconclusive. In systemic lupus erythematosus and rheumatoid arthritis, most studies agree that late onset of the disease is associated with involvement of fewer organs and better prognosis.[6,7] However, in the case of pSS, published data on the topic are scarce. Previous studies suggest differences in clinical and immunologic phenotypes between patients with early and late onset of the disease. Furthermore, the risk of developing lymphoma as a complication of pSS seems to be age-dependent, according to some authors.[8] An advanced age at diagnosis is also regarded as a risk factor for increased mortality, along with, for example, male sex, parotid enlargement, extraglandular involvement, and some immunologic abnormalities.[9,10] In particular, age seems to be an important factor in the clinical phenotype of pSS.[2,11] Brito-Zerón et al. suggested that the systemic phenotype of pSS is strongly influenced by personal determinants, such as age, gender, ethnicity, and place of residence, which are key geoepidemiological players driving the expression of systemic disease at diagnosis.[12]

Clinical variability in pSS can hinder both, early diagnosis and personalization, and selection of appropriate treatment. This is especially important in the early and late phenotype of the disease to accelerate the correct diagnosis while still in its early stages. To date, few papers and clinical observations on this issue in pSS have been published. In addition, there are few analyses available in the literature on the subsequent course of pSS in patients with early and late onset of the disease.

Objectives

This study aimed to assess the activity and clinical phenotype of pSS according to the age of disease onset (early- compared to late-onset phenotypes) and assess the activity of the disease over long-term follow-up.

Materials and methods

Patient selection

A total of 228 patients over 18 years of age who were diagnosed with pSS in our department from 2009 to 2020 based on the 2016 pSS classification criteria, were considered eligible for this study.[13] Patients with an additional systemic connective tissue disease, especially systemic lupus erythematosus (SLE) or rheumatoid arthritis (RA), were excluded. The selected study group consisted of 46 patients with early-onset pSS (≤35 years of age at the time of diagnosis and 32 patients with late-onset pSS (≥65 years of age at the time of diagnosis).

Assessment of disease activity and follow-up

Patients underwent routine labial salivary gland biopsy (LSGB) under local anesthesia with 10% lidocaine solution for histopathological assessment of characteristic lymphocytic infiltrates typical of pSS following the current guidelines[14] (focal lymphocytic sialadenitis and focus score ≥1 foci/4 mm^2). Disease activity was assessed in all patients using the European League Against Rheumatism (EULAR) Sjögren Syndrome Disease Activity Index (ESSDAI).[15] Laboratory tests were performed following current guidelines for the diagnosis and assessment of pSS activity, including assessment of the presence of rheumatoid factor (rheumatoid factor (RF), nephelometric method), antinuclear antibodies (ANA and immunofluorescence (IF) method), antibodies to extractable nuclear antigens (extractable nuclear antigen (ENA), enzyme-linked immunosorbent assay (ELISA)), C3 and C4 components of the complement system, and evaluation of immunoglobulin concentrations. Assessment of disease activity was carried out at least twice: at the time of the diagnosis of pSS and during the last follow-up visit (at least 6 months after the 1st visit). The average follow-up duration was 36 months.

This study was approved by the ethics committee of the Wroclaw Medical University, Wrocław, Poland (decision No. 836/2020) and was conducted in compliance with the Declaration of Helsinki. Written informed consent to participation in this study was obtained from all patients.

Statistical analysis

Statistical analysis was performed using STATISTICA v. 10 software package (StatSoft Inc., Tulsa, USA). The Mann–Whitney U test was used to compare the distributions of quantitative variables in 2 independent groups, i.e., to compare the ESSDAI point values and age between the early- and late-onset groups. The χ^2 test was used to assess relationships between dichotomous variables. Statistical significance was considered at $p \leq 0.05$.

Results

Among the 228 patients diagnosed with pSS, 20% (n = 46) had early-onset disease (≤35 years of age at the time of diagnosis and 14% (n = 32) had late-onset disease (≥65 years of age at the time of diagnosis). The majority of patients were diagnosed with pSS after the age of 35 but before the age of 65 (66% of patients (n = 150)). Symptoms of eye and mouth dryness were observed in 93% (n = 43) and 85% (n = 39) of patients with early-onset pSS and 96% (n = 31) and 100% (n = 32) of patients with late-onset pSS, respectively (the differences were not statistically significant; see Table 1). Salivary gland biopsy was not performed in 2 patients from each subgroup due to a lack of consent (4 patients in total). Focus score (FS) ≥1 was found in 90% (n = 27) of patients with late-onset pSS and 82% (n = 36) of patients with early-onset pSS. Specific anti-SSA antibodies were more common in patients with early-onset (89%, n = 41) than with late-onset pSS (72%, n = 23), but this difference was not statistically significant. Anti-SSB antibodies were found in a similar proportion of patients in each subgroup. The RF was more common among older patients (72% compared to 67%; p = 0.86). The C3 hypocomplementemia was found in approx. 15% of patients in each subgroup, while a reduced C4 serum concentration was more often observed among patients over the age of 64 (p = 0.28). In the global assessment of disease activity using ESSDAI, there was a higher pSS activity among younger patients (on average, 7.8 compared to 6.0 points; p = 0.11; Table 2). For the individual ESSDAI domains, the 2 subgroups differed with regard to lymphadenopathy and hematological domains, with organ involvement significantly more common among patients under the age of 36.

Table 1. Characteristic of patients with pSS depending on age at the time of diagnosis

Parameters	Patient age ≤35 years	Patient age ≥65 years	p-value
Number of patients	46	32	–
Age at time of pSS diagnosis SD	29 (min 17; max 35) 5.3	70 (min 65; max 85) 5.0	–
Mean age at the last visit (SD)	32 (5.2)	74 (5.5)	–
Positive ocular symptoms n % of patients	 43 93	 31 96	1.0
Positive oral symptoms n % of patients	 39 85	 32 100	0.62
Positive Schirmer test n % of patients	 40 87	 31 96	0.86
Focus score ≥1 n % of patients	N/A 2 36 82	N/A 2 27 90	0.86
Positive anti-SSA ab n % of patients	 41 89	 23 72	0.6
Positive anti-SSB ab n %	 30 65	 20 62	1.0
Positive RF (nv 0–14 IU/mL) n % of patients	 31 67	 23 72	0.86
Low C3 (nv 0.9–1.8 g/L) n %	N/A 1 7 15	 5 16	1.0
Low C4 (nv 0.1–0.4 g/L) n % of patients	N/A 1 3 7	 5 16	0.28

pSS – primary Sjögren's syndrome; n – number of patients; ab – antibodies; RF – rheumatoid factor; nv – normal value.

Table 2. Evaluation of pSS activity depending on a patient's age at the time of diagnosis

Parameters	Patient's age ≤35 years	Patient's age ≥65 years	p-value	z-score
ESSDAI score at the time of pSS diagnosis	7 (median) 9 (IQR)	5 (median) 5 (IQR)	0.11	1.48
ESSDAI domains (n/% of patients, max value-points in the domain): constitutional lymphadenopathy glandular articular cutaneous pulmonary renal muscular peripheral nervous system central nervous system hematological biological	 7/15 (max 6) 10/22 (max 4) 19/41 (max 4) 22/48 (max 4) 5/11 (max 9) 7/15 (max 10) 2/4 (max 5) 0 0 0 27/59 29/63	 1/3 (max 3) 1/3 (max 8) 9/28 (max 4) 18/56 (max 4) 5/16 (max 6) 9/28 (max 15) 0 0 1/3 (max 10) 0 6/19 16/50	 0.14 <0.05 0.49 0.69 0.73 0.28 0.51 0.41 <0.03 0.57	–
New ESSDAI onset during the observation period [n/% of patients]	8/17	10/31	0.29	–
Lymphoma MGUS	0 0	0 2		–

pSS – primary Sjögren's syndrome; ESSDAI – European League Against Rheumatism (EULAR) Sjögren Syndrome Disease Activity Index n – number of patients; MGUS – monoclonal gammopathy of undetermined significance; IQR – interquartile range.

Discussion

Our findings show that in 2/3 of pSS patients, the disease manifests between the age of 36 and 64. Only in 1/3 of cases did the disease begin at a very young age (≤35 years) or at an older age (≥65 years), which is in line with previous observations.[16] However, since pSS is one of the most common diseases in rheumatology, this represents a relatively large group of patients.[17] The early-onset pSS phenotype dominates this population of patients. The age of disease onset may be relevant for the clinical course and prognosis. Patients with the early-onset phenotype were significantly more likely to have lymphadenopathy and hematological disorders (most often lymphopenia and neutropenia, data not presented), although we did not observe any significant differences in serological abnormalities between early- and late-onset groups. We also observed disease deterioration during long-term follow-up of the late-onset group, despite higher baseline disease activity in early-onset patients (in both cases, the differences were nonsignificant).

The pSS is associated with several immunological abnormalities, of which positive ANA results are the most frequently detected. Anti-SSA antibodies are the most specific abnormality, while cryoglobulins and hypocomplementemia are the main prognostic markers.[18] Our analysis showed that anti-SSA antibodies are present regardless of age, as is hypocomplementemia. Observations made by Chinese researchers indicated that patients with early-onset pSS were more likely to have reduced complement C3 levels,[19] which was not confirmed by our study of a Caucasian population. However, our observations do confirm previous reports of a higher incidence of hematological disorders among younger patients, even though the studies involved different ethnic groups (Asians compared to Caucasians). Direct involvement of antibodies against muscarinic type 3 receptors located on leukocytes has been implicated in the pathomechanism of leucopenia during the course of pSS.[20] To date, anti-acetylcholine type 3 receptor (M3R) antibodies have been shown to be more common in younger patients and patients with hyperglobulinemia.[21]

According to the previous research, patients with the early-onset phenotype of pSS have a higher incidence of lymphadenopathy, RF and anti-SSA antibodies.[8,22] Although Tishler et al. reported more frequent organ involvement in the form of parotid gland enlargement, joint involvement and central nervous system involvement in patients with early-onset pSS, these results were not statistically significant.[5] In our patient sample, lymphadenopathy was more common in young patients. However, we did not observe any difference in the frequency of RF and anti-SSA antibodies. Admittedly, RF was recorded slightly more often in elderly patients, but the differences were statistically insignificant.

The RF is a key marker of pSS and is found in the majority of patients. As the likelihood of finding RF in a significant titer increases with age,[23] we expected to observe it more frequently in the older subgroup in our analysis. Indeed, the prevalence of RF in older patients (≥65 years) was higher than in patients with early disease onset (72% compared to 67%), although these differences were not statistically significant. The similar prevalence of RF in pSS patients irrespective of age may prove the involvement of RF in the pathogenesis and development of pSS. Determination of RF titers may play a central role in differentiating pSS from non-autoimmune causes of sicca syndrome. However, they are not included in the current pSS classification criteria[13] despite the attempts in 2012 to include RF among the primary criteria domains.[24] Furthermore, it is thought that the presence of RF in pSS patients may be linked to increased disease activity and lymphoma,[25] especially when considered in combination with other recognized risk factors for developing lymphoproliferative complications, such as an older age, enlargement of the salivary glands, reduced C4 component of the complement system, and the presence of cryoglobulins, leukopenia or monoclonal gammopathy. In our analysis, no patients were diagnosed with lymphoma. By contrast, in another published study, lymphomas were seen more commonly in older patients.[16]

Ramos-Casals et al. reported that adult pSS patients with early disease onset at the age of 35 had a higher frequency of autoantibodies and incidence of lymphomas than patients with late disease onset. They concluded that age at disease onset was of prognostic value,[8] which we did not confirm in any way in the present study. The likely insufficient (too small) study population is one potential explanation, and further studies are needed to confirm this hypothesis. Recent data also suggest that the risk of developing lymphoma depends on different predisposing factors in relation to the age of the onset of the disease, and that the distribution of lymphoma is different across time among early- and late-onset patient populations.[16] In our observations, among patients ≥65 years, only monoclonal gammopathy of undetermined significance (MGUS) was observed in 2 patients, which might relate to pSS activity or a patient's age (higher risk of MGUS in this age group). About 3% of people over the age of 50 and 5% of people aged 70 and older have M protein in their blood; the highest incidence is among adults aged 85 and older.[26,27]

The ESSDAI questionnaire is used to assess organ damage in pSS. It consists of 12 domains addressing the most important – although not all – clinical manifestations of pSS. The guidelines developed by Seror et al. specify the exact duration and detailed definitions assigned to each individual symptom.[15] In the present study, we assessed disease activity using ESSDAI at the time of diagnosis and subsequent visits. On average, the last visit took place 36 months after the diagnosis of pSS in both subgroups.

All patients were treated according to locally and globally accepted pSS treatment guidelines, depending on their symptoms and organ involvement. It is particularly

noteworthy that, in patients with the late phenotype, we were more likely to observe disease deterioration over long-term follow-up reflected by an increase in ESSDAI, although this change was not statistically significant. These findings contrast with recently published observations where a diagnosis of pSS at a younger age was associated with a poorer prognosis of the disease course.[28] Similar to a multicenter study involving a large group of patients,[12] in our patient population, higher ESSDAI was identified in patients with early-onset compared to late-onset pSS (7.8 compared to 6.0) at baseline, but statistically significant differences were ultimately not demonstrated.

Deviations in blood count and lymphadenopathy are observed more often in younger pSS patients. According to some authors, lymphadenopathy in young patients, as compared to the older patients, is an independent factor for the development of lymphoma in pSS.[16] Generally, identification of lymphadenopathy may allow earlier pSS diagnosis in these patients, for whom the diagnosis may be complicated because of the less pronounced expression of sicca features.[24] In our observations, more than half of patients ≤35 years of age (85%) reported symptoms of dry eyes and mouth, but this rate of dryness was still lower than in older patients (100%).

In most publications to date, lung lesions are typical for patients with late-onset pSS.[16,25] However, the data are still inconclusive.[16,22] According to Zhao et al., patients with pSS pulmonary involvement are more likely to have enlarged major salivary glands.[19] In our group of patients, lung lesions coexisted with enlargement of major salivary glands. The prevalence of organ involvement in both locations was independent of age, similarly to lymphocytic infiltrations in LSGB corresponding to pSS.[14] As demonstrated by Kakugawa et al., LSGB and FS results correlate with the presence and activity of lung lesions.[29] The authors showed that higher FS values were observed mainly in pSS patients with respiratory tract involvement. Furthermore, in our patient group, we more often observed FS ≥ 1 and lung involvement in elderly patients. Among the analyzed group, lung lesions were more common in patients with late-onset rather than early-onset disease phenotype. However, as these differences were not statistically significant, there is still the need to monitor young patients for this complication.

Another characteristic symptom of pSS is the inflammation of small joints.[30] Joint involvement was one of the most frequent clinical manifestations of pSS in our patients. No differences were noted concerning the frequency of musculoskeletal system involvement depending on age, in line with reports from other researchers.[5] Articular involvement occurred in about half of patients in each subgroup, and should thus be considered as a part of the diagnostics of patients with arthritis and a significant RF titer.

Renal involvement in the course of pSS is rarely observed, i.e., it presents in less than 10% of patients. Infiltration of the kidney by plasma cells is a key feature and is similar to lymphoplasmacytic infiltration of the salivary glands.[31] In our group of patients, renal changes occurred sporadically and only in patients with early onset of the disease. These findings are in line with a study by Jain et al. concerning renal involvement in pSS patients, where renal involvement was mainly observed in young people with symptoms of sicca.[32] Unlike the cited work, in our patient sample, renal changes were not associated with more frequent arthritis. However, the small proportion of patients with this complication (4%) prevents more detailed conclusions from being drawn.

Limitations

One of the limitations of the present study is the small group of patients with late and early onset of the disease, which results from the natural course of pSS. Moreover, the follow-up time was relatively short (36 months on average). Long-term follow-up is particularly crucial due to SLE and pSS coexistence at older age.

Conclusions

Based on the findings of this study, about 30% of pSS patients present with the early or late phenotype of the disease. Patients with early-onset pSS differed from those with late-onset pSS only in a higher incidence of peripheral lymphadenopathy and cytopenia. This observation has significant clinical implications as it draws attention to the need for diagnostics of pSS in young patients with organ manifestations and dryness symptoms, which are not always strongly expressed. The involvement of the lung and joints is common in pSS regardless of patient age. The observed quantitative differences (although statistically nonsignificant) in the prevalence of lung lesions in patients with the late-onset phenotype suggest the need to verify our observations in larger samples of patients. There was no difference in the frequency of lymphocytic FS infiltrations in patients ≥65 compared to ≤35 years of age, as there were no statistically significant differences in patients' serological profiles.

ORCID iDs

Agata Sebastian https://orcid.org/0000-0001-6332-8714
Marta Madej https://orcid.org/0000-0002-4523-9272
Maciej Sebastian https://orcid.org/0000-0002-1258-6358
Ewa Morgiel https://orcid.org/0000-0002-9506-698X
Piotr Wawryka https://orcid.org/0000-0002-9400-4920
Piotr Wiland https://orcid.org/0000-0001-9999-0267

References

1. Kaminski B. Laryngological manifestations of Sjögren's syndrome. *Reumatologia*. 2019;57(1):37–44. doi:10.5114/reum.2019.83237
2. Ramos-Casals M, Brito-Zeron P, Siso-Almirall A, Bosch X. Primary Sjögren's syndrome. *BMJ*. 2012;344:e3821. doi:10.1136/bmj.e3821
3. Qin B, Wang J, Yang Z, et al. Epidemiology of primary Sjögren's syndrome: A systematic review and meta-analysis. *Ann Rheum Dis*. 2015; 74(11):1983–1989. doi:10.1136/annrheumdis-2014-205375

4. Stefanski AL, Tomiak C, Pleyer U, Dietrich T, Burmester GR, Dörner T. The diagnosis and treatment of Sjögren's syndrome. *Dtsch Arztebl Int*. 2017;114(20):354–361. doi:10.3238/arztebl.2017.0354
5. Tishler M, Yaron I, Shirazi I, Yaron M. Clinical and immunological characteristics of elderly onset Sjögren's syndrome: A comparison with younger onset disease. *J Rheumatol*. 2001;28(4):795–797. PMID: 11327252
6. Koh ET, Boey ML. Late onset lupus: A clinical and immunological study in a predominantly Chinese population. *J Rheumatol*. 1994; 21(8):1463–1467. PMID:7983647
7. Stevens MB. Connective tissue disease in the elderly. *Clin Rheum Dis*. 1986;12(1):11–32. PMID:3522080
8. Ramos-Casals M, Cervera R, Font J, et al. Young onset of primary Sjögren's syndrome: Clinical and immunological characteristics. *Lupus*. 1998;7(3):202–206. doi:10.1191/096120398678920019
9. Singh AG, Singh S, Matteson EL. Rate, risk factors and causes of mortality in patients with Sjögren's syndrome: A systematic review and meta-analysis of cohort studies. *Rheumatology*. 2016;55(3):450–460. doi:10.1093/rheumatology/kev354
10. Parisis D, Chivasso C, Perret J, Soyfoo MS, Delporte C. Current state of knowledge on primary Sjögren's syndrome, an autoimmune exocrinopathy. *J Clin Med*. 2020;9(7):2299. doi:10.3390/jcm9072299
11. Ramos-Casals M, Solans R, Rosas J, et al; GEMESS Study Group. Primary Sjögren's syndrome in Spain: Clinical and immunologic expression in 1010 patients. *Medicine (Baltimore)*. 2008;87(4):210–219. doi:10.1097/MD.0b013e318181e6af
12. Brito-Zerón P, Acar-Denizli N, Ng WF, et al; Sjögren Big Data Consortium. Epidemiological profile and north-south gradient driving baseline systemic involvement of primary Sjögren's syndrome. *Rheumatology (Oxford)*. 2020;59(9):2350–2359. doi:10.1093/rheumatology/kez578
13. Shiboski CH, Shiboski SC, Seror R, et al; International Sjögren's Syndrome Criteria Working Group. 2016 American College of Rheumatology/European League Against Rheumatism Classification Criteria for Primary Sjögren's Syndrome: A consensus and data-driven methodology involving three international patient cohorts. *Arthritis Rheumatol*. 2017;69(1):35–45. doi:10.1002/art.39859
14. Fisher BA, Jonsson R, Daniels T, et al; Sjögren's histopathology workshop group (appendix) from ESSENTIAL (EULAR Sjögren's syndrome study group). Standardisation of labial salivary gland histopathology in clinical trials in primary Sjögren's syndrome. *Ann Rheum Dis*. 2017;76(7):1161–1168. doi:10.1136/annrheumdis-2016-210448
15. Seror R, Bowman SJ, Brito-Zeron P, et al. EULAR Sjögren's syndrome disease activity index (ESSDAI): A user guide. *RMD Open*. 2015;20; 1(1):e000022. doi:10.1136/rmdopen-2014-000022
16. Goules AV, Argyropoulou OD, Pezoulas VC, et al. Primary Sjögren's syndrome of early and late onset: Distinct clinical phenotypes and lymphoma development. *Front Immunol*. 2020;11:594096. doi:10.3389/fimmu.2020.594096
17. Witte T. Sjögren-Syndrom [in German]. *Z Rheumatol*. 2019;78(6):511–517. doi:10.1007/s00393-019-0625-8
18. Zhang NZ, Shi CS, Yao QP, et al. Prevalence of primary Sjögren's syndrome in China. *J Rheumatol*. 1995;22:659–661. PMID:7791159
19. Zhao Y, Li Y, Wang L, et al. Primary Sjögren syndrome in Han Chinese. *Medicine (Baltimore)*. 2015;94(16):e667. doi:10.1097/MD.0000000000000667
20. Namkoong E, Lee SW, Kim N, Choi Y, Park K. Effect of anti-muscarinic autoantibodies on leukocyte function in Sjögren's syndrome. *Mol Immunol*. 2017;90:136–142. doi:10.1016/j.molimm.2017.07.007
21. Jayakanthan K, Ramya J, Mandal SK, Sandhya P, Gowri M, Danda D. Younger patients with primary Sjögren's syndrome are more likely to have salivary IgG anti-muscarinic acetylcholine receptor type 3 antibodies. *Clin Rheumatol*. 2016;35(3):657–662. doi:10.1007/s10067-016-3186-0
22. Haga HJ, Jonsson R. The influence of age on disease manifestations and serological characteristics in primary Sjögren's syndrome. *Scand J Rheumatol*. 1999;28(4):227–232. doi:10.1080/03009749950155599
23. Ingegnoli F, Castelli R, Gualtierotti R. Rheumatoid factors: Clinical applications. *Dis Markers*. 2013;35(6):727–734. doi:10.1155/2013/726598
24. Shiboski SC, Shiboski CH, Criswell LA, et al. American College of Rheumatology Classification Criteria for Sjögren's Syndrome: A data-driven, expert consensus approach in the SICCA cohort. *Arthritis Care Res (Hoboken)*. 2012;64(4):475–487. doi:10.1002/acr.21591
25. Baldini C, Ferro F, Luciano N, Bombardieri S, Grossi E. Artificial neural networks help to identify disease subsets and to predict lymphoma in primary Sjögren's syndrome. *Clin Exp Rheumatol*. 2018;112(3):137–144. PMID:30156549
26. Sebastian A, Madej M, Sebastian M, et al. Prevalence and clinical presentation of lymphoproliferative disorder in patients with primary Sjögren's syndrome. *Rheumatol Int*. 2020;40(3):399–404. doi:10.1007/s00296-020-04522-7
27. Brito-Zerón P, Retamozo S, Gandía M, et al. Monoclonal gammopathy related to Sjögren syndrome: A key marker of disease prognosis and outcomes. *J Autoimmunol*. 2012;39(1–2):43–48. doi:10.1016/j.jaut.2012.01.010
28. Anquetil C, Hachulla E, Machuron F, et al. Is early-onset primary Sjögren's syndrome a worse prognosis form of the disease? *Rheumatology*. 2019;58(7):1163–1167. doi:10.1093/rheumatology/key392
29. Kakugawa T, Sakamoto N, Ishimoto H, et al. Lymphocytic focus score is positively related to airway and interstitial lung diseases in primary Sjögren's syndrome. *Respir Med*. 2018;137:95–102. doi:10.1016/j.rmed.2018.02.023
30. Mirouse A, Séror R, Vicaut E, et al. Arthritis in primary Sjögren's syndrome: Characteristics, outcome and treatment from French multicenter retrospective study. *Autoimmunol Rev*. 2019;18(1):9–14. doi:10.1016/j.autrev.2018.06.015
31. François H, Mariette X. Renal involvement in primary Sjögren syndrome. *Nat Rev Nephrol*. 2016;12(2):82–93. doi:10.1038/nrneph.2015.174
32. Jain A, Srinivas BH, Emmanuel D, et al. Renal involvement in primary Sjögren's syndrome: A prospective cohort study. *Rheumatol Int*. 2018;38(12):2251–2262. doi:10.1007/s00296-018-4118-x

Association of arterial hemodynamics with left ventricular systolic function in hypertensive patients: A longitudinal study

Anna Teresa Goździk[1,A,C–F], Ewelina Jasic-Szpak[1,A,D–F], Jakub Michałowicz[2,C,E,F], Monika Przewłocka-Kosmala[1,A,E,F], James Edward Sharman[3,A,B,D–F], Wojciech Kosmala[1,A–F]

[1] Institute of Heart Diseases, Wroclaw Medical University, Poland
[2] Student Scientific Organization, Institute of Heart Diseases, Wroclaw Medical University, Poland
[3] Menzies Institute for Medical Research, University of Tasmania, Hobart, Australia

A – research concept and design; B – collection and/or assembly of data; C – data analysis and interpretation; D – writing the article; E – critical revision of the article; F – final approval of the article

Advances in Clinical and Experimental Medicine, ISSN 1899–5276 (print), ISSN 2451–2680 (online) *Adv Clin Exp Med*. 2021;30(11):1147–1156

Address for correspondence
Anna Teresa Goździk
E-mail: anna.gozdzik@umed.wroc.pl

Funding sources
None declared

Conflict of interest
None declared

Received on July 10, 2021
Reviewed on July 27, 2021
Accepted on August 31, 2021

Published online on October 5, 2021

Abstract

Background. Left ventricular (LV) systolic impairment, particularly in the longitudinal direction, is considered an early and sensitive marker of hypertensive heart disease and increased cardiovascular risk. The evidence indicates that aortic stiffness and central hemodynamic factors are important determinants of LV performance, mediating the interaction between the heart and vascular load. Despite the existence of cross-sectional analyses linking central blood pressure (BP) parameters with LV mechanics, no longitudinal data are available which include serial measurements in the course of antihypertensive treatment.

Objectives. To investigate the associations between changes in LV longitudinal and circumferential function with alterations in arterial hemodynamics and ventricular-arterial coupling (VAC) in patients with uncomplicated hypertension during a 12-month follow-up.

Materials and methods. In this retrospective study, 216 patients (age 64.3 ±7.6 years) underwent echocardiography including left ventricular longitudinal (GLS) and circumferential strain (GCS) analysis, brachial BP measurements, VAC (combining echocardiography and brachial BP), and arterial hemodynamics using radial tonometry at baseline and after 12 months of antihypertensive therapy. Patients were grouped into 2 subsets: with improvement in GLS (n = 103) and with deterioration in GLS (n = 113).

Results. No significant differences were observed in the majority of cardiovascular, demographic or clinical characteristics between the groups. The subset with improvement in GLS demonstrated more favorable changes over follow-up in pulse wave velocity ($p = 0.03$), central augmentation pressure ($p = 0.01$) and ventricular-arterial coupling ($p = 0.04$) compared to patients showing deterioration in GLS. In the multivariable analysis, independent determinants of changes in GLS were: GLS at baseline (−0.48; $p < 0.001$), changes from baseline to follow-up in central augmentation pressure (−0.29; $p = 0.002$) and ventricular-arterial coupling (−0.25; $p = 0.004$). Independent determinants of analogous changes in GCS were: GCS at baseline (−0.46; $p < 0.001$) and changes in central augmentation pressure (−0.22; $p = 0.02$).

Conclusions. Left ventricular longitudinal and circumferential functional remodeling over time in hypertensive patients is associated with arterial hemodynamics and ventricular-arterial coupling.

Key words: hypertension, pulse wave analysis, arterial hemodynamics, ventricular-arterial coupling, longitudinal and circumferential strain

Cite as
Goździk AT, Jasic-Szpak E, Michałowicz J, Przewłocka-Kosmala M, Sharman JE, Kosmala W. Association of arterial hemodynamics with left ventricular systolic function in hypertensive patients: A longitudinal study. *Adv Clin Exp Med*. 2022;30(11):1147–1156. doi:10.17219/acem/141863

DOI
10.17219/acem/141863

Background

Left ventricular (LV) functional abnormalities have been widely recognized as an early manifestation of hypertensive heart disease (HHD) contributing to the increased cardiovascular risk.[1–4] The introduction of new imaging techniques, particularly speckle tracking echocardiography, provided evidence that in addition to LV diastolic derangements, LV systolic impairment, especially in the longitudinal direction, should be considered an early and sensitive marker of LV functional compromise, resulting from the detrimental effect of hypertension (HT).[5,6] Changes in LV circumferential contractility in the natural history of disease processes are not well understood; however, the relatively delayed development of this dysfunction has been reported consistently.[7–11]

Accumulating evidence indicates that aortic stiffness and central hemodynamic factors are important determinants of LV performance, mediating the interaction between the heart and vascular load.[12] Specifically, LV pressure load and myocardial function are associated with hemodynamics in the proximal aorta. Increased aortic stiffness amplifies early systolic load (evidenced by an increase in central pressure augmentation) and impairs ventricular-arterial coupling (VAC), which adversely affects cardiac function. Moreover, alterations in LV and aortic physiology enhance the risk of heart failure, especially heart failure with preserved ejection fraction (HFpEF), thus paving the way for adverse outcomes, such as HT.[13]

The association between central loading factors, assessed noninvasively with pulse wave analysis (PWA) from peripheral (e.g. brachial) arteries, and LV performance and structure has been demonstrated in previous studies.[14–21] However, no diagnostic approach has been developed that would favor the use of specific central hemodynamic parameters. Moreover, to our knowledge, no longitudinal data are available concerning the correlation of central hemodynamic parameters, including VAC, with LV mechanics, in the course of antihypertensive treatment.

Objectives

The aim of this study was to investigate the relationship between alterations in LV longitudinal and circumferential function with changes in arterial hemodynamic characteristics and VAC in patients with uncomplicated HT during a 12-month follow-up.

Materials and methods

Study subjects

This study was a retrospective analysis of 216 patients with uncomplicated HT, including 105 men and 111 women who participated in the BP GUIDE study,[22] and had complete datasets including LV deformation and PWA parameters. Among inclusion criteria were: 18–75 years of age, lack of pregnancy, and antihypertensive therapy including from 1 to 3 hypotensive drugs. Exclusion criteria included: severely abnormal LV mass index (>59 g/m$^{2.7}$ in women and >64 g/m$^{2.7}$ in men), clinical history of coronary artery disease or renal disease, serum creatinine >1.6 mg/dL, secondary HT, uncontrolled HT (office brachial blood pressure (BP) >180/100 mm Hg), aortic valve stenosis, or upper limb obstructive atherosclerosis. All patients were in the sinus rhythm to ensure the reliability of myocardial deformation assessment and PWA.

Protocol

Each participant underwent echocardiography, including LV longitudinal and circumferential strain analysis, brachial BP measurements, and estimated central hemodynamics assessment using radial tonometry at baseline and after 12 months of supervised HT management. Medication quantity was determined by daily defined dose (DDD) and according to the World Health Organization standards for exact quantifications of drug amount and standardization.[23] Patients were stratified according to the changes in global longitudinal strain (GLS) over the follow-up period (follow-up value minus baseline value) into 2 groups: with improvement in GLS and with deterioration in GLS. The study was conducted in accordance with The Declaration of Helsinki, and the protocol was approved by the institutional bioethics committee. All subjects gave their informed consent for inclusion before they participated in the study.

Echocardiography

Echocardiographic imaging was performed using Vivid E9 and Vivid 7 equipment (GE; Vingmed Ultrasound AS, Horten, Norway) with phased array 2.5 MHz multifrequency transducers. The assessment of LV function at baseline and 12-month follow-up was carried out by a single expert observer (W.K.) who was blinded to the clinical data.

Conventional and tissue Doppler imaging

The measurements of cardiac dimensions, wall thicknesses, LV ejection fraction, and Doppler parameters of mitral inflow and mitral annular velocities were obtained according to the recommendations of the American Society of Echocardiography and the European Association of Cardiovascular Imaging.[24]

The assessment of LV mass and ejection fraction were calculated by real-time three-dimensional echocardiography. The left atrium (LA) volume was measured using Simpson's technique from the apical four-chamber and two-chamber views at the end of ventricular systole, just

before mitral valve opening. The LA volume index was computed by adjusting LA volume to body surface area. The LV inflow parameters were evaluated using pulsed wave Doppler from the apical four-chamber view with the sample volume placed between the tips of mitral leaflets, and included peak early (E) and late diastolic flow velocity (A), along with deceleration time of the E-wave (DT). Pulse wave tissue Doppler was used to define peak early diastolic tissue velocity (e′) at the septal and lateral parts of the mitral annulus. The ratio of mitral inflow early diastolic velocity to the average e′ velocity obtained from the septal and lateral sides of the mitral annulus (E/e′) was calculated to estimate LV filling pressure.[25]

Speckle tracking imaging

Left ventricular deformation was assessed using a semi-automated two-dimensional speckle tracking technique (EchoPac; General Electric Healthcare, Horten, Norway) that analyzed all segments of the left ventricle in the 3 apical views (longitudinal strain) and parasternal short axis view at the papillary muscle level (circumferential strain). The LV strain measurements were performed at a frame rate of 60–80 frames/s. The measurements included the greatest negative value on the strain curve. Global longitudinal (GLS) and circumferential strains (GCS) were calculated as the averages of all LV segments interrogated. If more than 2 segments in a single view remained poorly tracked despite manual correction of the region of interest, global deformation parameters were not computed. All echocardiographic parameters were averaged over 3 consecutive cardiac cycles and reported as absolute values.

BP and hemodynamic measurements

Office brachial BP was measured in duplicate after 10 min of rest in the sitting position using a validated device (Omron HEM 907; Omron Healthcare, Kyoto, Japan). Central hemodynamics were estimated using radial tonometry (SphygmoCor; AtCor Medical, Sydney, Australia) with calibration of radial waveforms, using brachial systolic blood pressure (SBP) and diastolic blood pressure (DBP). This approach seeks to preserve the level of difference in SBP between brachial and central arterial sites, but underestimates the true central aortic SBP.[26] Hence, the focus of this analysis was on waveform indices, including augmented pressure and augmentation index from both, the untransformed radial waveform as well as the derived central waveform. Augmented pressure was assessed as the pressure difference between the 1st and 2nd systolic peaks on the pressure waveforms. Augmentation index was calculated as a percentage of augmented pressure to pulse pressure on the central and radial waveforms. To correct for differences in heart rate (HR), augmented pressure and augmentation index values were adjusted to a standard of 75 bpm. Pulse pressure was computed by the difference between SBP and DBP at brachial and central sites. Pulse pressure amplification was calculated as the ratio of brachial to central pulse pressure. Twenty-four-hour ambulatory BP was recorded using TM 2430 equipment (A&D Mercury, Thebarton, Australia).

Combined BP-echocardiography variables

The ventricular-arterial coupling ratio was calculated as the quotient of aortic (EaI) and LV end-systolic elastance (ELVI) indices, where EaI and ELVI were defined as the ratio of end-systolic pressure to echocardiographic-derived stroke volume index and end-systolic volume index, respectively. End-systolic pressure was computed from the equation 0.9 × brachial SBP.[27] Peripheral vascular resistance index was calculated by mean arterial pressure/cardiac index (the product of two-dimensional stroke volume and HR indexed to body surface area).

Statistical analyses

Data are presented as mean values ± standard deviation (SD) for continuous variables and as counts and percentages for categorical variables. Homogeneity of variances was assessed using the Levene's test. Between groups, comparisons were performed using an unpaired two-sided Students t-test for continuous variables and χ^2 test for categorical variables. The associations of changes in GLS and GCS from baseline to follow-up with other variables were analyzed using Pearson's correlation coefficient and multivariable linear regression analysis. The components of multivariable models were selected on the basis of anticipated and demonstrated univariate associations. Changes in particular parameters were calculated by subtracting the baseline value from the follow-up value, and were expressed in the units of their measurements. The reproducibility of strain measurements was evaluated by the Bland–Altman method (mean difference and 95% confidence interval (95% CI)). All calculations were carried out with standard statistical software (STATISTICA v. 13; StatSoft Inc., Tulsa, USA). The level of statistical significance was set at a two-sided p-value <0.05.

Results

Patients were grouped into 2 subsets depending on the change in the value of GLS after 12 months of antihypertensive therapy: with improvement in GLS (n = 103) and with deterioration in GLS (n = 113).

Patient profile

Baseline demographic, clinical and cardiovascular characteristics according to the change in GLS are presented in Table 1. A significantly lower GLS at baseline was found

Table 1. Baseline demographic, clinical and cardiovascular characteristics according to the change in global longitudinal strain over a 12-month follow-up

Variables	GLS deterioration at follow-up n = 113	GLS improvement at follow-up n = 103	p-value
Age [years]	64.9 ±7.2	63.7 ±8.0	0.23
Male sex, n (%)	51 (45)	52 (50)	0.60
BMI [kg/m^2]	29.4 ±4.6	29.7 ±5.1	0.55
Creatinine [mg/dL]	0.88 ±0.18	0.88 ±0.18	0.96
eGFR [mL/min/1.73 m^2]	82.1 ±14.8	84.1 ±15.1	0.33
Mean 24-hour SBP [mm Hg]	131.1 ±11.5	134.1 ±12.7	0.073
Mean 24-hour DBP [mm Hg]	75.5 ±7.5	77.1 ±7.6	0.13
bSBP [mm Hg]	132.9 ±14.9	130.6 ±12.9	0.24
bDBP [mm Hg]	76.9 ±9.2	77.4 ±9.8	0.66
bPP [mm Hg]	56.0 ±11.8	53.1 ±10.9	0.07
PWV [m/s]	9.5 ±2.2	9.4 ±2.1	0.59
cAGPH HR 75 [%]	21 ±8.7	21 ±9.7	0.87
cAP HR 75 [mm Hg]	9.0 ±4.9	8.9 ±5.1	0.92
rAIx [%]	81 ±13	82 ±16	0.64
PVRI [U/m^2]	53.5 ±23.4	54.3 ±14.4	0.76
Eai	4.2 ±1.9	4.3 ±1.0	0.57
ELVi	8.7 ±3.0	8.2 ±2.5	0.22
VAC	0.51 ±0.27	0.55 ±0.15	0.13
LV diastolic diameter [cm]	4.4 ±0.5	4.3 ±0.4	0.31
LV mass index [g/m^2]	30.9 ±5.3	31.3 ±5.5	0.56
LA volume index [mL/m^2]	32.9 ±9.7	33.5 ±11.3	0.72
LV ejection fraction [%]	62.2 ±4.9	60.8 ±5.7	0.072
GLS [%]	19.4 ±2.1	17.7 ±2.1	**<0.001**
GCS [%]	17.3 ±2.8	17.1 ±2.8	0.64
E/A	0.99 ±0.3	0.96 ±0.2	0.32
DT [ms]	226.9 ±44.5	221.7 ±48.8	0.42
e' septal [cm/s]	6.3 ±1.5	6.1 ±1.4	0.35
e' lateral [cm/s]	8.3 ±1.9	8.0 ±2.0	0.34
E/e'	10.0 ±3.1	9.6 ±2.7	0.37
DDD	2.5 ±1.5	2.4 ±1.4	0.45
ACEi, n (%)	35 (31)	30 (29)	0.77
ARB, n (%)	72 (64)	68 (66)	0.72
CCB, n (%)	33 (29)	35 (34)	0.45
Diuretics, n (%)	44 (39)	39 (38)	0.87
β-blockers, n (%)	11 (10)	11 (11)	0.82

GLS – global longitudinal strain; BMI – body mass index; eGFR – estimated glomerular filtration rate; SBP – systolic blood pressure; DBP – diastolic blood pressure; bSBP – brachial systolic blood pressure; bDBP – brachial diastolic blood pressure; bPP – brachial pulse pressure; PWV – pulse wave velocity; cAGPH HR 75 – central augmentation index at heart rate 75 beats/min; cAP HR 75 – central augmentation pressure at heart rate 75 beats/min; PVRI – peripheral vascular resistance index; Eai – effective arterial elastance index; ELVi – left ventricular elastance index; VAC – ventricular-arterial coupling; LV – left ventricular; LA – left atrium; GCS – global circumferential strain; E/A – ratio of peak early to peak late diastolic mitral inflow velocity; DT – deceleration time; e' – peak early diastolic mitral annular velocity; E/e' – ratio of peak early diastolic mitral inflow velocity to peak early diastolic mitral annular velocity; rAIx – radial augmentation index; DDD – daily defined dose of hypotensive drugs; ACEi – angiotensin-converting enzyme inhibitors; ARB – angiotensin receptor blockers; CCB – calcium channel blockers. The eGFR was calculated according to the CKD-EPI formula (www.nice.org.uk (July 2014)) "Chronic kidney disease in adults: assessment and management". Values in bold are statistically significant.

in patients with the improvement in GLS at follow-up. There were no significant integroup differences in patient age, proportion of male sex, body mass index (BMI), daily defined dose (DDD) of antihypertensive drugs, as well as echocardiographic, BP, or hemodynamic measurements.

Blood pressure and cardiovascular characteristics

The subset with improvement in GLS demonstrated more favorable changes over follow-up in pulse wave velocity, central augmentation pressure at HR 75 beats/min, VAC, GCS, and septal peak early diastolic mitral annular velocity compared to patients with deterioration in GLS (Table 2).

Correlates of LV functional characteristics

Univariate associations of changes in GLS and GCS from baseline to follow-up, with baseline values of demographic, clinical and cardiovascular characteristics are presented in Table 3, and analogous associations with changes from baseline to follow-up in clinical and cardiovascular parameters are shown in Table 4. Among significant correlates of change in GLS at 12 months were pulse wave velocity, VAC, effective arterial elastance index, central augmentation pressure, and index at HR 75 beats/min, whereas significant correlates of change in GCS were DBP, central augmentation pressure and index at HR of 75 beats/min.

Multivariable linear regression models illustrated that the independent determinants of changes in GLS at a follow-up were GLS at baseline and changes over follow-up in central augmentation pressure and VAC, whereas the independent determinants of changes in GCS were GCS at baseline and changes over follow-up in central augmentation pressure or index (Table 5). Changes over follow-up in central augmentation pressure and index were not combined into a single multivariable model due to strong collinearity (r = 0.85). Similar but not statistically significant results were demonstrated for radial augmentation index when used instead of central augmentation parameters (Table 6).

Change in effective arterial elastance index over follow-up was tested in multivariable models instead of change in VAC (a very strong collinearity between these 2 variables with r = 0.95), but did not prove to be a significant determinant of either delta GLS (p = 0.069) or delta GCS (p = 0.71).

Table 2. Changes in clinical and cardiovascular characteristics according to changes in global longitudinal strain over a 12-month follow-up

Variables	GLS deterioration at follow-up n = 113	GLS improvement at follow-up n = 103	p-value
Δ DDD	−0.36 ±0.95	−0.19 ±0.93	0.20
Δ Mean 24-hour SBP [mm Hg]	4.1 ±10.5	1.9 ±12.9	0.18
Δ Mean 24-hour DBP [mm Hg]	1.4 ±6.1	1.2 ±8	0.90
Δ bSBP [mm Hg]	−1.2 ±15.9	−1.3 ±12.3	0.96
Δ bDBP [mm Hg]	0.05 ±9.0	−0.7 ±8.9	0.54
Δ bPP [mm Hg]	−1.3 ±10.8	−0.6 ±8.2	0.62
Δ PWV [m/s]	0.3 ±1.6	−0.3 ±1.9	**0.026**
Δ cAGPH HR 75 [%]	1.2 ±7.5	−0.5 ±6.3	0.09
Δ cAP HR 75 [mm Hg]	0.7 ±4.5	−0.7 ±3.4	**0.012**
Δ rAIx [%]	1.4 ±12.7	−1.2 ±10.5	0.11
Δ PVRI [U/m^2]	4.4 ±24.3	−1 ±28.2	0.15
Δ Eai	0.3 ±1.7	−0.1 ±1.7	0.079
Δ ELVi	0.1 ±1.1	−0.1 ±0.8	0.29
Δ VAC	0.05 ±0.24	−0.01 ±0.20	**0.049**
Δ LV diastolic diameter [cm]	−0.06 ±0.4	0.004 ±0.5	0.33
Δ LV mass index [g/m^2]	0.07 ±2.6	−0.25 ±2.0	0.43
Δ LA volume index [mL/m^2]	−0.48 ±7.1	0.32 ±9.2	0.48
Δ LV ejection fraction [%]	−0.05 ±5.3	1.3 ±5.8	0.085
Δ GLS [%]	−1.4 ±1.2	1.5 ±1.0	**<0.001**
Δ GCS [%]	−0.2 ±2.8	1.1 ±2.5	**<0.001**
Δ E/A	−0.02 ±0.27	0.02 ±0.22	0.28
Δ DT [ms]	7.2 ±52.9	5.0 ±55.6	0.78
Δ e′ septal [cm/s]	−0.4 ±1.3	0.09 ±1.3	**0.005**
Δ e′ lateral [cm/s]	−0.6 ±1.5	−0.2 ±1.8	0.094
Δ E/e′	0.5 ±2.3	0.3 ±2.8	0.56

Δ – change at 12-month follow-up (follow-up value minus baseline value); DDD – daily defined dose of hypotensive drugs; SBP – systolic blood pressure; DBP – diastolic blood pressure; bSBP – brachial systolic blood pressure; bDBP – brachial diastolic blood pressure; bPP – brachial pulse pressure; PWV – pulse wave velocity; cAGPH HR 75 – central augmentation index at heart rate 75 beats/min; cAP HR 75 – central augmentation pressure at heart rate 75 beats/min; Eai – effective arterial elastance index; PVRI – peripheral vascular resistance index; LV – left ventricular; LA – left atrial; GLS – global longitudinal strain; GCS – global circumferential strain; VAC – ventricular-arterial coupling; E/A – ratio of peak early to peak late diastolic mitral inflow velocity; DT – deceleration time; e′ – peak early diastolic mitral annular velocity; E/e′ – ratio of peak early diastolic mitral inflow velocity to peak early diastolic mitral annular velocity; rAIx – radial augmentation index. Values in bold are statistically significant.

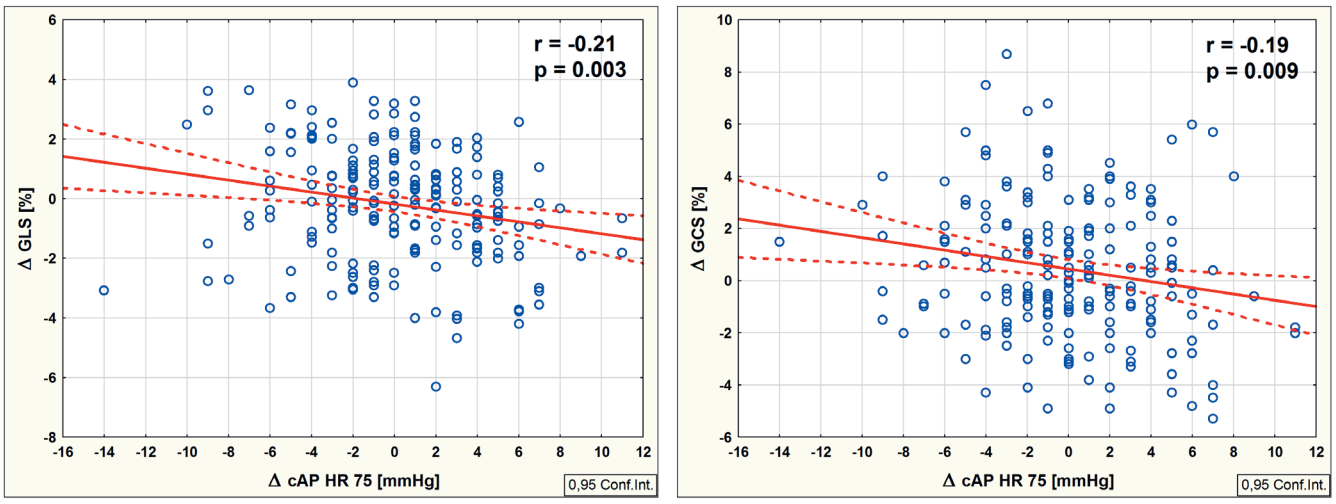

Fig. 1. Associations between changes in central augmentation pressure and changes in left ventricular global longitudinal and circumferential deformation over a 12-month follow-up. cAP HR 75 – central augmentation pressure at heart rate 75 beats/min; GLS – global longitudinal strain; GCS – global circumferential strain

Table 3. Univariable associations of changes in global longitudinal strain and circumferential strain at a 12-month follow-up with demographic, clinical and cardiovascular characteristics at baseline

Variables	Δ GLS		Δ GCS	
	r	p-value	r	p-value
Age [years]	–0.01	0.90	0.01	0.83
BMI [kg/m^2]	0.03	0.62	0.01	0.97
DDD	–0.05	0.42	–0.03	0.69
Mean 24-hour SBP [mm Hg]	0.08	0.22	0.19	**0.007**
Mean 24-hour DBP [mm Hg]	0.07	0.31	0.18	**0.009**
bSBP [mm Hg]	–0.04	0.57	0.04	0.58
bDBP [mm Hg]	0.05	0.44	0.07	0.34
bPP [mm Hg]	–0.09	0.18	–0.01	0.90
PWV [m/s]	0.01	0.82	0.01	0.90
cAGPH HR 75 [%]	0.04	0.51	–0.04	0.55
cAP HR 75 [mm Hg]	0.02	0.77	–0.01	0.85
rAIx [%]	0.08	0.26	–0.05	0.50
PVRI [U/m^2]	0.08	0.24	0.02	0.82
Eai	0.09	0.20	0.05	0.48
ELVi	–0.10	0.15	–0.13	0.077
VAC	0.17	**0.016**	0.15	**0.035**
LV diastolic diameter [cm]	–0.07	0.33	0.13	0.076
LV mass index [g/m^2]	0.03	0.69	0.05	0.48
LA volume index [mL/m^2]	–0.03	0.69	0.09	0.19
LV ejection fraction [%]	–0.13	0.078	–0.12	0.10
GLS [%]	–0.48	**<0.001**	–0.16	**0.027**
GCS [%]	–0.08	0.27	–0.46	**<0.001**

BMI – body mass index; DDD – daily defined dose of hypotensive drugs; SBP – systolic blood pressure; DBP – diastolic blood pressure; bSBP – brachial systolic blood pressure; bDBP – brachial diastolic blood pressure; bPP – brachial pulse pressure; PWV – pulse wave velocity; cAGPH HR 75 – central augmentation index at heart rate 75 beats/min; cAP HR 75 – central augmentation pressure at heart rate 75 beats/min; PVRI – peripheral vascular resistance index; Eai – effective arterial elastance index; ELVi – left ventricular elastance index; VAC – ventricular-arterial coupling; LV – left ventricular; LA – left atrium; GLS – global longitudinal strain; GCS – global circumferential strain; rAIx – radial augmentation index. Values in bold are statistically significant.

Scatterplots illustrating associations between changes in central augmentation pressure at a HR of 75 beats/min and LV longitudinal and circumferential function are presented in Fig. 1.

Sensitivity analysis

To check the robustness of results, we changed the input variables by restricting the dataset to the upper and lower delta GLS tertiles. This analysis confirmed the relationships between multivariable predictors (for example, the changes over follow-up in central augmentation pressure and index, or VAC), and changes in GLS and GCS (Table 7).

Reproducibility

The intra-observer variability of myocardial deformation measurements was assessed in 15 randomly selected examinations, and was analyzed twice on 2 separate days within a four-week time interval. The variability was –0.3% (–0.7; 0.2) for the LV longitudinal strain and 0.5% (–0.5; 1.4) for the circumferential strain.

Discussion

The current study confirmed the link between LV function and central hemodynamic and aortic characteristics by showing independent associations between temporal and treatment-associated changes in GLS, and changes in central augmentation pressure and VAC, as well as between analogous changes in GCS and central augmentation pressure. Thus, our findings emphasize the role of central loading factors in the pathophysiology of HHD, and support the need for extending BP assessments beyond standard cuff measurements to effectively manage myocardial complications of HT.

Existing evidence indicates the importance of both central and peripheral BP measurements due to their associations with cardiac, renal and vascular injury. Recognition of target organ damage is essential for clinical

Table 4. Univariable associations of changes in global longitudinal strain and circumferential strain with changes in clinical and cardiovascular characteristics at a 12-month follow-up

Variables	Δ GLS		Δ GCS	
	r	p-value	r	p-value
Δ DDD	0.10	0.16	0.11	0.15
Δ Mean 24-hour SBP [mm Hg]	–0.07	0.34	0.04	0.63
Δ Mean 24-hour DBP [mm Hg]	–0.01	0.93	0.01	0.88
Δ bSBP [mm Hg]	–0.07	0.30	–0.09	0.24
Δ bDBP [mm Hg]	–0.12	0.094	–0.15	**0.039**
Δ bPP [mm Hg]	0.02	0.98	0.01	0.94
Δ PWV	–0.17	**0.015**	0.05	0.52
Δ cAGPH HR 75 [%]	–0.15	**0.034**	–0.18	**0.013**
Δ cAP HR 75 [mm Hg]	–0.21	**0.003**	–0.19	**0.009**
Δ rAIx [%]	–0.13	0.063	–0.14	0.051
Δ PVRI [U/m^2]	–0.13	0.059	0.01	0.99
Δ Eai	–0.17	**0.011**	–0.04	0.60
Δ ELVi	0.09	0.20	–0.01	0.87
Δ VAC	–0.20	**0.003**	–0.02	0.83
Δ LV diastolic diameter [cm]	0.12	0.094	0.04	0.56
Δ LV mass index [g/m^2]	–0.01	0.84	0.02	0.74
Δ LA volume index [mL/m^2]	0.06	0.40	0.02	0.83
Δ LV ejection fraction [%]	0.13	0.072	0.02	0.77

Δ – change at 12-month follow-up (follow-up value minus baseline value); DDD – daily defined dose of hypotensive drugs; SBP – systolic blood pressure; DBP – diastolic blood pressure; bSBP – brachial systolic blood pressure; bDBP – brachial diastolic blood pressure; bPP – brachial pulse pressure; PWV – pulse wave velocity; cAGPH HR 75 – central augmentation index at heart rate 75 beats/min; cAP HR 75 – central augmentation pressure at heart rate 75 beats/min; PVRI – peripheral vascular resistance index; Eai – effective arterial elastance index; LV – left ventricular; LA – left atrial; GLS – global longitudinal strain; VAC – ventricular-arterial coupling; rAIx – radial augmentation index. Values in bold are statistically significant.

Table 5. Multivariable associations of the change in global longitudinal and circumferential strains at a 12-month follow-up. Models with central augmentation parameters

Variables	Model 1 Δ GLS $R^2 = 0.29$			Model 2 Δ GLS $R^2 = 0.28$			Model 3 Δ GCS $R^2 = 0.25$			Model 4 Δ GCS $R^2 = 0.26$		
	β	SE	p-value	β	SE	p-value	β	SE	p-value	β	SE	p-value
GLS at baseline	–0.45	0.07	**<0.001**	–0.46	0.07	**<0.001**	–	–	–	–	–	–
GCS at baseline	–	–	–	–	–	–	–0.45	0.07	**<0.001**	–0.47	0.07	**<0.001**
Δ cAP HR 75	–0.17	0.07	**0.016**	–	–	–	–0.16	0.07	**0.024**	–	–	–
Δ cAGPH HR 75	–	–	–	–0.13	0.07	0.051	–	–	–	–0.19	0.07	**0.006**
Δ VAC	–0.16	0.07	**0.014**	–0.15	0.07	**0.019**	0.03	0.07	0.68	0.04	0.07	0.59
Δ PWV	–0.07	0.07	0.27	–0.09	0.07	0.18	0.11	0.07	0.14	0.10	0.07	0.17
Δ Mean 24-hour SBP	0.03	0.07	0.62	0.02	0.07	0.76	0.04	0.07	0.63	0.03	0.07	0.71
Δ DDD	–0.01	0.07	0.83	0.01	0.07	0.91	0.04	0.07	0.60	0.03	0.07	0.64

Δ – change at 12-month follow-up (follow-up value minus baseline value); GLS – global longitudinal strain; GCS – global circumferential strain; cAP HR 75 – central augmentation pressure at heart rate 75 beats/min; cAGPH HR 75 – central augmentation index at heart rate 75 beats/min; VAC – ventricular-arterial coupling; PWV – pulse wave velocity; SBP – systolic blood pressure; DDD – daily defined dose of hypertension drugs; SE – standard error. Values in bold are statistically significant.

risk stratification in hypertensive patients, and reducing the occurrence and severity of these complications represents a major goal of current therapy. Central BP and associated indices including augmented pressure, central pulse pressure, and effective arterial elastance index have been found to be more closely related to the target organ damage expressed as LV hypertrophy, cardiac dysfunction, and increased carotid intima media thickness, and are believed to reflect LV afterload more accurately than brachial BP measurements.[28–31] Nonetheless, derived measures of central augmentation index are highly correlated with peripheral (radial) augmentation index[32] (e.g.,

Table 6. Multivariable associations of the change in global longitudinal and circumferential strains at a 12-month follow-up. Models with radial augmentation index

Variables	Model 1 Δ GLS $R^2 = 0.28$			Model 2 Δ GCS $R^2 = 0.24$		
	β	SE	p-value	β	SE	p-value
GLS at baseline	–0.46	0.07	**<0.001**	–	–	–
GCS at baseline	–	–	–	–0.46	0.07	**<0.001**
Δ rAIx	–0.11	0.07	0.10	–0.13	0.07	0.057
Δ VAC	–0.15	0.07	**0.026**	0.04	0.07	0.53
Δ PWV	–0.10	0.07	0.13	0.08	0.07	0.25
Δ Mean 24-hour SBP	0.02	0.07	0.72	0.03	0.07	0.70
Δ DDD	–0.003	0.07	0.97	0.05	0.07	0.53

Δ – change at 12-month follow-up (follow-up value minus baseline value); GLS – global longitudinal strain; GCS – global circumferential strain; cAP HR 75 – central augmentation pressure at heart rate 75 beats/min; cAGPH HR 75 – central augmentation index at heart rate 75 beats/min; VAC – ventricular-arterial coupling; PWV – pulse wave velocity; SBP – systolic blood pressure; DDD – daily defined dose of hypertension drugs; rAIx – radial augmentation index. Values in bold are statistically significant.

Table 7. Sensitivity analysis

Variables	GLS deterioration at follow-up n = 72	GLS improvement at follow-up n = 172	p-value	Δ GLS		Δ GCS	
				r	p-value	r	p-value
Δ PWV	0.33 ±1.75	–0.23 ±2.18	0.10	–0.14	0.11	0.01	0.88
Δ cAGPH HR 75 [%]	1.29 ±7.79	–1.16 ±5.97	**0.048**	–0.19	**0.029**	–0.20	**0.035**
Δ cAP HR 75 [mm Hg]	0.71 ±4.65	–1.06 ±3.60	**0.017**	–0.25	**0.004**	–0.27	**0.004**
Δ VAC	0.08 ±0.30	–0.02 ±0.23	**0.034**	–0.22	**0.010**	–0.02	0.81

GLS – global longitudinal strain; Δ – change at 12-month follow-up (follow-up value minus baseline value); GCS – global circumferential strain; PWV – pulse wave velocity; cAGPH HR 75 – central augmentation index at heart rate 75 beats/min; cAP HR 75 – central augmentation pressure at heart rate 75 beats/min; VAC – ventricular-arterial coupling. Values in bold are statistically significant.

r = 0.96); therefore, we would expect similar associations of changes in both central and radial augmentation index with changes in GLS and GCS. These associations were observed in the current study, which highlights the potential value of using non-transformed peripheral waveform parameters as risk stratification tools to supplement derived central BP measures that may be subject to error from cuff calibration and generalized transfer functions.[33–35]

The link between LV load and myocardial function is well-documented.[36] The value of LV multidirectional deformation results from loading conditions and myocardial determinants, including passive tissue characteristics, crossover of myofibers in the subendocardial and subepicardial layers, and direction of myofibers. Impairment in GLS represents the first step in the cascade of LV remodeling in the natural history of HHD, and may parallel or even precede other clinical forms of myocardial affection such as LV hypertrophy, diastolic dysfunction, or left atrial structural and functional abnormalities.[37–42] Conversely, LV circumferential performance deteriorates in more advanced stages of the disease, and may even increase the asymptomatic phase of heart failure (stage B) to compensate for the dysfunction in the longitudinal direction.[10,43–48]

This paper demonstrated that changes in LV longitudinal systolic deformation over follow-up were associated with alterations in relevant LV afterload-associated indices, among which central augmentation pressure remained an independent predictor after multivariable adjustments for possible confounders. Similar to GLS, the independent contribution from central augmentation pressure parameters was evident for LV circumferential strain as well. Moreover, we discovered that the interaction between the left ventricle and arterial system as assessed by VAC, representing net cardiovascular performance, independently determined changes in LV longitudinal strain. Importantly, our results demonstrated superiority of comprehensive evaluation of LV afterload, using non-invasive hemodynamic parameters derived from PWA over cuff BP measurement, in the context of LV function changes during antihypertensive therapy.

A stronger association between hypertension-related abnormalities of myocardial performance with pulse wave parameters rather than with brachial BP has been reported in previous papers;[17,49–51] however, a lack of research currently exists regarding the analogous interaction with respect to changes in LV strain over time. Accordingly, our analysis expounds upon prior reports by using repeated observations at the individual level, which may support

a causal nature of demonstrated relationships. However, as this study is retrospective, a post hoc analysis of the results from a randomized clinical trial should be regarded as hypothesis-generating. Despite the different trajectories in the early phase of HHD, both GLS and GCS are prone to the adverse influence of LV afterload. Thus, the extension of diagnostic focus over these 2 components of LV systolic function from the beginning of patient follow-up may be reasonable to track myocardial pathology in order to assist in therapeutic decision-making. Recognition for the role of hemodynamic loading factors and myocardial deformation, especially GLS – a widely recognized prognosticator in patient management strategy, might provide further clinical benefits. Our results provisionally support the concept of using non-invasive large artery hemodynamic assessment as a clinical rather than a research-only tool.

Limitations

This study population profile encompassing low to medium risk subjects with uncomplicated HT constrains the ability to extrapolate the results to other cohorts, especially with severe HT or advanced HHD. The estimations of central hemodynamics in the current analysis were acquired noninvasively and using a calibration, based on brachial cuff systolic and DBP. Thus, the readings will not be the same as invasively measured BP waveforms.

Conclusions

In hypertensive patients, LV longitudinal and circumferential functional remodeling over time is associated with arterial hemodynamic characteristics. This may indicate the need for pulse wave analysis to optimize patient care.

ORCID iDs

Anna Teresa Goździk https://orcid.org/0000-0002-8182-5586
Ewelina Jasic-Szpak https://orcid.org/0000-0002-4976-2589
Jakub Michałowicz https://orcid.org/0000-0002-4940-4108
Monika Przewłocka-Kosmala https://orcid.org/0000-0002-4054-6521
James Edward Sharman https://orcid.org/0000-0003-2792-0811
Wojciech Kosmala https://orcid.org/0000-0003-3807-8201

References

1. Fung MJ, Thomas L, Leung DY. Left ventricular function and contractile reserve in patients with hypertension. *Eur Heart J Cardiovasc Imaging*. 2018;19(11):1253–1259. doi:10.1093/ehjci/jex338
2. Lee WH, Liu YW, Yang LT, Tsai WC. Prognostic value of longitudinal strain of subepicardial myocardium in patients with hypertension. *J Hypertens*. 2016;34(6):1195–1200. doi:10.1097/HJH.0000000000000903
3. Modin D, Biering-Sorensen SR, Mogelvang R, Landler N, Jensen JS, Biering-Sorensen T. Prognostic value of echocardiography in hypertensive versus nonhypertensive participants from the general population. *Hypertension*. 2018;71(4):742–751. doi:10.1161/HYPERTENSIONAHA.117.10674
4. Cheng S, McCabe EL, Larson MG, et al. Distinct aspects of left ventricular mechanical function are differentially associated with cardiovascular outcomes and all-cause mortality in the community. *J Am Heart Assoc*. 2015;4(10):e002071. doi:10.1161/JAHA.115.002071
5. Mancusi C, Losi MA, Izzo R, et al. Higher pulse pressure and risk for cardiovascular events in patients with essential hypertension: The Campania Salute Network. *Eur J Prev Cardiol*. 2018;25(3):235–243. doi:10.1177/2047487317747498
6. Galderisi M, Trimarco B. Global longitudinal strain: A novel hallmark of cardiac risk in arterial hypertension. *J Hypertens*. 2016;34(6):1050–1051. doi:10.1097/HJH.0000000000000920
7. de Simone G, Mancusi C, Esposito R, De Luca N, Galderisi M. Echocardiography in arterial hypertension. *High Blood Press Cardiovasc Prev*. 2018;25(2):159–166. doi:10.1007/s40292-018-0259-y
8. Shin SM, Shim WJ, Park SM. Early changes of left ventricular function in young adults with never-treated hypertension and no left ventricular hypertrophy: Relationships to ambulatory blood pressure monitoring. *Clin Exper Hypertens*. 2014;36(7):517–523. doi:10.3109/10641963.2013.863326
9. Sun JP, Xu T, Yang Y, et al. Layer-specific quantification of myocardial deformation may disclose the subclinical systolic dysfunction and the mechanism of preserved ejection fraction in patients with hypertension. *Int J Cardiol*. 2016;219:172–176. doi:10.1016/j.ijcard.2016.06.035
10. Ballo P, Nistri S, Cameli M, et al. Association of left ventricular longitudinal and circumferential systolic dysfunction with diastolic function in hypertension: A nonlinear analysis focused on the interplay with left ventricular geometry. *J Card Fail*. 2014;20(2):110–120. doi:10.1016/j.cardfail.2013.12.009
11. Kraigher-Krainer E, Shah AM, Gupta DK, et al. Impaired systolic function by strain imaging in heart failure with preserved ejection fraction. *J Am Coll Cardiol*. 2014;63(5):447–456. doi:10.1016/j.jacc.2013.09.052
12. Kaess BM, Rong J, Larson MG, et al. Relations of central hemodynamics and aortic stiffness with left ventricular structure and function: The Framingham Heart Study. *J Am Heart Assoc*. 2016;5(3):e002693. doi:10.1161/JAHA.115.002693
13. Kaess BM, Rong J, Larson MG, et al. Aortic stiffness, blood pressure progression, and incident hypertension. *JAMA*. 2012;308(9):875–881. doi:10.1001/2012.jama.10503
14. Russo C, Jin Z, Takei Y, et al. Arterial wave reflection and subclinical left ventricular systolic dysfunction. *J Hypertens*. 2011;29(3):574–582. doi:10.1097/HJH.0b013e328342ca56
15. Russo C, Jin Z, Palmieri V, et al. Arterial stiffness and wave reflection: Sex differences and relationship with left ventricular diastolic function. *Hypertension*. 2012;60(2):362–368. doi:10.1161/HYPERTENSIONAHA.112.191148
16. Kim HL, Seo JB, Chung WY, Kim SH, Kim MA, Zo JH. Independent association between brachial-ankle pulse wave velocity and global longitudinal strain of left ventricle. *Int J Cardiovasc Imaging*. 2015;31(8):1563–1570. doi:10.1007/s10554-015-0744-5
17. Ye Z, Coutinho T, Pellikka PA, Villarraga HR, Borlaug BA, Kullo IJ. Associations of alterations in pulsatile arterial load with left ventricular longitudinal strain. *Am J Hypertens*. 2015;28(11):1325–1331. doi:10.1093/ajh/hpv039
18. Krishnasamy R, Hawley CM, Stanton T, et al. Left ventricular global longitudinal strain is associated with cardiovascular risk factors and arterial stiffness in chronic kidney disease. *BMC Nephrol*. 2015;16:106. doi:10.1186/s12882-015-0098-1
19. Negishi K, Yang H, Wang Y, et al. Importance of calibration method in central blood pressure for cardiac structural abnormalities. *Am J Hypertens*. 2016;29(9):1070–1076. doi:10.1093/ajh/hpw039
20. Protogerou AD, Argyris AA, Papaioannou TG, et al. Left-ventricular hypertrophy is associated better with 24-h aortic pressure than 24-h brachial pressure in hypertensive patients: The SAFAR study. *J Hypertens*. 2014;32(9):1805–1814. doi:10.1097/HJH.0000000000000263
21. Zhang Y, Kollias G, Argyris AA, et al. Association of left ventricular diastolic dysfunction with 24-h aortic ambulatory blood pressure: The SAFAR study. *J Hum Hypertens*. 2015;29(7):442–448. doi:10.1038/jhh.2014.101
22. Sharman JE, Marwick TH, Abhayaratna WP, Stowasser M. Rationale and design of a randomized study to determine the value of central Blood Pressure for GUIDing managEment of hypertension: The BP GUIDE study. *Am Heart J*. 2012;163(5):761–767. doi:10.1016/j.ahj.2012.02.017
23. WHO Collaborating Centre for Drug Statistics Methodology. Norwegian Institute of Public Health. Daily Defined Dose: Definition and General Considerations. www.whocc.no/ddd/definition_and_general_considera. Accessed January 10, 2019.

24. Lang RM, Bierig M, Devereux RB, et al. Recommendations for cardiac chamber quantification by echocardiography in adults: An update from the American Society of Echocardiography and the European Association of Cardiovascular Imaging. *Eur Heart J Cardiovasc Imaging*. 2015;16(3):233–271. doi:10.1093/ehjci/jev014
25. Nagueh SF, Smiseth OA, Appleton CP, et al. Recommendation for the evaluation of left ventricular diastolic function by echocardiography: An update from the American Society of Echocardiography and the European Association of Cardiovascular Imaging. *J Am Soc Echocardiogr*. 2016;29(4):277–314. doi:10.1016/j.echo.2016.01.011
26. Sharman JE, Avolio AP, Baulmann J, et al. Validation of non-invasive central blood pressure devices: ARTERY Society task force consensus statement on protocol standardization. *Eur Heart J*. 2017;38(37): 2805–2812. doi:10.1093/eurheartj/ehw632
27. Chen CH, Fetics B, Nevo E, et al. Noninvasive single-beat determination of left ventricular endsystolic elastance in humans. *J Am Coll Cardiol*. 2001;38(7):2028–2034. doi:10.1016/s0735-1097(01)01651-5
28. Kollias A, Lagou S, Zeniodi ME, Boubouchairpoulou N, Sterigou GS. Association of central versus brachial blood pressure with Target-Organ Damage: Systematic review and meta-analysis. *Hypertension*. 2016;67(1):183–190. doi:10.1161/HYPERTENSIONAHA.115.06066
29. Sharman JE, Laurent S. Central blood pressure in the management of hypertension: Soon reaching the goal? *J Hum Hypertens*. 2013; 27(7):405–411. doi:10.1038/jhh.2013.23
30. Armstrong MK, Schultz MG, Picone DS, Sharman JE. Aortic to brachial artery stiffness gradient is not blood pressure independent. *J Hum Hypertens*. 2019;33(5):385–392. doi:10.1038/s41371-018-0154-y
31. Climie RE, Schultz MG, Fell JW, Romero L, Otahal P, Sharman JE. Central to brachial blood pressure amplification in type 2 diabetes: A systematic review and meta-analysis. *J Hum Hypertens*. 2019;33(2):94–105. doi:10.1038/s41371-018-0124-4
32. Millasseau SC, Patel SJ, Redwood SR, Ritter JM, Chowienczyk PJ. Pressure wave reflection assessed from the peripheral pulse: Is a transfer function necessary? *Hypertension*. 2003;41(5):1016–1020. doi:10.1161/01.HYP.0000057574.64076.A5
33. Picone DS, Schultz MG, Otahal P, et al. Accuracy of cuff-measured blood pressure: Systematic reviews and meta-analyses. *J Am Coll Cardiol*. 2017;70(5):572–586. doi:10.1016/j.jacc.2017.05.064
34. Schultz MG, Picone DS, Armstrong MK, et al. Validation study to determine the accuracy of central blood pressure measurement using the sphygmocor xcel cuff device. *Hypertension*. 2020;76(1):244–250. doi:10.1161/HYPERTENSIONAHA.120.14916
35. Picone DS, Schultz MG, Peng X, et al. Intra-arterial analysis of the best calibration methods to estimate aortic blood pressure. *J Hypertens*. 2019;37(2):307–315. doi:10.1097/HJH.0000000000001902
36. Kosmala W, Przewlocka-Kosmala M, Sharman JE, Schultz MG, Marwick TH. Stability of left ventricular longitudinal and circumferential deformation over time and standard loading conditions. *Eur Heart J Cardiovasc Imaging*. 2017;18(9):1001–1007. doi:10.1093/ehjci/jew135
37. Kosmala W, Plaksej R, Strotmann JM, et al. Progression of left ventricular functional abnormalities in hypertension patients with heart failure: An ultrasonic two dimensional speckle tracking study. *J Am Soc Echocardiogr*. 2008;21(12):1309–1317. doi:10.1016/j.echo.2008.10.006
38. Lembo M, Esposito R, Li F, et al. Impact of pulse pressure on left ventricular global longitudinal strain in normotensive and newly diagnosed, untreated hypertensive patients. *J Hypertens*. 2016;34(6): 1201–1207. doi:10.1097/HJH.0000000000000906
39. Przewlocka-Kosmala M, Jasic-Szpak E, Rojek A, Kabaj M, Sharman JE, Kosmala W. Association of central blood pressure with left atrial structural and functional abnormalities in hypertensive patients: Implications for atrial fibrillation prevention. *Eur J Prev Cardiol*. 2019; 26(10):1018–1027. doi:10.1177/2047487319839162
40. Szelenyi Z, Fazakas A, Szenasi G, et al. The mechanism of reduced longitudinal left ventricular systolic function in hypertensive patients with normal ejection fraction. *J Hypertens*. 2015;33(9):1962–1969. doi:10.1097/HJH.0000000000000624
41. Kosmala W, Marwick TH, Stanton T, Abhayaratna WP, Stowasser M, Sharman JE. Guiding hypertension management using central blood pressure: Effect of medication withdrawal on left ventricular function. *Am J Hypertens*. 2016;29(3):319–325. doi:10.1093/ajh/hpv108
42. Huang H, Ruan Q, Lin M, Yan L, Huang Ch, Fu L. Investigation on left ventricular multidirectional deformation in patients of hypertension with different LVEF. *Cardiovascular Ultrasound*. 2017;15(1):14. doi:10.1186/s12947-017-0106-7
43. Russo C, Jin Z, Elkind MS, et al. Prevalence and prognostic value of subclinical left ventricular systolic dysfunction by global longitudinal strain in a community-based cohort. *Eur J Heart Fail*. 2014;16(12): 1301–1309. doi:10.1002/ejhf.154
44. Tadic M, Majstorovic A, Pencic B, et al. The impact of high-normal blood pressure on left ventricular mechanics: A three-dimensional and speckle tracking echocardiography study. *Int J Cardiovasc Imaging*. 2014;30(4):699–711. doi:10.1007/s10554-014-0382-3
45. Tadic M, Cuspidi C. Left ventricular strain and arterial hypertension: Is longitudinal strain ready for primetime? *J Clin Hypertens*. 2020;22(4): 683–685. doi:10.1111/jch.13833
46. Przewlocka-Kosmala M, Kosmala W, Mazurek W. Left ventricular circumferential function in patients with essential hypertension. *J Hum Hypertens*. 2006;20(9):666–671. doi:10.1038/sj.jhh.1002054
47. Morris DA, Otani K, Bekfani T, et al. Multidirectional global left ventricular systolic function in normal subjects and patients with hypertension: Multicenter evaluation. *J Am Soc Echocardiogr*. 2014;27(5): 493–500. doi:10.1016/j.echo.2014.01.017
48. Kim D, Shim CHY, Hong GR, et al. Differences in left ventricular functional adaptation to arterial stiffness and neurohormonal activation in patients with hypertension: A study with two-dimensional layer-specific speckle tracking echocardiography. *Clin Hypertens*. 2017;23:21. doi:10.1186/s40885-017-0078-9
49. Hwang JW, Kang SJ, Lim HS, et al. Impact of arterial stiffness on regional myocardial function assessed by speckle tracking echocardiography in patients with hypertension. *J Cardiovasc Ultrasound*. 2012;20(2):90–96. doi:10.4250/jcu.2012.20.2.90
50. Kim HL, Lim WH, Jae-Bin Seo JB, et al. Association between arterial stiffness and left ventricular diastolic function in relation to gender and age. *Medicine (Baltimore)*. 2017;96(1):e5783. doi:10.1097/MD.0000000000005783
51. Krzesiński P, Uziębło-Życzkowska B, Gielerak G, Stańczyk A, Kurpaska M, Piotrowicz K. Global longitudinal two-dimensional systolic strain is associated with hemodynamic alterations in arterial hypertension. *J Am Soc Hypertens*. 2015;9(9):680–689. doi:10.1016/j.jash.2015.06.014

Cholecystokinin-mediated pharmacological preconditioning effects on ischemic rat hearts: Possible signaling pathways

Yuan Cheng[B], Mengzuo Wu[B], Min Liu[C], Birong Zhou[C], Xianhe Lin[D], Bangning Wang[A,E,F]

Department of Cardiology, The First Affiliated Hospital of Anhui Medical University, Hefei, China

A – research concept and design; B – collection and/or assembly of data; C – data analysis and interpretation;
D – writing the article; E – critical revision of the article; F – final approval of the article

Advances in Clinical and Experimental Medicine, ISSN 1899–5276 (print), ISSN 2451–2680 (online) *Adv Clin Exp Med*. 2021;30(11):1157–1165

Address for correspondence
Bangning Wang
E-mail: wangbangning453@sina.com

Funding sources
None declared

Conflict of interest
None declared

Received on March 18, 2021
Reviewed on May 28, 2021
Accepted on June 10, 2021

Published online on September 10, 2021

Abstract

Background. Cholecystokinin (CCK-8) has been shown to exhibit pharmacological preconditioning and cardioprotective effects. However, the molecular mechanisms involved in CCK-8-induced pharmacological preconditioning have not yet been clarified.

Objectives. The current study explored the molecular mechanisms involved in CCK-8-mediated pharmacological preconditioning effects on ischemic rat hearts.

Materials and methods. Pharmacological preconditioning was induced in male Wistar rats by administration of CCK-8 (20 μg/kg) 24 h before heart isolation. The PI3K inhibitor LY294002 (10 mg/kg and 20 mg/kg) and the HIF-1α inhibitor YC-1 (1 mg/kg and 2 mg/kg) were administered 30 min before the administration of CCK-8. The hearts were subjected to ischemia-reperfusion (IR) injury using a Langendorff apparatus. Myocardial injury was quantified by measuring the release of LDH-1, CK-MB and cTnT. The levels of HIF-1α and p-Akt expression and the ratio of p-GSK-3β/GSK-3β, were assessed in the heart homogenates.

Results. Pharmacological preconditioning with CCK-8 reduced IR-induced increases in the release of LDH, CK-MB and cTnT. Moreover, it restored the expression of HIF-1α and p-Akt, and the p-GSK-3β/GSK-3β ratio. However, administration of LY294002 or YC-1 with CCK-8 significantly abolished the cardioprotective effects of pharmacological preconditioning. The PI3K and HIF-1α inhibitors also abolished the effects of CCK-8 preconditioning on HIF-1α, p-Akt and p-GSK-3β/GSK-3β.

Conclusions. Based on these findings, it may be concluded that the molecular mechanisms participating in CCK-8-induced pharmacological preconditioning involve HIF-1α, PI3K, Akt, and GSK-3β signaling pathways.

Key words: ischemia, reperfusion, LY294002, cholecystokinin, pharmacological preconditioning

Cite as
Cheng Y, Wu M, Liu M, Zhou B, Lin X, Wang B. Cholecystokinin-mediated pharmacological preconditioning effects on ischemic rat hearts: Possible signaling pathways. *Adv Clin Exp Med*. 2021;30(11):1157–1165. doi:10.17219/acem/138745

DOI
10.17219/acem/138745

Background

Interruption of blood flow in the form of ischemia induces severe heart injury, and early restoration of blood flow is essential to salvage ischemic heart. Thrombolysis or angioplasty is typically employed in clinical settings to restore the blood supply to ischemic heart.[1] However, reperfusion of the ischemic heart itself produces myocardial injury, which is referred to as "reperfusion injury".[2] Therefore, the term "ischemia-reperfusion-induced myocardial injury" is used to denote myocardial injury that occurs during ischemia and reperfusion (IR). At present, there are no well-established pharmacological agents to prevent IR-induced heart injury. Accordingly, there is a need to find new interventions/pharmacological agents that can limit or prevent IR-induced myocardial injury.

Ischemic preconditioning is a novel technique that renders the heart less vulnerable to prolonged ischemia-reperfusion injury by prior exposure of the heart to short episodes of IR.[3] Researchers have extrapolated the concept of ischemic preconditioning in the form of pharmacological preconditioning, in which short episodes of ischemia are induced by pharmacological agents.[4,5] Several studies have shown the usefulness of pharmacological preconditioning in conferring resistance to various tissues and organs,[6] including the heart.[7]

Cholecystokinin (CCK-8) is a neuropeptide secreted by enteroendocrine cells of the duodenum.[8] Preclinical studies have shown potential beneficial effects of CCK-8 distinct from its typical gastrointestinal effects related to satiety and food intake.[9] Specifically, CCK-8 has been shown to affect anxiety,[10] pain,[11] spatial memory ability,[12] and IR-induced liver injury.[13] Furthermore, a recent study reported an association of CCK-8 with reduction of apoptosis in IR-induced renal injury.[14] Based on the findings of studies conducted in animals, CCK-8 may also exert beneficial effects in humans. However, there are insufficient clinical studies proving the usefulness of CCK-8 in humans. In continuation of preclinical studies, CCK-8 has been shown to influence pathophysiological states of the heart through CCK-1 and CCK-2 receptors.[15] For example, CCK-8 has been shown to attenuate myocardial fibrosis following ischemia-reperfusion injury.[16] A previous study documented that exogenous administration of CCK-8 exhibits pharmacological preconditioning and produces cardioprotective effects against IR injury.[17] However, the molecular mechanisms involved in CCK-8-induced pharmacological preconditioning have not been explored.

Hypoxia-inducible factor 1-α (HIF-1α) is a transcriptional factor that is reported to play an important role in the cardioprotective effects of different forms of preconditioning.[18,19] Phosphoinositide 3-kinase (PI3K), protein kinase B (Akt), and glycogen synthase kinase-3β (GSK-3β) also play important roles in conferring cardioprotection during ischemic, remote and pharmacological preconditioning.[20,21] Considering the significant role of these signaling pathways in different types of preconditioning-induced cardioprotection, we attempted to explore the role of the HIF-1α, PI3K, Akt, and GSK-3β signaling pathways in CCK-8-induced pharmacological preconditioning on IR model rat hearts.

Objectives

The present study aimed to investigate the role of the HIF-1α, PI3K, Akt, and GSK-3β signaling pathways in CCK-8-induced pharmacological preconditioning on IR model rat hearts.

Materials and methods

Drugs and animals

Three-month-old male Wistar albino rats weighing 210–240 g were used in this study. The animals were fed a normal pellet diet containing fiber (5%), protein (20%) and fat (5–10%). Ultraviolet radiation-treated water was provided in bottles for drinking purposes. The animals were exposed to 12 h of light and 12 h of dark at 25 ±2°C and 55–60% relative humidity. The doses of CCK-8,[17] PI3K inhibitor LY294002[22,23] and HIF-1 inhibitor YC-1[24] were determined based on the previous literature. Kits for the quantification of lactate dehydrogenase 1 (LDH-1), the MB isoform of creatine kinase (CK-MB), cardiac troponins (cTnT), HIF-1α, p-Akt, and p-GSK-3β were procured from MyBioSource, Inc. (San Diego, USA).

Approval of animal experiments

The experiments were approved by the Animal Ethical Committee of The First Affiliated Hospital of Anhui Medical University, Hefei, China (approval No. 202103050053).

Pharmacological preconditioning

Pharmacological preconditioning was induced by administering a single dose of CCK-8 (20 μg/kg) intravenously (i.v.), 24 h before isolating the hearts.[17]

Ischemia-reperfusion injury

After 24 h of pharmacological preconditioning, rats were sacrificed by an overdose of 4.5% isoflurane (gaseous anesthetic agent) and the hearts were quickly isolated. Heparin (1000 units/kg) was administered through the intraperitoneal (i.p.) route 30 min before sacrificing the rats, to prevent clot formation in the coronary arteries. The isolated hearts were perfused with Krebs–Henseleit (KH) solution (118 mM NaCl, 4.7 mM KCl, 1.2 mM $MgSO_4$, 1.25 mM

$CaCl_2$, 1.2 mM KH_2PO_4, 25 mM $NaHCO_3$, and 11 mM glucose, pH = 7.4) at 37°C using a Langendorff system (emka TECHNOLOGIES, Paris, France). Perfusion was stopped for 30 min to induce global ischemia to the heart. Thereafter, the flow of KH was restored for 120 min to institute reperfusion.[25,26]

Quantitative assessment of myocardial injury

The extent of IR-induced myocardial injury was quantified by measuring the release of 3 heart-specific biochemicals, namely LDH-1, CK-MB and cTnT, in the coronary effluent, using commercially available kits. The measurement of LDH-1 was performed using lithium L-lactate and NAD^+ to yield pyruvic acid and a reduced form of nicotinamide adenine dinucleotide (NADH); absorbance was then measured at 340 nm using a spectrophotometer (Cary 60; Agilent Technologies, Santa Clara, USA). LDH-1 was quantified as enzymatic activity recorded in IU/L. The quantification of CK-MB was performed by adding adenosine diphosphate (ADP) to the sample (containing CK-MB) to obtain ATP, which then reacted with glucose in the presence of hexokinase. Thereafter, nicotinamide adenine dinucleotide phosphate ($NADP^+$) and glucose-6-phosphate dehydrogenase were added to generate nicotinamide adenine dinucleotide phosphate (NADPH), and the absorbance was determined at 340 nm using a spectrophotometer (Cary 60; Agilent Technologies). Like LDH-1, CK-MB was also quantified as enzymatic activity in IU/L. The cTnT levels in the coronary effluent were quantified using a sandwich enzyme-linked immunosorbent assay (ELISA) kit with a cTnT antibody (capture antibody) precoated microplate. The addition of a sample containing cTnT to the wells led to the binding of cTnT to the capture antibody. Next, detection reagent A (biotin-conjugated antibody), detection reagent B (avidin-conjugated horseradish peroxidase (HRP)) and tetramethylbenzidine (a substrate of HRP) were added to yield a color, which was measured at 450 nm using an ELISA reader (BioTek, Winooski, USA).

Quantification of HIF-1α, p-Akt and p-GSK-3β

After 120 min of reperfusion, the hearts were removed and homogenized in phosphate-buffered saline (PBS) solution (137 mM NaCl, 2.7 mM KCl, 10 mM Na_2HPO_4, 1.8 mM KH_2PO_4, pH = 7.4) for 15 min in a refrigerated microtube tissue homogenizer at 4°C (Thomas Scientific, Swedesboro, USA) to obtain the homogenate. The homogenate was centrifuged (Beckman Coulter Life Sciences, Indianapolis, USA) at 5000 g for 10 min at 4°C to obtain clear supernatant, which was then employed for biochemical estimations. Using the heart homogenate supernatants, the expression of HIF-1α, p-Akt and p-GSK-3β/GSK-3β was quantified using commercially available ELISA kits.

Experimental protocol

For this study, 7 groups, each containing 8 animals, were used. The animals were randomly assigned to the following groups: 1) non-ischemic group, in which the hearts were isolated for biochemical estimation of HIF-1α, p-Akt and p-GSK-3β/GSK-3β; 2) IR injury group, in which hearts were subjected to 30 min of ischemia and 120 min of reperfusion; 3) CCK-8 pharmacological preconditioning group; 4 and 5) LY294002 in CCK-8 pharmacological preconditioning group, in which LY294002 (10 and 20 mg/kg) was administered before CCK-8 preconditioning; and 6 and 7) YC-1 in CCK-8 pharmacological preconditioning groups, in which YC-1 (1 and 2 mg/kg, i.p.) was administered before CCK-8 preconditioning.

Statistical analyses

Statistical analyses were performed using GraphPad Prism v. 8 (GraphPad Software, San Diego, USA). Data are reported as the mean ± standard deviation (SD). A normality test was conducted to check the appropriateness of applying analysis of variance (ANOVA). After passing the normality test, the results for LDH-1, CK-MB and cTnT were analyzed with two-way ANOVA. The results of all other parameters were analyzed using one-way ANOVA. These analyses were followed by Tukey's post hoc test. The results of parametric tests are represented as figures. The data were also analyzed using non-parametric tests (Table 1,2), namely the Kruskal–Wallis test (for biochemical parameters) and Friedman's test (for heart injury-specific parameters), followed by Dunn's post hoc test. Statistical significance was fixed at $p < 0.05$.

Results

Influence of CCK-8 pharmacological preconditioning on IR-induced myocardial injury

There was a significant increase in the release of heart-specific biochemical markers, namely LDH-1 (Fig. 1), CK-MB (Fig. 2) and cTnT (Fig. 3) in the coronary effluent, in response to 30 min of ischemia and 120 min of reperfusion. There was an approximately sixteen-fold increase in LDH-1, 8-fold increase in CK-MB and 12-fold increase in cTnT release during the reperfusion phase in comparison to non-ischemic hearts. The increased release of these biochemicals in the coronary effluent suggests a significant increase in IR injury to the heart. Notably, pharmacological preconditioning in the form of CCK-8 administration 24 h before ischemic injury significantly attenuated the release of LDH-1, CK-MB and cTnT in the coronary effluent. In CCK-8-preconditioned rats, the increase in heart injury biomarkers was reduced, i.e., eight-fold increase for LDH-1,

Table 1. Effect of different interventions on the heart injury parameters in isolated heart. Values are given as median (interquartile range (IQR)). The analysis was done using Friedman's test with Dunn's post hoc analysis

Sample No.	Groups	LDH-1		CK-MB		cTnT	
		before ischemia	during reperfusion	before ischemia	during reperfusion	before ischemia	during reperfusion
1.	IR injury	24.0 [21.25–25.75]	508.5 [505.0–510.8][a]	14.0 [13.00–17.75]	159.5 [156.5–161.8][a]	15.0 [13.50–16.75]	188.5 [185.3–190.0][a]
2.	CCK-8 pharmacological preconditioning	35.0 [32.25–36.75]	82.0 [79.25–84.75][b]	24.0 [22.25–25.50]	34.0 [32.25–36.00][b]	12.0 [10.25–13.00]	24.5 [20.75–26.75][b]
3.	LY294002 (10 mg/kg) in CCK-8 pharmacological preconditioning	30.50 [29.25–32.75]	210.5 [207.0–213.8][c]	20.5 [19.25–21.75]	94.5 [90.50–96.75][c]	18.0 [17.00–19.75]	110.0 [109.0–111.0][c]
4.	LY294002 (20 mg/kg) in CCK-8 pharmacological preconditioning	30.0 [27.5–32.5]	469.0 [464.8–473.5][c]	27.0 [26.0–28.0]	138.5 [136.3–139.8][c]	21.0 [19.00–22.75]	178.5 [174.3–181.5][c]
5.	YC-1 (1 mg/kg) in CCK-8 pharmacological preconditioning	30.0 [27.5–32.5]	247.0 [244.0–253.5][c]	27.0 [26.0–28.0]	104.5 [102.3–107.8][c]	19.5 [17.25–20.75]	121.5 [119.3–122.8][c]
6.	YC-1 (2 mg/kg) in CCK-8 pharmacological preconditioning	37.5 [36.00–38.75]	488.0 [484.8–489.8][c]	25.5 [24.0–26.0]	149.0 [146.3–151.8][c]	23.0 [21.25–24.75]	183.0 [178.3–185.8][c]

[a] $p < 0.05$ compared to results before ischemia; [b] $p < 0.05$ compared to results after IR injury after reperfusion; [c] $p < 0.05$ compared to results after CCK-8 preconditioning; IR – ischemia-reperfusion; CCK-8 – cholecystokinin.

Table 2. Effect of different interventions on biochemical parameters in isolated rat hearts. The data were analyzed using Kruskal–Wallis test and post hoc analysis was done using Dunn's multiple comparison test. Values are given as median (interquartile range (IQR)).

Sample No.	Groups	HIF-1α	p-Akt	p-GSK-3β/GSK-3β ratio
1.	non-ischemic	100.0 [99.25–100.0]	100.0 [99.25–100.0]	1.0 [0.91–1.1]
2.	IR injury	46.5 [43.5–48.0][a]	46.5 [43.5–48.0][a]	0.31 [0.29–0.34][b]
3.	CCK-8 pharmacological preconditioning	88.5 [87.0–92.75][b]	88.5 [87.0–92.75][b]	0.90 [0.88–0.92][b]
4.	LY294002 (10 mg/kg) in CCK-8 pharmacological preconditioning	69.50 [68.25–70.75][c]	69.5 [68.25–70.25][c]	0.74 [0.72–0.76][c]
5.	LY294002 (20 mg/kg) in CCK-8 pharmacological preconditioning	56.0 [54.25–57.0][c]	56.0 [54.2–57.0][c]	0.56 [0.53–0.58][c]
6.	YC-1 (1 mg/kg) in CCK-8 pharmacological preconditioning	64.0 [63.0–65.75][c]	64.0 [63.0–65.75][c]	0.64 [0.61–0.67][c]
7.	YC-1 (2 mg/kg) in CCK-8 pharmacological preconditioning	52.5 [52.0–55.0][c]	52.5 [52.0–55.0][c]	0.43 [0.37–0.44][c]

[a] $p < 0.05$ compared to results before ischemia; [b] $p < 0.05$ compared to results after IR injury after reperfusion; [c] $p < 0.05$ compared to results after CCK-8 preconditioning; IR – ischemia-reperfusion; CCK-8 – cholecystokinin.

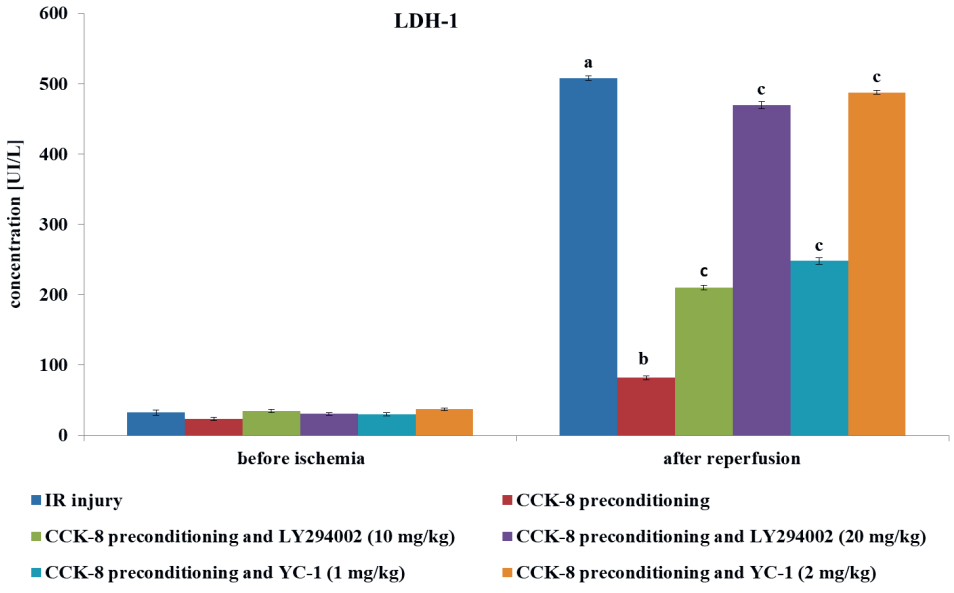

Fig. 1. Influence of cholecystokinin (CCK-8) preconditioning and other interventions on the release of LDH-1 in the coronary effluent

Values are given as mean ±SD; ANOVA results: $F(1,84) = 984.2$ for time, $F(5,84) = 453.9$ for treatment, $n = 8$, $p < 0.001$; a – $p < 0.05$ compared to before ischemia; b – $p < 0.05$ compared to IR injury after reperfusion; c – $p < 0.05$ compared to CCK-8 preconditioning; IR – ischemia-reperfusion; SD – standard deviation; ANOVA – analysis of variance.

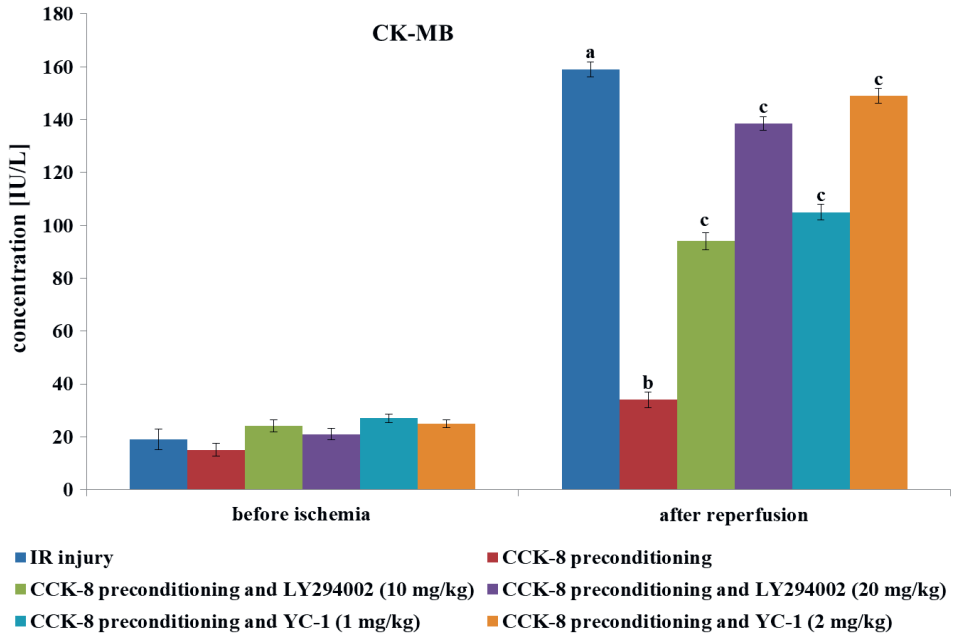

Fig. 2. Influence of cholecystokinin (CCK-8) preconditioning and other interventions on the release of CK-MB in the coronary effluent

Values are given as mean ±SD; ANOVA results: $F(1,84) = 783.1$ for time, $F(5,84) = 395.6$ for treatment, $n = 8$, $p < 0.001$; a – $p < 0.05$ compared to before ischemia; b – $p < 0.05$ compared to IR injury after reperfusion; c – $p < 0.05$ compared to CCK-8 preconditioning; IR – ischemia-reperfusion; SD – standard deviation; ANOVA – analysis of variance.

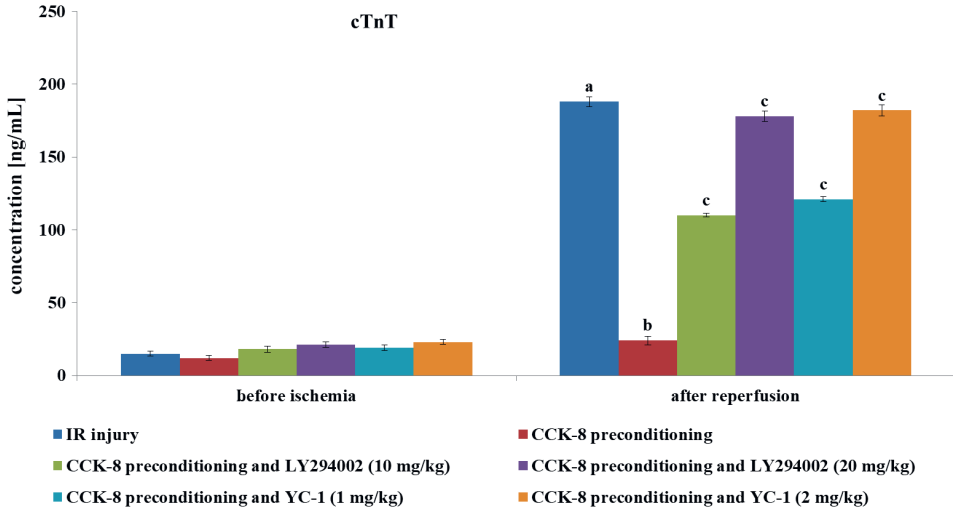

Fig. 3. Influence of cholecystokinin (CCK-8) preconditioning and other interventions on the release of cTnT in the coronary effluent

Values are given as mean ±SD; ANOVA results: $F(1,84) = 812.8$ for time, $F(5,84) = 412.7$ for treatment, $n = 8$, $p < 0.001$; a – $p < 0.05$ compared to before ischemia; b – $p < 0.05$ compared to IR injury after reperfusion; c – $p < 0.05$ compared to CCK-8 preconditioning; IR – ischemia-reperfusion; SD – standard deviation; ANOVA – analysis of variance.

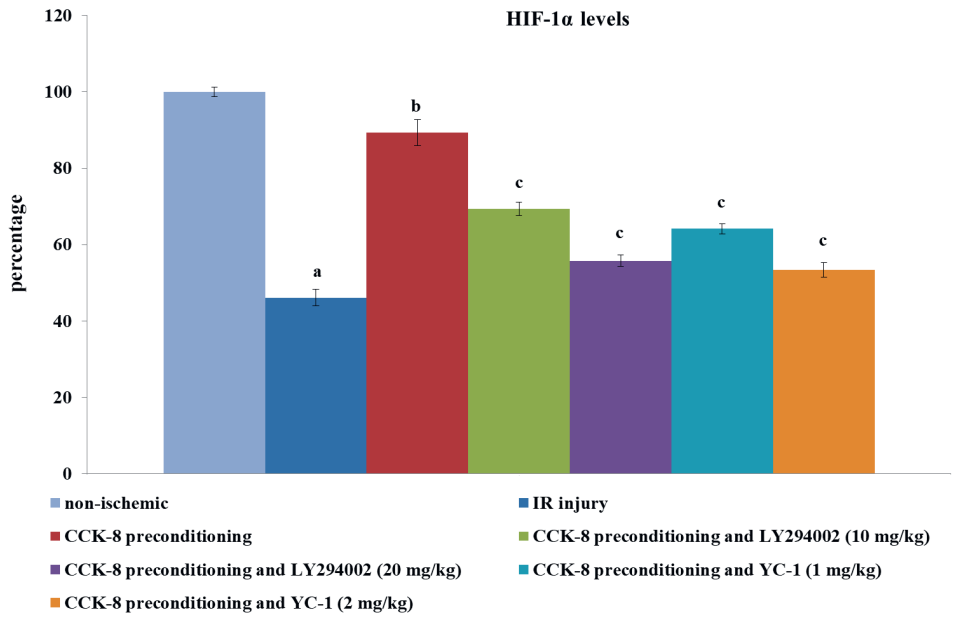

Fig. 4. Influence of cholecystokinin (CCK-8) preconditioning and other interventions on ischemia-reperfusion-induced changes in the expression of HIF-1α

Values are reported as mean ±SD; ANOVA results: $F(6,49) = 634.8$, $n = 8$, $p < 0.001$; a – $p < 0.05$ compared to non-ischemic; b – $p < 0.05$ compared to IR injury; c – $p < 0.05$ compared to CCK-8 preconditioning; IR – ischemia-reperfusion; SD – standard deviation; ANOVA – analysis of variance.

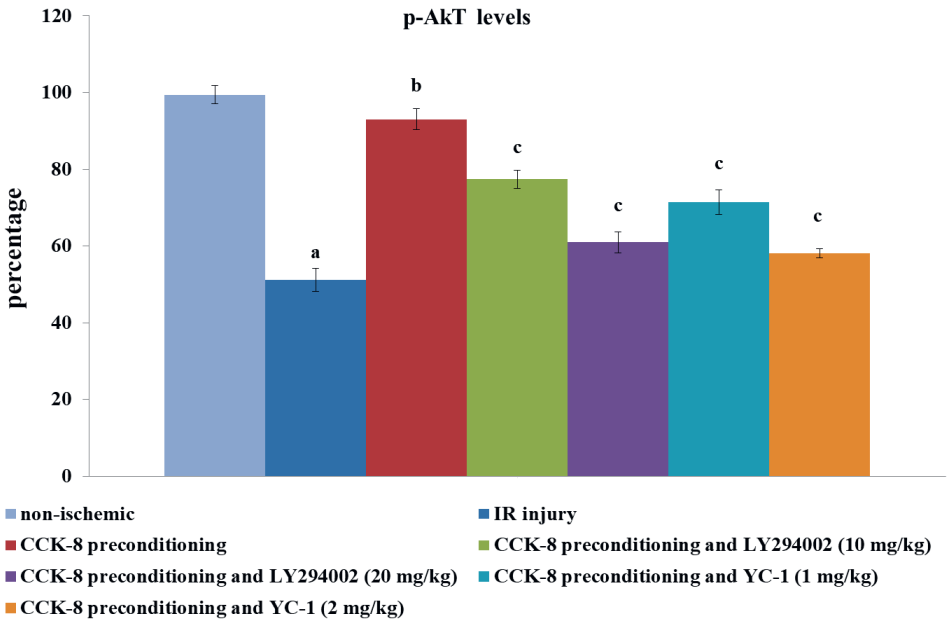

Fig. 5. Influence of cholecystokinin (CCK-8) preconditioning and other interventions on IR-induced changes in the p-Akt levels

Values are given as mean ±SD; ANOVA results: F(6,49) = 530.1, n = 8, p < 0.001; a – p < 0.05 compared to non-ischemic; b – p < 0.05 compared to IR injury; c – p < 0.05 compared to CCK-8 preconditioning; IR – ischemia-reperfusion; SD – standard deviation; ANOVA – analysis of variance.

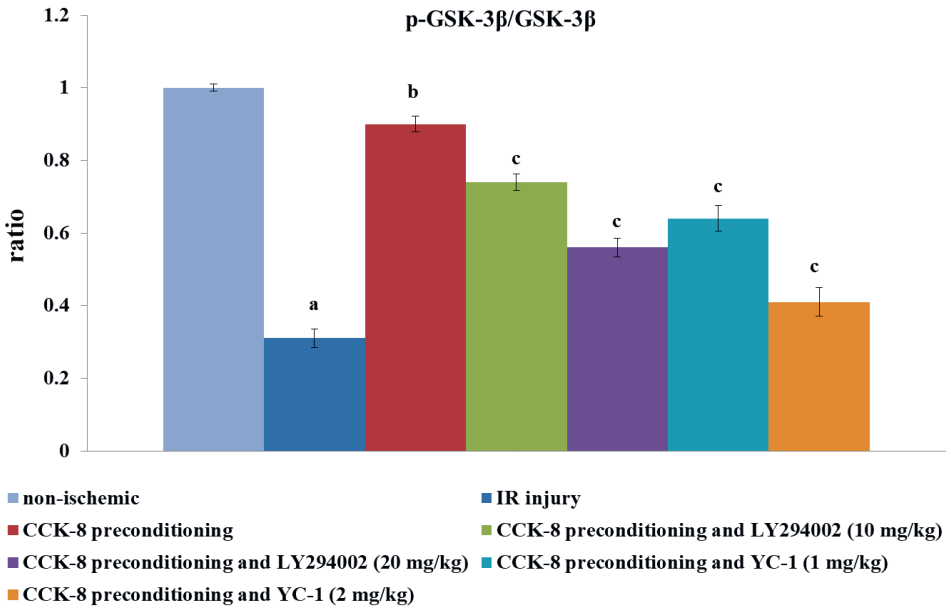

Fig. 6. Influence of cholecystokinin (CCK-8) preconditioning and other interventions on IR-induced changes in the p-GSK-3β/GSK-3β ratio in the heart homogenates

Values are given as mean ±SD; ANOVA results: F(6,49) = 785.3, n = 8, p < 0.001; a – p < 0.05 compared to non-ischemic; b – p < 0.05 compared to IR injury; c – p < 0.05 compared to CCK-8 preconditioning; IR – ischemia-reperfusion; SD – standard deviation; ANOVA – analysis of variance.

four-fold increase for CK-MB, and seven-fold increase for cTnT. Overall, the parameters were nearly two-fold lower than in the IR injury group. This result suggests that CCK-8 produced pharmacological preconditioning and significantly protected the rat hearts from IR injury.

Influence of CCK-8 pharmacological preconditioning on IR-induced biochemical changes in the heart

Apart from attenuating heart injury, pharmacological preconditioning with CCK-8 prevented ischemia-reperfusion-induced changes in the expression levels of the biochemical markers such as HIF-1α, p-Akt and p-GSK-3β. In IR-subjected rats, there was a significant decrease in the expression of HIF-1α (Fig. 4) and p-Akt (Fig. 5), and in p-GSK-3β/GSK-3β ratio (Fig. 6) in comparison to normal, non-ischemic hearts. In the IR group, the expression of HIF-1α in hearts was reduced 2.16-fold, the expression of p-Akt 1.94-fold and the p-GSK-3β/GSK-3β ratio 3.1-fold in comparison to non-ischemic hearts. However, pharmacological preconditioning with CCK-8 led to significant restoration of HIF-1α and p-Akt expression and p-GSK-3β/GSK-3β ratio in the heart homogenates. In CCK-8-preconditioned hearts, the expression of HIF-1α in hearts was reduced 1.2-fold, the expression of p-Akt 1.1-fold and the p-GSK-3β/GSK-3β ratio 1.4-fold. Thus, there was an approximately two-fold greater increase in the above biochemical parameters in the CCK-8 preconditioning group compared to the IR injury group.

Influence of LY294002 and YC-1 on CCK-8 pharmacological preconditioning-induced changes in IR-subjected rat hearts

In light of the significant increase in the expression of HIF-1α and p-Akt in CCK-8 preconditioning-subjected rat hearts, the influence of LY294002 and YC-1 on CCK-8-induced changes was explored. Administration of LY294002 (PI3K inhibitor) or YC-1 (HIF-1α inhibitor) prior to CCK-8 preconditioning significantly abolished CCK-8-induced cardioprotective effects in IR-subjected rat hearts. There was a significant and dose-dependent increase in the levels of LDH-1 (Fig. 1), CK-MB (Fig. 2) and cTnT (Fig. 3) in rat hearts treated with LY294002 (10 mg/kg and 20 mg/kg) and YC-1 (1 mg/kg and 2 mg/kg). Compared to CCK-8 preconditioning, administration of LY294002 led to a 2.56-fold (10 mg/kg) and 5.72-fold (20 mg/kg) increase in LDH-1 release; 2.76-fold (10 mg/kg) and 4.07-fold (20 mg/kg) increase in CK-MB release; and 4.58-fold (10 mg/kg) and 7.42-fold (20 mg/kg) increase in cTnT release during the reperfusion phase. Similarly, in comparison to CCK-8 preconditioning, administration of YC-1 led to a 3.02-fold (1 mg/kg) and 5.94-fold (2 mg/kg) increase in LDH-1 release; 3.08-fold (1 mg/kg) and 4.38-fold (2 mg/kg) increase in CK-MB release; and 5.04-fold (1 mg/kg) and 7.58-fold (2 mg/kg) increase in cTnT release during the reperfusion phase. These results indicate that higher doses of LY294002 (20 mg/kg) and YC-1 (2 mg/kg) almost completely abolished the effects of CCK-8 preconditioning, and that the effects in those groups were comparable to the IR injury group.

Moreover, there was a significant decrease in the levels of HIF-1α (Fig. 4) and p-Akt expression (Fig. 5) and in p-GSK-3β/GSK-3β ratio (Fig. 6) in the heart homogenates in LY294002 and YC-1-administered rats. In comparison to CCK-8 preconditioning, administration of LY294002 led to a 1.28-fold (10 mg/kg) and 1.60-fold (20 mg/kg) decrease in HIF-1α; 1.20-fold (10 mg/kg) and 1.52-fold (20 mg/kg) decrease in p-Akt; and 1.21-fold (10 mg/kg) and 1.60-fold (20 mg/kg) decrease in p-GSK-3β/GSK-3β ratio. Administration of YC-1 led to a 1.39-fold (1 mg/kg) and 1.67-fold (2 mg/kg) decrease in HIF-1α; 1.30-fold (1 mg/kg) and 1.60-fold (2 mg/kg) decrease in p-Akt; and 1.40-fold (1 mg/kg) and 2.19-fold (2 mg/kg) decrease in p-GSK-3β/GSK-3β ratio. Similar to the parameters of cardiac injury, higher doses of LY294002 (20 mg/kg) and YC-1 (2 mg/kg) almost completely abolished the effects of CCK-8 preconditioning on biochemical parameters, and the effects in those groups were comparable to the IR injury group.

Discussion

In this present investigation, pharmacological preconditioning with CCK-8 was found to provide significant cardioprotection against IR-induced myocardial injury. There was a significant reduction in the release of cardiac injury markers, namely LDH-1, CK-MB, and cTnT, in the coronary effluent of ischemia-reperfusion injury model rats. Pharmacological preconditioning is an extrapolation of ischemic preconditioning, in which instead of short episodes of ischemia, a pharmacological agent is employed.[27] Several pharmacological agents are known to exhibit pharmacological preconditioning-like effects.[28] In the current study, cardioprotective effects were evaluated after 24 h of CCK-8 administration. Therefore, the results suggest that CCK-8 exerts late phase preconditioning on hearts. The results of the present study are in line with the results of a previous study showing the delayed phase of cardioprotective effects of CCK-8-induced pharmacological preconditioning.[17]

In this present study, along with the cardioprotective effects of CCK-8-induced preconditioning, we observed significant restoration of biochemical markers in IR-subjected rat hearts. In response to IR, there was a significant decrease in the expression of HIF-1α and p-Akt and in p-GSK-3β/GSK-3β ratio. However, pharmacological preconditioning with CCK-8 led to significant restoration of HIF-1α and p-Akt expression and of p-GSK-3β/GSK-3β ratio in the heart homogenates. The HIF-1α is a hypoxia-inducible transcriptional factor and its key role in ischemic[29] and remote preconditioning-induced cardioprotection has been previously demonstrated.[30] The present finding of an increase in HIF-1α level in response to CCK-8 preconditioning is supported by previous studies showing that CCK-8 may increase the expression of HIF-1α.[31] Furthermore, the present study demonstrated that the administration of a selective pharmacological inhibitor of HIF-1α, namely YC-1, significantly abrogated the cardioprotective effects of CCK-8-induced pharmacological preconditioning. Accordingly, it may be suggested that CCK-8-induced pharmacological preconditioning involves the activation of a HIF-1α-dependent signaling pathway.

The relationship between p-Akt and CCK-8-induced pharmacological preconditioning was also assessed in the current study. The results showed that CCK-8-induced pharmacological preconditioning was associated with restoration of p-Akt expression and p-GSK-3β/GSK-3β ratio. Previous studies have described that PI3K-Akt-GSK-3β constitutes an important signaling cascade mediating various biological effects, including ischemic, remote and pharmacological preconditioning-induced cardioprotection.[32,33] PI3K leads to phosphorylation of Akt to increase its activity,[34] and the phosphorylated form of Akt leads to phosphorylation of GSK-3β.[35] Of note, phosphorylation of GSK-3β leads to a decrease in its activity and, thus, a decrease in the p-GSK-3β/GSK-3β ratio indicates the potentiation of its activity.[36]

In this present study, pharmacological inhibition of PI3K using LY294002 led to significant attenuation

of the cardioprotective actions of CCK-8-induced pharmacological preconditioning. Moreover, LY294002 abolished the restorative effects of CCK-8-induced pharmacological preconditioning on biochemical markers in the heart homogenates. To the best of our knowledge, this is the first study describing that the cardioprotective effects of CCK-8-induced pharmacological preconditioning are mediated through the PI3K-Akt-GSK-3β signaling pathway. Moreover, it is the first study describing that CCK-8-induced pharmacological preconditioning involves the activation of the HIF-1α-dependent signaling pathway. Previous studies have shown that hypoxia may trigger the activation of PI3K-Akt to increase the expression of HIF-1α, which may contribute to the resistance of the heart to ischemic injury.[37,38] However, the present study did not delineate the precise sequence of the intracellular signaling pathway involving PI3K-Akt-GSK-3β and HIF-1α in CCK-8-induced pharmacological preconditioning. Furthermore, roles of the RISK (reperfusion injury salvage kinase) and SAFE (survivor activating factor enhancement) signaling pathways in CCK-8-mediated protective effects in IR-induced myocardial injury have been reported.[39] Accordingly, there are potential roles for these signaling pathways in CCK-8-mediated preconditioning effects.

Clinically, there are limited options to protect the heart from ischemic injury; therefore, CCK-8 may serve as a useful pharmacological tool to protect against ischemia-reperfusion injury. In particular, CCK-8 may be useful in situations where myocardial ischemia is unavoidable, such as coronary artery balloon angioplasty, coronary artery bypass surgery, excision and transportation of a donor heart, and before exercise in patients with known demand-induced ischemia. Mechanistically, CCK-8 administration in the form of pharmacological preconditioning may trigger cardioprotective signaling, involving activation of the PI3K-Akt-GSK-3β pathway.

Limitations and future directions

The present study did not reveal the precise sequence of the HIF-1α and PI3K-Akt-GSK-3β signaling pathways in CCK-8-induced pharmacological preconditioning. Thus, the role of the RISK and SAFE signaling pathways in CCK-8-mediated preconditioning effects warrant further investigation. Moreover, future studies should explore the clinical effects of CCK-8 preconditioning in patients suffering from ischemic heart diseases.

Conclusions

The findings of this study suggest that the molecular mechanisms participating in CCK-8-induced pharmacological preconditioning involve the HIF-1α, PI3K, Akt, and GSK-3β signaling pathway.

ORCID iDs

Yuan Cheng https://orcid.org/0000-0002-4026-5607
Mengzuo Wu https://orcid.org/0000-0003-2550-1007
Min Liu https://orcid.org/0000-0002-4421-4540
Birong Zhou https://orcid.org/0000-0002-9527-7453
Xianhe Lin https://orcid.org/0000-0001-7899-4234
Bangning Wang https://orcid.org/0000-0002-5165-0375

References

1. Urban PL, Cowley M, Goldberg S, et al. Intracoronary thrombolysis in acute myocardial infarction: Clinical course following successful myocardial reperfusion. *Am Heart J.* 1984;108(4 Pt 1):873–878. doi:10.1016/0002-8703(84)90448-4
2. Chandra R, Baumann FG, Goldman RA. Myocardial reperfusion, a cause of ischemic injury during cardiopulmonary bypass. *Surgery*. 1976;80(2):266–276. PMID:941098
3. Hausenloy DJ, Yellon DM. Ischaemic conditioning and reperfusion injury. *Nat Rev Cardiol*. 2016;13(4):193–209. doi:10.1038/nrcardio.2016.5
4. Benke K, Mátyás C, Sayour AA, et al. Pharmacological preconditioning with gemfibrozil preserves cardiac function after heart transplantation. *Sci Rep*. 2017;7(1):14232. doi:10.1038/s41598-017-14587-3
5. Luca MC, Liuni A, Muxel S, et al. Chronic pharmacological preconditioning against ischemia. *Clin Hemorheol Microcirc*. 2011;49(1–4):287–293. doi:10.3233/CH-2011-1479
6. Goulton CS, Patten AR, Kerr JR, Kerr DS. Pharmacological preconditioning with GYKI 52466: A prophylactic approach to neuroprotection. *Front Neurosci*. 2010;4:54. doi:10.3389/fnins.2010.00054
7. Gabrielová E, Bartošíková L, Nečas J, Modrianský M. Cardioprotective effect of 2,3-dehydrosilybin preconditioning in isolated rat heart. *Fitoterapia*. 2019;132:12–21. doi:10.1016/j.fitote.2018.10.028
8. Chandra R, Liddle RA. Cholecystokinin. *Curr Opin Endocrinol Diabetes Obes*. 2007;14(1):63–67. doi:10.1097/MED.0b013e3280122850
9. Cawthon CR, de La Serre CB. The critical role of CCK in the regulation of food intake and diet-induced obesity. *Peptides*. 2021;2021:170492. doi:10.1016/j.peptides.2020.170492
10. Ochi R, Fujita N, Goto N, et al. Region-specific brain area reductions and increased cholecystokinin positive neurons in diabetic OLETF rats: Implication for anxiety-like behavior. *J Physiol Sci*. 2020;70(1):42. doi:10.1186/s12576-020-00771-0
11. Roca-Lapirot O, Fossat P, Ma S, et al. Acquisition of analgesic properties by the cholecystokinin (CCK)/CCK2 receptor system within the amygdala in a persistent inflammatory pain condition. *Pain*. 2019;160(2):345–357. doi:10.1097/j.pain.0000000000001408
12. Sadeghi M, Reisi P, Radahmadi M. The effects of CCK-8S on spatial memory and long-term potentiation at CA1 during induction of stress in rats. *Iran J Basic Med Sci*. 2017;20(12):1368–1376. doi:10.22038/IJBMS.2017.9619
13. Zhang Y, Zhu J, Guo L, et al. Cholecystokinin protects mouse liver against ischemia and reperfusion injury. *Int Immunopharmacol*. 2017;48:180–186. doi:10.1016/j.intimp.2017.03.028
14. Liu C, Chen K, Wang H, et al. Gastrin attenuates renal ischemia/reperfusion injury by a PI3K/Akt/Bad-mediated anti-apoptosis signaling. *Front Pharmacol*. 2020;11:540479. doi:10.3389/fphar.2020.540479
15. Dong X, Wang C, Zhang J, et al. Cholecystokinin expression in the development of postinfarction heart failure. *Cell Physiol Biochem*. 2017;43(6):2479–2488. doi:10.1159/000484454
16. Wang C, Zhang C, Wu D, et al. Cholecystokinin octapeptide reduces myocardial fibrosis and improves cardiac remodeling in post myocardial infarction rats. *Int J Biochem Cell Biol*. 2020;125:105793. doi:10.1016/j.biocel.2020.105793
17. Li H, An C. Exploring the role of neurogenic pathway-linked cholecystokinin release in remote preconditioning-induced cardioprotection. *Acta Cir Bras*. 2020;35(9):e202000906. doi:10.1590/s0102-86502020009000006
18. Jiang L, Zeng H, Ni L, et al. HIF-1α preconditioning potentiates antioxidant activity in ischemic injury: The role of sequential administration of dihydrotanshinone I and protocatechuic aldehyde in cardioprotection. *Antioxid Redox Signal*. 2019;31(3):227–242. doi:10.1089/ars.2018.7624
19. Yang L, Xie P, Wu J, et al. Sevoflurane postconditioning improves myocardial mitochondrial respiratory function and reduces myocardial ischemia-reperfusion injury by up-regulating HIF-1. *Am J Transl Res*. 2016;8(10):4415–4424. PMID:27830025

20. Rossello X, Riquelme JA, Davidson SM, Yellon DM. Role of PI3K in myocardial ischaemic preconditioning: Mapping pro-survival cascades at the trigger phase and at reperfusion. *J Cell Mol Med*. 2018;22(2): 926–935. doi:10.1111/jcmm.13394
21. Zi C, Zhang C, Yang Y, Ma J. Penehyclidine hydrochloride protects against anoxia/reoxygenation injury in cardiomyocytes through ATP-sensitive potassium channels, and the Akt/GSK-3β and Akt/mTOR signaling pathways. *Cell Biol Int*. 2020;44(6):1353–1362. doi:10.1002/cbin.11329
22. Fujiwara M, Izuishi K, Sano T, et al. Modulating effect of the PI3-kinase inhibitor LY294002 on cisplatin in human pancreatic cancer cells. *J Exp Clin Cancer Res*. 2008;27(1):76. doi:10.1186/1756-9966-27-76
23. Jiang H, Fan D, Zhou G, Li X, Deng H. Phosphatidylinositol 3-kinase inhibitor (LY294002) induces apoptosis of human nasopharyngeal carcinoma in vitro and in vivo. *J Exp Clin Cancer Res*. 2010;29(1):34. doi:10.1186/1756-9966-29-34
24. Yan J, Zhou B, Taheri S, Shi H. Differential effects of HIF-1 inhibition by YC-1 on the overall outcome and blood–brain barrier damage in a rat model of ischemic stroke. *PLoS One*. 2011;6(11):e27798. doi:10.1371/journal.pone.0027798
25. Bradic J, Milosavljevic I, Bolevich S, et al. Dipeptidyl peptidase 4 inhibitors attenuate cardiac ischaemia-reperfusion injury in rats with diabetes mellitus type 2. *Clin Exp Pharmacol Physiol*. 2020;48(4):575–584. doi:10.1111/1440-1681.13450
26. Watanabe M, Okada T. Langendorff perfusion method as an ex vivo model to evaluate heart function in rats. *Methods Mol Biol*. 2018;1816: 107–116. doi:10.1007/978-1-4939-8597-5_8
27. Ravindran S, Kurian GA. Preconditioning the rat heart with sodium thiosulfate preserved the mitochondria in response to ischemia-reperfusion injury. *J Bioenerg Biomembr*. 2019;51(3):189–201. doi:10.1007/s10863-019-09794-8
28. Naderi R, Imani A, Faghihi M. Phenylephrine produces late pharmacological preconditioning in the isolated rat heart. *Eur J Pharmacol*. 2010;627(1–3):203–208. doi:10.1016/j.ejphar.2009.10.052
29. Semenza GL. Hypoxia-inducible factor 1: Regulator of mitochondrial metabolism and mediator of ischemic preconditioning. *Biochim Biophys Acta*. 2011;1813(7):1263–1268. doi:10.1016/j.bbamcr.2010.08.006
30. Cai Z, Luo W, Zhan H, Semenza GL. Hypoxia-inducible factor 1 is required for remote ischemic preconditioning of the heart. *Proc Natl Acad Sci U S A*. 2013;110(43):17462–17467. doi:10.1073/pnas.1317158110
31. Chao C, Goluszko E, Lee YT, et al. Constitutively active CCK2 receptor splice variant increases Src-dependent HIF-1 alpha expression and tumor growth. *Oncogene*. 2007;26(7):1013–1019. doi:10.1038/sj.onc.1209862
32. Li J, Xuan W, Yan R, et al. Remote preconditioning provides potent cardioprotection via PI3K/Akt activation and is associated with nuclear accumulation of β-catenin. *Clin Sci (Lond)*. 2011;120(10):451–462. doi:10.1042/CS20100466
33. Semenza GL. Hypoxia-inducible factor 1: Regulator of mitochondrial metabolism and mediator of ischemic preconditioning. *Biochim Biophys Acta*. 2011;1813(7):1263–1268. doi:10.1016/j.bbamcr.2010.08.006
34. Karar J, Maity A. PI3K/AKT/mTOR pathway in angiogenesis. *Front Mol Neurosci*. 2011;4:51. doi:10.3389/fnmol.2011.00051
35. Hermida MA, Dinesh Kumar J, Leslie NR. GSK3 and its interactions with the PI3K/AKT/mTOR signalling network. *Adv Biol Regul*. 2017;65: 5–15. doi:10.1016/j.jbior.2017.06.003
36. Patel P, Woodgett JR. Glycogen synthase kinase 3: A kinase for all pathways? *Curr Top Dev Biol*. 2017;123:277–302. doi:10.1016/bs.ctdb.2016.11.011
37. Zhao R, Feng J, He G. Hypoxia increases Nrf2-induced HO-1 expression via the PI3K/Akt pathway. *Front Biosci (Landmark Ed)*. 2016;21: 385–396. doi:10.2741/4395
38. Zhang SB, Liu TJ, Pu GH, Li BY, Gao XZ, Han XL. MicroRNA-374 exerts protective effects by inhibiting SP1 through activating the PI3K/Akt pathway in rat models of myocardial ischemia-reperfusion after sevoflurane preconditioning. *Cell Physiol Biochem*. 2018;46(4):1455–1470. doi:10.1159/000489186
39. Yang X, Yue R, Zhang J, et al. Gastrin protects against myocardial ischemia/reperfusion injury via activation of RISK (reperfusion injury salvage kinase) and SAFE (survivor activating factor enhancement) pathways. *J Am Heart Assoc*. 2018;7(14):e005171. doi:10.1161/JAHA.116.005171

A novel therapeutic approach to NASH: Both polyethylene glycol 3350 and lactulose reduce hepatic inflammation in C57BL/6J mice

Pinar Gokcen[1,B–F], Oguzhan Ozturk[1,C–F], Gupse Adali[1,B,C,E,F], Ilkay Tosun[2,C,E,F], Halef Okan Dogan[3,B,E,F], Haki Kara[4,C,E,F], Yucel Yalman[4,E,F], Hamdi Levent Doganay[1,B,E,F], Kamil Ozdil[1,A–C,E,F]

[1] Department of Gastroenterology, Health Sciences University, Ümraniye Training and Research Hospital, Istanbul, Turkey
[2] Department of Pathology, Health Sciences University, Ümraniye Training and Research Hospital, Istanbul, Turkey
[3] Department of Biochemistry, Sivas Cumhuriyet University School of Medicine, Turkey
[4] Faculty of Veterinary Medicine, Sivas Cumhuriyet University, Turkey

A – research concept and design; B – collection and/or assembly of data; C – data analysis and interpretation; D – writing the article; E – critical revision of the article; F – final approval of the article

Advances in Clinical and Experimental Medicine, ISSN 1899–5276 (print), ISSN 2451–2680 (online) *Adv Clin Exp Med*. 2021;30(11):1167–1174

Address for correspondence
Pinar Gokcen
E-mail: pinar-gokcen@hotmail.com

Funding sources
None declared

Conflict of interest
None declared

Received on March 29, 2021
Reviewed on June 27, 2021
Accepted on July 26, 2021

Published online on September 22, 2021

Abstract

Background. The gut-liver axis is one of the most emphasized topics in the pathogenesis of non-alcoholic fatty liver disease (NAFLD). Intestinal microbiota dysbiosis has been shown to be a predictor of disease severity and progression to fatty liver disease. Therefore, research addressing gut-based therapies has become popular.

Objectives. To investigate the effect of lactulose and polyethylene glycol 3350 (PEG 3350) in mice with induced obesity and NAFLD at a non-diarrheal dose.

Materials and methods. Thirty-six C57BL/6J male mice were divided into 6 groups. The first 2 groups (n = 6 each) were used as an induced obesity model (group A) and NAFLD model (group B) for 8 weeks. The remaining 24 animals were categorized into control diet group, high-fat diet (HFD) group, HFD + lactulose group, and HFD + PEG 3350 group. Serum and liver tissue samples were obtained for biochemical and histopathological analyses, respectively.

Results. The HFD + lactulose treatment group displayed a significant decrease in liver weight (1.3 (1.3–1.4) kg compared to 1.8 (1.6–1.9) kg) and NAFLD activity score (NAS) (1.5 (1.0–3.0) compared to 5.0 (4.0–5.0), respectively; p = 0.0043, p = 0.0021) when compared with the HFD group. However, a decrease in body weight (35.0 (34.6–36.0) kg compared to 40.9 (34.7–41.9) kg) and hepatosteatosis (HS) rate (33.3% compared to 100.0%) were not statistically significant (p = 0.1796, p = 0.0606, respectively). The HFD + PEG 3350 treatment group showed a statistically significant decrease in body weight (32.4 (30.2–33.9) kg compared to 40.9 (34.7–41.9) kg), liver weight (1.5 (1.3–1.5) kg compared to 1.8 (1.6–1.9) kg), HS rate (16.7% compared to 100.0%) and NAS (0.5 (0.0–1.0) compared to 5.0 (4.0–5.0); p = 0.0086, p = 0.0086, p = 0.0151, and p = 0.0021, respectively) when compared with the HFD group.

Conclusions. We demonstrated that non-diarrheal dose of lactulose and PEG 3350 reduced hepatic inflammation in mice with induced NAFLD. It was also observed that PEG 3350 decreased HS and body weight. We believe these mechanisms can be utilized as novel therapeutic approaches in NAFLD in prospective human studies.

Key words: hepatosteatosis, lactulose, non-alcoholic fatty liver disease, non-alcoholic steatohepatitis, polyethylene glycol 3350

Cite as
Gokcen P, Ozturk O, Adali G, et al. A novel therapeutic approach to NASH: Both polyethylene glycol 3350 and lactulose reduce hepatic inflammation in C57BL/6J mice. *Adv Clin Exp Med*. 2021;30(11):1167–1174. doi:10.17219/acem/140506

DOI
10.17219/acem/140506

Background

Non-alcoholic fatty liver disease (NAFLD) is an ever-increasing major public health problem worldwide, and due to the high rates of hepatitis B immunization and the introduction of the hepatitis C vaccine, likely the most common cause of chronic liver disease. Non-alcoholic steatohepatitis (NASH) is a histologically more aggressive subgroup of NAFLD and is more frequently associated with the development of fibrosis and cirrhosis. In the general population, the prevalence of NAFLD is 25%, and the prevalence of NASH is 3–5%.[1]

The pathogenesis of NAFLD is not yet fully understood, although the "multiple-hit" hypothesis is widely accepted. The 1st hit involves increased lipid flows to hepatocytes, which induces the liver to become more susceptible to oxidative stress and lipid peroxidation with increased lipid uptake, free fatty acid production and de novo lipogenesis. Then, mitochondrial dysfunction and the 2nd hit occurs, resulting in hepatocyte damage, inflammation and fibrosis.[2] Although the majority of NAFLD patients are overweight or obese, there is also a subgroup of patients with normal body mass index (BMI); such situation is defined as lean NAFLD. Therefore, other factors in the pathogenesis besides insulin resistance, dyslipidemia and obesity are thought to be involved.

The gut–liver axis is one of the most emphasized topics in the pathogenesis of NAFLD, with intestinal microbiota dysbiosis being shown as a predictor of disease severity and progression to fatty liver disease.[3] Therefore, research on gut-based therapies has become popular. Lactulose is a drug mainly used in the treatment of constipation, hepatic encephalopathy and salmonellosis, and it is one of the oldest prebiotics known as the 'bifidus factor'. Oral lactulose administration exerts its positive effect on gut microbiota by increasing bifidobacteriaceae and lactobacillaceae.[4] The ability of lactulose to reduce hyperammonemia in hepatic encephalopathy is thought to be mainly due to amelioration of dysbiosis.[5] Polyethylene glycol 3350 (PEG 3350) is a high-molecular-weight, water-soluble polymer and a commonly used drug for bowel lavage due to its low rate of side effects. Post-lavage changes in the microbiota composition have been shown in fecal samples of patients who had colonoscopy preparation with PEG 3350.[6]

Objectives

In our study, we developed NAFLD mice models with a high-fat diet (HFD) involving butter and aimed to investigate the effect of lactulose and PEG 3350 at non-diarrheal doses on lipid profile, obesity and NAFLD (defined as NAFLD activity score (NAS) ≥3). The NAS system reflects fundamental histological features (steatosis, ballooning and inflammation) and is a well-accepted standard used for assessing NAFLD severity and responses to treatment.[8]

Materials and methods

Animals

Thirty-six C57BL/6J male mice were used in the study. Animals were eight-week old, weighing 24–28 g, and were obtained from the Bilkent University Experimental Animals Laboratory (Ankara, Turkey). Animals were held in a twelve-hour dark/light cycle at an average temperature of 22°C, and were randomized into 6 groups (n = 6) prior to housing. Before starting the experiment, the mice were given a standard diet (5.5% of the energy from fat) and water for 2 weeks to stabilize their metabolic status. The animal study was approved by the Animal Ethics Committee of Cumhuriyet University School of Sivas (Sivas, Turkey; approval No. 295/25.06.2019). All the surgical and experimental procedures were in accordance with institutional animal care guidelines.

Experimental design

The study was designed in 2 stages (Fig. 1). The 1st stage involved inducing obesity (group A, n = 6) and NAFLD (group B, n = 6) with a HFD diet (pellets, 60% of the energy from butter). Group A and group B mice received a standard diet and HFD, 3–6 g/day for 8 weeks, respectively. Daily weights, food, and water consumption were observed during the experiment. Finally, the 2 groups were fasted for 24 h prior to euthanasia for histopathological evaluation of the liver and the acquisition of blood samples from the femoral artery. When it was seen that NAFLD was induced in group B mice, the 16-week treatment trial phase was initiated. The remaining 24 animals were categorized into 4 groups: HFD, HFD + lactulose, and HFD + PEG 3350. Lactulose and PEG 3350 were given to mice by dissolving in drinking water at a dose of 0.44 g/day and 0.3 g/kg/day, respectively.[7] The frequency and consistency of defecation were monitored. Diarrhea was identified as an undesirable side effect, although it did not affect any animals. Serum and liver tissue samples were obtained in a similar manner to the mouse model of induced NAFLD at baseline and at 8 weeks.

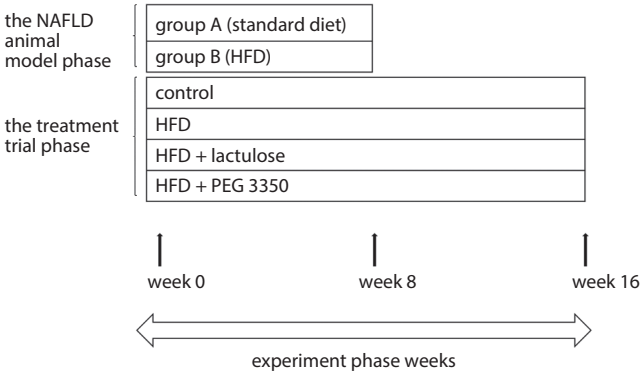

Fig. 1. Experimental study design

NAFLD – non-alcoholic fatty liver disease; HFD – high-fat diet.

Biochemical analysis and histopathological evaluation

Blood samples from euthanized mice were centrifuged for 10 min at 4000 rpm and 4°C, then were analyzed for glucose, total cholesterol (TC), triglycerides (TG), low-density lipoprotein cholesterol (LDL-C), and high-density lipoprotein-cholesterol (HDL-C) using cobas® 8000 analyzer (Roche, Basel, Switzerland). Liver tissues were dissected, fixed with 10% neutral formalin and sent to the pathology laboratory to be examined. After the automated tissue processing and paraffin blocking steps, 5 µm-thick sections were taken, then stained with hematoxylin and eosin (H&E) in an automated stainer (Leica ST5020; Leica, Buffalo Grove, USA). Each section was assessed under light microscope by 2 independent pathologists for histopathological evaluations. Hepatosteatosis (HS) was graded based on the percentage of fat within the hepatocytes: grade 0 (<5%), grade 1 (5–33%), grade 2 (34–66%), and grade 3 (>66%). The NAFLD activity score (NAS) was calculated using the scoring system developed by Kleiner et al.[8]

Statistical methods

Statistical data were analyzed using IBM SPSS v. 23.0 (IBM Corp., Armonk, USA). Descriptive statistics were given as a median (1st quartile–3rd quartile (Q1–Q3)) for continuous variables. Mann–Whitney U test was used to compare nonparametric variables. In comparison of categorical variables, the χ^2 test was used when conditions were met; otherwise, the Fisher's exact test was used. A p-value of ≤0.05 was considered statistically significant.

Results

The NAFLD animal model at 8 weeks

Body and liver weights of group B mice fed with HFD were significantly higher than group A mice at 8 weeks (p = 0.0021, p = 0.0043). While HS was not found in group A, 5 mice had HS in group B, and their fatty liver rates were determined as 10% in 3 mice, 15% in 1 mouse and 30% in 1 mouse (p = 0.0151). The NAS was found to be 4.0 (2.0–4.0) in group B mice and 0.0 (0.0–0.0) in group A (p = 0.0021) (Table 1).

Table 1. Comparison of the animal weight, liver weight, hepatosteatosis (HS), and NAS of C57BL/6J mice receiving standard and HFD (butter) in an eight-week period

Variables	Group A (control) (n = 6)	Group B (HFD) (n = 6)	p-value
Animal weight [g], median (Q1–Q3)	24.9 (24.4–25.2)	33.5 (30.9–36.0)	0.0021
Liver weight [g], median (Q1–Q3)	0.9 (0.9–0.9)	1.2 (1.0–1.4)	0.0043
HS, n (%)	0 (0.0)	5 (83.3)	0.0151
NAS, median (Q1–Q3)	0.0 (0.0–0.0)	4.0 (2.0–4.0)	0.0021

HFD – high-fat diet; NAS – non-alcoholic fatty liver disease (NAFLD) activity score; the data are shown as median, (Q1–Q3: 1st–3rd quartile) and p-values were for the Mann–Whitney U test, except HS (χ^2 test, df = 1).

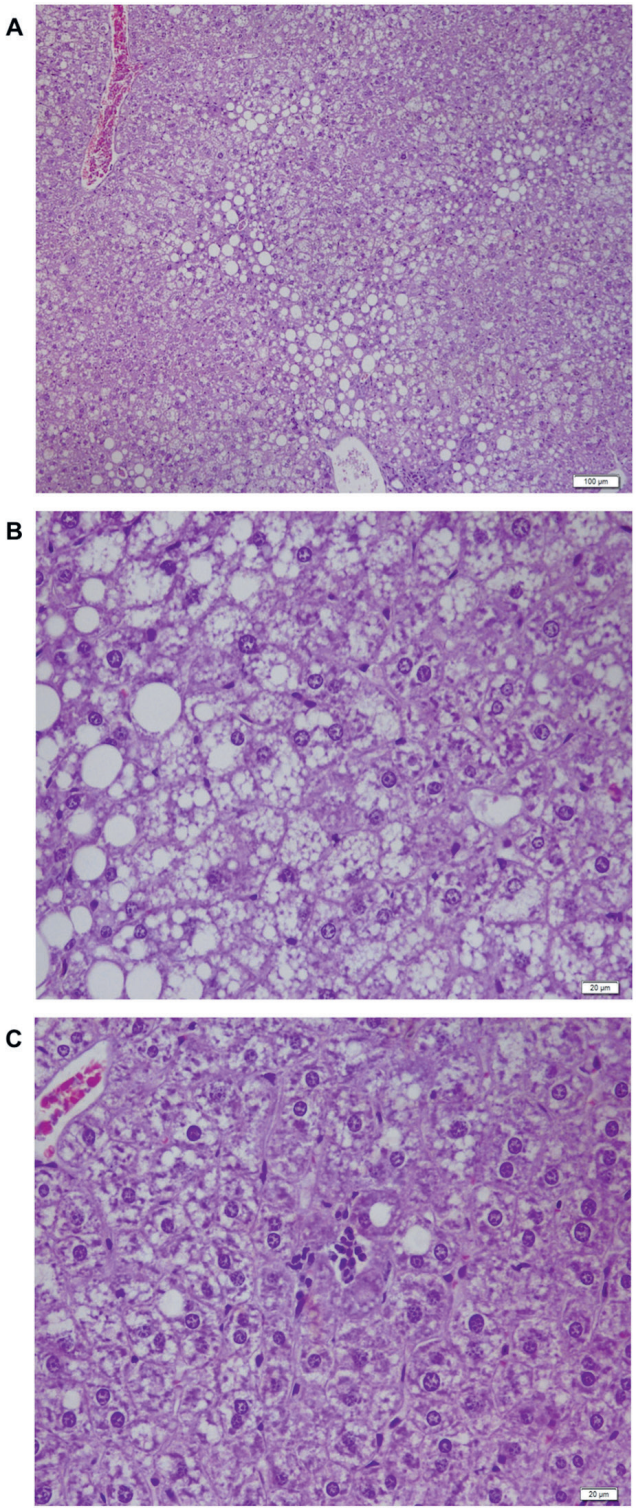

Fig. 2. Microscopic images of liver histology in high-fat diet (HFD) mice. A. Grade 2 microvesicular steatosis, ×4 magnification; B. Hepatocellular ballooning, ×10 magnification; C. Lobular inflammation, ×10 magnification; stained with hematoxylin and eosin (H&E)

Control diet compared to high-fat diet at 16 weeks

Macroscopic appearance of liver tissues was smooth and dark red in control mice. In histopathological examination of the control group, none of the mice had HS and NAS was determined to be 0.0 (0.0–0.0). Conversely, the liver tissues of HFD mice were granular, fragile and yellow-gray. All of them had HS, and fatty rates were determined as 10% in 3 mice, 30% in 1 mouse and 40% in 2 mice. The NAS in the HFD mice was calculated as 5.0 (4.0–5.0) and was significantly higher than in the controls ($p = 0.0021$). The H&E staining images samples of the liver tissue in HFD mice are displayed in Fig. 2. Also, serum lipid levels were significantly higher in HFD, except TG (Table 2).

High-fat diet compared to high-fat diet + lactulose

High-fat diet + lactulose mice had lower level of liver, but not lower body weight when compared with HFD mice ($p = 0.0043$ and $p = 0.1796$, respectively). Two of HFD + lactulose mice had HS (fatty rates were 15% and 30%; $p = 0.0606$). The NAS was 1.5 (1.0–3.0), which was significantly lower than in HFD mice ($p = 0.0021$). There was no difference between the groups in terms of body weight, glucose level and lipid parameters (Table 2).

High-fat diet compared to high-fat diet + PEG 3350

Body and liver weight of HFD + PEG 3350 mice were lower than those of HFD mice (both $p = 0.0086$). In the histopathological evaluation of the liver, only 1 mouse in the HFD + PEG 3350 group had 30% HS, and the NAS was 0.5 (0.0–1.0), which was significantly lower than in the HFD group ($p = 0.0151$, $p = 0.0021$). There was no difference between the groups in terms of glucose and lipid parameters, except TG. Higher TG levels were observed in HFD + PEG 3350 mice ($p = 0.0021$) (Table 2).

High-fat diet + lactulose compared to high-fat diet + PEG 3350

The body weight of the HFD + PEG 3350 mice was lower when compared with HFD + lactulose mice ($p = 0.0259$). However, there was no statistically significant difference between the groups in terms of liver weight, HS and NAS (Table 2).

Comparison of body weight, liver weight and NAS in all groups is shown in Fig. 3, and differences in biochemical parameters are shown in Fig. 4.

Table 2. Comparison of the liver and laboratory analysis of high-fat diet (HFD), HFD + lactulose and HFD + PEG 3350 mice in a sixteen-week period

Variables	Control (n = 6)	HFD (n = 6)	HFD + lactulose (n = 6)	HFD + PEG 3350 (n = 6)	p-value*	p-value**	p-value***	p-value****
Liver analysis								
Animal weight [g], median (Q1–Q3)	26.8 (26.7–27.2)	40.9 (34.7–41.9)	35.0 (34.6–36.0)	32.4 (30.2–33.9)	0.0021	0.1796	0.0086	0.0259
Liver weight [g], median (Q1–Q3)	1.4 (1.3–1.5)	1.8 (1.6–1.9)	1.3 (1.3–1.4)	1.5 (1.3–1.5)	0.0043	0.0043	0.0086	0.4848
HS, n (%)	0 (0.0)	6 (100.0)	2 (33.3)	1 (16.7)	0.0021	0.0606	0.0151	1.0000
NAS, median (Q1–Q3)	0.0 (0.0–0.0)	5.0 (4.0–5.0)	1.5 (1.0–3.0)	0.5 (0.0–1.0)	0.0021	0.0021	0.0021	0.1320
Laboratory analysis								
TC [mg/dL], median (Q1–Q3)	74.5 (71.0–76.0)	141.0 (136.0–157.0)	156.0 (148.0–157.0)	162.0 (159.0–165.0)	0.0021	0.2402	0.0649	0.0151
LDL-C [mg/dL], median (Q1–Q3)	9.6 (9.2–10.2)	34.2 (26.5–43.3)	26.5 (24.7–28.3)	24.7 (24.0–25.40)	0.0021	0.1796	0.0649	0.1796
HDL-C [mg/dL], median (Q1–Q3)	60.4 (57.8–61.3)	129.4 (109.0–145.3)	139.6 (136.0–142.8)	137.2 (136.7–137.6)	0.0021	0.4848	0.3939	0.3939
TG [mg/dL], median (Q1–Q3)	93.0 (86.0–133.0)	107.5 (102.0–127.0)	107.0 (102.0–108.0)	213.5 (212.0–215.0)	0.3939	0.6991	0.0021	0.0021
Glucose [mg/dL], median (Q1–Q3)	147.5 (130.0–148.0)	196.0 (191.0–218.0)	209.0 (204.0–211.0)	165.0 (155.0–170.0)	0.0095	0.2857	0.0571	0.0357

The data are shown as median (Q1–Q3: 1st–3rd quartile) and p-values were for the Mann–Whitney U test, except HS (χ^2 test, df = 1); HDL-C – high-density lipoprotein cholesterol; HFD – high-fat diet; HS – hepatosteatosis; LDL-C – low-density lipoprotein cholesterol; NAS – non-alcoholic fatty liver disease (NAFLD) activity score; PEG 3350 – polyethylene glycol 3350; TC – total cholesterol; TG – triglycerides; *between control and HFD groups; **between HFD and HFD + lactulose groups; ***between HFD and HFD + PEG 3350 groups; ****between HFD + lactulose and HFD + PEG 3350 groups.

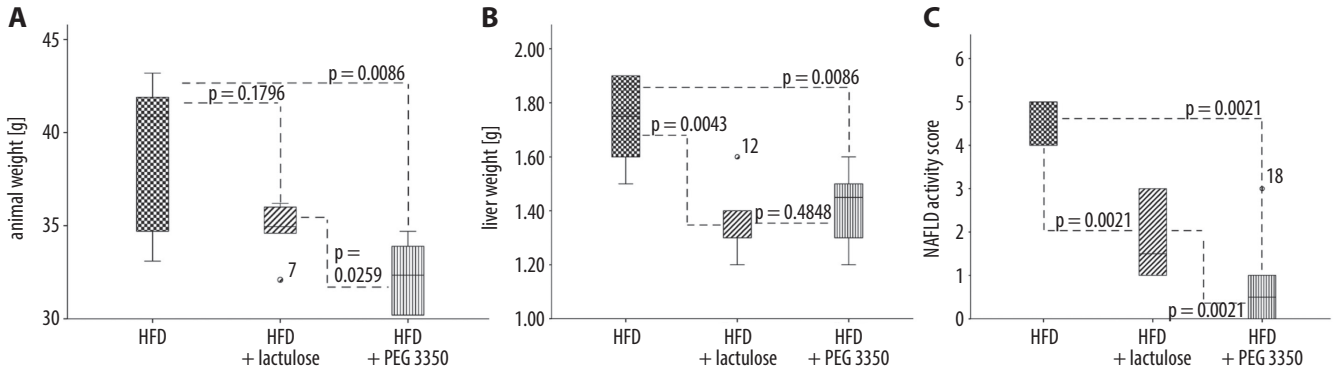

Fig. 3. High-fat diet (HFD) + lactulose and HFD + PEG 3350 mice had lower body weight (A), liver weight (B) and NAS (C) when compared with HFD mice. The data are shown as median, (Q1–Q3) (p-value for the Mann–Whitney U test)

NAFLD – non-alcoholic fatty liver disease; NAS – NAFLD activity score.

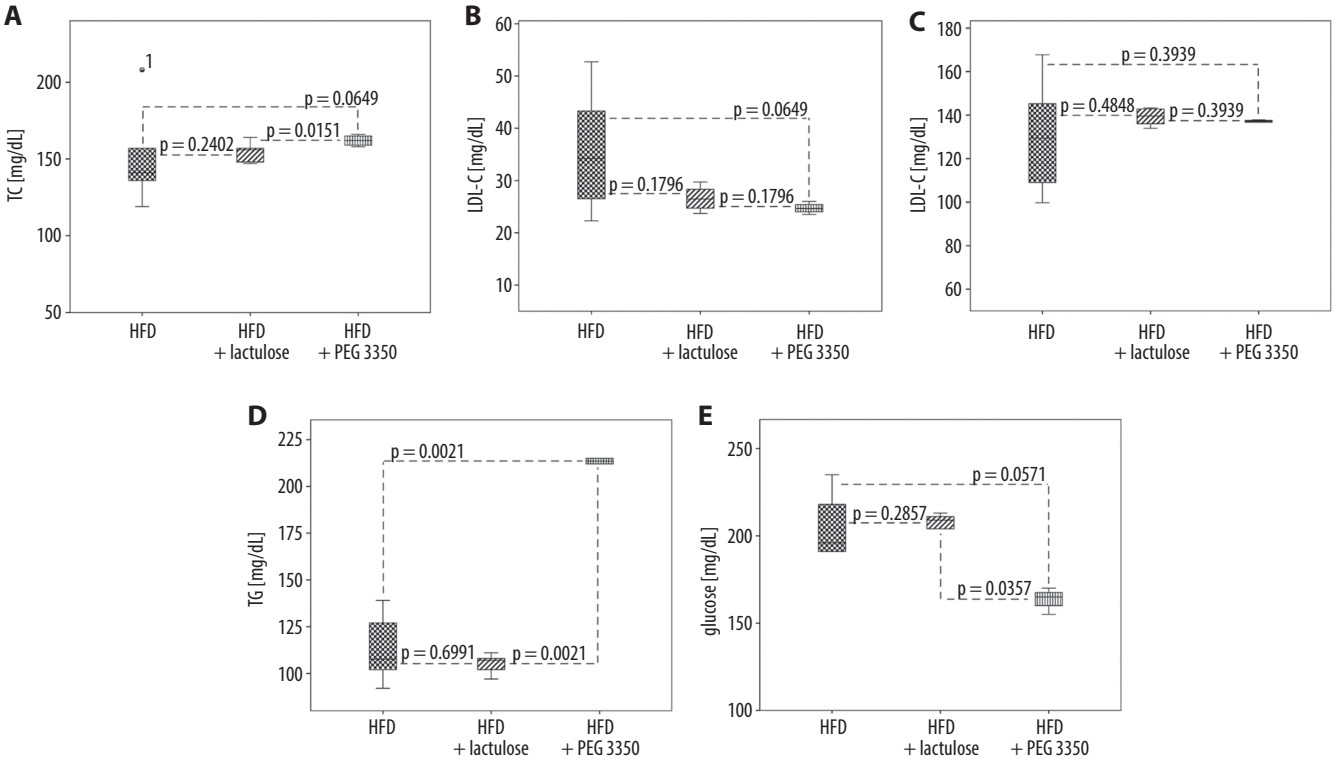

Fig. 4. Comparison of high-fat diet (HFD), HFD + lactulose and HFD + PEG 3350 mice by biochemical parameters including TC (A), LDL-C (B), HDL-C (C), TG (D), and glucose (E). The data are shown as median (Q1–Q3; p-value for the Mann–Whitney U test)

TC – total cholesterol; LDL-C – low-density lipoprotein cholesterol; HDL-C – high-density lipoproten cholesterol; TG – triglycerides.

Discussion

The pathogenesis of NAFLD is still not clearly elucidated and there are no accepted therapeutic options, except for diet and lifestyle changes. Diets lacking methionine and kaolin, and rich in sucrose and fructose or fat are often preferred to induce NAFLD. Butter is one of the well-known hyperlipidemic oils frequently included in our dietary habits. We observed that both obesity and NASH models were induced in all mice fed a HFD, which included 60% of energy provided through butter (both p = 0.0021). This is similar to a previous study in rats fed chow with a similar butter ratio, which also developed HS, although no weight gain was observed.[9] In a study investigating the effect of fatty diets on intestinal flora, fecal DNA samples of mice receiving butter were compared with mice receiving olive oil and a standard diet. It was observed that the proteobacteria family, which is frequently indicated in NASH-intestinal pathogenesis, was more prevalent in the mice receiving butter.[10] In this study, HDL-C/LDL-C ratios

were sorted as olive oil > butter > standard diet. Similarly, we observed increased HDL-C and LDL-C in mice receiving butter. Furthermore, in a human study this concurrent increase was observed in healthy volunteers given a diet containing moderate butter ratio (4.5%).[11] It is thought that HDL-C compensates for LDL-C, so there is no increased cardiovascular risk in this population. Based on this result, it is recommended that butter should be minimized in the diet of hyperlipidemic patients, but moderate butter intake can be allowed in normolipidemic individuals. We observed another interesting finding in the lipid profile of HFD mice, namely, the absence of increased TG levels. Essentially, TG accumulation in the liver is thought to be one of the fundamentals of NAFLD pathogenesis. In a rat model of NAFLD, the highest TG level was seen in the 1st week and then decreased, and this was explained by the decreased food intake in the following weeks.[12] In the present study, while the amount of food intake consumed throughout the experiment was constant, there was no correlation between TG level and NAFLD.

The liver is directly affected by changes in the intestine due to portal vein flow. Stool analysis of patients with NAFLD showed that their intestinal flora density was different from healthy individuals. For example, in the presence of NASH, bacteroidete (bacteroidaceae, prevotellaceae, rikenellaceae) density was increased, while the density of actinobacteria (bifidobacteriaceae) decreased.[13] In the same study, it was shown that *Escherichia*, which was responsible for the high endogenous serum alcohol production, increased liver damage in patients with NASH. Hence, bacteroidetes and *Ruminococcus*, which are known to produce alcohol, are considered an independent risk factor for NAFLD and fibrosis, respectively.[3] When fecal DNA analysis was performed in a patient with NAFLD, it was shown that the density of fusobacteriaceae and prevotellaceae, which are known as short chain fatty acid (SCFA) producing bacteria, increased, and the fecal SCFA concentrations were high.[14] Consequently, dysbiosis, increased SCFA production and altered permeability of the intestinal barrier are thought to lead to NAFLD and even fibrosis at later stages.

In our study, we observed that a non-diarrheal dose of lactulose improved hepatic inflammation without significant weight loss. This result suggests that lactulose may play a role in the treatment of lean NAFLD. It has been shown that *Lactobacillus plantarum* spp. NA136 and *Lactobacillus johnsonii* spp. BS15, known as probiotics, inhibited hepatic steatosis and regressed hepatic inflammation in mice.[15,16] Additionally, lactulose reduced the high concentration of SCFA seen in the stools of NAFLD patients, and caused the regression of steatosis.[4] In another study performed in rats with induced NASH, lactulose decreased both portal vein serum endotoxin levels and hepatic inflammation, but had no effect on HS.[17] Unlike in that study, we started lactulose treatment concurrent with HFD, and the duration of treatment was longer (8 weeks compared to 16 weeks). However, we observed a similar result being decreased NAS but no effect on HS.

Lactulose may contain up to 30% carbohydrates in the form of water-soluble liquid syrups, such as those used in this study. However, we observed no increase in glucose levels. In a recent randomized controlled study of healthy volunteers, neither form of lactulose was found to have a significant effect on serum glucose levels, and no hyperglycemic effect was observed in diabetic patients.[18,19] Interestingly, lactulose leads to positive changes in carbohydrate metabolism, creating fiber and acarbose effects and increasing glucose tolerance in patients with diabetes mellitus.[20] In the jejunal loops of rats given lactulose, it was observed that glucose absorption was decreased by 40%, but amino acid absorption was not.[21] It is thought that bacterial endotoxins reduce the production of pancreatic insulin, and therefore, any treatment that reduces the production of endotoxin will have an antidiabetic effect.[22] The decreased hepatic inflammation in our HFD + lactulose group could be due to the beneficial effects of lactulose on insulin resistance, as we observed no differences in terms of serum lipid levels between HFD + lactulose and HFD mice. Similarly, Mao et al. found no changes in biochemical parameters with the same dose of lactulose (15%, ~0.44 g/day) given in our study in C57BL/6J mice for 2 weeks.[7] However, we showed an approx. 23% decrease of LDL-C level with lactulose, although this was not statistically significant. Serum cholesterol levels decreased by 17% in hyperlipidemic patients receiving lactulose treatment for 4 weeks, and this decrease continued for 4 weeks following the cessation of treatment.[23]

Polyethylene glycol 3350, because of its high molecular weight and non-absorbable structure, is frequently used for intestinal perfusion studies and colonoscopy preparations, with high doses of PEG 3350 required for colonic lavage. It has also started to be preferred as a long-term treatment option for functional constipation, softening the stool without inducing diarrhea. The PEG 3350 dose that we used was calculated by adapting the lower dose (17 g/day) used in humans to the weight of a mouse. We observed decreased liver and body weight, 83.3% less HS and lower NAS in the HFD + PEG 3350 mice at non-diarrheal dose. To our knowledge, this is the first study to investigate the effect of PEG 3350 on NAFLD treatment, and we believe these results may depend on its weight-reducing effect. Essentially, the studies investigating the effect of PEG 3350 on intestinal flora were performed at a high dose, similar to that used for colonic lavage. Some of these studies showed no significant difference between prelavage and postlavage bacterial cultures,[24,25] while Drago et al. showed the decreased density of *Lactobacillus* and increased density of proteobacteria, which is known to cause severe diarrheal attacks.[6] Contrary, rikenellaceae had been shown to decrease in pediatric patients with NAFLD and increased

in individuals who had colonic lavage with PEG.[6,26] Hence, more studies are needed using formulas with different doses of PEG 3350 to determine its positive effect on the gut microbiota.

Since PEG 3350 is not considered a long-term treatment, there are few studies investigating the effects of PEG 3350 on lipid profile. In our study, we detected higher serum TG levels in the HFD + PEG 3350 treatment group despite a decrease in HS and NAS. We believe this interesting finding suggests that PEG 3350 reduces lipid uptake by the liver at the receptor level, without affecting serum lipids. For instance, it was observed that a liver-specific inhibitor that inhibited acetyl CoA carboxylase decreased hepatic steatosis, but increased serum TG levels in an insulin-resistant rat model.[27] Likewise, we observed no changes in terms of lipid parameters, except TG. It was shown that intestinal transit time decreased by 20%, but there was no change in TC and TG levels in rats given PEG 4000 at a non-diarrheal dose.[28] We also detected lower serum glucose levels in HFD + PEG 3350 mice, which was close to but not statistically significant ($p = 0.0571$). Similarly, in humans, it was observed that there was no difference between PEG 3350 and placebo in terms of glucose levels in the treatment of functional constipation for 2 weeks.[29] This provides a safe side effect profile in individuals with insulin resistance.

Limitations

This study has some limitations. First, fecal bacterial DNA analysis was not performed to evaluate the effect of drugs on the intestinal flora. Second, sequential biochemical analysis of serum lipid and glucose and aminotransferase tests were not done due to insufficient blood samples.

Conclusions

Currently, there are no approved therapies for NAFLD. Drug development efforts have focused on pathogenic mechanisms including gut–liver axis. We developed an obesity and NAFLD mouse model through the administration of a HFD. Then, we observed decreases in HS by 66.7% and 83.3% in the HFD + lactulose and HFD + PEG 3350 treatment groups, respectively. Significant decreases in NAS were found in HFD + lactulose (1.5 (1.0–3.0)) and HFD + PEG 3350 (0.5 (0.0–1.0)) treatment groups when compared with the HFD group (5.0 (4.0–5.0)). The decrease in body weight was determined as 11% and 16.5%, respectively. Considering that more than 10% weight loss reduces not only steatosis but also fibrosis in NAFLD, it seems likely that lactulose and PEG 3350 may have an effect in the treatment of obesity and NAFLD. We recommend that human studies should be conducted to address this.

ORCID iDs

Pinar Gokcen https://orcid.org/0000-0002-6742-6976
Oguzhan Ozturk https://orcid.org/0000-0002-7718-8684
Gupse Adali https://orcid.org/0000-0003-2157-0304
Ilkay Tosun https://orcid.org/0000-0003-3380-7591
Halef Okan Dogan https://orcid.org/0000-0001-8738-0760
Haki Kara https://orcid.org/0000-0002-0295-0582
Yucel Yalman https://orcid.org/0000-0001-6506-3836
Hamdi Levent Doganay https://orcid.org/0000-0002-2263-6689
Kamil Ozdil https://orcid.org/0000-0003-2556-3064

References

1. Younossi Z, Anstee QM, Marietti M, et al. Global burden of NAFLD and NASH: Trends, predictions, risk factors and prevention. *Nat Rev Gastroenterol Hepatol*. 2018;15(1):11–20. doi:10.1038/nrgastro.2017.109
2. Safari Z, Gérard P. The links between the gut microbiome and non-alcoholic fatty liver disease (NAFLD). *Cell Mol Life Sci*. 2019;76(8):1541–1558. doi:10.1007/s00018-019-03011-w
3. Boursier J, Mueller O, Barret M, et al. The severity of non-alcoholic fatty liver disease is associated with gut dysbiosis. *Hepatology*. 2016;63(3):764–775. doi:10.1002/hep.28356
4. Zhai S, Zhu L, Qin S, Li L. Effect of lactulose intervention on gut microbiota and short chain fatty acid composition of C57BL/6J mice. *Microbiologyopen*. 2018;7(6):e00612. doi:10.1002/mbo3.612
5. Wang JY, Bajaj JS, Wang JB, et al. Lactulose improves cognition, quality of life, and gut microbiota in minimal hepatic encephalopathy: A multicenter, randomized controlled trial. *J Dig Dis*. 2019;20(10):547–556. doi:10.1111/1751-2980.12816
6. Drago L, Toscano M, De Grandi R, Casini V, Pace F. Persisting changes of intestinal microbiota after bowel lavage and colonoscopy. *Eur J Gastroenterol Hepatol*. 2016;28(5):532–537. doi:10.1097/MEG.0000000000000581
7. Mao B, Li D, Ai C, Zhao J, Zhang H, Chen W. Lactulose differently modulates the composition of luminal and mucosal microbiota in C57BL/6J mice. *J Agric Food Chem*. 2016,64(31):6240–6247. doi:10.1021/acs.jafc.6b02305
8. Kleiner DE, Brunt EM, Van Natta M, et al. Nonalcoholic steatohepatitis clinical research network: Design and validation of a histological scoring system for non-alcoholic fatty liver disease. *Hepatology*. 2015;41(6):1313–1321. doi:10.1002/hep.20701
9. Nalloor TJP, Kumar N, Narayanan K, Palanimuthu VR. Long-term exposure to a butter-rich diet induces mild-to-moderate steatosis in Chang liver cells and Swiss albino mice models. *J Basic Clin Physiol Pharmacol*. 2017;28(3):257–265. doi:10.1515/jbcpp-2016-0058
10. Prieto I, Hidalgo M, Segarra AB, et al. Influence of a diet enriched with virgin olive oil or butter on mouse gut microbiota and its correlation to physiological and biochemical parameters related to metabolic syndrome. *PLoS One*. 2018;13(1):e0190368. doi:10.1371/journal.pone.0190368
11. Engel S, Tholstrup T. Butter increased total and LDL cholesterol compared with olive oil but resulted in higher HDL cholesterol compared with a habitual diet. *Am J Clin Nutr*. 2015;102(2):309–315. doi:10.3945/ajcn.115.112227
12. Wardani HA, Rahmadi M, Ardianto C, Balan SS, Kamaruddin NS, Khotib J. Development of non-alcoholic fatty liver disease model by high-fat diet in rats. *J Basic Clin Physiol Pharmacol*. 2019;30(6):/j/jbcpp.2019.30.issue-6/jbcpp-2019-0258/jbcpp-2019-0258.xml. doi:10.1515/jbcpp-2019-0258
13. Zhu L, Baker SS, Gill C, et al. Characterization of gut microbiomes in non-alcoholic steatohepatitis (NASH) patients: A connection between endogenous alcohol and NASH. *Hepatology*. 2013;57(2):601–609. doi:10.1002/hep.26093
14. Rau M, Rehman A, Dittrich M, et al. Fecal SCFAs and SCFA-producing bacteria in gut microbiome of human NAFLD as a putative link to systemic T-cell activation and advanced disease. *United European Gastroenterol J*. 2018;6(10):1496–1507. doi:10.1177/2050640618804444
15. Zhao Z, Wang C, Zhang L, et al. *Lactobacillus plantarum* NA136 improves the non-alcoholic fatty liver disease by modulating the AMPK/Nrf2 pathway. *Appl Microbiol Biotechnol*. 2019;103(14):5843–5850. doi:10.1007/s00253-019-09703-4

16. Xin J, Zeng D, Wang H, et al. Preventing non-alcoholic fatty liver disease through *Lactobacillus johnsonii* BS15 by attenuating inflammation and mitochondrial injury and improving gut environment in obese mice. *Appl Microbiol Biotechnol*. 2014;98(15):6817–6829. doi:10.1007/s00253-014-5752-1
17. Fan JG, Xu ZJ, Wang GL. Effect of lactulose on establishment of a rat non-alcoholic steatohepatitis model. *World J Gastroenterol*. 2005; 11(32):5053–5056. doi:10.3748/wjg.v11.i32.5053
18. Steudle J, Schön C, Wargenau M, et al. Blood glucose response after oral intake of lactulose in healthy volunteers: A randomized, controlled, cross-over study. *World J Gastrointest Pharmacol Ther*. 2018; 9(3):22–30. doi:10.4292/wjgpt.v9.i3.22
19. Lieberthal M, Conn HO, Bircher J. *Hepatic Encephalopathy*. Michigan, USA: Medi-Ed Press; 1988.
20. Huchzermeyer H, Schumann C. Lactulose: A multifaceted substance. *Z Gastroenterol*. 1997;35(10):945–955. PMID:9370144
21. Hosaka H, Tokunaga K, Sakumoto I. The influence of lactulose on intestinal absorption. *Gastroenterol Jpn*. 1972;7:316–317. doi:10. 1007/BF02779812
22. Cornell RP. Endogenous gut-derived bacterial endotoxin tonically primes pancreatic secretion of insulin in normal rats. *Diabetes*. 1985; 34(12):1253–1259. doi:10.2337/diab.34.12.1253
23. Conte D, Bardella MT, Bernardi M, Pacetti G, Bianchi PA. Hypocholesterinemic effect of lactulose in man. *Panminerva Med*. 1977;19: 1–4. PMID:834472
24. Beck DE, Harford FJ, DiPalma JA. Comparison of cleansing methods in preparation for colonic surgery. *Dis Colon Rectum*. 1985;28(7):491–495. doi:10.1007/BF02554091
25. Morotomi M, Guillem JG, Pocsidio J, et al. Effect of polyethylene glycol-electrolyte lavage solution on intestinal microflora. *Appl Environ Microbiol*. 1989;55(4):1026–1028. doi:10.1128/AEM.55.4.1026-1028.1989
26. Del Chierico F, Nobili V, Vernocchi P, et al. Gut microbiota profiling of pediatric non-alcoholic fatty liver disease and obese patients unveiled by an integrated meta-omics-based approach. *Hepatology*. 2017;65(2):451–464. doi:10.1002/hep.28572
27. Kim CW, Addy C, Kusunoki J, et al. Acetyl CoA carboxylase inhibition reduces hepatic steatosis but elevates plasma triglycerides in mice and humans: A bedside to bench investigation. *Cell Metab*. 2017; 26(2):394–406. doi:10.1016/j.cmet.2017.07.009
28. van der Wulp MY, Cuperus FJ, Stellaard F, et al. Laxative treatment with polyethylene glycol does not affect lipid absorption in rats. *J Pediatr Gastroenterol Nutr*. 2012;55(4):457–462. doi:10.1097/MPG. 0b013e3182555ba9
29. Di Palma JA, Smith JR, Cleveland MvB. Overnight efficacy of polyethylene glycol laxative. *Am J Gastroenterol*. 2002;97(7):1776–1779. doi:10.1111/j.1572-0241.2002.05840.x

Effect of adenosine triphosphate, benidipine and their combinations on bevacizumab-induced kidney damage in rats

Hüseyin Kocaturk[2,A,C,E,F], Fevzi Bedir[2,B,F], Ömer Turangezli[2,B,F], Remzi Arslan[3,C,F], Taha Abdulkadir Çoban[4,C,F], Durdu Altuner[1,C,F], Halis Suleyman[1,D,E,F]

[1] Department of Pharmacology, Faculty of Medicine, Erzincan Binali Yıldırım University, Turkey
[2] Department of Urology, Erzurum Regional Training and Research Hospital, Health Sciences University, Turkey
[3] Department of Pathology, Faculty of Medicine, Atatürk University, Erzurum, Turkey
[4] Department of Biochemistry, Faculty of Medicine, Erzincan Binali Yıldırım University, Turkey

A – research concept and design; B – collection and/or assembly of data; C – data analysis and interpretation; D – writing the article; E – critical revision of the article; F – final approval of the article

Advances in Clinical and Experimental Medicine, ISSN 1899–5276 (print), ISSN 2451–2680 (online) *Adv Clin Exp Med*. 2021;30(11):1175–1183

Address for correspondence
Halis Suleyman
E-mail: halis.suleyman@gmail.com

Funding sources
None declared

Conflict of interest
None declared

Received on March 23, 2021
Reviewed on June 15, 2021
Accepted on July 22, 2021

Published online on September 22, 2021

Abstract

Background. Bevacizumab-induced vascular endothelial growth factor (VEGF) inhibition may lead to a decrease in adenosine triphosphate (ATP) levels, an increase in intracellular Na^+ and Ca^{2+} concentrations and an increase in reactive oxygen species (ROS) generation, as well as to cell damage.

Objectives. To investigate the biochemical and histopathological effects of ATP, benidipine and ATP in combination with benidipine on bevacizumab-induced kidney damage in rats.

Materials and methods. Rats were divided into 5 treatment groups: bevacizumab (BVZ) alone, ATP + bevacizumab (ABVZ), benidipine + bevacizumab (BBVZ), ATP + benidipine + bevacizumab (ABBVZ), and healthy controls (HC). Adenosine triphosphate (25 mg/kg), benidipine (4 mg/kg orally), ATP (25 mg/kg) + benidipine (4 mg/kg), or saline were administered to albino Wistar rats. One hour after treatment, bevacizumab was injected at a dose of 10 mg/kg to induce kidney damage. Two doses of bevacizumab were delivered 15 days apart. Adenosine triphosphate + benidipine were administered once a day for 1 month.

Results. Malondialdehyde (MDA), total oxidant status (TOS), creatinine, and blood urea nitrogen (BUN) levels of the BVZ, BBVZ, ABVZ, ABBVZ, and HC groups were ranked from highest to lowest. Conversely, total glutathione (tGSH) and total antioxidant status (TAS) kidney tissue values were ranked from lowest to highest, respectively. Hemorrhage, tubular necrosis and grade 3 focal tubular atrophy were observed in the BVZ group. Atrophy and grade 2 necrosis were observed in the BBVZ group and atrophy and grade 1 necrosis were observed in the ABVZ group. Only grade 1 atrophy was observed in the ABBVZ group.

Conclusions. Adenosine triphosphate reduced bevacizumab-induced renal toxicity significantly more effectively than benidipine. However, the combination of ATP + benidipine further reduced bevacizumab-induced renal toxicity relative to benidipine or ATP alone. These data indicate that ATP + benidipine might be a potential therapeutic strategy for the prevention of bevacizumab-induced renal toxicity.

Key words: bevacizumab, rat, nephrotoxicity, ATP, benidipine

Cite as
Kocaturk H, Bedir F, Turangezli Ö, et al. Effect of adenosine triphosphate, benidipine and their combinations on bevacizumab-induced kidney damage in rats. *Adv Clin Exp Med*. 2021;30(11):1175–1183. doi:10.17219/acem/140440

DOI
10.17219/acem/140440

Background

Bevacizumab is a monoclonal hybrid antibody that binds and neutralizes vascular endothelial growth factor (VEGF).[1] Inhibition of VEGF signaling is a common therapeutic strategy in oncology for the development of new drugs.[2] Bevacizumab and other anti-VEGFs that have been successfully used in the treatment of renal cell carcinoma and colorectal cancer have become some of the most prescribed drugs in the present day.[3] Bevacizumab and other VEGF-targeting monoclonal antibodies are also used intravitreally for the treatment of exudative macular degeneration.[4] However, the development of overt proteinuria, new-onset hypertension and nephrotic syndrome have been frequently reported during bevacizumab therapy.[1] The latest data demonstrate that even intravitreal injections of VEGF inhibitors lead to significant systemic absorption and a measurable decrease in the VEGF activity, and this event has been reported to result in hypertension, proteinuria, glomerular disease, and thrombotic microangiopathy.[5] Even though bevacizumab-associated glomerulonephritis and nephrotic syndrome have been confirmed by means of renal biopsy, the mechanism of action has not yet been clarified.[1] However, the data cited above suggest that bevacizumab nephrotoxicity is due to decreased VEGF.

There are data in the literature showing that VEGF increases intracellular adenosine triphosphate (ATP) levels and reduces the production of reactive oxygen species (ROS).[6] These findings also suggest that decreased VEGF may result in decreased ATP levels and increased ROS production. Decreased ATP causes the inhibition of the Na^+/K^+-ATPase pump in the cell membrane and, consequently, increases in intracellular Na^+ and Ca^{2+} concentrations.[7] Increased levels of Ca^{2+} induce ROS production and cause the Ca^{2+} channels to open. This event leads to further increases in intracellular calcium levels and cell toxicity.[8,9] These data indicate that bevacizumab nephrotoxicity may cause increased intracellular Ca^{2+} levels and ROS as a result of decreased ATP.

Previous work has shown that ATP is a molecule mostly produced by oxidative phosphorylation under aerobic conditions in mitochondria.[10] Chiang et al. have reported that ATP elevates VEGF levels and promotes epithelization.[11] Here, we evaluate the effects of benidipine, an L-type calcium channel blocking antihypertensive agent,[12] on bevacizumab-induced kidney damage. It has been previously reported that benidipine prevents an increase in oxidant parameters and has positive effects on antioxidant levels in damaged tissues.[13]

Objectives

The data cited above suggest that an ATP and benidipine combination may be useful in the treatment of bevacizumab-associated nephrotoxicity. Thus, the aim of this study is to investigate the effects of ATP and benidipine, administered alone and in combination, on bevacizumab-induced renal damage in rats, using biochemical and histopathological techniques.

Materials and methods

Animals

A total of 30 male albino Wistar rats with a body weight of 250–267 g were used in the experiment. All rats were obtained from the Atatürk University Medical Experimental Practice and Research Center (Erzurum, Turkey). Prior to the experiment, the animals were housed and fed under suitable conditions at normal room temperature (22°C) in a suitable laboratory setting. The protocols and procedures were approved by the local Animal Experimentation Ethics Committee (meeting No. 8 on July 28, 2020).

Pharmacological agents

Bevacizumab (100 mg/4 mL) was supplied by Roche Switzerland (Basel, Switzerland), benidipine was supplied by Deva (Istanbul, Turkey), thiopental sodium was supplied by İ.E ULAGAY (Istanbul, Turkey), and ATP was supplied by Zdorove Narodu (Kharkiv, Ukraine).

Experimental groups

Rats were divided into 5 treatment groups: bevacizumab (BVZ) alone, ATP + bevacizumab (ABVZ), benidipine + bevacizumab (BBVZ), ATP + benidipine + bevacizumab (ABBVZ), and healthy controls (HC).

Experimental procedure

Adenosine triphosphate was administered at a dose of 25 mg/kg intraperitoneally (ip.) to the ABVZ group of rats. Benidipine was administered orally by gavage at a dose of 4 mg/kg to the BBVZ group. Adenosine triphosphate (25 mg/kg, ip.) and benidipine (4 mg/kg, orally) were administered simultaneously to the ABBVZ group. Normal saline (0.9% NaCl) was administered to the HC group. One hour after the administration of ATP, benidipine or saline, bevacizumab was injected ip. at a dose of 10 mg/kg to the BVZ, ABVZ, BBVZ, and ABBVZ groups. A total of 2 doses of bevacizumab were delivered with an interval of 15 days. Adenosine triphosphate and benidipine were administered once daily for 1 month. The animals were sacrificed using a high dose of thiopental sodium (50 mg/kg) at the end of this period. The kidneys were removed immediately after the animals were sacrificed. Malondialdehyde (MDA), total glutathione (tGSH) levels, total oxidant status (TOS), and total antioxidant status (TAS) values were measured in the renal

tissue. Renal tissue samples were also examined histopathologically. Creatinine and blood urea nitrogen (BUN) levels were measured in blood samples taken before the animals were sacrificed.

Biochemical analyses

MDA measurement

The MDA measurement was conducted applying the method developed by Ohkawa et al.[14] Briefly, 25 µL of sodium dodecyl sulfate (80 g/L) and 1 mL of a mixture of 200 g/L acetic acid and 1.5 mL 8 g/L 2-thiobarbituric acid were added to 25 µL of the sample and heated at 95°C for 60 min. After cooling down, the samples were centrifuged at 4000 rpm for 10 min. The absorbance of the upper layer was then measured at 532 nm. The amount of MDA in the sample was calculated on a calibration graph drawn using 1,1,3,3-tetraethoxypropane as a standard.

tGSH measurement

The method of Sedlak et al. was applied for tGSH analysis.[15] For deproteinization, the samples were processed with metaphosphoric acid in a ratio of 1:1 and centrifuged accordingly. Briefly, 150 µL of measurement mixture (5.85 mL of 100 mM Na-phosphate buffer, 2.8 mL of 1 mM 5,5-dithio-bis-(2-nitrobenzoic acid) (DTNB), 3.75 mL of 1 mM nicotinamide adenine dinucleotide phosphate (NADPH), and 80 µL of 625 U/L glutathione reductase) was added to 50 µL of the supernatant acquired from the sample. Measurements were conducted at 412 nm according to a standard graph prepared with oxidized glutathione (GSSG).

Measurements of TOS and TAS

The TOS and TAS levels of tissue homogenates were determined using a novel automated measurement method and commercially available kits (Rel Assay Diagnostics, Gaziantep, Turkey), both developed by Erel.[16,17] The TAS method is based on bleaching of the characteristic color of a more stable 2,2'-azino-bis (3-ethylbenzothiazoline-6-sulfonic acid) (ABTS) radical cation with antioxidants and measurements performed at 660 nm. The results are expressed as nmol hydrogen peroxide (H_2O_2) equivalent/L. For the TOS method, the oxidants present in the sample oxidize the ferrous ion-o-dianisidine complex to ferric ion. The oxidation reaction is enhanced by glycerol molecules, which are abundantly present in the reaction medium. The ferric ion produces a colored complex with xylenol orange in an acidic medium. The color intensity, which was measured at 530 nm spectrophotometrically, is related to the total amount of oxidant molecules present in the sample. The results are expressed as µmol Trolox equivalent/L. The percentage ratio of TOS to TAS was used as the oxidative stress index (OSI). The OSI was calculated as TOS divided by 100 × TAS.

Creatinine measurement

The quantitative assay for serum creatinine was conducted with spectrophotometric analysis using a Roche Cobas 8000 autoanalyzer (Roche Diagnostics, Basel, Switzerland). This kinetic colorimetric test was performed based on the Jaffe method. A yellow-orange color complex was formed with the creatinine picrate in alkaline solution. This complex was measured at a wavelength of 505 nm. The rate of stain formation is proportional to the creatinine concentration found in the sample. "Rate-blanking" (rate shield) was used to minimize the bilirubin interference. For the purposes of correcting the nonspecific reaction caused by serum/plasma pseudo-creatinine chromogens, including proteins and ketones, serum or plasma outcomes were corrected with –26 µmol/mL (–0.3 mg/dL).

BUN measurement

The quantitative assay for serum urea levels was also conducted with the spectrophotometric method using a Roche Cobas 8000 autoanalyzer. The levels were calculated using the formula BUN = urea × 0.48. The kinetic test with urease and glutamate dehydrogenase is based on urea hydrolysis into ammonium and carbonate ions (urea + 2 $H_2O \rightarrow {}^{(Urease)} \rightarrow 2\ NH_4^+ + CO_3^{2-}$). In the 2nd reaction, L-glutamate is formed when 2-oxoglutarate reacts with ammonium in the presence of glutamate and dehydrogenase (GLDH) and coenzyme NADH in the medium ($NH4^+$ + 2-oxoglutarate + NADH $\rightarrow {}^{(GLDH)} \rightarrow$ L-glutamate + NAD^+ + H_2O NADH). In this reaction, 2 moles of NADH are oxidized to NAD^+ for every mole of urea hydrolyzed. The rate of decrease in the concentration is directly proportional to the urea concentration in the sample. The measurement was conducted at a wavelength of 340 nm.

Histopathological analyses

Renal tissues were fixed with 10% neutral buffered formalin for a period of at least 24 h. The tissues were then embedded in paraffin blocks and sliced horizontally using a microtome into 4-µm sections. A minimum of 3 sections were obtained from each sample and were stained with hematoxylin and eosin (H&E) for histomorphological assessment. The stained sections were assessed by an independent pathologist (who was blinded to the experimental treatments) using an AXIO LAB A1 Zeiss microscope (Carl Zeiss AG, Jena, Germany). The severity of the histopathological findings in each section was scored between 0 and 3. The assignment of the severity grades was as follows: 0 – normal tissue; 1 – mild damage; 2 – moderate damage; and 3 – severe damage.

Statistical analyses

The biochemical results are shown as mean ± standard deviation (SD). With the exception of the MDA results, the significance of the differences between groups was tested using one-way analysis of variance (ANOVA). For the MDA analysis, a Kruskal–Wallis test was performed. Tukey's tests were used for post hoc comparisons, except for TOS. For TOS, the homogeneity of variances assumption was not met and the Games–Howell test was used.

The values obtained with histopathological grading are expressed as median and the difference between groups was analyzed using the Kruskal–Wallis test, with the Dunn's test used for post hoc comparisons. All statistical analyses were performed using SPSS for Windows v. 18.0 software (SPSS Inc., Chicago, USA), and a value of $p < 0.05$ was considered significant.

Results

Biochemical findings

MDA and tGSH analyses

As seen in Fig. 1, the amount of MDA in the kidney tissue of the animals was different across study groups (Kruskal–Wallis H: 26.99, $p < 0.001$, Table 1). The MDA levels in the BVZ group increased significantly compared to the HC group ($p < 0.001$), ABVZ ($p < 0.001$), BBVZ ($p < 0.001$), and the ABBVZ groups ($p < 0.001$). The amount of MDA in the kidney tissue of the ABVZ group was found to be lower than in the BBVZ group ($p < 0.001$). The MDA level was also found to be the lowest in the ABBVZ group. The difference in MDA levels between the ABBVZ group and the HC group was statistically insignificant ($p = 0.471$).

Bevacizumab administration also caused a decrease in tGSH in kidney tissue ($F(4,25) = 521.8$, $p < 0.001$; Fig. 2, Table 1). The level of tGSH decreased more significantly in the ABVZ group according to the BBVZ group. The tGSH levels of the ABBVZ group were the closest to that of the HC group (but still statistically different, $p = 0.024$). The combination of ATP + benidipine was the best at preventing the reduction of tGSH.

TOS and TAS analyses

The TOS and TAS levels were found to be significantly different across the study groups ($F(4,25) = 783.1$, $p < 0.001$; $F(4,25) = 583.9$, $p < 0.001$, respectively; Table 1). As can be seen in Fig. 3 and Fig. 4, while bevacizumab increased the TOS levels ($p < 0.001$) in the kidney tissue of the animals, it decreased the TAS levels ($p < 0.001$). The drugs with the best efficacy for preventing increased TOS were in the ABBVZ ($p < 0.001$), ABVZ ($p < 0.001$) and BBVZ groups ($p < 0.001$), respectively. Likewise, the drugs with

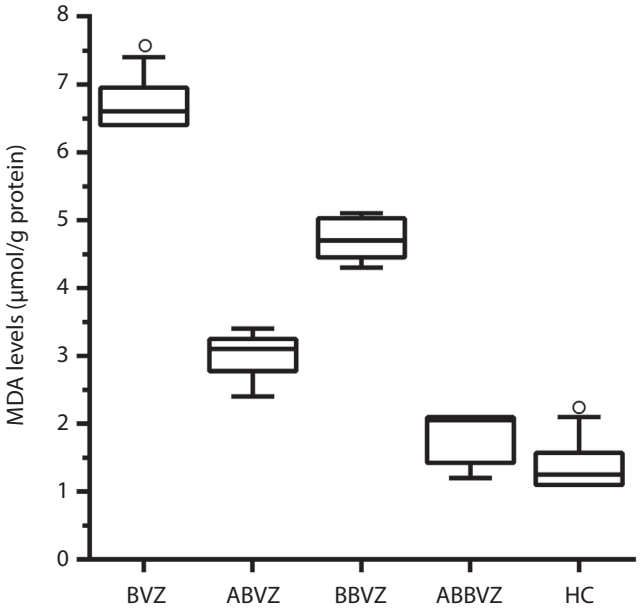

Fig. 1. Malondialdehyde (MDA) levels in the renal tissue of the study groups (BVZ = 6.7 ±0.4, ABVZ = 3.02 ±0.34, BBVZ = 4.7 ±0.3, ABBVZ = 1.8 ±0.4, and HC = 1.4 ±0.4)

Horizontal line – median; bottom line of the box – Q1 (25th); topline of the box – Q3 (75th); whiskers – minimum and maximum observation (excluding outlier); empty circles – outliers 1.5 × interquartile range (IQR) (Q3–Q1); BVZ – bevacizumab alone group; ABVZ – ATP + bevacizumab group; BBVZ – benidipine + bevacizumab group; ABBVZ – ATP + benidipine + bevacizumab; HC – healthy controls group; ATP – adenosine triphosphate.

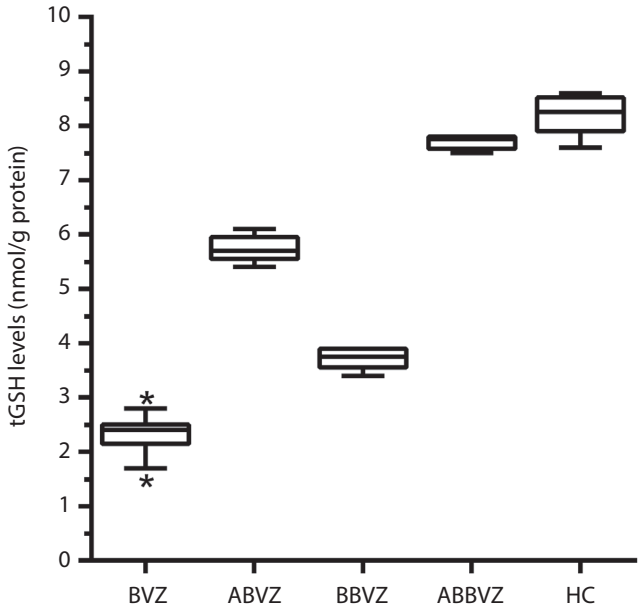

Fig. 2. Total glutathione (tGSH) levels in the renal tissue of the study groups (BVZ = 2.3 ±0.35, ABVZ = 5.7 ±0.24, BBVZ = 3.7 ±0.18, ABBVZ = 7.7 ±0.13, and HC = 8.2 ±0.37)

Horizontal line – median; bottom line of the box – Q1 (25th); topline of the box – Q3 (75th); whiskers – minimum and maximum observation (excluding outlier); asterisks – outliers 3 × interquartile range (IQR) (Q3–Q1); BVZ – bevacizumab alone group; ABVZ – ATP + bevacizumab group; BBVZ – benidipine + bevacizumab group; ABBVZ – ATP + benidipine + bevacizumab; HC – healthy controls group; ATP – adenosine triphosphate.

Table 1. The p-values of post hoc comparisons for variables between study groups

Variable	p-values of post hoc comparisons									
	1 vs 2	1 vs 3	1 vs 4	1 vs 5	2 vs 3	2 vs 4	2 vs 5	3 vs 4	3 vs 5	4 vs 5
MDA	<0.001	0.331	0.009	0.471	<0.001	<0.001	<0.001	<0.001	1.000	0.096
tGSH	<0.001	<0.001	<0.001	0.024	<0.001	<0.001	<0.001	<0.001	<0.001	<0.001
TOS	<0.001	<0.001	<0.001	0.266	<0.001	<0.001	<0.001	<0.001	<0.001	<0.001
TAS	<0.001	<0.001	<0.001	0.104	<0.001	<0.001	<0.001	<0.001	<0.001	<0.001
Creatinine	<0.001	0.037	<0.001	0.966	<0.001	<0.001	<0.001	0.005	0.082	<0.001
BUN	<0.001	<0.001	<0.001	0.515	<0.001	<0.001	<0.001	<0.001	<0.001	<0.001

Numbers represent groups: 1 – healthy control (HC), 2 – bevacizumab (BVZ), 3 – ATP + bevacizumab (ABVZ), 4 – benidipine + bevacizumab (BBVZ), 5 – ATP + benidipine + bevacizumab (ABBVZ).
MDA – malondialdehyde; tGSH – total glutathione; TOS – total oxidant status; TAS – total antioxidant status; BUN – blood urea nitrogen.

the best efficacy for preventing decreased TAS were in the ABBVZ, ABVZ and BBVZ groups, respectively. The group with the TOS and TAS values closest to the HC group was compared with the ABBVZ group ($p = 0.266$, $p = 0.104$, respectively).

Creatinine and BUN analyses

Creatinine and BUN levels were also found to be significantly different across groups ($F(4,25) = 105.8$, $p < 0.001$; $F(4,25) = 724.5$, $p < 0.001$, respectively; Table 1). Compared to the other groups, creatinine and BUN levels in the blood serum samples of the animal group treated with bevacizumab demonstrated a significant increase ($p < 0.001$, $p < 0.001$, respectively; Fig. 5 and Fig. 6). The administration of ATP significantly decreased the bevacizumab-related increase in creatinine and BUN levels ($p < 0.001$, $p < 0.001$, respectively). The increase in creatinine and BUN levels was also significantly decreased in the BBVZ group ($p < 0.001$, $p < 0.001$, respectively). However, the differences in creatinine and BUN levels were statistically significant in favor of the ABVZ group, compared to the BBVZ group ($p = 0.005$, $p < 0.001$, respectively). The combination of ATP + benidipine was found to be the best for prevention of the increased creatinine and BUN levels. Also, the differences in creatinine and BUN levels between the ABBVZ and HC groups were statistically insignificant ($p = 0.966$, $p = 0.515$, respectively).

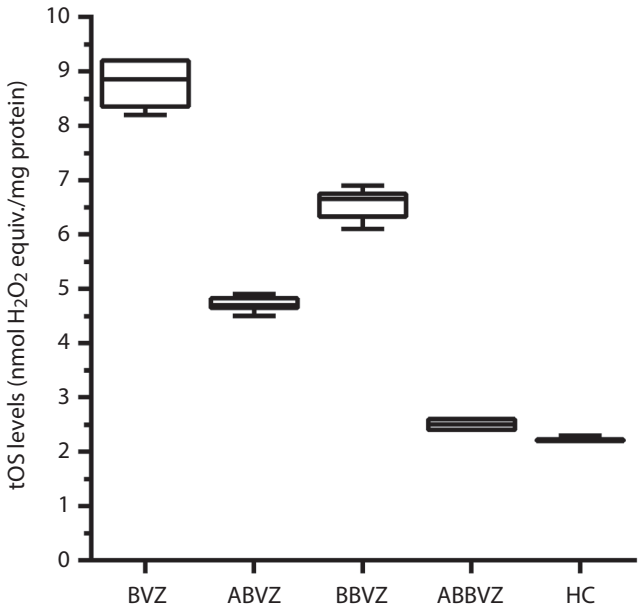

Fig. 3. Total oxidant status (TOS) levels in the renal tissue of the study groups (BVZ = 8.8 ±0.44, ABVZ = 4.7 ±0.13, BBVZ = 6.6 ±0.26, ABBVZ = 2.5 ±0.09, and HC = 2.2 ±0.06)

Horizontal line – median, bottom line of the box – Q1 (25th); topline of the box – Q3 (75th); whiskers – minimum and maximum observation (excluding outlier); BVZ – bevacizumab alone group; ABVZ – ATP + bevacizumab group; BBVZ – benidipine + bevacizumab group; ABBVZ – ATP + benidipine + bevacizumab; HC – healthy controls group; ATP – adenosine triphosphate.

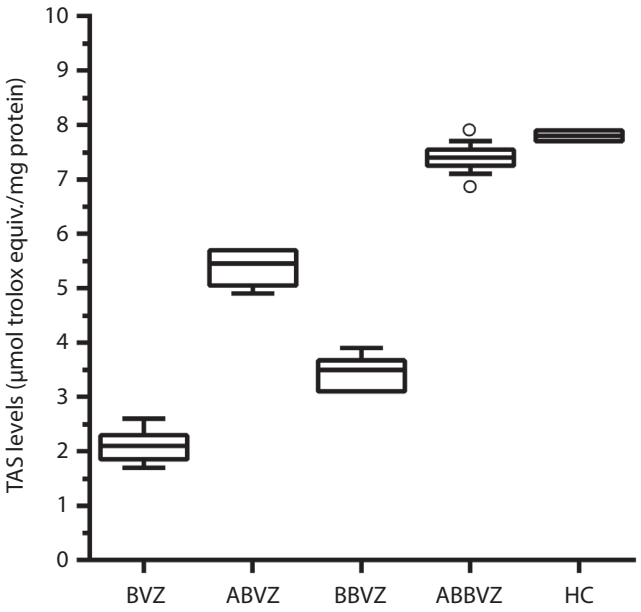

Fig. 4. Total antioxidant status (TAS) levels in the renal tissue of the study groups (BVZ = 2.1 ±0.27, ABVZ = 5.4 ±0.30, BBVZ = 3.4 ±0.32, ABBVZ = 7.4 ±0.19, and HC = 7.8 ±0.07)

Horizontal line – median; bottom line of the box – Q1 (25th); topline of the box – Q3 (75th); whiskers – minimum and maximum observation (excluding outlier); empty circles – outliers 1.5 × interquartile range (IQR) (Q3–Q1); BVZ – bevacizumab alone group; ABVZ – ATP + bevacizumab group; BBVZ – benidipine + bevacizumab group; ABBVZ – ATP + benidipine + bevacizumab; HC – healthy controls group; ATP – adenosine triphosphate.

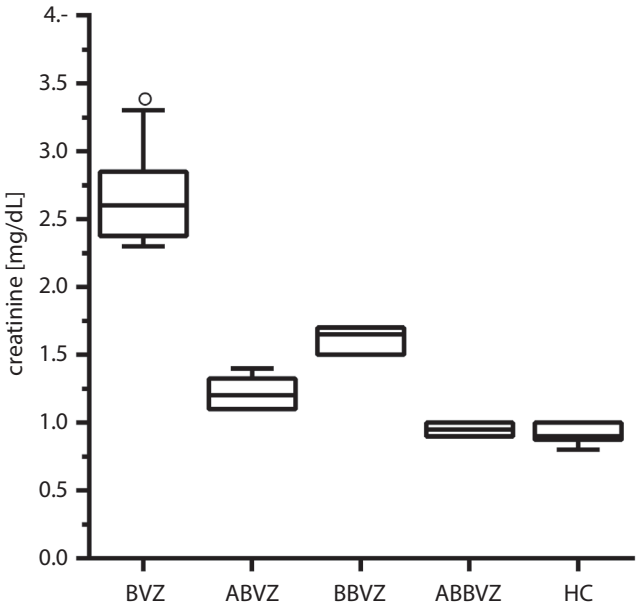

Fig. 5. Creatinine levels in the blood serum of the study groups (BVZ = 2.6 ±0.35, ABVZ = 1.2 ±0.11, BBVZ = 1.6 ±0.09, ABBVZ = 0.9 ±0.05, and HC = 0.9 ±0.07)

Horizontal line – median; bottom line of the box – Q1 (25th); topline of the box – Q3 (75th); whiskers – minimum and maximum observation (excluding outlier); empty circles – outliers 1.5 × interquartile range (IQR) (Q3–Q1); BVZ – bevacizumab alone group; ABVZ – ATP + bevacizumab group; BBVZ – benidipine + bevacizumab group; ABBVZ – ATP + benidipine + bevacizumab; HC – healthy controls group; ATP – adenosine triphosphate.

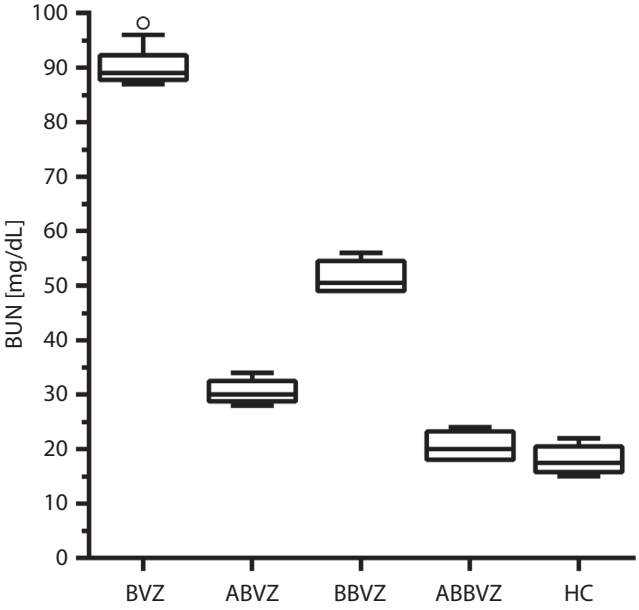

Fig. 6. Blood urea nitrogen (BUN) levels in the blood serum of the study groups (BVZ = 90 ±3.22, ABVZ = 30 ±2.17, BBVZ = 51 ±2.88, ABBVZ = 20 ±2.59, and HC = 18 ±2.6)

Horizontal line – median; bottom line of the box – Q1 (25th); topline of the box – Q3 (75th); whiskers – minimum and maximum observation (excluding outlier); empty circles – outliers 1.5 × interquartile range (IQR) (Q3–Q1); BVZ – bevacizumab alone group; ABVZ – ATP + bevacizumab group; BBVZ – benidipine + bevacizumab group; ABBVZ – ATP + benidipine + bevacizumab; HC – healthy controls group; ATP – adenosine triphosphate.

Histopathological findings

Figure 7A shows that no pathological findings were observed in the renal tissue of the HC group. Also, no histopathological damage was detected in the glomeruli of any animal group. However, grade 3 hemorrhage, tubular necrosis and focal tubular atrophy were observed in the kidneys of animals from the BVZ group (Fig. 7B, Table 2). While grade 1 atrophic tubular structures and focal single cell necrosis were observed in the ABVZ group (Fig. 7C, Table 2), the damage to these structures in the BBVZ group was evaluated as grade 2 (Fig. 7D, Table 2). No pathological findings, except grade 1 atrophic tubules, were observed in the kidneys of the ABBVZ group (Fig. 7E, Table 2).

Discussion

This study focused on the effects of ATP, benidipine and the combination of ATP and benidipine on possible rat renal damage induced with bevacizumab, using biochemical and histopathological methods. The biochemical examinations revealed increased levels of oxidant parameters such as MDA and TOS in the renal tissue of animals treated with bevacizumab, while the levels of antioxidant parameters such as tGSH and TAS were decreased significantly.

Malondialdehyde is a toxic product released by ROS as a result of the peroxidation of cell membrane lipids.[18] Malondialdehyde cross-binds to membrane components and initiates a polymerization reaction that causes serious damage to membrane receptors and proteins.[19] Glutathione (GSH), unlike MDA, is an endogenous antioxidant molecule neutralizing ROS.[20]

The TOS and TAS are substantial markers used in identifying the total oxidant and antioxidant capacity.[16,17] Oxidative stress intensity increases TOS levels and decreases TAS levels. The physiological balance between oxidant and antioxidant changing in favor of oxidants is regarded as oxidative stress.[21] In the BVZ group, animals showed increased TOS and MDA levels, and decreased TAS and tGSH levels, suggesting that bevacizumab induced oxidative stress. Moreover, oxidative stress is defined as the excessive production of ROS that cannot be prevented by the effects of antioxidants and the disruption of cell redox equilibrium.[22] The results of the current experiment, in combination with previous data, suggest that bevacizumab results in oxidative stress in the renal tissue. However, no data are available in the literature to directly show that bevacizumab induced the oxidative damage.

In the blood samples, it was observed that bevacizumab administration significantly increased creatinine and BUN levels. Increased creatinine and BUN levels in the BVZ group indicate that oxidative damage developed in the kidneys. Many studies report that oxidative stress can impair renal functions and antioxidant administration is beneficial in the treatment of oxidative renal damage.[23,24] In a recently

Table 2. Histopathological effect of ATP and benidipine on bevacizumab-induced tubular and glomerular damage

Groups	Tubular damage			Glomerular damage		
	hemorrhage	atrophy	necrosis	hemorrhage	atrophy	necrosis
HC	0	0	0	0	0	0
BVZ	3[a]	3[a]	3[a]	0	0	0
ABVZ	0[b]	1[c]	1[c]	0	0	0
BBVZ	0[b]	2	2	0	0	0
ABBVZ	0[b]	1[c]	0[b]	0	0	0

Results were presented as median values. [a] $p < 0.001$, according to HC; [b] $p < 0.001$, according to BVZ group; [c] $p < 0.05$, according to BVZ group. Kruskal–Wallis test was performed, as post hoc Dunn's test was used. Study group symbols: HC – healthy control; BVZ – bevacizumab alone; ABVZ – ATP + bevacizumab; BBVZ – benidipine + bevacizumab; ABBVZ – ATP + benidipine + bevacizumab; ATP – adenosine triphosphate.

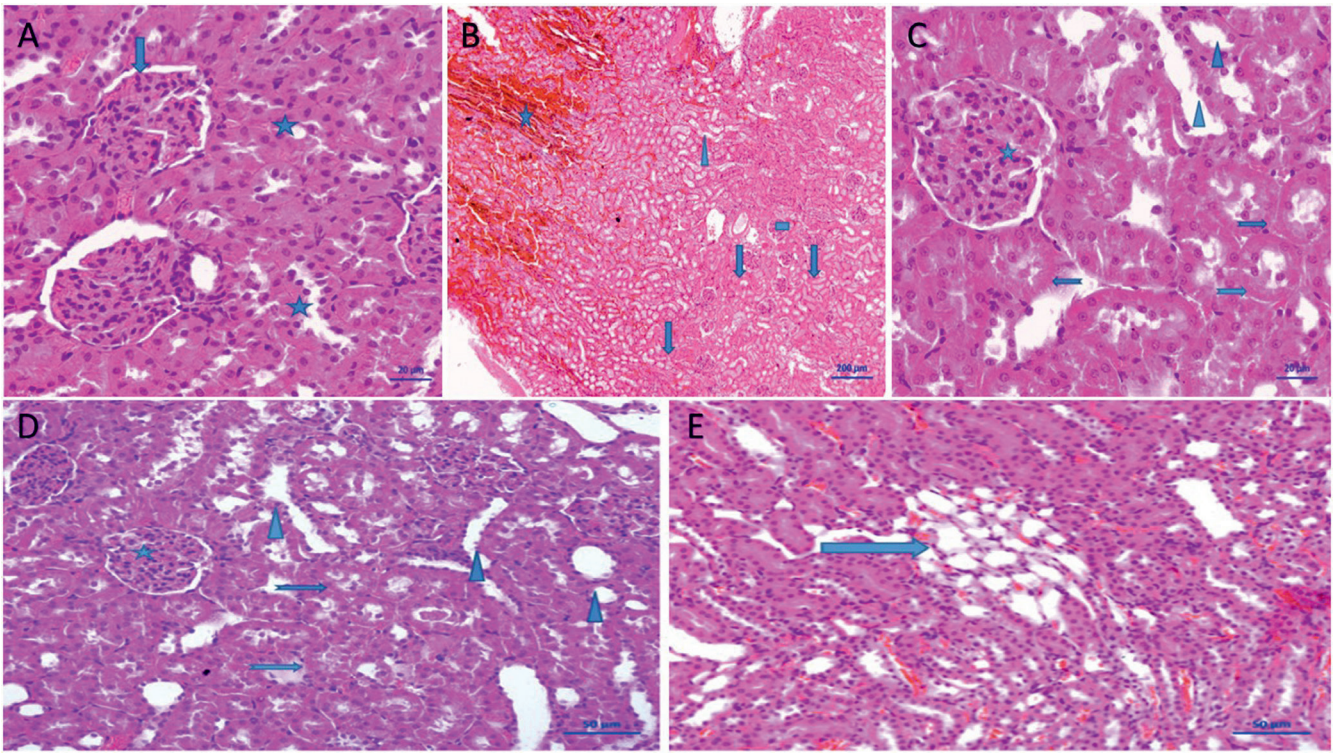

Fig. 7. A. Healthy renal tissue (hematoxylin and eosin (H&E) staining, ×20 magnification); B. Cross-section showing diffuse bleeding areas (asterisks), tubular necrosis areas (arrows), focal tubular atrophy (triangle), and normal glomerular (square) structures in the BVZ group (H&E staining, ×200 magnification); C. Cross-section showing normal glomeruli (asterisks) and tubule structures, as well as diffuse atrophic tubule structures (triangle) and focal single-cell necrosis (arrows) in the ABVZ group (H&E staining, ×20 magnification); D. Section showing normal glomeruli (asterisks) and tubule structures, diffuse atrophic tubules (triangle), and focal single cell necrosis (arrows) in the BBVZ group (H&E staining, ×50 magnification); E. Cross-section showing atrophic tubules (arrow) in the ABBVZ group (H&E staining, ×50 magnification)

conducted study, serum creatinine and BUN were utilized to assess oxidative renal impairment and an increase in these parameters was associated with oxidative damage.[25] Studies have also shown that increased creatinine and BUN levels are due to permanent damage to the renal tubules.[26]

In the current study, it was also determined that ATP alleviated the bevacizumab-induced rat kidney damage by preventing oxidative stress. These results suggest that inhibition of a chain reaction involving decreased VEGF and ATP, Na^+/K^+-ATPase pump inhibition, increased intracellular Na^+ and Ca^{2+} concentrations, and the triggering of ROS production, respectively, may have resulted from bevacizumab administration. Previous studies have suggested that ATP promotes epithelialization by increasing VEGF levels.[11] A recent study by Yıldırım et al. also reports that ATP heals oxidative dermal damage induced by sunitinib, a target-driven anticancer drug.[27] It has also been found that VEGF inhibition is accountable for the oxidative heart and dermal damage associated with tyrosine kinase inhibitors (target-driven anticancer drugs), and that this damage was minimized by the administration of ATP.[28,29]

The current biochemical and histopathological results show that the oxidative renal damage associated with bevacizumab is also suppressed by benidipine. As stated above, benidipine is a Ca^{2+} channel blocker drug with antioxidant properties.[12,13] This pharmacological agent has a strong effect and long duration of action with a high affinity for calcium channels.[30] Benidipine is not only known to inhibit

L-type Ca^{2+} channels, but also N- and T-type Ca^{2+} channels,[31] and the nephroprotective effect of benidipine is presumed to be due to the blockade of these 3 channels.[30] It has also been reported that benidipine suppresses the increase of serum creatinine, lipid peroxidation and intracellular calcium levels due to renal ischemia, while preventing a decrease in renal ATP.[32] Thus, the possible mechanisms by which benidipine prevents bevacizumab-induced oxidative kidney damage are likely due to its antioxidant properties, inhibitory effects on ATP depletion, and its Ca^{2+} channel blocking effects.

It has also been shown that increased intracellular Ca^{2+} levels are associated with ROS production and cell damage.[8,9] However, benidipine suppressed bevacizumab-associated kidney damage less than ATP, suggesting that the effects of benidipine may be primarily due to its inhibitory effect on VEGF production. Indeed, Jesmin et al. have reported that benidipine inhibits the excessive production of VEGF.[33] Considering the mechanism of action of bevacizumab,[1] these findings support our original hypothesis that ATP, benidipine, and especially ATP combined with benidipine, may be effective against bevacizumab toxicity. In the current study, the treatments that reduced bevacizumab-associated oxidative kidney damage most effectively were the ATP and benidipine combination, ATP and benidipine, in descending order.

In the present study, histopathological signs of damage, such as severe necrosis, atrophy and hemorrhage, were observed in the renal tubules of the BVZ group. However, there was no damage to the glomeruli. Similarly, Assayag et al. found that tubular necrosis developed in a patient who was administered bevacizumab. However, since bevacizumab was used in combination with other chemotherapeutic drugs, it could not be conclusively determined that this damage was related to bevacizumab.[34] Another study also reported tubular necrosis in patients treated with bevacizumab and VEGF inhibitors.[35] Zhao et al., using light microscopy, could not determine if bevacizumab caused morphological damage to the glomeruli. However, a subsequent electron microscopy analysis demonstrated that the glomeruli experienced certain morphological changes following bevacizumab administration.[36]

Limitations

In future studies, pro-inflammatory cytokine levels should also be investigated to clarify the protective effects of the combination of ATP and benidipine on bevacizumab toxicity.

Conclusions

The administration of bevacizumab resulted in tubular necrosis with oxidative stress in the renal tissue of animals. Benidipine significantly reduced the damage associated with bevacizumab, and ATP reduced it even more significantly. However, a combination of ATP and benidipine was the most effective in reducing bevacizumab-associated oxidative stress and tubular damage. Thus, the results of our trial revealed that ATP and benidipine reduce bevacizumab-related renal toxicity. However, the combination of ATP and benidipine is suggested to be a potential therapeutic strategy for the prevention of bevacizumab toxicity.

ORCID iDs

Hüseyin Kocaturk https://orcid.org/0000-0002-7254-7692
Fevzi Bedir https://orcid.org/0000-0003-0506-0777
Ömer Turangezli https://orcid.org/0000-0002-1792-9620
Remzi Arslan https://orcid.org/0000-0002-3198-4706
Taha Abdulkadir Çoban https://orcid.org/0000-0003-1711-5499
Durdu Altuner https://orcid.org/0000-0002-5756-3459
Halis Suleyman https://orcid.org/0000-0002-9239-4099

References

1. George BA, Zhou XJ, Toto R. Nephrotic syndrome after bevacizumab: Case report and literature review. *Am J Kidney Dis*. 2007;49(2):23–29. doi:10.1053/j.ajkd.2006.11.024
2. Estrada CC, Maldonado A, Mallipattu SK. Therapeutic inhibition of VEGF signaling and associated nephrotoxicities. *Am Soc Nephrol*. 2019;30(2):187–200. doi:10.1681/ASN.2018080853
3. Touyz RM, Herrmann J. Cardiotoxicity with vascular endothelial growth factor inhibitor therapy. *NPJ Precis Oncol*. 2018;2(1):1–11. doi:10.1038/s41698-018-0056-z
4. Khneizer G, Al-Taee A, Bastani B. Self-limited membranous nephropathy after intravitreal bevacizumab therapy for age-related macular degeneration. *J Nephropathol*. 2017;6(3):134–137. doi:10.15171/jnp.2017.23
5. Hanna RM, Barsoum M, Arman F, Selamet U, Hasnain H, Kurtz I. Nephrotoxicity induced by intravitreal vascular endothelial growth factor inhibitors: Emerging evidence. *Kidney Int*. 2019;96(3):572–580. doi:10.1016/j.kint.2019.02.042
6. Guo D, Wang Q, Li C, Wang Y, Chen X. VEGF stimulated the angiogenesis by promoting the mitochondrial functions. *Oncotarget*. 2017;8(44):77020–77027. doi:10.18632/oncotarget.20331
7. McCord JM. Oxygen-derived free radicals in postischemic tissue injury. *N Engl J Med*. 1985;312(3):159–163. doi:10.1056/NEJM198501173120305
8. Gordeeva A, Zvyagilskaya R, Labas YA. Cross-talk between reactive oxygen species and calcium in living cells. *Biochemistry (Mosc)*. 2003;68(10):1077–1080. doi:10.1023/a:1026398310003
9. Orrenius S, Burkitt MJ, Kass GE, Dypbukt JM, Nicotera P. Calcium ions and oxidative cell injury. *Ann Neurol*. 1992;32(1):33–42. doi:10.1002/ana.410320708
10. Bulanova E, Bulfone-Paus S. P2 receptor-mediated signaling in mast cell biology. *Purinergic Signal*. 2010;6(1):3–17. doi:10.1007/s11302-009-9173-z
11. Chiang B, Essick E, Ehringer W, et al. Enhancing skin wound healing by direct delivery of intracellular adenosine triphosphate. *Am J Surg*. 2007;193(2):213–218. doi:10.1016/j.amjsurg.2006.08.069
12. Ohtani K, Usui S, Kaneko S, et al. Benidipine reduces ischemia reperfusion-induced systemic oxidative stress through suppression of aldosterone production in mice. *Hypertens Res*. 2012;35(3):287–294. doi:10.1038/hr.2011.183
13. Hassan MQ, Akhtar MS, Akhtar M, Ali J, Haque SE, Najmi AK. Edaravone, a potent free radical scavenger and a calcium channel blocker attenuate isoproterenol induced myocardial infarction by suppressing oxidative stress, apoptotic signaling and ultrastructural damage. *Ther Adv Cardiovasc Dis*. 2016;10(4):214–223. doi:10.1177/1753944716630653
14. Ohkawa H, Ohishi N, Yagi K. Assay for lipid peroxides in animal tissues by thiobarbituric acid reaction. *Anal Biochem*. 1979;95(2):351–358. doi:10.1016/0003-2697(79)90738-3
15. Sedlak J, Lindsay RH. Estimation of total, protein-bound, and nonprotein sulfhydryl groups in tissue with Ellman's reagent. *Anal Biochem*. 1968;25:192–205. doi:10.1016/0003-2697(68)90092-4

16. Erel O. A new automated colorimetric method for measuring total oxidant status. *Clin Biochem*. 2005;38(12):1103–1111. doi:10.1016/j.clinbiochem.2005.08.008
17. Erel O. A novel automated method to measure total antioxidant response against potent free radical reactions. *Clin Biochem*. 2004;37(2):112–119. doi:10.1016/j.clinbiochem.2003.10.014
18. Davies K, Goldberg A. Oxygen radicals stimulate intracellular proteolysis and lipid peroxidation by independent mechanisms in erythrocytes. *J Biol Chem*. 1987;262(17):8220–8226. PMID:3597372
19. Goulart M, Batoreu M, Rodrigues A, Laires A, Rueff J. Lipoperoxidation products and thiol antioxidants in chromium exposed workers. *Mutagenesis*. 2005;20(5):311–315. doi:10.1093/mutage/gei043
20. Urso ML, Clarkson PM. Oxidative stress, exercise, and antioxidant supplementation. *Toxicology*. 2003;189(1–2):41–54. doi:10.1016/s0300-483x(03)00151-3
21. Kisaoglu A, Borekci B, Yapca OE, Bilen H, Suleyman H. Tissue damage and oxidant/antioxidant balance. *Eurasian J Med*. 2013;45(1):47–49. doi:10.5152/eajm.2013.08
22. Pisoschi AM, Pop A. The role of antioxidants in the chemistry of oxidative stress: A review. *Eur J Med Chem*. 2015;97(5):55–74. doi:10.1016/j.ejmech.2015.04.040
23. Erdemli ME, Zayman E, Erdemli Z, Gul M, Gul S, Bag HG. Protective effects of melatonin and vitamin E in acetamiprid-induced nephrotoxicity. *Environ Sci Pollut Res Int*. 2020;27(9):1–12. doi:10.1007/s11356-019-06754-y
24. Ghaznavi H, Mehrzadi S, Dormanesh B, et al. Comparison of the protective effects of melatonin and silymarin against gentamicin-induced nephrotoxicity in rats. *J Evid Based Complementary Altern Med*. 2016;21(4):49–55. doi:10.1177/2156587215621672
25. Kocaturk H, Bedir F, Altay MS, et al. The effect of desloratadine on ischemia reperfusion induced oxidative and inflammatory renal injury in rats. *Ren Fail*. 2020;42(1):531–538. doi:10.1080/0886022X.2020.1769656
26. Dickey DT, Muldoon LL, Doolittle ND, Peterson DR, Kraemer DF, Neuwelt EA. Effect of N-acetylcysteine route of administration on chemoprotection against cisplatin-induced toxicity in rat models. *Cancer Chemother Pharmacol*. 2008;62(2):235–241. doi:10.1007/s00280-007-0597-2
27. Yıldırım N, Karatas A, Cengiz M, et al. Protective effect of adenosine triphosphate against sunitinib-related skin damage in rats. *Hum Exp Toxicol*. 2020;39(12):1737–1746. doi:10.1177/0960327120940365
28. Aldemir M, Simsek M, Kara A, et al. The effect of adenosine triphosphate on sunitinib-induced cardiac injury in rats. *Hum Exp Toxicol*. 2020;39(8):1046–1053. doi:10.1177/0960327120909874
29. Akagunduz B, Ozcicek F, Kara AV, et al. Effects of adenosine triphosphate on vandetanib induced skin damage in rats. *Cutan Ocul Toxicol*. 2020;39(4):323–327. doi:10.1080/15569527.2020.1802742
30. Yao K, Nagashima K, Miki H. Pharmacological, pharmacokinetic, and clinical properties of benidipine hydrochloride, a novel, long-acting calcium channel blocker. *J Pharmacol Sci*. 2006;100(4):243–261. doi:10.1254/jphs.dtj05001x
31. Wang B, Yang J, Fan L, Wang Y, Zhang C, Wang H. Osteogenic effects of antihypertensive drug benidipine on mouse MC3T3-E1 cells in vitro. *J Zhejiang Univ Sci B*. 2021;22(5):410–420. doi:10.1631/jzus.B2000628
32. Karasawa A, Kubo K. Protection by benidipine hydrochloride (KW-3049), a calcium antagonist, of ischemic kidney in rats via inhibitions of Ca-overload, ATP-decline and lipid peroxidation. *Jpn J Pharmacol*. 1990;52(4):553–562. doi:10.1254/jjp.52.553
33. Jesmin S, Sakuma I, Hattori Y, Fujii S, Kitabatake A. Long-acting calcium channel blocker benidipine suppresses expression of angiogenic growth factors and prevents cardiac remodeling in a Type II diabetic rat model. *Diabetologia*. 2020;45(3):402–415. doi:10.1007/s00125-001-0765-6
34. Assayag M, Rouvier P, Gauthier M, et al. Renal failure during chemotherapy: Renal biopsy for assessing subacute nephrotoxicity of pemetrexed. *BMC Cancer*. 2017;17(1):770. doi:10.1186/s12885-017-3705-7
35. Usui J, Glezerman IG, Salvatore SP, Chandran CB, Flombaum CD, Seshan SV. Clinicopathological spectrum of kidney diseases in cancer patients treated with vascular endothelial growth factor inhibitors: A report of 5 cases and review of literature. *Hum Pathol*. 2014;45(9):1918–1927. doi:10.1016/j.humpath.2014.05.015
36. Zhao N, Xu Q, Wang M, et al. Mechanism of kidney injury caused by bevacizumab in rats. *Int J Clin Exp Pathol*. 2014;7(12):8675–8683. PMID:25674232

Protective effect of metformin on lithium-induced nephrogenic diabetes insipidus: An experimental study in rats

Halil Ibrahim Tas[2,A–C,F], Eyup Burak Sancak[1,A,B,D,E]

[1] Department of Urology, Faculty of Medicine, Çanakkale Onsekiz Mart University, Turkey
[2] Department of Psychiatry, Faculty of Medicine, Ordu University, Turkey

A – research concept and design; B – collection and/or assembly of data; C – data analysis and interpretation; D – writing the article; E – critical revision of the article; F – final approval of the article

Advances in Clinical and Experimental Medicine, ISSN 1899–5276 (print), ISSN 2451–2680 (online) *Adv Clin Exp Med*. 2021;30(11):1185–1193

Address for correspondence
Eyup Burak Sancak
E-mail: eyupburaksancak@comu.edu.tr

Funding sources
This research was supported by Çanakkale Onsekiz Mart University, The Scientific Research Coordination Unit, Project No. 2579. The funding bodies had no role in the design of the study and collection, analysis and interpretation of data, or in writing the manuscript.

Conflict of interest
None declared

Acknowledgements
This work was supported by Çanakkale Onsekiz Mart University, The Scientific Research Coordination Unit, project No. TSA-2018-2579.

Received on April 23, 2021
Reviewed on June 12, 2021
Accepted on July 21, 2021

Published online on September 22, 2021

Abstract

Background. Lithium is widely used in the treatment of bipolar disorders and may lead to nephrogenic diabetes insipidus (NDI), following long-term treatment. Metformin is considered the preferred initial therapy for patients with type 2 diabetes mellitus (T2D).

Objectives. To investigate the protective effect of metformin on the kidney damage caused by lithium administration.

Materials and methods. Using an animal model of chronic lithium-induced NDI, rats were divided into 4 groups: sham, metformin, lithium, and lithium + metformin. The effects of these treatments were examined using serum electrolytes, blood and tissue total antioxidant status, total oxidant status, the oxidative stress index, urine and blood osmolality, and tissue aquaporin-2 (AQP2) levels. Additionally, histopathological changes, including congestion, hydropic swelling, tubular necrosis, tubular atrophy, and Bowman's capsule dilatation, were evaluated. The total histopathological score was obtained by summing the scores for each pathological finding.

Results. In the lithium group, biochemical variables indicating NDI, including sodium, chloride and blood osmolality, increased, and urine osmolality decreased, compared to the sham group. With metformin treatment, the blood osmolality decreased from 328.17 mOsm/kg to 306.33 mOsm/kg, and urine osmolality increased from 349.67 mOsm/kg to 754.50 mOsm/kg ($p = 0.004$ and $p = 0.001$, respectively). Tissue AQP2 levels decreased with lithium administration but stabilized with metformin treatment. Additionally, in comparison to the lithium group, the total histopathological score in the metformin group declined from 8.0 to 2.0 ($p = 0.002$).

Conclusions. Metformin may help protect the kidneys from lithium-induced NDI through the AQP2 regulating effect and a reduction in oxidative stress.

Key words: metformin, bipolar disorder, aquaporin-2, lithium, nephrogenic diabetes insipidus

Cite as
Tas HI, Sancak EB. Protective effect of metformin on lithium-induced nephrogenic diabetes insipidus: An experimental study in rats. *Adv Clin Exp Med*. 2021;30(11):1185–1193. doi:10.17219/acem/140403

DOI
10.17219/acem/140403

Background

Lithium has been widely used for the treatment of bipolar disorders and depression.[1,2] However, lithium administration has well-documented side effects on several biological systems.[2] One of the main targets of lithium are the kidneys, and a long-term lithium treatment may induce progressive nephrotoxicity. A significant part of the lithium-induced deterioration of renal function occurs in the form of nephrogenic diabetes insipidus (NDI), characterized by polyuria and polydipsia.[1,3] Nephrogenic diabetes insipidus develops as a result of impaired urine concentration due to the changes in the absorption of water and sodium at the level of collecting tubules. Previous studies have shown that the urinary concentration defect, associated with lithium toxicity, is mainly connected to a decrease in the amount of aquaporin-2 (AQP2) protein in the collecting duct principal cells.[4] Another mechanism responsible for lithium-induced nephrotoxicity is a change in the epithelial sodium channels (ENaCs), collecting channels, which are essential sites for sodium reabsorption.[1] It has been shown that when inhibition of the functioning of ENaCs in the collecting ducts is prevented, the expected polyuria due to lithium is also inhibited, and introduction of lithium into the cell through ENaCs is a central step in the development of NDI.[5] Furthermore, oxidative stress has been proposed as an alternative mechanism for lithium toxicity in renal tissue through impairment of the mitochondrial respiratory system, that leads to an increased generation of free radicals through lipid peroxidation of the cell membrane.[2]

Metformin, an activator of 5′-AMP-activated protein kinase (AMPK), is one of the most popular oral glucose-lowering medications, and is preferred by most guideline committees as an optimal initial medical therapy for patients with type 2 diabetes mellitus (T2D).[6] The useful mechanisms of metformin on cell metabolism that are known to have a protective effect on the kidney include the activation of an upstream kinase (i.e., liver kinase B1), increased cellular AMP levels and consequent AMPK activation.[7] Recent studies have shown that metformin increases osmotic water permeability by increasing AQP2 accumulation in the renal apical plasma membrane.[8] Similarly, metformin was found to prevent high-sodium-induced upregulation of ENaC expression.[9] Metformin has also been shown to reduce cell damage during oxidative stress.[10]

Objectives

Metformin, having a positive effect on almost all stages of lithium-induced renal injury, is a critical drug to investigate the prevention of lithium-induced renal injury. In this study, we assess the protective effect of metformin against the renal adverse effects of lithium use.

Materials and methods

Trial design

A randomized controlled animal study was carried out. Ethical approval was obtained from the Çanakkale Onsekiz Mart University (Turkey) Ethical Board of Animal Studies (approval No. 2018/1800054097). The study was conducted following the CONSORT guidelines,[11,12] and the methods used for the animal experiments are in accordance with the National Institutes of Health Guide for the Care and Use of Laboratory Animals (National Institutes of Health (NIH), Bethesda, USA).

Study setting

Twenty-four adult male Wistar albino rats weighing 250–300 g were purchased from the Laboratory Animal Production Unit of Çanakkale Onsekiz Mart University (Turkey) and maintained for an adaptation period of 1 week under standard conditions with a temperature of 22 ±2°C, a relative humidity of 70 ±4% and a 12 h light/dark cycle. All animals were provided with standard commercial pellet diets and tap water ad libitum.

Randomization

After the adaptation period, the animals were divided using a random numbers list into 4 groups of 6 rats each as follows:

Group 1 (sham operation group, n = 6) – fed a standard diet for 2 weeks and placed in a metabolic cage for 24 h on the 14th day. Blood and right kidney tissue samples were taken on the 15th day.

Group 2 (lithium group, n = 6) – fed a lithium-rich diet (LiCl; Li; 40 mmol/kg of dry food) for 2 weeks and placed in a metabolic cage for 24 h on the 14th day. Blood and right kidney tissue samples were taken on the 15th day.

Group 3 (metformin group, n = 6) – administered metformin (metformin hydrochloride, 800 mg/kg, by gavage) for 2 weeks and placed in a metabolic cage on the 14th day for 24 h. Blood and right kidney tissue samples were taken on the 15th day.

Group 4 (lithium + metformin group, n = 6) – fed with a lithium rich diet and administered metformin (LiCl; Li; 40 mmol/kg of dry food + metformin hydrochloride, 800 mg/kg, by gavage) for 2 weeks and placed in a metabolic cage on the 14th day for 24 h. Blood and right kidney tissue samples were taken on the 15th day (Fig. 1).

Biochemical analysis

At the end of the experiment, all animals were deeply anesthetized with ketamine (50–60 mg/kg). Blood samples were collected from all subjects into tubes and centrifuged at 4000 rpm for 10 min. The resultant serum samples were

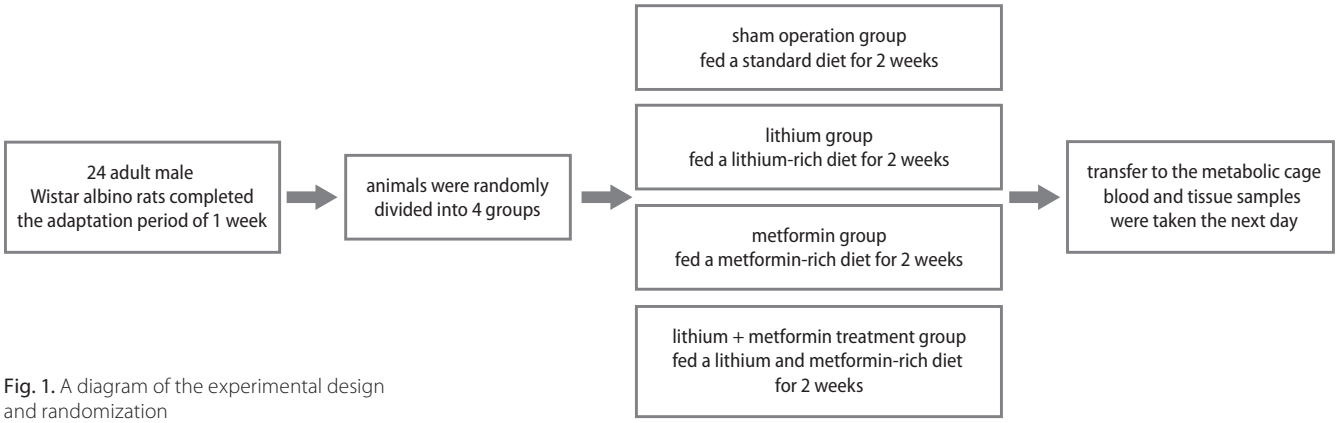

Fig. 1. A diagram of the experimental design and randomization

aliquoted into polypropylene tubes and stored at –80°C until biochemical analysis. Urine samples were stored at 4°C until analysis. The right kidney was removed and sagittally divided in half, with half used for tissue biochemistry and the other half for the histopathological analysis. Finally, the rats were sacrificed by decapitation.

Blood and tissue biochemical markers were measured by spectrophotometric methods. Tissues from all experimental groups were prepared at 4°C to determine their total antioxidant status (TAS) and total oxidant status (TOS) levels. After washing with a phosphate-buffered solution (PBS), the tissue samples were weighed and cut into small pieces. The tissues were then homogenized using a Mixer Mill MM 400 (Retsch, Haan, Germany). Assays were performed on the supernatant of the homogenate, which was prepared by centrifugation at 4°C. The protein contents of the tissues were calculated according to the method developed by Lowry et al.[13]

Serum and tissue TAS (product code: RL0017) and TOS (product code: RL0024) were determined with spectrophotometric kits (Rel Assay Diagnostics, Gaziantep, Turkey). The ratio percentage of TOS (μmol H_2O_2 equivalent/L) to TAS (μmol Trolox equivalent/L) potential was used to calculate the oxidative stress index (OSI) — the indicator of the degree of oxidative stress.

Albumin, creatinine (Crea), chlorine (Cl), potassium (K), sodium (Na), lithium (Li), total protein, and urea were analyzed using Roche Diagnostic kits and Cobas c501 auto analyzer (Roche Diagnostics, Indianapolis, USA). Urine and blood osmolalities (mOsm/kg) were determined with the freezing point depression method, using an automatic cryoscopic osmometer (Osmomat 030-D; Gonotec, Berlin, Germany). The main outcome variable of the study was urine osmolality.

Histopathological analysis

Kidney tissue samples were fixed in a 10% neutral buffered formaldehyde solution for light microscopic examination. After the fixation, the samples were placed into cassettes and washed under running water for 2 h. To remove water, the tissues were passed through a series of increasing alcohol concentrations (60%, 70%, 80%, 90%, 96%, and 100%). The tissues were then passed through xylol for polishing and then were embedded in molten paraffin. Hematoxylin and eosin (H&E) staining and immunohistochemical AQP2 evaluation were performed on the 4-μm thick sections obtained from the paraffin blocks. The sections were evaluated on a Leica DCM 3000 (Leica Microsystems, Wetzlar, Germany), computer-assisted imaging system, using the Leica Q Vin 3 program, and pictures of the histological sections were taken. A score table was formed after the evaluations with H&E staining.

For the H&E staining method, sections taken from the experimental groups were kept in a 60°C oven for 60 min, then moved into xylol for 3 × 10 min and cleansed from paraffin. The slides were then passed through a series of increasing alcohol concentrations (70%, 90%, 96%, and 100%), washed in running water for 1 min, then stained in Harris hematoxylin for 2 min, and finally washed in running water for 2 × 2 min. The specimens were then soaked in a 1% ammonia-water mixture and washed again in running water for 1 min. The slides were kept in eosin for 2 min and passed through a series of increasing alcohol concentrations (70%, 80%, 96%, and 100%), xylolized for 2 × 1 min, and covered with entellan. To make a numerical evaluation of the total area size in the tissue, data were generated for each group and each animal in the whole area, using a ×4 magnification lens. Evaluation of the histopathological changes included congestion, hydropic swelling, tubular necrosis, tubular atrophy, and Bowman's capsule dilatation. Tissue damage scores were assigned as follows: no visible change = 0, minimal or slight change = 1, moderate change = 2, and severe change = 3. After calculating the score of all rats for each of the histopathological changes, the total score was obtained by summing all of the scores together.

For immunohistochemical AQP2 staining, 4-μm thick sections were taken from the kidney tissue blocks of all experimental groups and transferred to slides. Sections were kept in a 60°C oven for 1 h and then moved to xylol for 3 × 10 min to achieve deparaffinization. The slides were then rehydrated through a series of increasing alcohol concentrations (70%, 80%, 96%, and 100%). Sections were passed through distilled water twice for 1 min to remove the alcohol. To remove

the antigen mask, 1/10 dilution citrate buffer (ap-9003-999; Thermo Fisher Scientific, Waltham, USA) was applied in a microwave. The endogenous peroxidase activity was blocked in the tissues with 3% hydrogen peroxide (TA-125-HP; Thermo Fisher Scientific) for 10 min after washing with distilled water. Sections were then washed with PBS and protein-blocked (TA-125 PBQ; Thermo Fisher Scientific) for 10 min.

The AQP2 antibody (ab15116; Abcam, Cambridge, UK) was incubated with the tissue for 60 min in a humid environment. The HRP Polymer Amplifier Quanto (TL-125-QPB; Thermo Fisher Scientific) was rested for 20 min. Washing with PBS was carefully completed at every stage. The 3, 3'-diaminobenzidine (DAB) staining was performed to identify AQP2-positive cells, and hematoxylin was then applied for 1 min for background staining. The stained sections were passed through a series of increasing alcohol concentrations, water was removed, and then they were kept in xylol for 5 min to achieve transparency. Then, the sections were covered with entellan. Animals in all groups were evaluated and scored for AQP2 levels as follows: none = 0, 1%–25% = 1, 26%–50% = 2, and 51%–100% = 3.

Sample size

Sample size calculation was based on the resource equation method. In comparison of 4 groups (k) for mean urine osmolality with the one-way analysis of variance (ANOVA) using 6 animals (n) in each group, the equation (degree of freedom (df) = (n × k) – k) revealed a df of 20, which is in the acceptable range of 10–20.[14,15]

Statistical analyses

Statistical analyses were conducted using IBM SPSS software, v. 24.0 (IBM Corp., Armonk, USA). The variables were investigated using analytical methods (Kolmogorov–Smirnov/Shapiro–Wilk test) to determine whether or not they were normally distributed (Table 1). The sample mean ± standard deviations were used to determine the average of the collected data if the quantitative variables were normally distributed; otherwise, the sample median (min–max) was used. One-way ANOVA tests were used to compare the biochemical and tissue parameters among the 4 groups. The Levene test was used to assess the homogeneity of the variances (Table 1). When an overall significance was observed, pairwise post hoc tests were performed using Tukey's test. The ANOVA results are presented as F test (degrees of freedom) (F(df)). Values of $p < 0.05$ were considered statistically significant. The histopathological findings and AQP2 levels were evaluated with the Kruskal–Wallis test, as they were ordinal variables. The Mann–Whitney U test was performed to test the significance of pairwise differences, using the Bonferroni correction to adjust for multiple comparisons.

Table 1. Analysis of variance (ANOVA) assumptions

Parameter	Independent groups	Test for normality (Shapiro–Wilk)	Homogeneity of variances (Levene's test)	Ordinal variable
Sodium	+	p > 0.05	0.091	–
Potassium	+	p > 0.05	0.650	–
Chloride	+	p > 0.05	0.858	–
Urea	+	p > 0.05	0.120	–
Creatinine	+	p > 0.05	0.435	–
Lithium	+	p > 0.05	0.901	–
TOS	+	p > 0.05	0.335	–
TAS	+	p > 0.05	0.334	–
OSI	+	p > 0.05	0.411	–
TOS (tissue)	+	p > 0.05	0.880	–
TAS (tissue)	+	p > 0.05	0.284	–
OSI (tissue)	+	p > 0.05	0.518	–
Blood osmolality	+	p > 0.05	0.562	–
Urine osmolality	+	p > 0.05	0.181	–
Aquaporin-2	+	unrelated	unrelated	+
Congestion	+	unrelated	unrelated	+
Hydropic swelling	+	unrelated	unrelated	+
Tubular necrosis	+	unrelated	unrelated	+
Tubular atrophy	+	unrelated	unrelated	+
Bowman's capsule dilatation	+	unrelated	unrelated	+
Total score	+	unrelated	unrelated	+

TOS – total oxidant status; TAS – total antioxidant status; OSI – oxidative stress index.

Results

Biochemical findings

The blood biochemical results for all groups are shown in Table 2. There were no significant differences between the sham and metformin groups for the plasma biochemistry values. When compared with the sham group, the Na, Cl, Li, TOS and OSI values were significantly higher in the lithium group (p = 0.018, p = 0.004, p = 0.002, p = 0.002, and p = 0.001, respectively). In the lithium + metformin group, the plasma Na, Cl, TOS and OSI values were lower compared to the lithium group (p = 0.035, p = 0.001, p = 0.003, and p = 0.001, respectively).

Tissue and osmolality analysis results for the groups are provided in Table 3. Compared to the sham group, the lithium group had significantly higher TOS, OSI, blood osmolality, and urine osmolality values (p = 0.010, p = 0.004, p = 0.004, and p = 0.002, respectively). In the lithium + metformin group, a reduction in TOS, OSI and blood osmolality, and an increase in urine osmolality values were observed compared to the lithium group (p = 0.004, p = 0.002, p = 0.004, and p = 0.001, respectively).

Histopathological findings

Histopathological analysis results and AQP2 levels for the groups are given in Table 4. No bleeding or interstitial fibrosis were observed in any of the sections. There were no

Table 2. Serum biochemical analysis

Serum parameters	Sham group (n = 6)	Metformin group (n = 6)	Lithium group (n = 6)	Lithium + metformin group (n = 6)	ANOVA	Post hoc
Sodium [mmol/L]	135.16 ±3.86	134.83 ±6.74	144.16 ±1.94[a]	136.00 ±6.22[b]	$F_{(3–20)}$ = **5.23** **p = 0.008**	**p = 0.018**[a] **p = 0.035**[b]
Potassium [mmol/L]	5.53 ±0.59	5.47 ±0.61	5.51 ±0.69	5.54 ±0.98	$F_{(3–20)}$ = 0.11 p = 0.998	p = 0.999[a] p = 0.998[b]
Chloride [mmol/L]	98.15 ±1.52	98.80 ±1.91	103.06 ±1.36[a]	99.10 ±1.83[b]	$F_{(3–20)}$ = **12.54** **p < 0.001**	**p = 0.004**[a] **p = 0.001**[b]
Urea [mg/dL]	36.33 ±4.87	37.03 ±3.93	42.00 ±8.33	37.43 ±3.06	$F_{(3–20)}$ = 1.34 p = 0.288	p = 0.300[a] p = 0.481[b]
Creatinine [mg/dL]	0.27 ±0.03	0.26 ±0.03	0.29 ±0.03	0.25 ±0.02	$F_{(3–20)}$ = 1.62 p = 0.216	p = 0.316[a] p = 0.213[b]
Lithium [mmol/L]	0.003 ±0.008	0.003 ±0.005	0.045 ±0.005[a]	0.043 ±0.005[a]	$F_{(3–20)}$ = **89.00** **p < 0.001**	**p = 0.002**[a] **p = 0.001**[a]
TOS	12.98 ±2.16	11.87 ±1.98	21.27 ±4.35[a]	14.39 ±2.54[b]	$F_{(3–20)}$ = **12.56** **p < 0.001**	**p = 0.002**[a] **p = 0.001**[b]
TAS	0.86 ±0.23	0.88 ±0.17	0.64 ±0.14	0.80 ±0.12	$F_{(3–20)}$ = 2.30 p = 0.108	p = 0.167[a] p = 0.427[b]
OSI	15.87 ±5.03	14.11 ±5.03	33.69 ±7.21[a]	18.25 ±3.92[b]	$F_{(3–20)}$ = **16.32** **p < 0.001**	**p = 0.004**[a] **p = 0.001**[b]

Values are expressed as mean ± standard deviation (SD). ANOVA – analysis of variance; TOS – total oxidant status (μmol H_2O_2 equivalent/L); TAS – total antioxidant status (μmol Trolox equivalent/L); OSI – oxidative stress index; a – compared with the sham group; b – compared with the lithium group. Data in bold indicate statistically significant associations.

Table 3. Tissue oxidant/antioxidant status and osmolality analysis

Serum and urine parameters	Sham group (n = 6)	Metformin group (n = 6)	Lithium group (n = 6)	Lithium + metformin group (n = 6)	ANOVA*	Post hoc
TOS	0.89 ±0.35	0.84 ±0.35	2.33 ±0.33[a]	0.94 ±0.27[b]	$F_{(3–20)}$ = **28.25** **p < 0.001**	**p = 0.010**[a] **p = 0.004**[b]
TAS	0.24 ±0.06	0.26 ±0.02	0.22 ±0.03	0.26 ±0.02	$F_{(3–20)}$ = 1.58 p = 0.226	p = 0.657[a] p = 0.213[b]
OSI	3.99 ±2.24	3.29 ±1.44	10.71 ±1.92[a]	3.59 ±1.23[b]	$F_{(3–20)}$ = **24.64** **p < 0.001**	**p = 0.004**[a] **p = 0.002**[b]
Blood osmolality [mOsm/kg]	304.3 ±3.3	306.3 ±2.8	328.2 ±4.6[a]	306.3 ±3.38[b]	$F_{(3–20)}$ = **59.08** **p = 0.002**	**p = 0.004**[a] **p = 0.004**[b]
Urine osmolality [mOsm/kg]	788.5 ±169.8	779.8 ±165.3	349.7 ±44.6[a]	754.5 ±147.3[b]	$F_{(3–20)}$ = **13.61** **p < 0.001**	**p = 0.002**[a] **p = 0.001**[b]

Values are expressed as mean ± standard deviation (SD). ANOVA – analysis of variance; TOS – total oxidant status (μmol H_2O_2 equivalent/L); TAS – total antioxidant status (μmol Trolox equivalent/L); OSI – oxidative stress index; a – compared with the sham group; b – compared with the lithium group. Data in bold indicate statistically significant associations. * p < 0.05 was considered statistically significant.

Table 4. Histopathological analysis and aquaporin-2 levels

Parameter	Sham group (n = 6)	Metformin group (n = 6)	Lithium group (n = 6)	Lithium + metformin group (n = 6)	Kruskal–Wallis test	Mann–Whitney U test
Aquaporin-2	3.0 (2–3)	3.0 (2–3)	1.5 (1–2)[a]	2.5 (2–3)[b]	**p = 0.008**	**p = 0.011**[a] **p = 0.009**[b]
Congestion	1 (0–1)	1 (0–1)	2 (1–3)[a]	1 (0–2)[b]	**p = 0.008**	**p = 0.004**[a] **p = 0.009**[b]
Hydropic swelling	0 (0–1)	1 (0–1)	2 (1–3)[a]	1 (0–2)	**p = 0.008**	**p = 0.008**[a] p = 0.058[b]
Tubular necrosis	0 (0–0)	0 (0–0)	1 (0–1)[a]	0 (0–0)[b]	p = 0.020	p = 0.056[a] p = 0.018[b]
Tubular atrophy	0 (0–1)	0 (0–1)	2 (0–3)[a]	1 (0–1)[b]	p = 0.026	p = 0.020[a] p = 0.075[b]
Bowman's capsule dilatation	0 (0–0)	0 (0–1)	2 (1–2)[a]	0 (0–1)[b]	**p = 0.001**	**p = 0.002**[a] **p = 0.004**[b]
Total score	1 (0–2)	2 (0–3)	9 (4–9)[a]	3 (1–4)[b]	**p = 0.001**	**p = 0.002**[a] **p = 0.002**[b]

Values are expressed as median (min–max). Evaluation of aquaporin level: 0 – none; 1 – <25%; 2 – 26–50%; 3 – >50%. Evaluation of congestion, hydropic swelling, tubular necrosis, tubular atrophy, and Bowman's capsule dilation: 0 – none; 1 – minimal; 2 – medium; 3 – severe. Total score – summing all of the histopathological scores.
A value of p < 0.013 after Bonferroni correction was considered statistically significant. Data in bold indicate statistically significant associations.
a – compared with the sham group; b – compared with the lithium group.

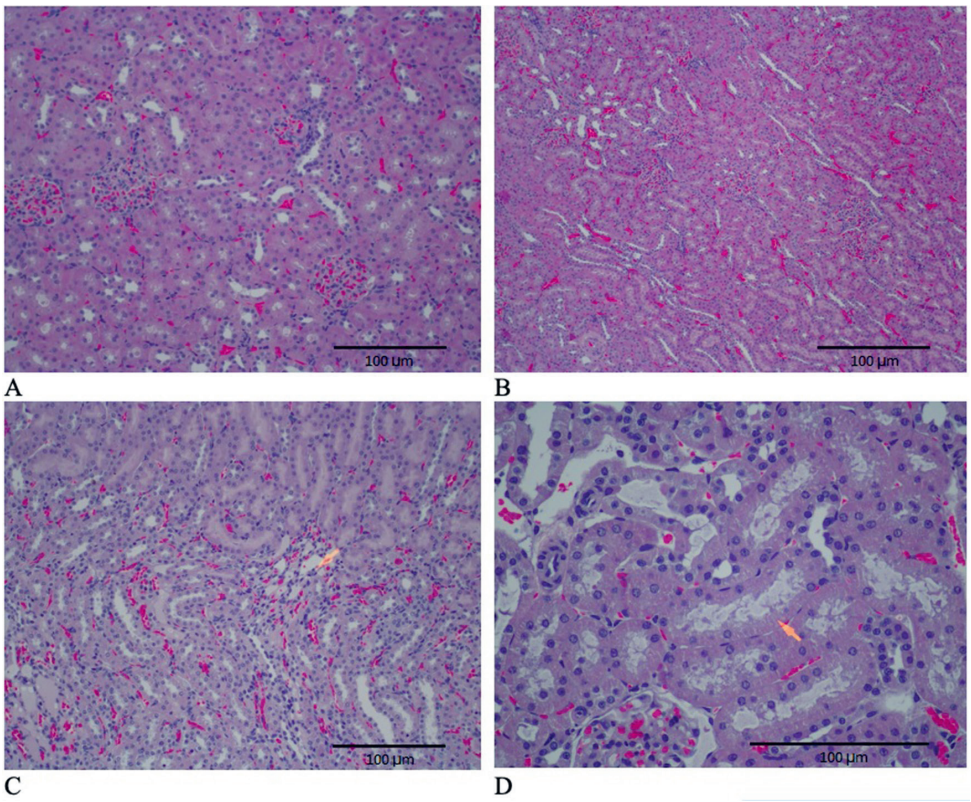

Fig. 2. A. Congestion in the control group; B. Congestion in the metformin group; C. The yellow arrow indicates the tubules showing atrophy in the lithium group; D. The yellow arrow indicates necrosis in the tubular epithelium in the metformin + lithium group (hematoxylin and eosin (H&E) staining, ×100 magnification)

significant differences in the variables between the sham and lithium + metformin groups. Congestion, hydropic swelling, and Bowman's capsule dilatation scores in the lithium group were higher than in the sham group (p = 0.004, p = 0.008, and p = 0.002, respectively). In the lithium + metformin group, the median congestion and Bowman's capsule dilatation pathological evaluation scores were lower compared to the lithium group (p = 0.009 and p = 0.004, respectively). The total score was higher in the lithium group when compared with the sham group (p = 0.002). However, compared with the lithium group, the overall score was significantly lower in the lithium + metformin group (p = 0.002; Fig. 2). The AQP2 levels were significantly lower in the lithium group compared to the sham group (p = 0.009), and significantly higher in the lithium + metformin group compared to the lithium group (p = 0.011; Fig. 3).

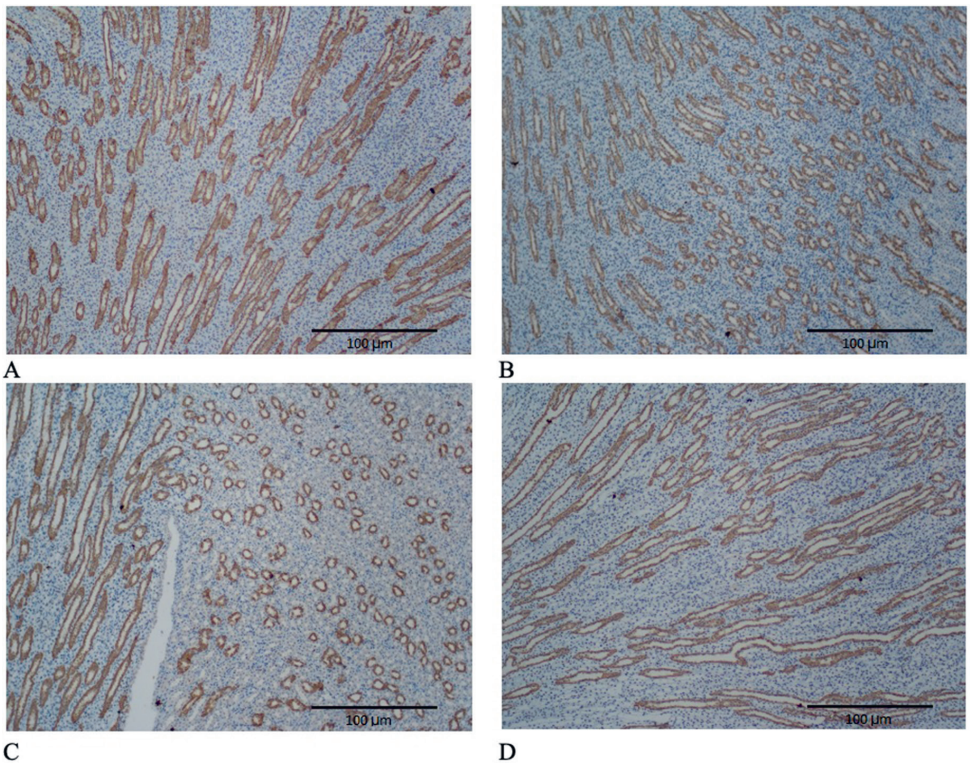

Fig. 3. Histological sections showing aquaporin-2 in the different groups (A. control; B. metformin; C. metformin + lithium; D. lithium (×100 magnification)

Discussion

Bipolar disorder is one of the leading causes of mental disability in the world. Lithium is widely used in the treatment of bipolar disorders and depression.[2] A long-term use of lithium is known to produce permanent nephrotoxicity.[1–3] Lithium causes damage to the kidneys by 3 mechanisms. The 1st one is a decrease in the amount of AQP2 in the kidney,[4] the 2nd one is changes in the ENaCs of the collecting tubules[1] and the 3rd one is oxidative stress due to mitochondrial damage in the kidney cells.[2] Ultimately, acquired NDI, characterized by polyuria and polydipsia, may develop.[1–4]

The most common kidney injury due to chronic lithium use is acquired NDI. Likewise, the most common cause of acquired NDI is lithium-induced NDI, which occurs in up to 50% of patients who receive the long-term lithium therapy.[1,4] Clinically, acquired NDI manifests as arginine vasopressin (AVP) resistant polyuria and polydipsia, and is often associated with natriuresis.[4] In animal models of acquired NDI, it has been shown that the AVP-regulated water channel AQP2 is consistently and markedly decreased in the principal cells of renal medulla collecting duct.[4,16]

Klein et al. have shown that metformin, an AMPK activator, increases phosphorylation of AQP2 in the rat inner medullary collecting ducts, and increases the apical plasma membrane accumulation of AQP2.[8] It was also reported that metformin increases osmotic water permeability by increasing AQP2 accumulation in the apical plasma membrane, and that metformin increases urine osmolality. In the current study, the AQP2 level was low in the lithium group ($p = 0.009$) when compared to the sham group, whereas it increased in the group receiving lithium + metformin when compared to the lithium group ($p = 0.011$).

The ENaC is a likely candidate for lithium entry. Studies by Christensen et al. on transgenic mice lacking ENaC showed that ENaC-mediated lithium entry into the collecting duct principal cells contributes to the pathogenesis of lithium-induced nephrotoxicity, and the absence of functional ENaCs in the transgenic mice protects them from acquired NDI.[5]

Zheng et al. also showed that metformin inhibits the high-sodium-induced upregulation of ENaC expression.[9] It was concluded that metformin with an AMPK activator might directly act in the endothelium by inhibiting ENaC expression and activity, thereby contributing to endothelial protection in response to the high-salt challenge.

The current study shows that the ENaC upregulation in the kidney caused by lithium salts is determined by metformin. Hypernatremia and hyperchloremia (seen in acquired NDI) were observed in the group receiving lithium, and sodium and chloride values in the group receiving lithium + metformin decreased to the levels close to those in the sham group. Similarly, when compared to the lithium group, urine osmolality in the lithium + metformin group reached levels close to those in the sham group.

Studies on oxidative stress in the kidneys caused by chronic lithium use are controversial. Vosahlikova

et al. found that chronic lithium exposure has different oxidative responses in lipid peroxidation products and malondialdehyde levels depending on the cell culture type.[17] In their study, the concentration of lipid peroxidation products in Jurkat cells decreased. On the other hand, in HEK293 cells, long-term Li exposure for 7 or 28 days resulted in a significant increase in the concentration of lipid peroxidation products. In their study on rats, Nciri et al. found that lithium increases the concentration of lipid peroxidation products by triggering oxidative stress in the kidneys, thus intensifying superoxide dismutase and catalase activity while reducing glutathione peroxidase activity from antioxidant enzymes.[18] Again, results in rat studies on TAS and antioxidant enzymes superoxide dismutase, glutathione peroxidase and catalase in cell culture differ.[19,20] However, a literature review did not reveal any research related to TOS and OSI in the kidneys in lithium damage, which shows the actual oxidative stress state.[13–16] In the current study, we observed that TOS values in both plasma and tissue increased with chronic lithium exposure. Although it was not statistically significant, there was a decrease in TAS values, and the OSI value increased significantly.

In recent publications, metformin was reported to reduce the generation of reactive oxygen species (ROS) and prevent mitochondria-mediated apoptosis. It was also suggested that this agent can protect against oxidative stress-induced cell death.[21,22] In the present study, we observed that TOS and OSI values decreased significantly along with metformin treatment, whereas TAS increased, although not significantly.

Histopathological results showed convincing evidence regarding the protective nature of metformin against lithium-induced nephrotoxicity. The total histopathological score was high in the lithium group but significantly lower in the metformin group.

Limitations

Certain limitations of this study should be mentioned. First, varying doses of metformin were not administered. In addition, the study was not fully blind. However, to prevent bias, one of the study authors, those who conducted the blood and tissue analysis, and the biostatisticians did not know the group assignments. The small size of our animal sample constitutes another limitation.

Conclusions

Nephrogenic diabetes insipidus is one of the most critical conditions preventing lithium use, which is widely administered for many psychological disorders. The current study is the 1st to investigate the effects of metformin on lithium-induced NDI. Metformin, which had positive effects on almost all lithium-induced nephrotoxicity parameters, may be a novel therapeutic option for acquired NDI. We conclude that AMPK activation by metformin ameliorates NDI by increasing AQP2 and urine concentrating ability in lithium-induced nephrotoxicity. These findings suggest that metformin may be a novel therapeutic option for lithium-induced NDI. Since metformin is commercially available for human use, further clinical studies can be conducted with ease.

ORCID iDs

Halil Ibrahim Tas https://orcid.org/0000-0001-5849-9068
Eyup Burak Sancak https://orcid.org/0000-0003-4154-2052

References

1. Oktem F, Ozguner F, Sulak O, et al. Lithium-induced renal toxicity in rats: Protection by a novel antioxidant caffeic acid phenethyl ester. *Mol Cell Biochem*. 2005;277(1–2):109–115. doi:10.1007/s11010-005-5426-5
2. ben Saad A, Rjeibi I, Ncib S, Zouari N, Zourgui L. Ameliorative effect of cactus (*Opuntia ficus indica*) extract on lithium-induced nephrocardiotoxicity: A biochemical and histopathological study. *Biomed Res Int*. 2017;2017:8215392. doi:10.1155/2017/8215392
3. Kalita-De Croft P, Bedford JJ, Leader JP, Walker RJ. Amiloride modifies the progression of lithium-induced renal interstitial fibrosis. *Nephrology (Carlton)*. 2018;23(1):20–30. doi:10.1111/nep.12929
4. Zheng P, Lin Y, Wang F, et al. 4-PBA improves lithium-induced nephrogenic diabetes insipidus by attenuating ER stress. *Am J Physiol Renal Physiol*. 2016;311(4):F763–F776. doi:10.1152/ajprenal.00225.2016
5. Christensen BM, Zuber AM, Loffing J, et al. alphaENaC-mediated lithium absorption promotes nephrogenic diabetes insipidus. *J Am Soc Nephrol*. 2011;22(2):253–261. doi:10.1681/ASN.2010070734
6. Sanchez-Rangel E, Inzucchi SE. Metformin: Clinical use in type 2 diabetes. *Diabetologia*. 2017;60(9):1586–1593. doi:10.1007/s00125-017-4336-x
7. Pavlov TS, Levchenko V, Ilatovskaya DV, et al. Lack of effects of metformin and AICAR chronic infusion on the development of hypertension in Dahl salt-sensitive rats. *Front Physiol*. 2017;8:227. doi:10.3389/fphys.2017.00227
8. Klein JD, Wang Y, Blount MA, et al. Metformin, an AMPK activator, stimulates the phosphorylation of aquaporin 2 and urea transporter A1 in inner medullary collecting ducts. *Am J Physiol Physiol*. 2016;310(10):F1008–F1012. doi:10.1152/ajprenal.00102.2016
9. Zheng WW, Li XY, Liu HB, et al. AMP-activated protein kinase attenuates high salt-induced activation of epithelial sodium channels (ENaC) in human umbilical vein endothelial cells. *Oxid Med Cell Longev*. 2016;2016:1–11. doi:10.1155/2016/1531392
10. Chen Q, Thompson J, Hu Y, Das A, Lesnefsky EJ. Metformin attenuates ER stress-induced mitochondrial dysfunction. *Transl Res*. 2017;190:40–50. doi:10.1016/j.trsl.2017.09.003
11. Moher D, Schulz KF, Altman D. The CONSORT statement: Revised recommendations for improving the quality of reports of parallel-group randomized trials. *JAMA*. 2001;285(9263):1987–1991. doi:10.1016/j.explore.2004.11.001
12. Moher D, Schulz KF, Altman DG. The CONSORT statement: Revised recommendations for improving the quality of reports of parallel group randomized trials. *BMC Med Res Methodol*. 2001;1:2. doi:10.1186/1471-2288-1-2
13. Lowry OH, Rosebrough NJ, Farr AL, Randall RJ. Protein measurement with the Folin phenol reagent. *J Biol Chem*. 1951;193(1):265–275. doi:10.1016/S0021-9258(19)52451-6
14. Charan J, Kantharia ND. How to calculate sample size in animal studies? *J Pharmacol Pharmacother*. 2013;4(4):303–306. doi:10.4103/0976-500X.119726
15. Arifin WN, Zahiruddin WM. Sample size calculation in animal studies using resource equation approach. *Malays J Med Sci*. 2017;24(5):101–105. doi:10.21315/mjms2017.24.5.11
16. Zhang Y, Hansson KM, Liu T, et al. Genetic deletion of ADP-activated P2Y12 receptor ameliorates lithium-induced nephrogenic diabetes insipidus in mice. *Acta Physiol*. 2019;225(2):e13191. doi:10.1111/apha.13191

17. Vosahlikova M, Roubalova L, Ujcikova H, et al. Na^+/K^+-ATPase level and products of lipid peroxidation in live cells treated with therapeutic lithium for different periods in time (1, 7, and 28 days): Studies of Jurkat and HEK293 cells. *Naunyn Schmiedebergs Arch Pharmacol*. 2019;392(7):785–789. doi:10.1007/s00210-019-01631-4
18. Nciri R, Allagui MS, Bourogaa E, et al. Lipid peroxidation, antioxidant activities and stress protein (HSP72/73, GRP94) expression in kidney and liver of rats under lithium treatment. *J Physiol Biochem*. 2012;68(1):11–18. doi:10.1007/s13105-011-0113-3
19. Musik I, Kiełczykowska M, Rajtar B, Świątek Ł, Polz-Dacewicz M, Kocot J. Lithium as a prooxidant? A possible protective role of selenium: In vitro study. *Ann Agric Environ Med*. 2017;24(3):423–427. doi:10.26444/aaem/74473
20. Musik I, Kocot J, Kiełczykowska M. Effect of sodium selenite on chosen anti-and pro-oxidative parameters in rats treated with lithium: A pilot study. *Pharmacol Reports*. 2015;67(3):446–450. doi:10.1016/j.pharep.2014.11.010
21. Vial G, Detaille D, Guigas B. Role of mitochondria in the mechanism(s) of action of metformin. *Front Endocrinol (Lausanne)*. 2019;10:294. doi:10.3389/fendo.2019.00294
22. Valiulienė G, Vitkevičienė A, Skliutė G, Borutinskaitė V, Navakauskienė R. Pharmaceutical drug metformin and MCl1 inhibitor S63845 exhibit anticancer activity in myeloid leukemia cells via redox remodeling. *Molecules*. 2021;26(8):1–13. doi:10.3390/molecules26082303

Echinatin mitigates H_2O_2-induced oxidative damage and apoptosis in lens epithelial cells via the *Nrf2/HO-1* pathway

Haijun Ran[1,B,D], Han Liu[2,B,C], Ping Wu[3,A,E,F]

[1] Nanchong Aier Mega Eye Hospital, China
[2] Department of Ophtalmology, Jiangjin Central Hospital of Chongqing, China
[3] Chongqing Aier Eye Hospital, China

A – research concept and design; B – collection and/or assembly of data; C – data analysis and interpretation;
D – writing the article; E – critical revision of the article; F – final approval of the article

Advances in Clinical and Experimental Medicine, ISSN 1899–5276 (print), ISSN 2451–2680 (online) *Adv Clin Exp Med*. 2021;30(11):1195–1203

Address for correspondence
Ping Wu
E-mail: wp2228094@163.com

Funding sources
None declared

Conflict of interest
None declared

Received on March 23, 2021
Reviewed on May 10, 2021
Accepted on June 18, 2021

Published online on September 9, 2021

Abstract

Background. Oxidative stress has been reported to be an early factor in the development of cataracts. Echinatin (Ech) is an active ingredient of licorice that exhibits antioxidant effects.

Objectives. To investigate the effects of Ech on oxidative stress-induced lens epithelial cell (LEC) damage.

Materials and methods. Human lens epithelial B3 cells (HLECs) were exposed to hydrogen peroxide (H_2O_2) and were pretreated with or without Ech. For rescue experiments, ML385, an inhibitor of the *Nrf2* pathway, was added into the medium.

Results. Echinatin reversed the H_2O_2-induced reduction of cell viability in B3 cells. Additionally, H_2O_2 induced oxidative stress, evidenced by an increase of reactive oxygen species (ROS) and malondialdehyde (MDA) levels, and a decrease in superoxide dismutase (SOD) and catalase (CAT) levels, which could be abolished by Ech. Echinatin treatment also reduced HLEC apoptosis induced by H_2O_2. In addition, Ech pretreatment promoted *Bcl-2* expression, and suppressed *Bax* and caspase-3 expression levels, in H_2O_2-treated B3 cells. Moreover, H_2O_2 significantly reduced *Nrf2* nuclear localization, as well as *HO-1* and *NQO1* expression, which could be reversed by Ech. Inhibition of *Nrf2* by ML385 aggravated H_2O_2-induced oxidative damage and apoptosis in HLECs, and the protective effects of Ech on H_2O_2-induced oxidative damage and apoptosis could be restored by ML385.

Conclusions. Echinatin mitigates H_2O_2-induced oxidative damage and apoptosis in HLECs via the *Nrf2/HO-1* pathway, suggesting that Ech may be a potential drug for the treatment of cataracts.

Key words: cataract, lens epithelial cells, apoptosis, oxidative stress, echinatin

Cite as
Ran H, Liu H, Wu P. Echinatin mitigates H_2O_2-induced oxidative damage and apoptosis in lens epithelial cells via the *Nrf2/HO-1* pathway. *Adv Clin Exp Med*. 2021;30(11):1195–1203. doi:10.17219/acem/139130

DOI
10.17219/acem/139130

Background

Cataracts have become the main cause of loss of useful vision worldwide.[1] It is currently believed that, with the exception of congenital cataracts, the apoptosis of lens epithelial cells (LECs) is the cytological basis for the formation of various types of cataracts.[2] Due to long-term exposure to light, the lens is continuously damaged by reactive oxygen species (ROS), which is considered to be a key factor in the development of cataracts.[3–5] Studies have confirmed that cataracts are directly related to the apoptosis of LECs caused by oxygen free radicals.[6,7] Thus, it is important to explore antioxidant drugs that can prevent the formation and development of cataracts.

The process of oxidative stress mainly involves a variety of stress-sensitive signaling pathways.[8,9] As one of the main cellular defense mechanisms against oxidative stress, *Nrf2* is crucial in resisting cell damage caused by endogenous and exogenous stress.[10] As the main regulator of the antioxidant response, *Nrf2* can induce the expression of target genes, such as NAD(P)H quinone oxidoreductase 1 (*NQO1*), heme oxygenase 1 (*HO-1*) and catalase (*CAT*). The dysfunction of *Nrf2* is inseparable from the development of cataract. Studies have shown that the protein and gene expression of *Nrf2* in the lens significantly decreases with age.[11,12] The decreased activity of *Nrf2* limits the transcription of its downstream antioxidant enzymes and causes the antioxidant system to fail, which ultimately leads to age-related cataracts.[12] Targeted activation of *Nrf2* signaling can protect LECs from damage induced by oxidative stress.[13,14]

Echinatin (Ech; 4,4'-dihydroxy-2-methoxychalcone; Fig. 1A), a retrochalcone, is an active ingredient of licorice and the main active form with pharmacokinetic function.[15] Studies have shown that Ech has a wide range of biological properties, including anti-inflammatory and anti-tumor effects.[16] Importantly, Liang et al.[17] confirmed that Ech may undergo electron transfer and proton transfer to cause antioxidant effects. However, to date, the effects of Ech on oxidative stress-induced LEC damage have not been reported, and its molecular mechanism is largely unclear. Hence, the present study attempted to investigate the potential role of Ech as an agent for controlling cataract progression against H_2O_2-induced oxidative stress and apoptosis in human B3 cells.

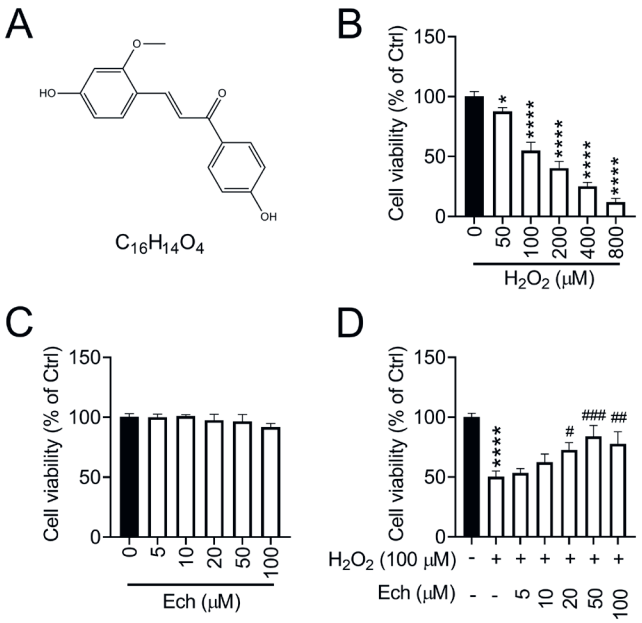

Fig. 1. Echinatin (Ech) attenuates the effects of H_2O_2 on the viability of human lens epithelial B3 cells (HLECs)

A. Structure of Ech; B. B3 cells were exposed to H_2O_2 (0–800 μM) for 24 h and the viability of B3 cells was analyzed using the MTT assay; C. B3 cells were treated with Ech (0–100 μM) for 12 h and the viability of B3 cells was analyzed using the MTT assay; D. B3 cells were pretreated with Ech (0–100 μM) for 12 h, followed by exposure to H_2O_2 (100 μM) for 24 h, and the viability of B3 cells was analyzed using the MTT assay; *p < 0.05, ****p < 0.0001, #p < 0.05, ##p < 0.01, ###p < 0.001.

Objectives

Oxidative stress has been shown to be an early factor in the development of cataracts. Echinatin is the active ingredient of licorice, and its pharmacological effects are closely related to antioxidants. Thus, the aim of the current study is to investigate the effects of Ech on oxidative stress-induced LEC damage.

Materials and methods

All in vitro experiments in the current study were carried out using human LECs (HLECs). This study does not contain any experiments using human participants or animal subjects.

Cell culture and treatment

The human lens epithelial cell (HLEC) line B3 cells were purchased from American Type Culture Collection (CRL-11421; ATCC, Manassas, USA). B3 cells were cultured in Dulbecco's modified Eagle's medium (Invitrogen, Carlsbad, USA) containing 10% fetal bovine serum (FBS; Invitrogen) and 100 mg/mL streptomycin in a humidified atmosphere with 5% CO_2 at 37°C. B3 cells at 80% confluence were treated with different concentrations of H_2O_2 (Sigma–Aldrich, Seelze, Germany; 0, 50, 100, 200, 400, and 800 μM) for 24 h. To investigate the role of Ech, B3 cells were pretreated with different concentrations of Ech (0, 5, 10, 20, 50, and 100 μM) for 12 h before the H_2O_2 treatment. For rescue experiments, B3 cells were pretreated with ML385 (5 μM; Sigma–Aldrich), a specific inhibitor of *Nrf2*, for 12 h in the presence or absence of Ech (50 μM), followed by exposure to H_2O_2. Echinatin ($C_{16}H_{14}O_4$; CAS No. 34221-41-5, M.W. 270.2, purity 99%) was purchased from Chengdu Alfa Biotechnology Co. Ltd. (Chengdu, China).

MTT assay

The cells (2×10^4) were seeded in a 96-well culture plate and incubated with H_2O_2 (0, 50, 100, 200, 400, and 800 μM) for 24 h alone or after pretreatment with Ech (0, 5, 10, 20, 50, and 100 μM) for 12 h. The cells were then incubated with 5 mg/mL MTT solution (Beyotime, Shanghai, China) for 4 h at 37°C. The supernatant was aspirated and dimethyl sulfoxide (DMSO) was added to the cells. The optical density at 490 nm was observed using a microplate reader (SpectraMax Id3; Molecular Devices, San Jose, USA).

Determination of intracellular ROS levels

The ROS level was gauged using 6-carboxy-2', 7'-dichlorodihydrofluorescein diacetate (DCHFDA; Beyotime) according to the manufacturer's protocol. Briefly, after exposure to corresponding treatment, the culture medium was removed and B3 cells were incubated with 25 μM of DCHFDA mix for 45 min at 37°C. The absorbance was detected at a wavelength of 488 nm.

Measurement of MDA, SOD and CAT

After centrifugation of cell lysates, the supernatants were collected. The protein concentration was measured according to the BCA Assay Kit instructions (Beyotime). Malondialdehyde (MDA) was measured using a lipid peroxidation MDA assay kit (Beyotime). The test working solution was added to the sample and mixed. The mixture was heated at 100°C for 15 min. After centrifugation, the supernatants were collected. The absorbance was detected at a wavelength of 532 nm and the results were expressed as nmol/mg protein.

Total superoxide dismutase (SOD) content was determined using a SOD assay kit (Beyotime), and the results were expressed as U/mg protein. A Cu/Zn-SOD inhibitor was added to the samples to inhibit the activity of the Cu/Zn-SOD enzyme, followed by incubation with the WST-8/enzyme working solution at 37°C for 30 min. The absorbance was detected at a wavelength of 450 nm. One SOD enzymatic activity unit (U) was defined as the amount of sample needed to achieve a 50% inhibition rate of WST-8 formazan dye.

Catalase (CAT) content was tested using a CAT assay kit (Beyotime). Catalase detection buffer and hydrogen peroxide solution were added to the sample, and then incubated at 25°C for 5 min. The reaction stop solution was added to the mixture, then it was inverted and mixed to stop the reaction. After adding the detection buffer and chromogenic working buffer, the mixture was incubated at 25°C for 15 min. The absorbance was detected at a wavelength of 520 nm, and the results were expressed as U/mg protein. All operations were performed in accordance with the manufacturer's instructions.

Measurement of apoptosis

Cells (1×10^6) were seeded and pretreated with or without Ech for 12 h, followed by exposure to 100 μM H_2O_2 for 24 h. Cells were fixed in 4% paraformaldehyde for 20 min at room temperature. The apoptosis of B3 cells was measured using the terminal deoxyribonucleotidyl transferase (TdT)-mediated dUTP nick end labeling (TUNEL) assay (Cell Death Detection Kit; Beyotime), according to the instructions of the manufacturer. The cells were visualized under a fluorescent microscope (Olympus Corp., Tokyo, Japan). Data were expressed as the ratio of TUNEL-positive cells to total cells.

Western blot assay

The protein expression in whole cell lysates or nuclear extracts was analyzed using western blot analysis. The radioimmunoprecipitation assay (RIPA) lysis buffer (Beyotime) was used to extract total protein from B3 cells. Next, a BCA protein assay kit (Beyotime) was used to quantify the proteins. Then, 30-μg protein samples were separated using 10% sodium dodecyl sulfate polyacrylamide gel electrophoresis (SDS-PAGE) and transferred to polyvinylidene fluoride (PVDF) membranes (Merck Millipore, Darmstadt, Germany). The membranes were then blocked using 5% skimmed milk for 1 h at room temperature, followed by incubation with primary antibodies against *Bcl-2* (Abcam, Cambridge, USA), *Bax* (Abcam), *Nrf2* (Cell Signaling Technology, Beverly, USA), *HO-1* (Abcam), *NQO1* (Cell Signaling Technology), and *GAPDH* (Cell Signaling Technology) at 4°C overnight. Subsequently, the membranes were incubated with horseradish peroxidase (HRP)-conjugated goat anti-rabbit secondary antibody (Abcam) for 1 h at room temperature, followed by exposure to the enhanced chemiluminescent reagent (Pierce, Rockford, USA). The intensity of proteins signals was quantified using Quantity One software v. 4.1.1 (Bio-Rad Laboratories, Hercules, USA).

Measurement of caspase-3 activity

As described previously,[18] caspase-3 activity was measured using a caspase-3 activity assay kit (Beyotime) according to the manufacturer's protocol. For each sample, an equal amount of protein (200 μg) was mixed with reaction buffer (50 μL) and caspase-3 substrate (5 μL) in the dark at 37°C for 30 min. The absorbance at 485 nm was measured using a microplate reader.

Statistical analyses

Data are expressed as mean ± standard deviation (SD) from at least 3 independent experiments, and the results were analyzed using GraphPad Prism v. 8.0 (GraphPad Software, San Diego, USA). Data from individual groups were confirmed to follow a normal distribution using

the Kolmogorov–Smirnov test. Comparisons between 2 groups were analyzed using Student's t-tests (Welch's correction was used in cases of unequal variance), and comparisons among multiple groups were analyzed using one-way analysis of variance (ANOVA), followed by Tukey's post hoc tests. A p-value of less than 0.05 was considered statistically significant.

Results

Echinatin attenuates the effects of H_2O_2 on viability of HLECs

We performed a MTT assay to evaluate the effects of H_2O_2 and Ech on the viability of B3 cells. The B3 cells were exposed to H_2O_2 (0–800 μM) for 24 h and the results showed that higher concentrations of H_2O_2 (100–800 μM) restrained cell viability in a dose-dependent manner (Fig. 1B). In view of the results that the treatment with 100 μM H_2O_2 for 24 h could reduce cell viability to approx. 50% compared to the control group, this concentration was chosen for subsequent experiments. Additionally, Ech (0–50 μM) did not affect the viability of HLECs (Fig. 1C). Moreover, the pretreatment with Ech (10–50 μM) illustrated a protective effect against H_2O_2-induced damage in a dose-dependent manner (Fig. 1D).

Echinatin reduces H_2O_2-induced oxidative damage in HLECs

Oxidative stress is considered to be an early factor in the development of cataracts.[19] B3 cells were treated with H_2O_2 for 24 h and exhibited the onset of oxidative stress manifested by the enhanced levels of ROS (Fig. 2A) and MDA (Fig. 2B), and suppressed levels of SOD (Fig. 2C) and CAT (Fig. 2D), compared to control cells. The cells pretreated with Ech restored levels similar to those of control cells in a dose-dependent manner (Fig. 2A–D), indicating that Ech had a protective effect on oxidative damage in HLECs.

Ech reduces cell apoptosis induced by H_2O_2 in HLECs

Apoptosis of LECs is the main cytological basis for the formation of various types cataract.[2] Here, the TUNEL assay was used to measure HLEC apoptosis after exposure to Ech and/or H_2O_2. The results illustrated that H_2O_2 exposure markedly induced apoptosis, compared to the control group (Fig. 3A,B). Additionally, Ech treatment could reduce HLEC apoptosis induced by H_2O_2 in a dose-dependent manner (Fig. 3A,B). Moreover, western blot analysis showed that the expression of the anti-apoptotic protein Bcl-2 was markedly suppressed, while the expression of the pro-apoptotic protein Bax was significantly enhanced after the exposure to H_2O_2, which could be

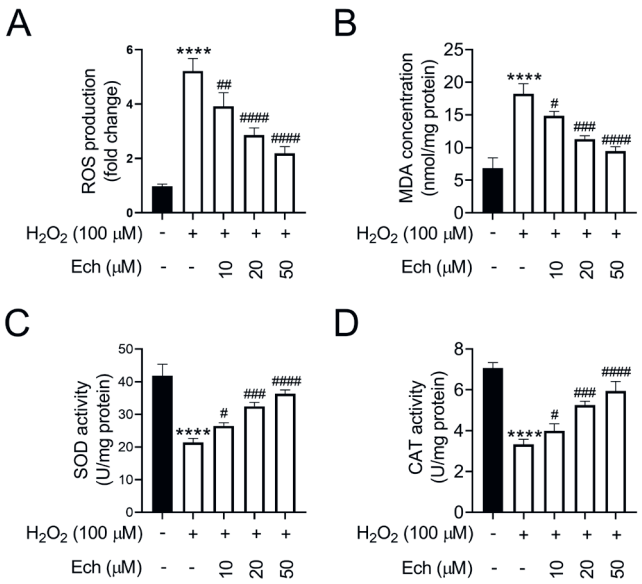

Fig. 2. Echinatin (Ech) alleviates H_2O_2-induced oxidative damage in human lens epithelial B3 cells (HLECs)

B3 cells were pretreated with Ech (10 μM, 20 μM and 50 μM) for 12 h, followed by exposure to H_2O_2 (100 μM) for 24 h. A. The levels of intracellular reactive oxygen species (ROS) were determined using the DCFHDA method; B. The content of malondialdehyde (MDA) was measured using a Lipid Peroxidation MDA Assay Kit; C. The levels of superoxide dismutase (SOD) were analyzed using a Total Superoxide Dismutase Assay Kit; D. The levels of catalase (CAT) were determined using a Catalase Assay Kit. ****p < 0.0001, #p < 0.05, ##p < 0.01, ###p < 0.001, ####p < 0.0001.

reversed by Ech pretreatment (Fig. 3C,D). Furthermore, Ech pretreatment eliminated the increase in caspase-3 activity induced by H_2O_2 (Fig. 3E).

Ech activates the *Nrf2/HO-1* pathway in H_2O_2-treated HLECs

To determine the effects of *Nrf2* on H_2O_2-induced HLECs, the expression levels of *Nrf2* and its downstream targets (*HO-1* and *NQO1*) were analyzed using the western blot assay. Since *Nrf2* nuclear translocation is an essential step for activation of the *Nrf2* pathway, the nuclear localization of *Nrf2* in B3 cells was also analyzed using the western blot assay. The results showed that H_2O_2 significantly reduced *Nrf2* nuclear localization, which could be reversed with Ech pretreatment (Fig. 4A,B). Moreover, compared to the control group, the expression levels of *HO-1* and *NQO1* were decreased after the exposure to H_2O_2, which could be reversed with Ech pretreatment (Fig. 4C,D). These data demonstrate that Ech may activate the *Nrf2/HO-1* pathway in H_2O_2-treated HLECs.

Inhibition of *Nrf2* by ML385 aggravates H_2O_2-induced oxidative damage and apoptosis in HLECs

We assessed the effect of ML385 (5 μM) alone on the viability of B3 cells, and the results confirmed that ML385 had

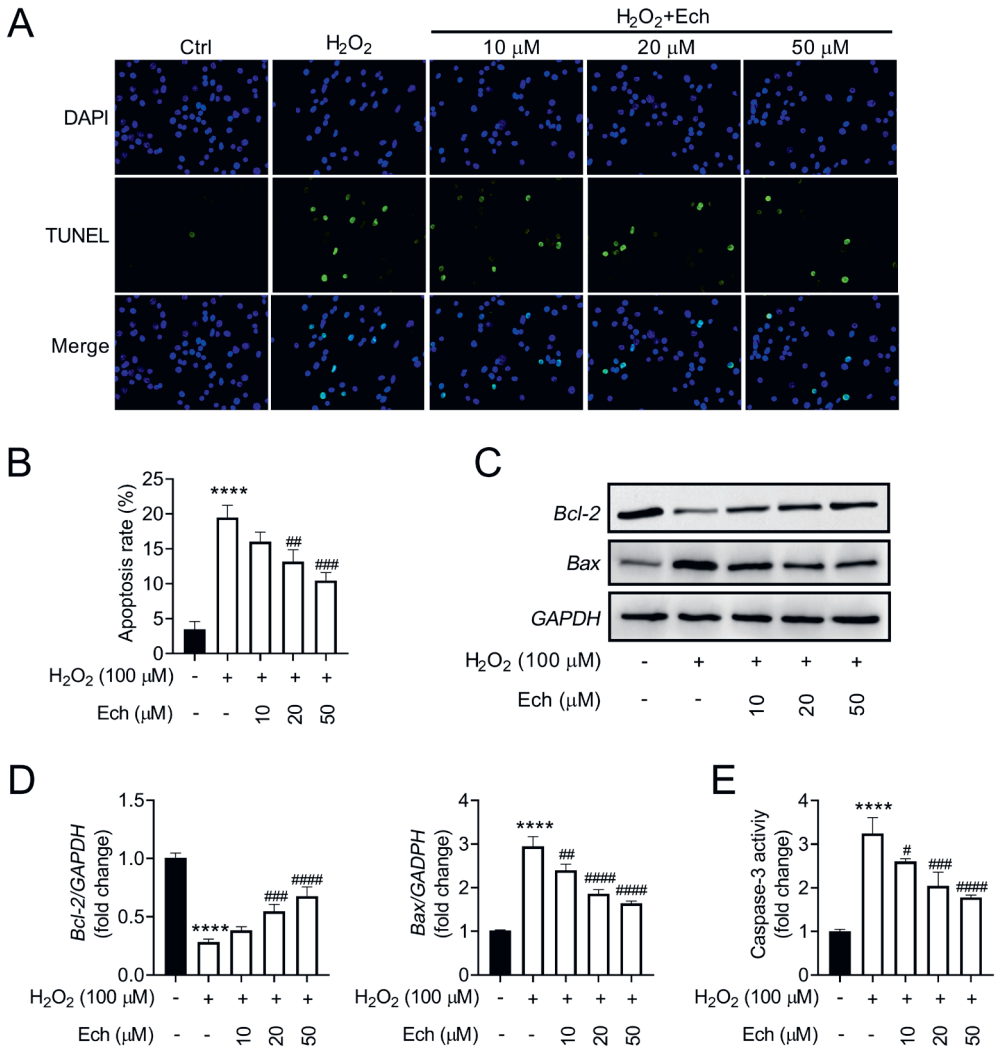

Fig. 3. Echinatin (Ech) reduces cell apoptosis induced by H_2O_2 in human lens epithelial B3 cells (HLECs)

B3 cells were pretreated with Ech (10 μM, 20 μM and 50 μM) for 12 h, followed by exposure to H_2O_2 (100 μM) for 24 h. A. The TUNEL assay was used to analyze the changes in apoptosis; B. Quantitative results of TUNEL-positive cells; C. The expression of *Bcl-2* and *Bax* was analyzed using the western blot assay; D – Quantitative results of *Bcl-2* and *Bax* levels; E. The activity of caspase-3 was analyzed using a corresponding kit; ****p < 0.0001, #p < 0.05, ##p < 0.01, ###p < 0.001, ####p < 0.0001.

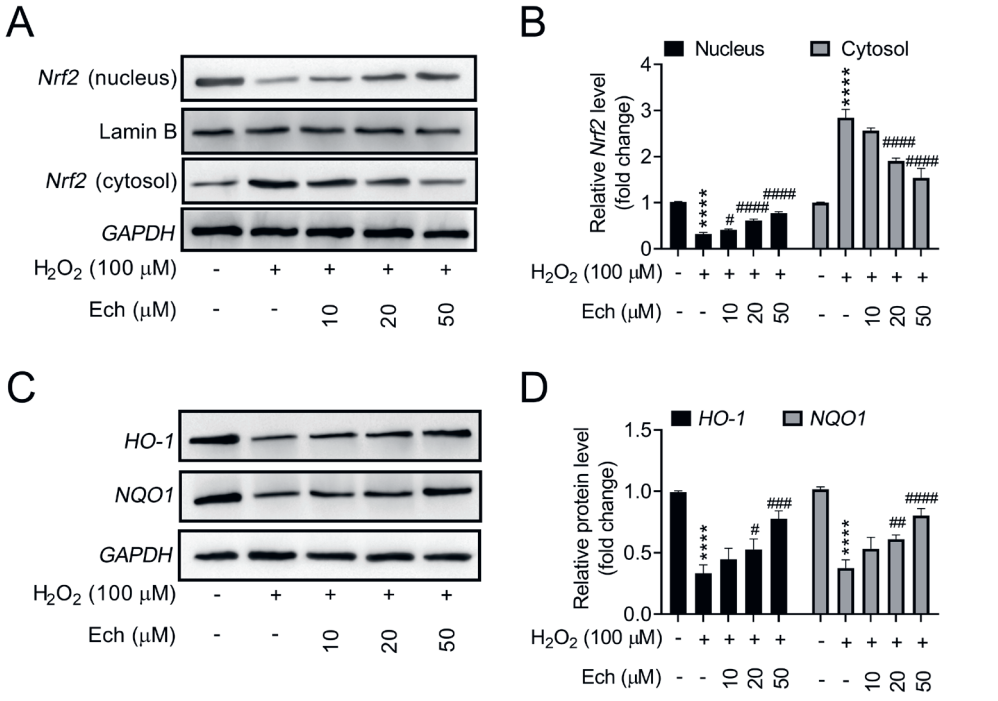

Fig. 4. Echinatin (Ech) activates the *Nrf2/HO-1* pathway in H_2O_2-treated human lens epithelial B3 cells (HLECs)

B3 cells were pretreated with Ech (10 μM, 20 μM and 50 μM) for 12 h, followed by exposure to H_2O_2 (100 μM) for 24 h. A. The expression of nuclear and cytosolic *Nrf2* was analyzed using the western blot assay; B. Quantitative results of *Nrf2* levels; C. The expression of *HO-1* and *NQO1* was analyzed using the western blot assay; D. Quantitative results of *HO-1* and *NQO1* levels; ****p < 0.0001, #p < 0.05, ##p < 0.01, ###p < 0.001, ####p < 0.0001.

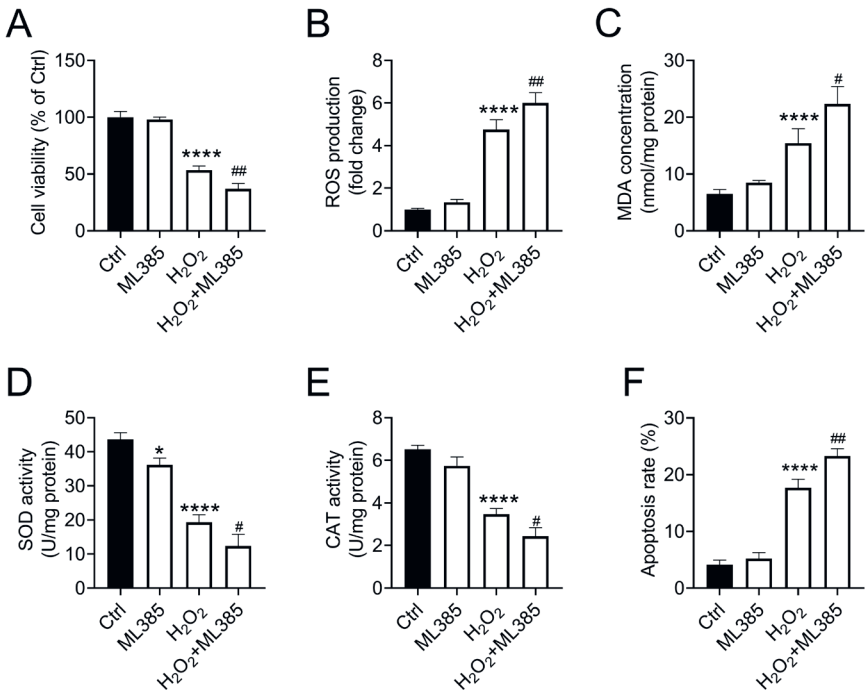

Fig. 5. ML385 aggravates H_2O_2-induced oxidative damage and cell apoptosis in human lens epithelial B3 cells (HLECs)

B3 cells were pretreated with ML385 (5 μM) for 12 h, followed by exposure to H_2O_2 (100 μM) for 24 h; the viability of B3 cells was analyzed using the MTT assay (A); reactive oxygen species (ROS) (B), malondialdehyde (MDA) (C), superoxide dismutase (SOD) (D), and catalase (CAT) (E) levels were determined using corresponding kits; F. The TUNEL assay was used to analyze cell apoptosis; *p < 0.05, ****p < 0.0001, #p < 0.05, ##p < 0.01, ###p < 0.001, ####p < 0.0001.

no effect on the viability of B3 cells, but aggravated the inhibitory effect of H_2O_2 on cell viability (Fig. 5A). Compared with the control group, ML385 increased ROS and MDA levels, and decreased SOD and CAT levels in B3 cells. Simultaneously, ML385 enhanced the oxidative stress damage caused by H_2O_2 (Fig. 5B–E). There was no change in the apoptosis rate between the ML385 group and the control group. Importantly, inhibition of *Nrf2* by ML385 also exacerbated H_2O_2-induced cell apoptosis in HLECs (Fig. 5F).

ML385 attenuates the protective effect of Ech on H_2O_2-induced oxidative damage and apoptosis in HLECs

To confirm that Ech could resist H_2O_2-induced cell damage by activating the *Nrf2* pathway, B3 cells were pretreated with Ech (50 μM) and ML385 (5 μM) for 12 h, followed by exposure to H_2O_2 (100 μM) for 24 h. The results showed that Ech restrained the enhancement of ROS and MDA, and weakened SOD and CAT induced by H_2O_2, whereas ML385 abolished the effects of Ech on oxidative stress (Fig. 6A–D). Similarly, the anti-apoptotic effects of Ech on H_2O_2-induced B3 cells also could be blocked by ML385 (Fig. 6E–G). These results reveal that Ech protected B3 cells against H_2O_2-induced oxidative injury and apoptosis via activation of the *Nrf2* pathway (Fig. 7).

Discussion

Oxidative stress has been proven to be an early factor in the development of cataracts,[19] and drugs that prevent this event are needed to resist adverse cellular reactions.[20] Oxidative stress damage refers to the comprehensive effect of exogenous or endogenous ROS on the cell signal transduction system, or to damage to nucleic acids, proteins and lipid molecules.[21] Hydrogen peroxide can induce the production of ROS in cells, leading to oxidative damage.[22] Early studies confirmed that high concentrations of H_2O_2 in the lens and aqueous humor can cause cataracts.[23] Exogenous H_2O_2 treatment is a simple and feasible cell model for studying LEC oxidative damage, which can effectively simulate the process of oxidative damage in LECs that results in cataracts.[24] Therefore, in the present study, 100 μM H_2O_2 was selected as an inducer of oxidative damage in B3 cells.

Previous work has confirmed that the use of antioxidants and certain metabolic receptor agonists can delay the occurrence of cataracts.[20] For instance, glycyrrhizin, a substance extracted from licorice, prevents sodium iodate-induced retinal pigment epithelium and retinal injury via the inhibition of ROS.[25] Echinatin has been shown to prevent or treat cardiovascular disease, tumors and diabetic nephropathy.[26–28] Recently, the antioxidant properties of Ech have been confirmed.[17] Kwak et al.[28] reported that Ech can exert anti-cancer effects by inducing ROS/endoplasmic reticulum stress (ERS)-dependent apoptosis. Tian et al.[26] proposed that Ech improves myocardial injury caused by ischemia and reperfusion by reducing oxidative stress and apoptosis of cardiomyocytes. However, the effects of Ech on the development of cataracts remain unclear. In the present study, Ech significantly improved the viability of H_2O_2-treated LECs. Simultaneously, Ech pretreatment prevented the production of ROS and MDA, and enhanced the activity of SOD and CAT in LECs treated with H_2O_2. These data suggest that Ech can effectively prevent oxygen free radicals from

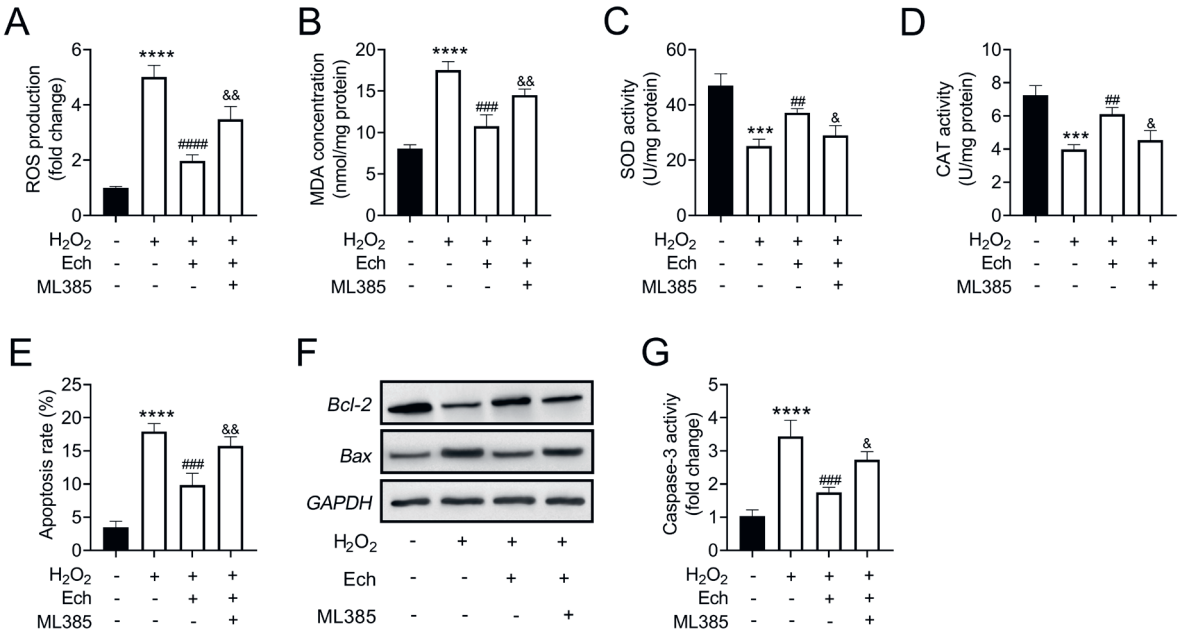

Fig. 6. ML385 attenuates the protective effect of echinatin (Ech) on H_2O_2-induced oxidative damage and apoptosis in human lens epithelial B3 cells (HLECs)

B3 cells were pretreated with Ech (50 μM) and ML385 (5 μM; an inhibitor of *Nrf2*) for 12 h, followed by exposure to H_2O_2 (100 μM) for 24 h; reactive oxygen species (ROS) (A), malondialdehyde (MDA) (B), superoxide dismutase (SOD) (C), and catalase (CAT) (D) levels were determined using corresponding kits; E. The TUNEL assay was used to analyze the changes in apoptosis; F. The expression of *Bcl-2* and *Bax* was analyzed using the western blot assay; G. The activity of caspase-3 was analyzed using a corresponding kit; ***p < 0.001, ****p < 0.0001, ##p < 0.01, ###p < 0.001, ####p < 0.0001, &p < 0.05, &&p < 0.01.

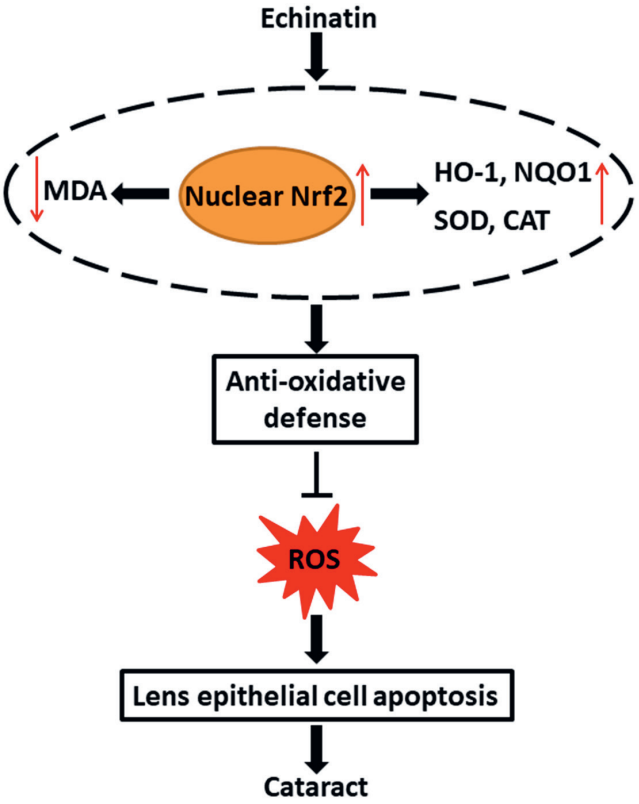

Fig. 7. Schematic diagram of the protective effect of echinatin (Ech) on H_2O_2-induced oxidative damage and apoptosis in human lens epithelial B3 cells (HLECs)

entering the lens, and has a protective effect on the oxidative damage of LECs induced by H_2O_2 by enhancing cell viability.

Studies on the prevention and treatment of primary or subsequent cataracts mainly focus on how to control the apoptosis of LECs.[29,30] Apoptosis is a type of programmed cell death different from cell necrosis,[31] where the mitochondrial apoptotic pathway plays a key role. The *Bcl-2* family and the caspase family play important roles in the mitochondrial pathway.[32,33] *Bcl-2* family members play a key role in maintaining the integrity of the outer mitochondrial membrane and regulate the release of cytochrome C, which determines the direction of apoptosis regulation in the apoptosis pathway.[34] Caspase is a protease system that can lead to the disintegration of apoptotic cells, among which caspase-3 is the main executor of apoptosis.[35,36] In addition to congenital cataracts, the apoptosis of LECs plays a vital role in the formation of other types of cataracts. Studies have shown that *p53*-dependent LECs can be induced to undergo apoptosis by ultraviolet radiation, which further leads to the formation of cataracts.[37,38] Tamada et al.[39] found that apoptosis in selenite cataracts may be an early event, which is reflected in the increase of caspase-3 enzyme activity. Similar studies have found that high glucose can also induce the apoptosis of LECs, which is essential for the formation of cataracts.[40,41] Moreover, cataracts are directly related to the apoptosis of LECs caused by oxygen free radicals.[42,43]

It has been reported that antioxidant genes and drugs can inhibit the oxidative damage caused by H_2O_2 by reducing the activity of ROS.[44,45] Lens epithelial cells initiate apoptosis-related signal transduction pathways under oxidative stress, which mediates the apoptosis of LECs and promote the development of cataracts. Reactive oxygen species promote the entry of cytochrome C into

the cytoplasm by oxidizing the thiol group on the adenine nucleotide transporter, and induce the caspase cascade, which ultimately leads to irreversible cell apoptosis.[46] Wu et al.[47] reported that the ERS inhibitor, salubrinal, reduces the H_2O_2-induced oxidative stress damage in HepG2 cells by inhibiting cell apoptosis. Here, we analyzed the effect of Ech on the apoptosis of LECs treated with H_2O_2. Similar to previous reports,[48] this study showed that H_2O_2 induced the apoptosis of HLECs, which may be an important mechanism for the development of cataracts caused by oxidative stress. Additionally, Ech reduced the apoptosis of HLECs induced by H_2O_2 treatment. Echinatin also inhibited the levels of *Bax* and caspase-3, and promoted the expression of *Bcl-2*. These results indicate that Ech can protect HLECs from apoptosis caused by oxidative stress.

Nrf2 signal transduction is a pivotal mechanism to maintain oxidation and antioxidant homeostasis, and to reduce oxidative stress damage.[49] Normally, *Nrf2* is anchored in the cytoplasm through Keap1. *Nrf2* is dissociated from Keap1 and transferred to the nucleus under the stimulation of oxidative stress, phosphorylation or electrophiles.[50] *HO-1* and *NQO1* are the key downstream factors of *Nrf2* signal transduction, which are very important in protecting cells from the oxidative damage.[51,52] Recent studies have shown that trimetazidine can delay the formation of age-related cataracts by regulating the expression of *Nrf2* and reducing the production of ROS.[53] Whitson et al.[54] found that LECs lacking glutathione (GSH) depend on the activation of the *Nrf2* signaling pathway to trigger oxidative stress. Moreover, *Nrf2* inhibitors may increase the oxidative stress of the lens, and *Nrf2* inducers can prevent cataract formation by reducing oxidative stress.[55] Therefore, *Nrf2* pathway activation can be used as a target for the prevention and treatment of age-related cataracts induced by oxidative stress. In the present study, we found that Ech abolished the inhibitory effect of H_2O_2 on *Nrf2* nuclear translocation in B3 cells, as well as the expression of *HO-1* and *NQO1*. Furthermore, administration of the *Nrf2* inhibitor ML385 could reverse the protective effect of Ech, suggesting that the potential antioxidant mechanism of Ech may include *Nrf2* signal transduction. Importantly, it has been reported that Ech can inhibit activation of the *NF-κB* pathway[56] and the *AKT/mTOR* pathway.[57] Therefore, the protective effect of Ech may also involve other signal pathways, a hypothesis that needs further study. In addition, because the potential toxicity and side effects of Ech and its derivatives are still unclear, there is still a lot of research to be performed before this drug can be applied in the clinic.

Limitations

The therapeutic effect of Ech should be further identified in an animal model of cataracts. In addition, more work needs to be done to elucidate its underlying molecular mechanisms.

Conclusions

As far as we know, the present study is the first demonstration that Ech can protect HLECs from the oxidative stress damage caused by the exposure to H_2O_2. More importantly, Ech pretreatment reduced cell apoptosis induced by H_2O_2, providing new directions in the search for novel drugs to prevent and treat cataracts.

ORCID iDs

Haijun Ran https://orcid.org/0000-0002-6170-2685
Han Liu https://orcid.org/0000-0002-6039-9362
Ping Wu https://orcid.org/0000-0002-8297-6140

References

1. Lee CM, Afshari NA. The global state of cataract blindness. *Curr Opin Ophthalmol*. 2017;28(1):98–103. doi:10.1097/icu.0000000000000340
2. Yan Q, Liu JP, Li DW. Apoptosis in lens development and pathology. *Differentiation*. 2006;74(5):195–211. doi:10.1111/j.1432-0436.2006.00068.x
3. Shahinfar J, Keshavarzi Z, Ahmadi M, et al. Serum oxidative stress markers in patients with senile cataract and healthy controls. *J Coll Physicians Surg Pak*. 2018;28(6):448–451. doi:10.29271/jcpsp.2018.06.448
4. Babizhayev MA, Yegorov YE. Biomarkers of oxidative stress and cataract. Novel drug delivery therapeutic strategies targeting telomere reduction and the expression of telomerase activity in the lens epithelial cells with N-acetylcarnosine lubricant eye drops: Anti-cataract which helps to prevent and treat cataracts in the eyes of dogs and other animals. *Curr Drug Deliv*. 2014;11(1):24–61. doi:10.2174/15672018113106660062.
5. Spector A. Oxidative stress-induced cataract: Mechanism of action. *FASEB J*. 1995;9(12):1173–1182. PMID:7672510
6. Lu B, Christensen IT. SUMOylation evoked by oxidative stress reduced lens epithelial cell antioxidant functions by increasing the stability and transcription of TP53INP1 in age-related cataracts. *Oxid Med Cell Longev*. 2019;2019:7898069. doi:10.1155/2019/7898069
7. Zou Y, Cui B, Liang P, et al. Inhibition of NLRP3 protects human lens epithelial cells against oxidative stress-induced apoptosis by NF-κB signaling. *Ophthalmic Res*. 2020;63(2):174–181. doi:10.1159/000504303
8. Tóbon-Velasco JC, Cuevas E, Torres-Ramos MA. Receptor for AGEs (RAGE) as mediator of NF-kB pathway activation in neuroinflammation and oxidative stress. *CNS Neurol Disord Drug Targets*. 2014;13(9):1615–1626. doi:10.2174/1871527313666140806144831
9. Beyfuss K, Hood DA. A systematic review of p53 regulation of oxidative stress in skeletal muscle. *Redox Rep*. 2018;23(1):100–117. doi:10.1080/13510002.2017.1416773
10. Hybertson BM, Gao B, Bose SK, McCord JM. Oxidative stress in health and disease: The therapeutic potential of *Nrf2* activation. *Mol Aspects Med*. 2011;32(4–6):234–246. doi:10.1016/j.mam.2011.10.006
11. Periyasamy P, Shinohara T. Age-related cataracts: Role of unfolded protein response, Ca(2+) mobilization, epigenetic DNA modifications, and loss of *Nrf2*/Keap1 dependent cytoprotection. *Prog Retin Eye Res*. 2017;60:1–19. doi:10.1016/j.preteyeres.2017.08.003
12. Gao Y, Yan Y, Huang T. Human age-related cataracts: Epigenetic suppression of the nuclear factor erythroid 2-related factor 2-mediated antioxidant system. *Mol Med Rep*. 2015;11(2):1442–1447. doi:10.3892/mmr.2014.2849
13. Ma TJ, Lan DH, He SZ, et al. *Nrf2* protects human lens epithelial cells against H(2)O(2)-induced oxidative and ER stress: The ATF4 may be involved. *Exp Eye Res*. 2018;169:28–37. doi:10.1016/j.exer.2018.01.018
14. Elanchezhian R, Palsamy P, Madson CJ, Lynch DW, Shinohara T. Age-related cataracts: Homocysteine coupled endoplasmic reticulum stress and suppression of *Nrf2*-dependent antioxidant protection. *Chem Biol Interact*. 2012;200(1):1–10. doi:10.1016/j.cbi.2012.08.017
15. Li T, Ye W, Huang B, et al. Determination and pharmacokinetic study of echinatin by UPLC-MS/MS in rat plasma. *J Pharm Biomed Anal*. 2019;168:133–137. doi:10.1016/j.jpba.2019.02.023.

16. Oh HN, Lee MH, Kim E, et al. Dual inhibition of EGFR and MET by echinatin retards cell growth and induces apoptosis of lung cancer cells sensitive or resistant to gefitinib. *Phytother Res*. 2020;34(2):388–400. doi:10.1002/ptr.6530
17. Liang M, Li X. Antioxidant mechanisms of echinatin and licochalcone A. *Molecules*. 2018;24(1):3. doi:10.3390/molecules24010003
18. Jung ES, Jang HJ, Hong EM, et al. The protective effect of 5-aminosalicylic acid against non-steroidal anti-inflammatory drug-induced injury through free radical scavenging in small intestinal epithelial cells. *Medicina (Kaunas)*. 2020;56(10):515. doi:10.3390/medicina56100515
19. Nita M, Grzybowski A. The role of the reactive oxygen species and oxidative stress in the pathomechanism of the age-related ocular diseases and other pathologies of the anterior and posterior eye segments in adults. *Oxid Med Cell Longev*. 2016;2016:3164734. doi:10.1155/2016/3164734
20. Liang B, Wei W, Wang J, et al. Protective effects of *Semiaquilegia adoxoides* n-butanol extract against hydrogen peroxide-induced oxidative stress in human lens epithelial cells. *Pharm Biol*. 2016;54(9):1656–1663. doi:10.3109/13880209.2015.1113993
21. Sies H. Oxidative stress: A concept in redox biology and medicine. *Redox Biol*. 2015;4:180–183. doi:10.1016/j.redox.2015.01.002
22. Sies H. Role of metabolic H_2O_2 generation: Redox signaling and oxidative stress. *J Biol Chem*. 2014;289(13):8735–8741. doi:10.1074/jbc.R113.544635
23. Spector A, Garner WH. Hydrogen peroxide and human cataract. *Exp Eye Res*. 1981;33(6):673–681. doi:10.1016/s0014-4835(81)80107-8
24. Li X, Meng F, Li H, et al. L-carnitine alleviates oxidative stress-related damage via MAPK signaling in human lens epithelial cells exposed to H_2O_2. *Int J Mol Med*. 2019;44(4):1515–1522. doi:10.3892/ijmm.2019.4283
25. He H, Wei D, Liu H, et al. Glycyrrhizin protects against sodium iodate-induced RPE and retinal injury though activation of AKT and *Nrf2/HO-1* pathway. 2019;23(5):3495–3504. doi:10.1111/jcmm.14246
26. Tian XH, Liu CL, Jiang HL, et al. Cardioprotection provided by echinatin against ischemia/reperfusion in isolated rat hearts. *BMC Cardiovasc Disord*. 2016;16:119. doi:10.1186/s12872-016-0294-3
27. Ke Z, Su Z, Zhang X, et al. Discovery of a potent angiotensin converting enzyme inhibitor via virtual screening. *Bioorg Med Chem Lett*. 2017;27(16):3688–3692. doi:10.1016/j.bmcl.2017.07.016
28. Kwak AW, Choi JS, Lee MH, Oh HN, Cho SS. Retrochalcone echinatin triggers apoptosis of esophageal squamous cell carcinoma via ROS- and ER stress-mediated signaling pathways. *Molecules*. 2019;24(22):4055. doi:10.3390/molecules24224055
29. Xiang J, Kang L, Gao H, et al. BLM can regulate cataract progression by influencing cell vitality and apoptosis. *Exp Eye Res*. 2019;178:99–107. doi:10.1016/j.exer.2018.08.022
30. Wang HM, Li GX, Zheng HS, Wu XZ. Protective effect of resveratrol on lens epithelial cell apoptosis in diabetic cataract rat. *Asian Pac J Trop Med*. 2015;8(2):153–156. doi:10.1016/s1995-7645(14)60307-2
31. Fleisher TA. Apoptosis. *Ann Allergy Asthma Immunol*. 1997;78(3):245–249, quiz 249–250. doi:10.1016/s1081-1206(10)63176-6
32. Piro LD. Apoptosis, *Bcl-2* antisense, and cancer therapy. *Oncology (Williston Park)*. 2004;18(13 Suppl 10):5–10. PMID:15651171
33. Fan TJ, Han LH, Cong RS, Liang J. Caspase family proteases and apoptosis. *Acta Biochim Biophys Sin (Shanghai)*. 2005;37(11):719–727. doi:10.1111/j.1745-7270.2005.00108.x
34. Bruckheimer EM, Cho SH, Sarkiss M, Herrmann J, McDonnell TJ. The *Bcl-2* gene family and apoptosis. *Adv Biochem Eng Biotechnol*. 1998;62:75–105. doi:10.1007/BFb0102306
35. Boatright KM, Salvesen GS. Caspase activation. *Biochem Soc Symp*. 2003;70(70):233–242. doi:10.1042/bss0700233
36. Fulda S. Therapeutic opportunities based on caspase modulation. *Semin Cell Dev Biol*. 2018;82:150–157. doi:10.1016/j.semcdb.2017.12.008
37. Galichanin K, Löfgren S, Bergmanson J, Söderberg P. Evolution of damage in the lens after in vivo close to threshold exposure to UV-B radiation: Cytomorphological study of apoptosis. *Exp Eye Res*. 2010;91(3):369–377. doi:10.1016/j.exer.2010.06.009
38. Ayala M, Strid H, Jacobsson U, Söderberg PG. p53 expression and apoptosis in the lens after ultraviolet radiation exposure. *Invest Ophthalmol Vis Sci*. 2007;48(9):4187–4191. doi:10.1167/iovs.06-0660
39. Tamada Y, Fukiage C, Nakamura Y, et al. Evidence for apoptosis in the selenite rat model of cataract. *Biochem Biophys Res Commun*. 2000;275(2):300–306. doi:10.1006/bbrc.2000.3298
40. Higashi Y, Higashi K, Mori A, et al. Anti-cataract effect of resveratrol in high-glucose-treated streptozotocin-induced diabetic rats. *Biol Pharm Bull*. 2018;41(10):1586–1592. doi:10.1248/bpb.b18-00328
41. Li D, Liu GQ, Lu PR. High glucose: Activating autophagy and affecting the biological behavior of human lens epithelial cells. *Int J Ophthalmol*. 2019;12(7):1061–1066. doi:10.18240/ijo.2019.07.02
42. Gu XL. MicroRNA-124 prevents H_2O_2-induced apoptosis and oxidative stress in human lens epithelial cells via inhibition of the NF-κB signaling pathway. *Pharmacology*. 2018;102(3–4):213–222. doi:10.1159/000491433
43. Zhang Y, Huang WR. Sanguinarine induces apoptosis of human lens epithelial cells by increasing reactive oxygen species via the MAPK signaling pathway. *Mol Med Rep*. 2019;19(5):4449–4456. doi:10.3892/mmr.2019.10087
44. Chen S, Sun P, Zhao X, et al. Gardenia jasminoides has therapeutic effects on L-NNA-induced hypertension in vivo. *Mol Med Rep*. 2017;15(6):4360–4373. doi:10.3892/mmr.2017.6542
45. Mitter SK, Song C, Qi X, et al. Dysregulated autophagy in the RPE is associated with increased susceptibility to oxidative stress and AMD. *Autophagy*. 2014;10(11):1989–2005. doi:10.4161/auto.36184
46. Sharma KK, Santhoshkumar P. Lens aging: Effects of crystallins. *Biochim Biophys Acta*. 2009;1790(10):1095–1108. doi:10.1016/j.bbagen.2009.05.008
47. Wu Z, Wang H, Fang S, Xu C. Roles of endoplasmic reticulum stress and autophagy on H_2O_2-induced oxidative stress injury in HepG2 cells. *Mol Med Rep*. 2018;18(5):4163–4174. doi:10.3892/mmr.2018.9443
48. Ma T, Chen T, Li P, et al. Heme oxygenase-1 (*HO-1*) protects human lens epithelial cells (SRA01/04) against hydrogen peroxide (H_2O_2)-induced oxidative stress and apoptosis. *Exp Eye Res*. 2016;146:318–329. doi:10.1016/j.exer.2016.02.013
49. Luo YH, Cheng HJ, Tsai FY, Tsou TC, Lin SY. Primary amine modified gold nanodots regulate macrophage function and antioxidant response: Potential therapeutics targeting of *Nrf2*. *Int J Nanomedicine*. 2020;15:8411–8426. doi:10.2147/ijn.s268203
50. Tamatam CM, Reddy NM, Potteti HR, et al. Preconditioning the immature lung with enhanced *Nrf2* activity protects against oxidant-induced hypoalveolarization in mice. *Nature*. 2020;10(1):19034. doi:10.1038/s41598-020-75834-8
51. Waz S, Heeba GH, Hassanin SO, Abdel-Latif RG. Nephroprotective effect of exogenous hydrogen sulfide donor against cyclophosphamide-induced toxicity is mediated by *Nrf2/HO-1/NF-κB* signaling pathway. *Life Sci*. 2020;264:118630. doi:10.1016/j.lfs.2020.118630
52. Ma JQ, Zhang YJ, Tian ZK, Liu CM. Bixin attenuates carbon tetrachloride induced oxidative stress, inflammation and fibrosis in kidney by regulating the *Nrf2/TLR4/MyD88* and *PPAR-γ/TGF-β1/Smad3* pathway. *Int Immunopharmacol*. 2020;90:107117. doi:10.1016/j.intimp.2020.107117
53. Fang W, Ye Q, Yao Y, et al. Protective effects of trimetazidine in retarding selenite-induced lens opacification. *Curr Eye Res*. 2019;44(12):1325–1336. doi:10.1080/02713683.2019.1633359
54. Whitson JA, Wilmarth PA, Klimek J, et al. Proteomic analysis of the glutathione-deficient LEGSKO mouse lens reveals activation of EMT signaling, loss of lens specific markers, and changes in stress response proteins. *Free Radic Biol Med*. 2017;113:84–96. doi:10.1016/j.freeradbiomed.2017.09.019
55. Liu XF, Hao JL, Xie T, et al. *Nrf2* as a target for prevention of age-related and diabetic cataracts by against oxidative stress. *Aging Cell*. 2017;16(5):934–942. doi:10.1111/acel.12645
56. Funakoshi-Tago M, Tanabe S, Tago K, et al. Licochalcone A potently inhibits tumor necrosis factor alpha-induced nuclear factor-kappaB activation through the direct inhibition of IkappaB kinase complex activation. *Mol Pharmacol*. 2009;76(4):745–753. doi:10.1124/mol.109.057448
57. Hong P, Liu QW, Xie Y, et al. Echinatin suppresses esophageal cancer tumor growth and invasion through inducing AKT/mTOR-dependent autophagy and apoptosis. *Cell Death Dis*. 2020;11(7):524. doi:10.1038/s41419-020-2730-7

High-sensitivity detection of clinically significant red blood cell antibodies by the column agglutination technique

Nurdina Charong[1,A–F], Nateelak Kooltheat[1,A–E], Thunyaluk Plyduang[2,B–D]

[1] School of Allied Health Sciences, Walailak University, Nakhon Si Thammarat, Thailand
[2] The Centre for Scientific and Technological Equipment, Walailak University, Nakhon Si Thammarat, Thailand

A – research concept and design; B – collection and/or assembly of data; C – data analysis and interpretation; D – writing the article; E – critical revision of the article; F – final approval of the article

Advances in Clinical and Experimental Medicine, ISSN 1899–5276 (print), ISSN 2451–2680 (online) *Adv Clin Exp Med*. 2021;30(11):1205–1214

Address for correspondence
Nurdina Charong
E-mail: nurdina.ch@mail.wu.ac.th

Funding sources
None declared

Conflict of interest
None declared

Received on May 11, 2021
Reviewed on May 29, 2021
Accepted on July 19, 2021

Published online on September 10, 2021

Abstract

Background. The detection of clinically significant antibodies to red blood cell antigens is important for the selection of compatible blood for patients. The conventional test tube technique (CTT) is commonly used as the gold standard test, but manual testing and visual detection of hemagglutination may produce errors. A more recently developed method, the column agglutination technique (CAT), facilitates ease of testing.

Objectives. To investigate the specificity and sensitivity of the CAT compared to the CTT for the screening of clinically significant antibodies from the Rh blood group.

Materials and methods. Standard antibodies to the Rh blood group, anti-D, -C and -E, were used as examples of clinically significant antibodies in transfusion science. The antibodies were serially diluted by two-fold, then reacted with screening cells with different antigen expression. The hemagglutination reaction was investigated using both techniques, and the grades and scores of the reactions were used to analyze the sensitivity and specificity of the CTT and CAT.

Results. The CAT had a better sensitivity than the CTT. The lowest antibody dilution of 1:8192 could be detected using CAT, while a dilution of only 1:2048 could be detected with CTT. However, the CTT and CAT were equal in specificity. The 2 techniques specifically detected all antibodies to the screening cells.

Conclusions. Both the CAT and CTT showed 100% specificity. However, the CAT exhibited more sensitivity than the CTT, and can be used in substitution of, or in parallel with, the CTT technique for red blood cell phenotyping, antibody screening, identification, and crossmatching.

Key words: column agglutination technique, conventional test tube, antibody screening, Rh antibody, anti-D

Cite as
Charong N, Kooltheat N, Plyduang T. High-sensitivity detection of clinically significant red blood cell antibodies by the column agglutination technique. *Adv Clin Exp Med*. 2021;30(11):1205–1214. doi:10.17219/acem/140317

DOI
10.17219/acem/140317

Background

Antibody screening in blood banking is used to detect unexpected antibodies to red blood cell antigens other than ABO antibodies, known as clinically significant antibodies.[1] These unexpected antibodies include minor blood groups antibodies, such as anti-Rh, -MNS, -P, -Lewis, -Kell, -Kidd, -Duffy, and -Diego.[2] According to the AABB standard for Blood Bank and Transfusion Service, antibody screening is performed in 2 situations. First, it is used to screen donor blood in order to prevent the passing of unexpected antibodies to patients and subsequent hemolytic transfusion reactions (HTRs). Second, antibody screening is used pre-transfusion to test a transfusion recipient's sample.[3] Positive antibody screening results in a donor's plasma lead to the rejection of the plasma unit and, if the transfusion recipient has unexpected antibodies, antibody identification and confirmation tests are necessary to select the antigen negative blood donor for compatibility testing.[4]

Unexpected antibodies can be divided into 2 types according to the source of immunization. Alloantibodies are produced by patient's immunization by foreign red blood cell antigens encountered through blood transfusion or pregnancy.[5] Autoantibodies are produced after a patient's immune system loses tolerance for self-antigens, which can occur with age and is associated with several diseases.[6] Depending upon how immunization occurs, unexpected antibodies can also be divided into immune type and naturally occurring antibodies. Immune antibodies, such as anti-Rh, -Kidd or -Duffy, are produced after immunization through blood transfusion or pregnancy.[7] These antibodies are mostly of the immunoglobulin G (IgG) type and react best at body temperature (37°C). Naturally occurring antibodies (e.g., anti-Lewis, -P) are not produced by immunization by red blood cell antigens, but by antigens that are structurally similar to those on red blood cells.[8] These antibodies are mostly of the IgM type and react best at temperatures below body temperature (4–22°C). Clinically significant unexpected antibodies are also characterized according to their impact on donor red blood cells after blood transfusion. Highly significant IgG antibodies, such as anti-Rh, react at body temperature, and can strongly induce HTRs and produce hemolytic disease of the fetus and newborn (HDFN).[9] The other type of unexpected antibodies, IgMs such as anti-I, -M and -N, react at low temperatures and normally cause a positive result in the direct antiglobulin test without hemolysis.[10]

Antibody screening is performed by reacting patient's or donor's serum/plasma with screening cells made from pooled Type O cells that have different minor red blood cell antigens.[11] Unexpected antibodies in the sample will bind to the corresponding antigens on the red blood cells and directly cause hemagglutination. For the IgG class of unexpected antibodies, the addition of secondary anti-human globulins (AHG) is needed to crosslink the nearby sensitized red blood cells.

Different techniques can be used for antibody identification and an ideal technique must be able to detect low levels of clinically significant antibodies, be easy to perform, and have a short turnaround time. The conventional test tube technique (CTT) uses a glass test tube as a container for the reaction. For this test, the serum sample is mixed with screening cells, incubated at room temperature (20–22°C) for the detection of IgM antibodies, and then incubated at body temperature (37°C) with AHG for the detection of IgG antibodies. The CTT is considered the gold standard for antibody screening, as it is easy to perform and it is cost effective.[12] However, the grading of hemagglutination by eye and shaking the test tube by hand requires expertise, and false positive and false negatives can occur easily depending on individual techniques. The column agglutination technique (CAT) is an alternative method for antibody screening that uses a microcolumn gel card as a container for the reaction. For this technique, the serum sample and cells are transferred and mixed in a column gel card, incubated at 37°C, and spun to read the hemagglutination reaction by visual inspection or use of an automated analyzer. The CAT is easier to carry out, more accurate and more precise than the CTT technique.[13] However, due to increased costs and the need for specific equipment, the CAT method is typically not used by small community hospitals.

Objectives

The aim of this study is to compare the CTT and CAT in terms of specificity, accuracy and precision for antibody screening. In order to find a suitable technique for the detection of low antibody titers, clinically significant antibodies of the Rh system (anti-D, -C, -E) were investigated.

Materials and methods

Reagents and equipment

Standard antibodies for Rh blood groups, anti-D, anti-C and anti-E, and antibody screening cells (lot: 62061) were purchased from the National Blood Centre (Thai Red Cross Society, Bangkok, Thailand). The expression of Rh antigens on the antibody screening red blood cells used in this study is shown in Table 1. The column agglutination platform and the AHG/LISS gel cards were commercially purchased (Diagnostic Grifols, Barcelona, Spain).

Antibody dilution and antibody screening cells

Standard antibodies for Rh blood groups (anti-D, anti-C and anti-E) were two-fold diluted up to 1:16384. A total of 500 µL of the antibodies were serially diluted with

Table 1. Expression of Rh antigens on antibody screening red blood cells

Screening cells	Rh					
	Wiener	D	C	E	c	e
O1	R1R1	+	+	0	0	+
O2	R1R2	+	+	+	+	+

an equal volume of 0.9% NaCl (normal saline solution (NSS)) using glass test tubes and a mechanical automatic pipette. The types of screening cells used were based upon expression of the Rh blood group antigens on the cell surface (Table 1). For the inspection of anti-D and anti-C, O1 or O2 screening cells were used. For the inspection of anti-E, only the O2 screening cells were used.

Antibody screening by CTT

The CTT for antibody screening was performed using the indirect antiglobulin test. First, 2 drops of diluted antibody were added to a 10 × 75 mm glass test tube. Next, 1 drop of a 3% screening cells suspension was added, and the solution was mixed and incubated at room temperature for 5 min. The tube was then centrifuged at 3000 rpm for 15 s and gently shaken for the visual inspection of hemagglutination. The solution was then further incubated at 37°C for 30 min, centrifuged for 15 s, and inspected again for hemagglutination. Incubated screening cells were then washed 3 times with NSS and the supernatant was completely discarded. Two drops of AHG (Thai Red Cross Society) were added to the tube to crosslink antibody-sensitized screening cells. The solution was then centrifuged for 15 s for the inspection of hemagglutination in the AHG phase. The reactions were graded and scored according to the standard AABB guidelines.[14]

Antibody screening by CAT

The antibody screening using CAT was performed according to the manufacturer's instructions. Using an AHG/LISS microcolumn gel card, 50 µL of 1% screening cells in NSS were added, followed by 25 µL of diluted antibody. The solution was then incubated at 37°C for 15 min in a gel card incubator. The gel card was then centrifuged at 900 × g for 9 min using a specific gel card centrifuge. Hemagglutination was visually graded, scored and compared with control.

Statistical analyses

This study compared the titer of antibodies that can be detected by antibody screening. The antibody titer range was the range of the two-fold diluted antibody. The mean titer was calculated by averaging the reacted antibody titers. The mean reaction score was calculated by averaging the reaction scores of the antibody tests for the screening of D, C or E antigens on screening red blood cells.

The Gaussian distribution of all data sets from the antibody screenings were analyzed with column statistics using the D'Agostino–Pearson omnibus normality test. The antibody titers detected with the CTT and CAT were compared using paired t-tests (parametric, Gaussian distribution) or Wilcoxon matched-pairs signed-rank tests (non-parametric, non-Gaussian distribution). Correlations between the CTT and CAT were analyzed using Pearson's correlations (parametric) or Spearman's correlations (non-parametric). The correlations between the CTT and CAT in the screening of unexpected antibodies were further analyzed with 2nd order polynomial (quadratic) to maximize the goodness of fit of the analyzed data. All statistical analyses were performed with a 95% confidence interval, $p = 0.05$, using GraphPad Prism v. 6.01 (GraphPad Software, San Diego, USA).

The sensitivity, specificity, accuracy, and precision of the CTT and CAT in the screening of anti-D, anti-C and anti-E were calculated using a confusion matrix.[15]

All methods and results are reported in agreement with the Standards for Quality Improvement Reporting Excellence (SQUIRE) guidelines.[16]

Results

Specificity, accuracy and precision of CTT and CAT for antibody screening

The testing of the CTT and CAT for antibody screening was done by reacting diluted antibodies with screening cells. The screening cells expressed different antigens of the Rh blood group, with O1 cells expressing only D and C antigens and O2 cells expressing D, C and E antigens (Table 1). The specificity of the antibody screening techniques was analyzed using the reaction between the screening cells and specific antibodies. The CTT and CAT both gave positive results for reactions between the O1 or O2 cells and anti-D and anti-C (Tables 2,3). The 2 techniques also gave negative results for the reaction of O1 and positive results for the reaction of O2, when testing with anti-E (Table 4). These results show that both the CTT and CAT have equal specificity in the screening of clinically significant antibodies to D, C and E antigens. Due to the use of E antigen-negative cells in the screening test, the specificity of anti-E was also calculated (Table 5). The precision of the antibody screening results performed by the CAT was consistent when compared to the CTT and showed a high accuracy for all tested antibodies (Table 5).

Table 2. Reaction gradings and scores of anti-D screening using CTT and CAT

Anti-D																							
Dilution (titer range)	conventional test tube technique (CTT)												column agglutination technique (CAT)										
	reaction grading						score						reaction grading						score				
	O1			O2			O1			O2			O1			O2			O1			O2		
	1st	2nd	3rd	1st	2nd	3rd	1st	2nd	3rd	1st	2nd	3rd	1st	2nd	3rd	1st	2nd	3rd	1st	2nd	3rd	1st	2nd	3rd
1:2	4+	4+	4+	4+	4+	4+	12	12	12	12	12	12	4+	4+	4+	4+	4+	4+	12	12	12	12	12	12
1:4	4+	4+	4+	4+	4+	4+	12	12	12	12	12	12	4+	4+	4+	4+	4+	4+	12	12	12	12	12	12
1:8	4+	4+	4+	4+	4+	4+	12	12	12	12	12	12	4+	4+	4+	4+	4+	4+	12	12	12	12	12	12
1:16	4+	4+	4+	4+	4+	4+	12	12	12	12	12	12	4+	4+	4+	4+	4+	4+	12	12	12	12	12	12
1:32	4+	4+	4+	4+	4+	4+	12	12	12	12	12	12	4+	4+	4+	4+	4+	4+	12	12	12	12	12	12
1:64	3+	4+	3+	3+	4+	3+	10	12	10	10	12	10	4+	4+	4+	4+	4+	4+	12	12	12	12	12	12
1:128	2+	2+	2+	3+	4+	3+	8	8	8	10	12	10	4+	4+	4+	4+	4+	4+	12	12	12	12	12	12
1:256	2+	2+	2+	2+	4+	3+	8	8	8	8	12	10	4+	4+	4+	4+	4+	4+	12	12	12	12	12	12
1:512	2+	1+	2+	2+	2+	2+	8	5	8	8	8	8	4+	4+	4+	4+	4+	4+	12	12	12	12	12	12
1:1024	2+	1+	2+	1+	1+	1+	8	5	8	5	5	5	3+	4+	3+	3+	4+	4+	10	12	10	10	12	12
1:2048	1+	1+	1+	1+	1+	1+	5	5	5	5	5	5	3+	3+	3+	3+	3+	3+	10	10	10	10	10	10
1:4096	0	0	0	0	0	0	2	2	2	2	2	2	2+	2+	2+	2+	2+	2+	8	8	8	8	8	8
1:8192	0	0	0	0	0	0	2	2	2	2	2	2	1+	1+	1+	1+	1+	1+	5	5	5	5	5	5
1:16384	0	0	0	0	0	0	2	2	2	2	2	2	0	0	0	0	0	0	2	2	2	2	2	2
Sum							113	109	113	112	120	114	Sum						143	145	143	143	145	145
Average							111.7 ±2.3			115.4 ±4.2			Average						143.7 ±1.2			144.3 ±1.2		
Total (mean reaction score)							227.0 ±2.0						Total (mean reaction score)						288.0 ±2.0					

Table 3. Reaction gradings and scores of anti-C screening using CTT and CAT

Anti-C																								
Dilution (titer range)	conventional test tube technique (CTT)												column agglutination technique (CAT)											
	reaction grading						score						reaction grading						score					
	O1			O2			O1			O2			O1			O2			O1			O2		
	1st	2nd	3rd	1st	2nd	3rd	1st	2nd	3rd	1st	2nd	3rd	1st	2nd	3rd	1st	2nd	3rd	1st	2nd	3rd	1st	2nd	3rd
1:2	4+	4+	4+	4+	4+	4+	12	12	12	12	12	12	4+	4+	4+	4+	4+	4+	12	12	12	12	12	12
1:4	4+	4+	4+	4+	4+	4+	12	12	12	12	12	12	4+	4+	4+	4+	4+	4+	12	12	12	12	12	12
1:8	4+	4+	4+	4+	4+	4+	12	12	12	12	12	12	4+	4+	4+	4+	4+	4+	12	12	12	12	12	12
1:16	4+	4+	4+	4+	4+	4+	12	12	12	12	12	12	4+	4+	4+	4+	4+	4+	12	12	12	12	12	12
1:32	4+	3+	3+	2+	2+	2+	12	10	10	8	8	8	4+	4+	4+	4+	3+	4+	12	12	12	12	10	12
1:64	3+	4+	3+	2+	1+	2+	10	12	10	10	5	8	4+	4+	4+	4+	3+	4+	12	12	12	12	10	12
1:128	2+	2+	2+	1+	1+	1+	8	8	8	5	5	5	4+	4+	4+	2+	3+	2+	12	12	12	8	10	8
1:256	2+	2+	1+	1+	1+	1+	8	8	5	5	5	5	3+	4+	3+	1+	2+	2+	10	12	10	5	8	8
1:512	1+	2+	1+	w+	1+	0	5	8	5	4	5	2	2+	3+	3+	0	1+	0	8	10	10	2	5	2
1:1024	w+	1+	w+	w+	0	0	4	5	4	4	2	2	1+	2+	2+	0	1+	0	5	8	8	2	5	5
1:2048	0	0	0	0	0	0	2	2	2	2	2	2	0	0	0	0	0	0	2	2	2	2	2	2
1:4096	0	0	0	0	0	0	2	2	2	2	2	2	0	0	0	0	0	0	2	2	2	2	2	2
1:8192	0	0	0	0	0	0	2	2	2	2	2	2	0	0	0	0	0	0	2	2	2	2	2	2
1:16384	0	0	0	0	0	0	2	2	2	2	2	2	0	0	0	0	0	0	2	2	2	2	2	2
Sum							103	107	98	92	86	86	Sum						115	122	120	97	104	103
Average							102.7 ±4.5			88.0 ±3.5			Average						119.0 ±3.6			101.3 ±3.8		
Total (mean reaction score)							190.7 ±5.7						Total (mean reaction score)						220.3 ±7.4					

w+ – weakly positive.

Table 4. Reaction gradings and scores of anti-E screening using CTT and CAT

Anti-E																								
Dilution (titer range)	conventional test tube technique (CTT)												column agglutination technique (CAT)											
	reaction grading						score						reaction grading						score					
	O1			O2			O1			O2			O1			O2			O1			O2		
	1st	2nd	3rd	1st	2nd	3rd	1st	2nd	3rd	1st	2nd	3rd	1st	2nd	3rd	1st	2nd	3rd	1st	2nd	3rd	1st	2nd	3rd
1:2	0	0	0	4+	4+	4+	2	2	2	12	12	12	0	0	0	4+	4+	4+	2	2	2	12	12	12
1:4	0	0	0	4+	4+	4+	2	2	2	12	12	12	0	0	0	4+	4+	4+	2	2	2	12	12	12
1:8	0	0	0	4+	4+	4+	2	2	2	12	12	12	0	0	0	4+	4+	4+	2	2	2	12	12	12
1:16	0	0	0	4+	4+	4+	2	2	2	12	12	12	0	0	0	4+	4+	4+	2	2	2	12	12	12
1:32	0	0	0	4+	4+	3+	2	2	2	12	12	10	0	0	0	4+	4+	4+	2	2	2	12	12	12
1:64	0	0	0	4+	3+	3+	2	2	2	12	10	10	0	0	0	4+	4+	3+	2	2	2	12	12	10
1:128	0	0	0	3+	2+	2+	2	2	2	10	8	8	0	0	0	3+	4+	3+	2	2	2	10	12	10
1:256	0	0	0	2+	2+	2+	2	2	2	8	8	8	0	0	0	3+	4+	3+	2	2	2	10	12	10
1:512	0	0	0	1+	2+	2+	2	2	2	5	8	8	0	0	0	2+	3+	2+	2	2	2	8	10	18
1:1024	0	0	0	1+	2+	1+	2	2	2	5	8	5	0	0	0	1+	2+	1+	2	2	2	5	8	5
1:2048	0	0	0	w+	1+	1+	2	2	2	4	5	5	0	0	0	1+	1+	1+	2	2	2	5	5	5
1:4096	0	0	0	0	0	0	2	2	2	2	2	2	0	0	0	1+	1+	1+	2	2	2	5	5	5
1:8192	0	0	0	0	0	0	2	2	2	2	2	2	0	0	0	0	0	0	2	2	2	2	2	2
1:16384	0	0	0	0	0	0	2	2	2	2	2	2	0	0	0	0	0	0	2	2	2	2	2	2
Sum							28	28	28	110	113	108	Sum						28	28	28	119	128	127
Average							28.0 ±0.0			115.3 ±2.5			Average						28.0 ±0.0			124.7 ±4.9		
Total (mean reaction score)							138.3 ±2.5						Total (mean reaction score)						152.7 ±4.9					

w+ – weakly positive.

Table 5. Sensitivity, specificity, accuracy, and precision of CTT and CAT in the screening of anti-D, anti-C and anti-E

Measure	Conventional test tube technique (CTT)			Column agglutination technique (CAT)		
	anti-D	anti-C	anti-E	anti-D	anti-C	anti-E
Sensitivity	0.7857	0.6786	0.7857	0.9286	0.6667	0.8571
Specificity	–	–	1	–	–	1
Accuracy	0.8757	0.6786	0.8929	0.9286	0.6667	0.9286
Precision	1	1	1	1	1	1
Matthews correlation coefficient	–	–	0.8044	–	–	0.866

Sensitivity of CTT and CAT for antibody screening

The screening of antibodies using CTT and CAT was performed according to the AABB standard protocols.[4] The reaction of hemagglutination was visually graded as negative (0), weakly positive (w+) or positive (1+, 2+, 3+, 4+). The same reaction was also scored as negative (2), weakly positive (4) or positive (5, 8, 10, 12).

The CTT detected anti-D, anti-C and anti-E at the lowest dilutions of 1:2048, 1:1024 and 1:2048, respectively. The reaction scores for the lowest dilutions of anti-D, anti-C and anti-E were 5, 4 and 4, respectively. The total scores for hemagglutination for anti-D, anti-C and anti-E were 227.0 ±2.0, 190.70 ±5.70 and 138.30 ±2.50, respectively (Tables 2–4).

The CAT detected anti-D, anti-C and anti-E at the lowest dilutions of 1:8192, 1:1024 and 1:4096, respectively. Reaction scores for the lowest dilutions of anti-D, anti-C and anti-E were all at 5. The total scores for hemagglutination for anti-D, anti-C and anti-E were 288.0 ±2.0, 220.3 ±7.4 and 152.7 ±4.9, respectively (Tables 2–4).

Column statistics were calculated and the Gaussian distribution of all data sets was tested. Data from the anti-D screening with CTT, and the anti-E screening with CTT and CAT, were normally distributed (Table S1). Data from the anti-D screening with CAT, and the anti-C screening with CTT and CAT, were not normally distributed

Table S1. Statistical analyses of reaction score in screening of anti-D, anti-C and anti-E using conventional tube test technique (CTT) and column agglutination technique (CAT)

Parameter	Scrn. of anti-D		Scrn. of anti-C		Scrn. of anti-E	
	CTT	CAT	CTT	CAT	CTT	CAT
Mean	8.107	10.29	6.810	7.869	7.881	8.905
Standard deviation	4.029	3.148	4.186	4.389	3.986	3.960
Standard error of mean	1.077	0.8414	1.119	1.173	1.065	1.058
Lower 95% CI of mean	5.781	8.468	4.392	5.335	5.579	6.618
Upper 95% CI of mean	10.43	12.10	9.227	10.40	10.18	11.19
D'Agostino–Pearson omnibus normality test						
K2	3.087	13.12	6.095	6.398	3.269	3.136
p-value	0.2136	0.0014	0.0475	0.0408	0.1950	0.2085
Passed normality test? (alpha = 0.05)	yes	no	no	no	yes	yes
p-value summary	ns	**	*	*	ns	ns
Coefficient of variation	49.69%	30.61%	61.48%	55.77%	50.58%	44.47%

* $p < 0.05$; ** $p < 0.01$; ns – not significant; Scrn. – screening.

(Table S1). Thus, parametric tests were used for data sets from the anti-E screenings, while non-parametric tests were applied to data sets from anti-D and anti-C screenings.

The results indicated that CAT had a significantly higher sensitivity than CTT (0.0313 compared to 0.0285, respectively, p = 0.0078; Fig. 1A–Fig. 3A).

Titer range, mean titer and mean reaction scores of antibodies detected using CTT and CAT

The sensitivity of the CTT and CAT was compared by examining the mean reaction scores, titer ranges and the mean titers of detectable antibodies. The CTT had mean reaction scores for the screening of anti-D, anti-C and anti-E of 227.0 ±2.0, 190.70 ±5.70 and 138.30 ±2.50, respectively. The antibody titer ranges detected using CTT for anti-D, anti-C and anti-E were all at 0–16387 (Tables 2–4). The CAT had mean reaction scores in the screening of anti-D, anti-C and anti-E of 288.0 ±2.0, 220.3 ±7.4 and 152.7 ±4.9, respectively. The antibody titer ranges detected with CTT for anti-D, anti-C and anti-E were all at 0–16387 (Tables 2–4). The column agglutination technique had a better sensitivity in antibody screening than CAT (Fig. 1B–Fig. 3B).

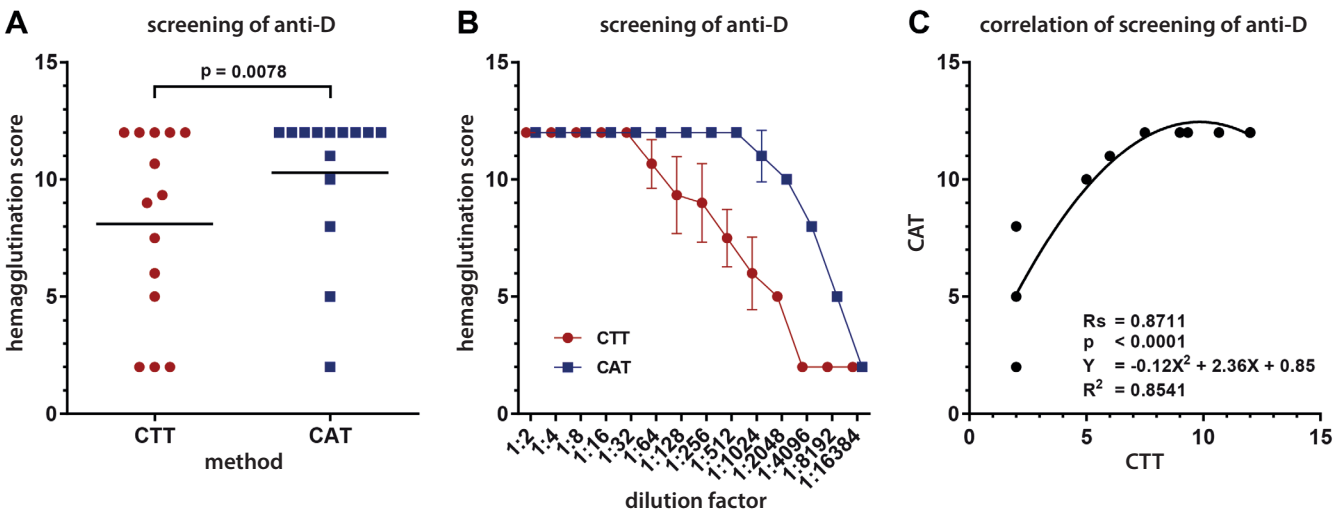

Fig. 1. Sensitivity comparison of the conventional test tube (CTT) and column agglutination techniques (CAT) in the screening of anti-D. Anti-D was two-fold diluted from 1:2 to 1:16348 and then screened with O1 and O2 cells using CTT and CAT. The hemagglutination of each reaction was scored. A. Sensitivity of CTT and CAT was compared with Wilcoxon matched-pairs signed-rank test; B. Antibody titers ranging from 1-16384 for anti-D detection using CTT and CAT were used; C. Correlation between CTT and CAT was analyzed with Spearman's correlation and non-linear curve fitting

Rs – Spearman's correlation coefficient; Y – correlation curve in screening of anti-D; R^2 – coefficient of determination.

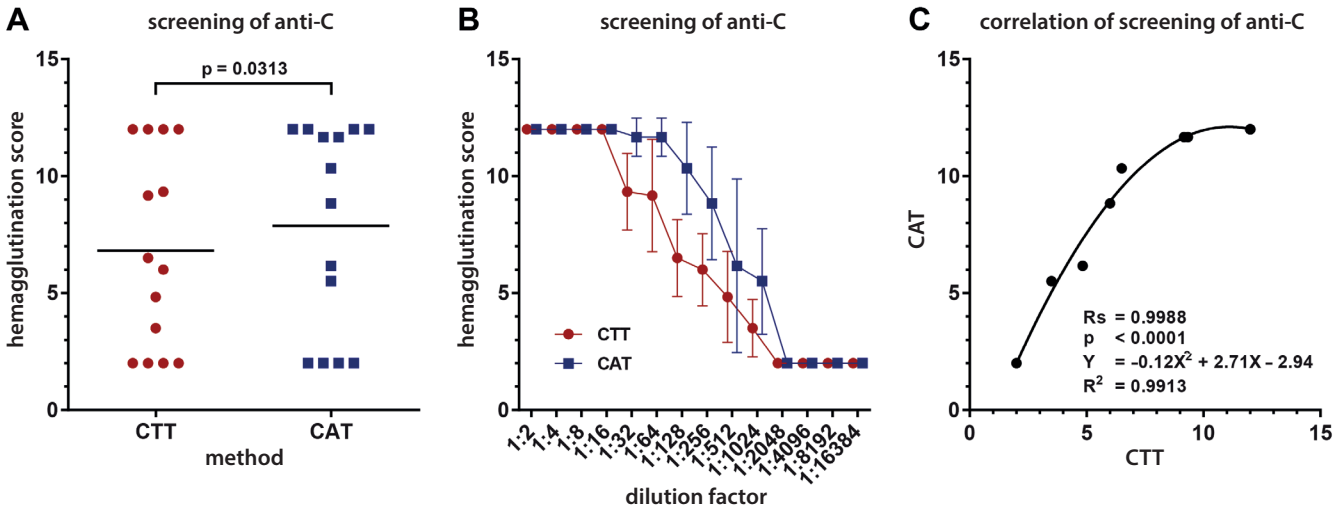

Fig. 2. Sensitivity comparison of the conventional test tube (CTT) and column agglutination techniques (CAT) in the screening of anti-C. Anti-C was two-fold diluted from 1:2 to 1:16348 then screened with O1 and O2 cells using CTT and CAT. The hemagglutination of each reaction was scored. A. Sensitivity of CTT and CAT was compared with Wilcoxon matched-pairs signed-rank test; B. Antibody titers ranging from 1 to 16384 for anti-C detection using CTT and CAT were used; C. Correlation between CTT and CAT was analyzed with Spearman's correlation and non-linear curve fitting

Rs – Spearman's correlation coefficient; Y – correlation curve in screening of anti-C; R^2 – coefficient of determination.

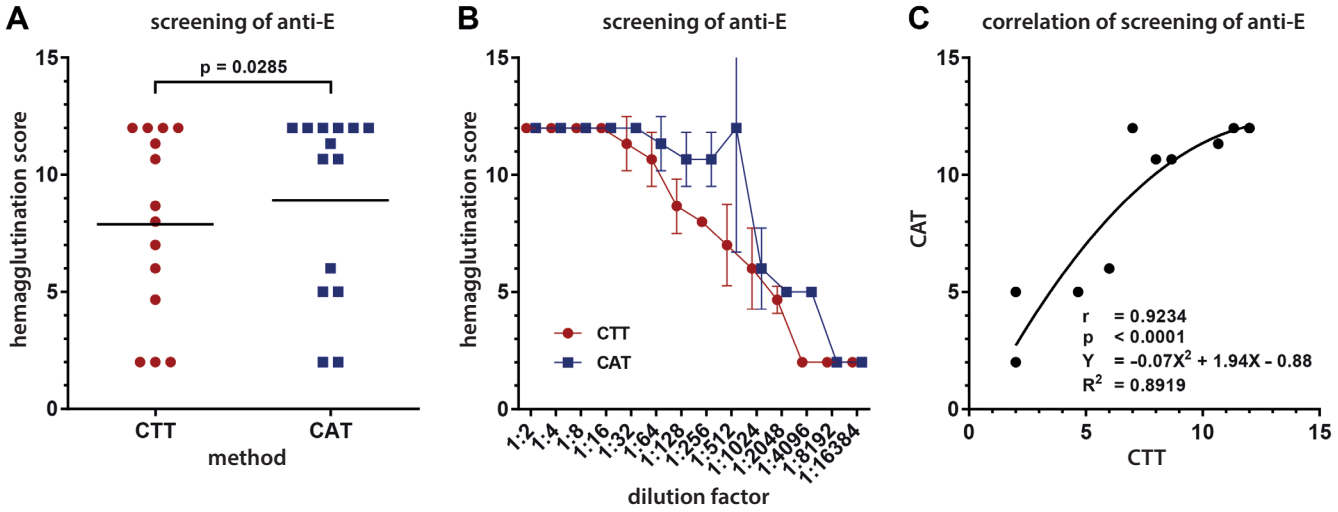

Fig. 3. Sensitivity comparison of conventional test tube (CTT) and column agglutination techniques (CAT) in the screening of anti-E. Anti-E was two-fold diluted from 1:2 to 1:16348 then screened with O1 and O2 cells using CTT and CAT. The hemagglutination of each reaction was scored. A. Sensitivity of CTT and CAT was compared by matched-pairs t-test; B. Antibody titers ranging from 1 to 16384 for anti-E detection using CTT and CAT were used; C. Correlation between CTT and CAT was analyzed with Pearson's correlation and non-linear curve fitting

Rs – Spearman's correlation coefficient; Y – correlation curve in screening of anti-C; R^2 – coefficient of determination.

Differences between CTT and CAT in screening for unexpected clinically significant Rh antibodies

Differences in the screening of anti-D, anti-C and anti-E were observed, as CAT has a higher sensitivity than CTT. The screening of anti-D using CAT was significantly different from screening with CTT, with a p-value of 0.0078, a Spearman's rank correlation coefficient of 0.8711 and a R-square of 0.8541 (Table 6, Fig. 1C). The screening of anti-C using CAT was significantly different from screening with CTT, with a p-value of 0.0313, a Spearman's rank correlation coefficient of 0.9988 and a R-square of 0.9913 (Table 6, Fig. 2C). The screening of anti-E using CAT was significantly different from screening with CTT with a p-value of 0.0285, a Pearson's correlation coefficient of 0.9234 and a R-square of 0.8919 (Table 6, Fig. 3C).

Discussion

The CTT is considered the gold standard for tests in the blood bank laboratory, including for ABO, Rh typing, antibody screening, antibody identification, and crossmatching.[5]

Table 6. Differences between conventional test tube technique (CTT) and column agglutination technique (CAT) in screening of unexpected clinically significant Rh antibodies

Parameter	Screening of unexpected antibody		
	anti-D	anti-C	anti-E
Pared t-test			
p-value	–	–	0.0285
t-statistic	–	–	2.463
Degrees of freedom (df)	–	–	13
Mean of differences	–	–	–0.5119
95% confidence interval	–	–	–0.9608 to –0.06297
R-square	–	–	0.3182
Pearson correlation coefficient (r)	–	–	0.9234
p-value	–	–	<0.0001
Wilcoxon matched-pairs signed-rank test			
p-value	0.0078	0.0313	–
Sum of positive	0.0	0.0	–
Negative ranks	–84.0	–69.0	–
Sum of signed ranks	–84.0	–69.0	–
Median of differences	–2.0	0.0	–
98.71% confidence interval	–5.0 to 0.0	–2.5 to 0.0	–
Spearman's rank correlation coefficient (Rs)	0.8711	0.9988	–
p-value	<0.0001	<0.0001	–

This technique uses only basic equipment, is cost-effective and gives significant results in the reading of the reaction. In addition, antibodies of both the IgM and IgG classes can be detected in a single tube at different temperature phases. However, the CTT technique depends on manual testing and reading by the eyes, which may be subject to human error, especially under a high workload. Moreover, the techniques used for tube shaking to resuspend the red cell pellet for observing agglutination may vary among laboratory staff.

In 1985, Lapierre et al. developed a new technique, CAT, for detection of the reaction between red blood cell antigens and antibodies for red blood cell phenotyping.[17] This method uses a microcolumn packed with gel particles, specific antibodies, LISS buffer, and Coombs/AHG reagent. The Food and Drug Administration (FDA) issued the first gel technology license in 1994 to Micro Typing System under the product name ID-MTS Card. The implementation of this technique in hospital laboratories and transfusion services within 5 years after the release of the first report indicated widespread satisfaction with the test.[18,19] The CAT is particularly useful as it can eliminate many of the variables associated with manual testing and provides stable endpoint agglutination. The CAT also minimizes sample preparation as can be performed using an automated analyzer, and the results can be repeatedly verified.[5]

The implementation of the CAT for pretransfusion testing was also reported in a community hospital, and indicated an increase in the overall number of antibodies and clinically significant antibodies detected with CAT, as compared to CTT, without significant differences in non-specific reactions.[20] Earlier studies also compared the CAT with the CTT in terms of ABO, Rh phenotyping, antibody screening, and crossmatching. A strong correlation between the CAT and CTT results for both anti-A and anti-B IgG titers was reported, but these authors suggested that the relationship between CTT and CAT for the titration of other kinds of antibodies should be further analyzed.[21] Another study also indicated that CAT results showed a high degree of concordance with the CTT, suggesting that the CAT could be brought into routine use. However, proper training and standardization are needed prior to the use of the CAT.[22] In addition, the costs associated with the CAT are increased compared to the CTT. In the current study, the cost per test for these 2 methods was calculated for a comparison, based on the estimated number of tests per day (10 tests/day) performed by a blood bank in a general or community hospital (Table 7). Interestingly, the estimated cost for CAT is 100% higher than that for CTT. Thus, CAT should not be recommended for routine use in the laboratory. However, using the CAT in parallel with the CTT for specific cases, as indicated in Fig. 4, is suggested to reduce the adverse effects of transfusion due to the secondary immunization of alloantibody (e.g., delayed hemolytic transfusion reaction (DHTR)).

Although many previous studies have reported on the advantages of using the CAT for detecting unexpected antibodies in terms of sensitivity and specificity, our study showed gaps in the antibody titers that can be detected with these methods. Frequently detectable antibodies to the Rh blood group antigens, anti-D, anti-C and anti-E, were used as model antibodies, which can be

Table 7. Cost comparison analysis of antibody screening by conventional tube test technique (CTT) and column agglutination technique (CAT)

Equipment/ reagent	CTT		CAT	
	system	cost* [USD/year]	system	cost* [USD/year]
Reaction container	10 × 75 Glass Test Tube (reusable) (PYREX VISTA, Corning Inc., Glendale, USA) (1000 tubes)	380 (0.38/Tube)	AHG/LISS Microcolumn (Disposable) (8 reactions/card, 50 cards/box) (DG Gel Coombs, Grifols, S.A., Barcelona, Spain) (19 boxes)	5947 (313/Box)
Screening cell	O1, O2 (25 µL/test, 10 mL/bottle/month) (National Blood Centre, Bangkok, Thailand) (12 bottles O1, 12 bottle O2)	28.8 (1.2/Bottle)	O1, O2 (25 µL/test, 10 mL/bottle/month) (National Blood Centre, Bangkok, Thailand) (12 bottles O1, 12 bottle O2)	28.8 (1.2/bottle)
Anti-human globulin reagent	AHG/Coomb's (50 µL/test, 10 mL/bottle) (National Blood Centre, Bangkok, Thailand) (37 bottles)	118.4 (3.2/Bottle)	–	–
Low ionic strength solution	LISS (100 µL/test, 10 mL/bottle) (National Blood Centre, Bangkok, Thailand) (74 bottles)	236.8 (3.2/Bottle)	–	–
Incubator	Heat Block (DVT-2B, BioVision Inc., Milpitas, USA)	360	Microcolumn Card Incubator (DG Therm, Grifols, S.A., Barcelona, Spain)	1625
Centrifuge	Serofuge (EBA 280 Serology Decanting Package 5, Andreas Hettich GmbH & Co. KG, Tuttlingen, Germany)	4481	Microcolumn Centrifuge (DG Spin, Grifols, S.A., Barcelona, Spain)	5063
Tube cleaning cost	every week (48 ×10 USD)	480	–	–
Total	7300 tests/year	6085	7300 tests/year	12663.8
Cost	per 1 test	0.83	per 1 test	1.73
Difference	CTT compared to CAT	208.12%		
	CAT compared to CTT	48.05%		

Cost analyzed from product supplied in Thailand. * 10 tests of antibody screening (O1, O2) per day, 7300 tests for 1 year.

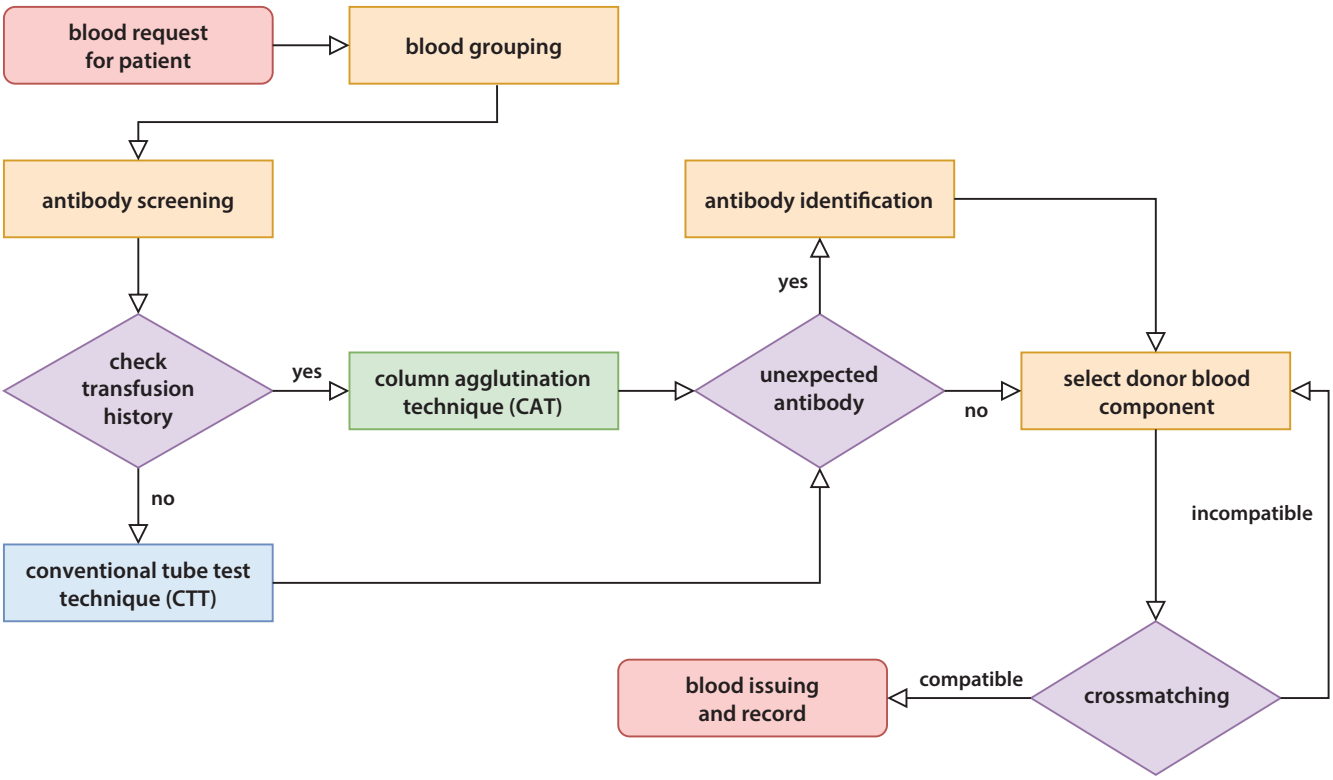

Fig. 4. Suggested guidelines for using column agglutination technique (CAT) in parallel with conventional tube test technique (CTT) in specific case of blood requesting

applied in the investigation of DHTR and HDFN in real-life situations. While the CAT was significantly comparable to the gold standard technique CTT ($p < 0.01$), the CAT had a higher sensitivity than the standard CTT, and the mean titer of CAT in the detection of anti-D, anti-C and anti-E was significantly higher than CTT ($p < 0.01$).

Thus, the use of CAT instead of CTT may be better in detecting lower-titer antibodies, especially for the clinically significant antibodies. In addition, to prevent DHTRs, CAT should be carried out for the detection of low-titer antibodies that have been previously detected in a patient, but where no agglutination appeared with the CTT. Nevertheless, IgM class unexpected antibodies cannot be detected using CAT, as this technique does not have the ability to detect antibodies at room temperature. Therefore, in the case of cold alloantibody detection, the use of CAT in pre-transfusion compatibility testing or crossmatching should be performed in parallel with CTT or using the neutral Gel card. Column agglutination technique has been reported to estimate anti A/B titer in an ABO incompatible kidney transplant, which indicated a sensitivity approx. 2.5-fold higher than CTT.[23] However, CAT was not suggested to determine a critical titer for anti-D titration, since it showed significantly higher titers than the CTT in all samples studied.[24]

Limitations

The current study indicates the superior sensitivity of the CAT technique with a wide-gap titer in the detection of commercially available antibodies to the Rh system, compared with the CTT. However, applying the CAT to detect the presence of significant unexpected antibodies in clinical samples is needed to confirm the advantages of the CAT over the CTT. The simpler CAT technique minimizes turnaround time and workload while maintaining standard operation and results, and can easily be performed by blood bank laboratory technologists.

Conclusions

The CAT can be used in substitution of, or in parallel with, the CTT for the screening of clinically significant antibodies (especially those with a low titer) to avoid secondary immunization of antibodies to minor red blood cell antigens after transfusion.

ORCID iDs

Nurdina Charong https://orcid.org/0000-0002-4432-2699
Nateelak Kooltheat https://orcid.org/0000-0001-7623-854X
Thunyaluk Plyduang https://orcid.org/0000-0002-9523-746X

References

1. Fung MK, Grossman BJ, Hillyer CD, Westhoff CM, eds. *Technical Manual*. 18th ed. Bethesda, USA: AABB; 2014:391-396.
2. Giblett ER. Blood group alloantibodies: An assessment of some laboratory practices. *Transfusion*. 1997;17(4):299–308. doi:10.1046/j.1537-2995.1977.17477216857.x
3. Nance ST. Red cell antibody detection by serology. *ISBT Sci Ser*. 2015; 10(Suppl 1):1–4:225–231. doi:10.1111/voxs.12128
4. Walker PS, Hamilton JR. Identification of antibodies to red cell antigens. In: Fung MK, Grossman BJ, Hillyer CD, Westhoff CM, eds. *Technical Manual*. 18th ed. Bethesda, USA: AABB; 2014:391–421.
5. Avent ND. *Transfusion and Transplantation Science*. Oxford, UK: Oxford University Press; 2018.
6. Tomer Y, Shoenfeld Y. Ageing and autoantibodies. *Autoimmunity*. 1988;1(2):141–149. doi:10.3109/08916938809001927
7. Daniels G, Poole J, de Silva M, et al. The clinical significance of blood group antibodies. *Transfus Med*. 2002;12(5):287–295. doi:10.1046/j.1365-3148.2002.00399.x
8. Quinley ED. *Immunohematology Principles and Practice*. Philadelphia, USA: Lippincott Williams and Wilkins; 2011.
9. Urbaniak SJ, Greiss MA. RhD haemolytic disease of the fetus and the newborn. *Blood Rev*. 2000;14(1):44–61. doi:10.1054/blre.1999.0123
10. Poole J, Daniels G. Blood group antibodies and their significance in transfusion medicine. *Transfus Med Rev*. 2007;21(1):58–71. doi:10.1016/j.tmrv.2006.08.003
11. Downes KA, Shulman IA. Antigen and antibody testing. In: Fung MK, Grossman BJ, Hillyer CD, Westhoff CM, eds. *Technical Manual*. 18th ed. Bethesda, USA: AABB; 2014:367–384.
12. Rumsey DH, Ciesielski DJ. New protocols in serologic testing: A review of techniques to meet today's challenges. *Immunohematology*. 2000; 16(4):131–137. PMID:15373603
13. Langston MM, Procter JL, Cipolone KM, Stroncek DF. Evaluation of the gel system for ABO grouping and D typing. *Transfusion*. 1999; 39(3):300–305. doi:10.1046/j.1537-2995.1999.39399219288.x
14. Roback JD, Grossman BJ, Harris T, Hillyer CD, eds. *Technical Manual*. 17th ed. Bethesda,USA: AABB; 2011:873-874.
15. Chicco D, Tötsch N, Jurman G. The Matthews correlation coefficient (MCC) is more reliable than balanced accuracy, bookmaker informedness, and markedness in two-class confusion matrix evaluation. *BioData Min*. 2021;14(1):13. doi:10.1186/s13040-021-00244-z
16. Ogrinc G, Davies L, Goodman D, et al. SQUIRE 2.0 (Standards for Quality Improvement Reporting Excellence): Revised publication guidelines from a detailed consensus process. *BMJ Qual Saf*. 2016;25:986–992. doi:10.1016/j.jamda.2021.06.006
17. Lapierre Y, Rigal D, Adam J, et al. The gel test: A new way to detect red cell antigen-antibody reactions. *Transfusion*. 1990;30(2):109–113. doi:10.1046/j.1537-2995.1990.30290162894.x
18. Cheng G, Chan A, Chun M, et al. Evaluation of the gel test for antibody screening in a tertiary hospital in Hong Kong: Insensitivity for some cold antibodies that are reactive at 37°C by conventional indirect antiglobulin tests. *Clin Lab Haematol*. 1995;17(1):81–84. doi:10.1111/j.1365-2257.1995.tb00323.x
19. Chan HF, Wong CH, Chui L, et al. The impact of a gel system on routine work in a general hospital blood bank. *Immunohematology*. 1996; 12(1):30–32. PMID:15387759
20. Delaflor-Weiss E, Chizhevsky V. Implementation of gel testing for antibody screening and identification in a community hospital: A 3-year experience. *Lab Med*. 2005;36(8):489–492. doi:10.1309/JAP6EC69BAAUG9B3
21. Cheng D, Hao Y. Comparative evaluation of the microcolumn gel card test and the conventional tube test for measurement of titres of immunoglobulin G antibodies to blood group A and blood group B. *J Int Med Res*. 2011;39(3):934–943. doi:10.1177/147323001103900328
22. Bhagwat SN, Sharma JH, Jose J, et al. Comparison between conventional and automated techniques for blood grouping and crossmatching: Experience from a tertiary care centre. *J Lab Physicians*. 2015;7(2):96–102. doi:10.4103/0974-2727.163130
23. Bhangale A, Pathak A, Pawar S, et al. Comparison of antibody titers using conventional tube technique versus column agglutination technique in ABO blood group incompatible renal transplant. *Asian J Transfus Sci*. 2017;11(2):131–134. doi:10.4103/0973-6247.214343
24. Novaretti MCZ, Jens E, Pagliarini T, et al. Comparison of conventional tube test with diamed gel microcolumn assay for anti-D titration. *Clin Lab Haematol*. 2003;25(5):311–315. doi:10.1046/j.1365-2257.2003.00540.x